# THE ROLE OF ACIDOSIS-SENSING IN THE REGULATION OF CHRONIC INFLAMMATION BY SKELETAL MUSCLE

**Thesis submitted for the degree of**

**Doctor of Philosophy**

**at the University of Leicester**

**by**

**Safia Sabr Ibrahim Blbas**

**Department of Infection, Immunity and Inflammation**

**College of Life Sciences**

**School of Medicine**

**University of Leicester**

**2017**

# Abstract


**The role of acidosis sensing in the regulation of chronic inflammation by skeletal muscle**

Safia Sabr Ibrahim Blbas

Many chronic inflammatory diseases including Chronic kidney disease (CKD) are characterised by loss of skeletal muscle or cachexia, which leads to decreased mobility and quality of life. Metabolic acidosis is common in CKD and stimulates muscle protein wasting which may further enhance chronic inflammation. *In vivo*, this muscle wasting by acidosis also requires the presence of glucocorticoid (GC). Metabolic acidosis is thought to act by inhibiting the pH-sensitive System A amino acid transporter protein SNAT2, resulting in impaired global protein synthesis and enhanced global proteolysis.

The L6 rat muscle cell model was used to study the effects of glucocorticoid Dexamethasone (DEX) on SNAT2 transport activity. The activity of this transporter was measured from the rate of α-[1-$^{14}$C]-MeAIB transport into the cells and related to the total protein content of the cultures. To obtain an experimental system in which changes in the SNAT2 protein could be assessed; GFP-tagged human SNAT2 (SNAT2-eGFP) was cloned and expressed in L6 and in the readily transfected cell line HEK293A.

DEX significantly inhibited SNAT2 activity in L6 cells. This effect was blunted by vanadate and abolished by vanadate plus amino acid deprivation (AAD). AAD is reported to stabilise SNAT2 protein, and vanadate inhibits both phosphotyrosine phosphatases (PTPs) and proteasomes. More specific PTP inhibitors failed to blunt DEX's effect on SNAT2 activity. DEX had no effect on SNAT2 mRNA expression but depleted SNAT2 protein assessed by immunoblotting, suggesting that DEX acts through changes in degradation rather than phosphorylation of SNAT2 protein. This was confirmed by blunting the effect of DEX with proteasome inhibitor MG132.

Transfection of L6 myoblasts with SNAT2-eGFP cDNA led to protein expression detected by fluorescence, but only a small increase in α-[1-$^{14}$C]-MeAIB transport. However, expression of SNAT2-eGFP in HEK-293A cells yielded a functionally active transporter protein which was isolated by GFP trapping and confirmed by mass spectrometry to be SNAT2. This isolated protein showed no evidence of phosphorylation, but SNAT2-eGFP fluorescence was significantly reduced by DEX and partly restored by MG132, again suggesting that DEX promotes SNAT2 degradation. SNAT2-eGFP over-expression also significantly activated the amino acid-dependent signalling pathway through mTORC1 to rpS6, a potential stimulator of global protein synthesis; and increased intracellular concentration of the SNAT2 substrate L-Met, a reported stimulator of mTORC1.

To test the hypothesis that SNAT2's transport of L-Met contributes to mTORC1 activation in L6 cells, SNAT2 was inhibited in L6 myoblasts by competitive

inhibition with excess MeAIB or by SNAT2 silencing with siRNA. Addition of L-Met alone to L6 cells detectably stimulated mTORC1/rpS6 signalling and MeAIB abolished this effect. However, it was not possible to show by siRNA silencing that SNAT2 alone mediated the effect of L-Met. SNAT2 silencing in L6 did however significantly blunt MAPK signalling (a key mediator of mechanical stress–induced anabolic signals during exercise), suggesting that SNAT2 contributes to anabolic pathways in addition to mTORC1.

# Acknowledgments

Foremost, I would like to express my sincere gratitude to my supervisor Dr. Alan Bevington for his continuous support and encouragement throughout my project without his endless help and guidance I could not easily have done this project: I could not have imagined having a better supervisor and thanks to him for his help in Figure 3.3 experiment. I would like to thank my second supervisor Dr Cordula Stover for her support. Thanks for my progress review panels Professor Nigel Brunskill and Dr Karl Herbert for their valuable comments and advice in my annual meetings.

I would also like to thank my sponsor Kurdistan Region Government for giving me this opportunity to do my PhD which was an eye opener and gaining the whole experience of living and studying abroad.

Special thanks to Mr Jeremy Brown for his assistance in lab works, teaching me the techniques, for making the lab a happy environment never getting bored and always remember that Jimi Hendrix is his favourite.

A big thank you with love to all whom I worked with in the renal lab during my PhD Dr Emma Watson, Dr Izabella Pawluczyk, Dr Karen Molyneux, Dr Nima Abbasian, Ziyad Aldosari, Abdullah Alruwaili, Doug Gould, Tom O'Sullivan, Dina Nilasari, thanks to Antoine Maresca MSc student worked under my supervision for counting SNAT2-GFP fluorescence. Special thanks to Violeta Diez Beltran for being a great friend and sister who has happy memories together never to be forgotten. I would also thank Patricia Higgins for making renal group like a family with her special tea time and showing me beautiful places in UK.

I want to dedicate all my hard work and success from the beginning of my journey as a student until today to the soul of my father and mother: it was always their dream for me to reach to this stage.

My sincere thanks also go to my father and mother in law for being great parents with all their emotional support and help. Big love to my sisters and brothers, old and new for their endless support, phone calls and never stop saying “What time you will come back”. A special thanks to my uncle Muhammad for being my role model and a great support throughout my life. Thanks to my friend Bayan Faraj for her help and advice in transformation experiment.

Finally, a massive love and thanks to my lovely husband Hawkar, for being amazing company during my journey, thanks for your patient waiting for me to come back late from lab every day and having faith in me that I can do this project, for your delicious cooks. I never felt lonely and hopeless with you being beside me, assisting me to solve problems and copying with study stress. Your encouragement was the greatest factor for my success.

# Table of contents

# List of figures

# List of tables

# List of abbreviations

| | |
|---|---|
| mTOR | Mechanistic or mammalian target of rapamycin |
| CKD | Chronic Kidney Disease |
| DEX | Dexamethasone |
| DFBS | Dialysed foetal bovine serum |
| DMEM | Dulbecco's Modified Eagle’s Medium |
| DMSO | Dimethyl sulfoxide |
| EBSS | Earle's Balanced Salt Solution |
| HBS | Hepes Buffered Saline |
| HBSS | Hanks’ Balanced Salt Solution |
| HEK293A | Human Embryonic Kidney Cells |
| HIA-FBS | Heat inactivated foetal bovine serum |
| MeAIB | Methylaminoisobutyric acid |
| MEM | Minimum Essential Medium |
| SNAT2 | Sodium-coupled neutral amino acid transporter |
| PI3K | Phosphoinositide 3-kinase |
| IGF1 | Insulin-like Growth Factor-1 |
| MAPK | Mitogen-activated protein kinase |
| ERK | Extracellular Signal-Regulated Kinase |
| JNK | c-Jun NH2-terminal kinase |
| UPP/S | Ubiquitin/Proteasome Pathway/System |
| Ang II | Angiotensin II |
| CRP | C-reactive protein |
| SGK-1 | Serum- and glucocorticoid-induced kinase-1 |
| GFR | Glomerular filtration rate |
| GPCRs | G protein-coupled receptors |
| GCN2 | general control non-derepressible 2 |
| S6K | ribosomal protein S6 kinase |
| 4E-BP1 | eukaryotic translation initiation factor 4E binding protein 1 |

| | |
|---|---|
| LAT1 | System L amino acid transporter1 |
| GC | Glucocorticoid |
| GR | Glucocorticoid receptor |

# Chapter 1 General introduction

## 1.1 The importance of skeletal muscle and muscle mass in human health

In addition to skeletal muscle's primary mechanical role in supporting movement and body posture, it also plays a vital role in maintaining health and good quality of life (Janssen *et al.,* 2000) by its metabolic effects on for example carbohydrate and protein metabolism. Skeletal muscle accounts for approximately 40% of total body weight and around half to one third of the total body protein. Muscle consists of 75% of water, 20% protein and the rest is carbohydrates, fat and inorganic salts (Frontera & Ochala, 2015). Consequently, muscle can be thought of as a metabolic organ, serving as a source of key nutrients, for example amino acids by acting as a protein reservoir (Carrero *et al.,* 2016). These effects are strongly dependent on the regulation of muscle mass and this regulation is largely performed by adjusting the balance between intramuscular protein synthesis and protein breakdown (McCarthy & Esser, 2010).

These important functions will decline with aging, therefore maintaining muscle quality and quantity is regarded as a significant goal in aged populations to prevent the complications arising from muscle wasting during aging (McLeod *et al.,* 2016). Size of the muscles is one of the important predictors of muscle quality and physical performance, as well as neurological aspects which influence the locomotor and physical strength of the muscle (Carrero *et al.,* 2016). In the process of muscle development, there is increase in the number and size of muscle fibres which contributes to muscle strength. Conversely decrease in number of fibres due to disease conditions such as cachexia leads to decreased muscle strength and increased frailty and loss of self-confidence which affect the individuals and their families and place a considerable burden on the health care sector (Romanick *et al.,* 2013). Skeletal muscle is one of the vital organs which, with reduced cardiac output, and reduction in lung function, contributes to the well-documented age-dependent reduction in maximum oxygen consumption ($VO_2^{max}$) which is a major contributor to age-related mortality rate (McLeod *et al.,* 2016). Decrease in muscle mass is common in elderly people with significant

outcomes such as sarcopenia and (indirectly) osteopenia which together make it difficult to maintain posture and unimpaired movement and consequently affect the quality of life in this population (Janssen *et al.,* 2002). A more recently recognised important feature of muscle is its role in cytokine biology – in particular by the release of muscle – derived cytokines (myokines). For example, skeletal muscle is one of the organs that produces Interleukin-15 (IL-15) which may play a role in regulation of contractile protein turnover and myoblast differentiation and adiposity (Argiles *et al.,* 2009). Skeletal muscle may also serve as anti-inflammatory organ (especially during exercise) releasing Interleukin-6 (IL-6) as a myokine which may exert an anti-inflammatory effect on Tumour Necrosis Factor -α (TNF-α) (Nielsen & Pedersen, 2008) as discussed in more detail in Section 1.5.

### 1.2 The clinical importance of chronic inflammation

Chronic inflammation, which has been defined as a response to a sustained inflammatory stimulus which cannot be eradicated (Serhan *et al.,* 2010), is one of the most important clinical features in many chronic diseases such as chronic kidney disease (CKD), diabetes mellitus, cancer, and cardiovascular diseases (CVD) and consequently it is a leading contributor to mortality. The U.S. Centres for Disease Control and Prevention reported that 63% of all deaths worldwide are linked to chronic inflammatory diseases, and about 70% of all deaths in USA (1.7 million each year) (Prasad & Aggarwal, 2014). Elevated C-reactive protein (CRP) as a marker of inflammation is associated with prolonged hospitalisation and high mortality rate, for example among dialysed CKD patients (Yeun *et al.,* 2000).

Inflammation is common in CKD (Cheung *et al.,* 2010) and this group of diseases provides a particularly clear example of the link between chronic inflammation and increased rates of morbidity and mortality when compared with the general population (Foley *et al.,* 1998). Prevalence of inflammation among CKD patients is different among different populations, possibly because genetic factors are a major contributor. For example, in the USA and European countries 30–60% of end-stage renal disease (ESRD) patients have high concentrations of inflammatory markers in their serum, while Asian patients are characterised by lower inflammatory marker levels. Elevated acute phase proteins such as CRP and amyloid A, and similarly elevated concentrations of inflammatory cytokines

especially IL-6 are found in renal disease (Nascimento *et al.,* 2002; Wong *et al.,* 1999) . Cardiovascular disease is very common in CKD (Foley *et al.,* 1998), and the classical causes of cardiovascular disease such as high blood pressure, or comorbidities such as diabetes mellitus, are not regarded as an adequate explanation of this high incidence in these patients. For this reason, chronic inflammation has been proposed as a major contributor to this high prevalence of cardiovascular disease among CKD populations, possibly because inflammation is associated with (and may promote) oxidative stress, insulin resistance, endothelial dysfunction and muscle wasting (Cheung *et al.,* 2010). Muscle wasting and changes in body composition are a common finding in patients with CKD and are strongly associated with increased risk of morbidity and mortality (Carrero *et al.,* 2016).

### 1.3 The role of muscle mass and body composition in chronic inflammation

In view of this link between body composition and clinical outcome in chronic inflammatory diseases such as CKD, measuring body composition accurately is important. Body mass index (BMI) which is defined as body weight in kilograms (kg) divided by the square of the patient's height in meters is a technically simple indirect indicator of body composition which can be used in a clinical setting (for example as a measure of obesity) and related to patients' fitness and wellbeing (Wells & Fewtrell, 2006). High BMI among CKD patients in general is not associated with good quality of life and fitness, especially among end stage renal disease (ESRD) patients because of increases in visceral fat which may lead to increased risk of developing cardio vascular diseases (Johansen & Lee, 2015). CKD is characterised by muscle wasting and this is even true among obese CKD patients who, at first sight, do not seem to be wasted, because they have high adipose tissue which masks their low percentage of lean tissue (Johansen & Lee, 2015). Therefore, measuring muscle mass is a better indicator of the functionality, potential for physical activity, and metabolic status in CKD patients (Carrero *et al.,* 2016). Measuring body composition, especially estimating the amount of muscle, is very important in chronically ill patients because of the role of the muscle (as explained in Section 1.1) in controlling many important metabolic

functions such amino acid supply to other organs and secretion of anti-inflammatory cytokines (Wolfe, 2006) (See also Section 1.5 and Figure 1.3).

In view of these important functions of the muscles, many techniques have been developed to measure muscle mass such as computed tomography (CT), magnetic resonance imaging (MRI), bioelectrical impedance, and dual energy X-ray absorptiometry (DEXA). Among these methods DEXA is regarded as the gold standard to measure muscle mass. It was originally developed to measure bone mineral mass but, because this requires penetrating the surrounding soft tissue such as muscle, and penetration of lower energy X-rays is to some extent impeded by soft tissue, muscle mass can also be measured (Frontera & Ochala, 2015; Wells & Fewtrell, 2006). This is possible because the technique can be used to discriminate between lean tissue (muscle) and adipose tissue (Shaw *et al.,* 2007).

### 1.4 The cell biology of muscle

Individual skeletal muscles consist of hundreds to thousands of elongated structures called muscle fibres or myofibres. Each is a multinucleated cell containing smaller rod-shaped units called myofibrils which in turn consist of overlapped thick and thin filaments, principally made up of the proteins myosin and actin respectively (Brooks, 2003) (Figure 1.1). Actin and myosin are present in all kind of muscles, but they are most abundant in skeletal muscle cells. The pattern of actin and myosin arrangement gives the skeletal muscle cell a striated appearance in each of its contractile units called sarcomeres, which are responsible for the process of contraction (Greig & Jones, 2010). The number of muscle fibres is determined from birth, but small changes happen in response to some factors such as injury or training (Brooks, 2003). This response to injury arises because skeletal muscle has a powerful regeneration system: in case of injury muscle cells can be regenerated within a short period and returned to functioning normally (Relaix & Zammit, 2012).The cellular basis for this skeletal muscle regeneration are the satellite cells. Satellite cells are mature mono-nuclear stem cells which have differentiation ability to fuse to each other to form myotubes that mature into myofibres or fuse with damaged segments of existing myofibres (Frontera & Ochala, 2015).

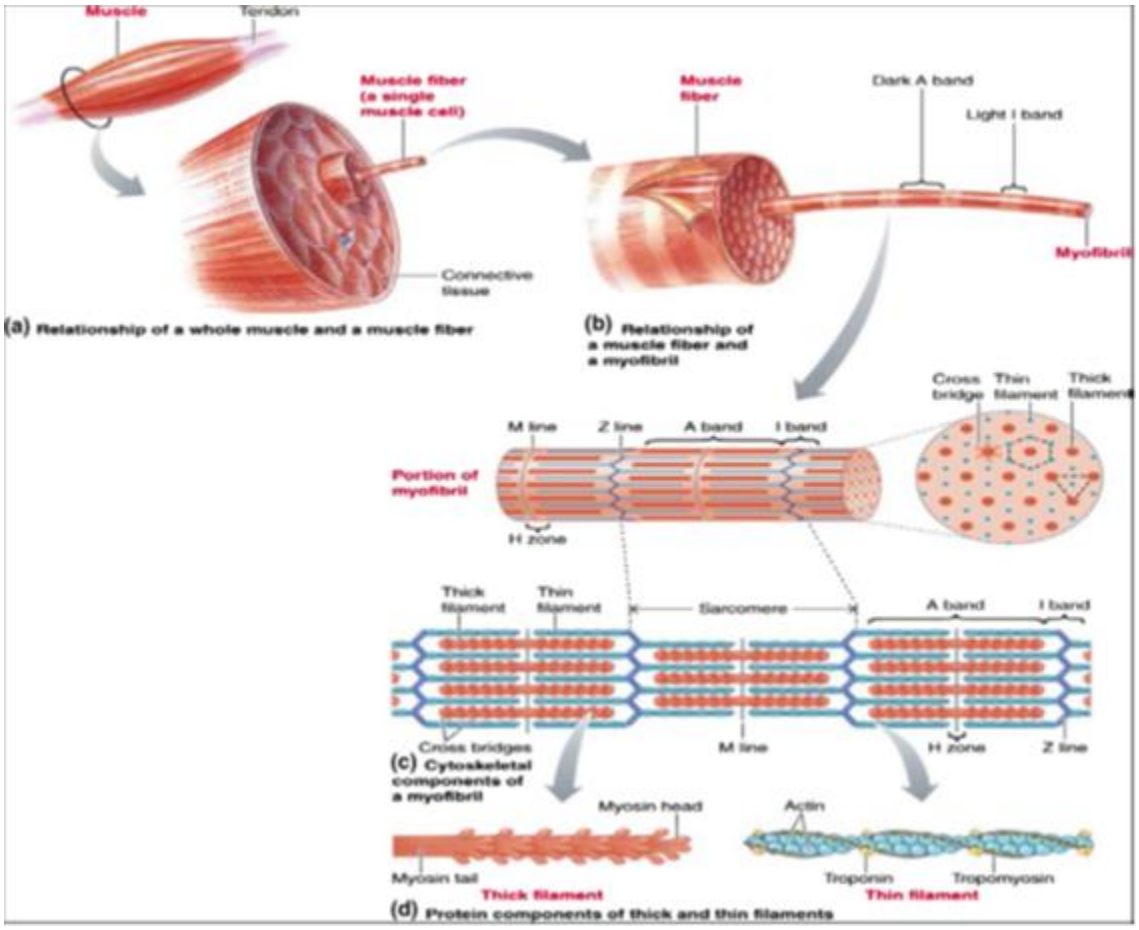


**Figure 1.1. Major features of skeletal muscle structure taken from (Frontera & Ochala, 2015).**

In healthy skeletal muscle, satellite cells are dormant cells located just below the basal lamina of myofibres. When they are activated (for example following injury) they form myoblasts first, then converting to myofibres by a process of cell fusion, initially forming multi-nuclear myotubes, but then mature myofibres which may contain hundreds of nuclei (Hall *et al.,* 2011b). Also, some of them form more undifferentiated cells and go back to dormancy - again to serve as precursors to maintain the satellite cell pool by this self-renewing process (Figure 1.2). This ability of satellite cells to differentiate to myofibres and generate more satellite cells at the same time is due to their heterogeneity (Relaix & Zammit, 2012). The process of satellite cell activation is a heavily regulated process, controlled by the expression of myogenic regulatory factors, MyoD (initiating proliferation) and myogenin (controlling differentiation). (Pallafacchina *et al.,* 2013). A study by Verdijk et al (2014) showed the importance of satellite cells in maintaining muscle

generation and strength throughout human life, with a reduction in type II muscle fibre-associated satellite cell content in relation to muscle fibre size with aging, implying a delay in muscle regeneration in elderly people (Verdijk *et al.,* 2014). Such impaired satellite cell function is also thought to contribute to muscle wasting (through impaired response to injury) in chronic inflammatory illnesses such as CKD (Wang *et al.,* 2011).

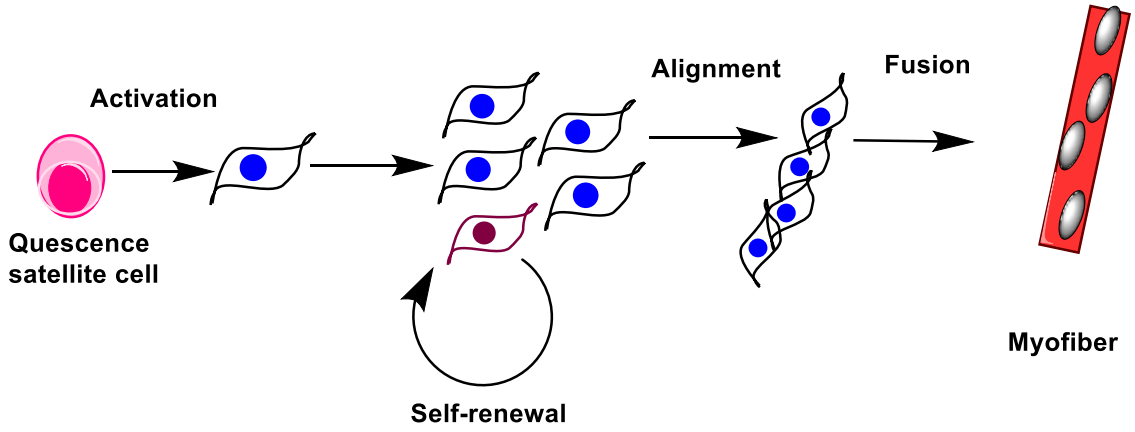


**Figure 1.2. Satellite cell activation, proliferation, self-renewal and myofibre formation.**
Information was taken from (Yablonka-Reuveni, 2011) to draw the diagram.

Muscle fibres can be broadly classified into two main categories, Type I and Type II according to their differences in myosin isoforms. These are also known as slow and fast twitch fibres respectively. Type II muscle fibres are further subdivided into IIA, IIX and IIB (the latter is only found in rodent) according to the contraction ability-slowest to fastest respectively (Greig & Jones, 2010). In addition to Type I fibres being classed as slower than Type II, they are more fatigue resistant and have an important role in supporting posture. In contrast, Type II muscle fibres are used in quick and intense physical activities (Greig & Jones, 2010). Type II fibres have a significant glycolytic capacity and express high glycolytic enzyme activity. In contrast Type I fibres do not require glycolysis as their major pathway of ATP synthesis but rely more heavily on mitochondrial metabolism (oxidative phosphorylation) with ATP synthesis sustained through the oxidative metabolism of fat and carbohydrate. However, a significant mitochondrial density and capacity for oxidative phosphorylation is also found in Type IIA fibres – the so-

called “fast oxidative fibres”. The relative proportions of each muscle fibre type in human muscle can vary within individuals from muscle to muscle (Johnson *et al.,* 1973) and also between individuals according to their physical activity, training (Methenitis *et al.,* 2017; Ross & Leveritt, 2001) and genetics (Simoneau & Bouchard, 1995): for example sprint athletes having more Type II fibres compared with endurance athletes (Costill *et al.,* 1987; Costill *et al.,* 1976) or individuals performing daily walking or low intensity exercise (Greig & Jones, 2010; Ross & Leveritt, 2001).

### 1.5 The role of exercise and muscle in controlling chronic inflammation

While chronic inflammation can cause muscle wasting (cachexia) (see Section 1.8), loss of skeletal muscle can also contribute to inflammation. Myokines (cytokines and chemokines released by muscle cells) may have a role in this (Okajima, 2013; Viana *et al.,* 2014). There is evidence that muscle cells can produce anti-inflammatory cytokines which have endocrine or paracrine effects to maintain anti-inflammatory/inflammatory balance in normal muscles and in surrounding tissues, especially during and after exercise (Brandt & Pedersen, 2010). Myokines whose release is regulated by muscle contraction include IL-6, IL-15, irisin, BDNF (Brain derived neurotrophic factor), ANGPTL4 (Angiopoien like 4), FGF21 (Fibroblast growth factor 21), myonectin and MCP-1(Monocyte chemo attractive protein-1) (Raschke & Eckel, 2013), although it has been suggested that not all of this contraction-mediated myokine release originates from the muscle fibres themselves. For example, some of this may derive from adipose tissue within the muscle (Raschke & Eckel, 2013).

A functionally important myokine is IL-6. Contraction of muscle fibres induces IL-6 production which has anti-inflammatory effects in short-term release and increases glucose uptake and fat oxidation by activating both AMPK and PI3kinase pathways (Brandt & Pedersen, 2010). IL-6 is mostly considered as a *pro*-inflammatory cytokine (Nielsen & Pedersen, 2008). However, the IL-6 released acutely from muscle in the context of exercise is different in its biological effects from the macrophage-derived IL-6 that is released in the context of an acute inflammatory response, for example during an infection. The IL-6 which is

produced by exercising muscle in the absence of significant muscle TNF-α production has an autocrine effect on its own production within the skeletal muscle, and an anti-inflammatory effect in surrounding tissues by suppressing the inflammatory cytokine TNF-α (Figure 1.3) which is also one of the pro-inflammatory cytokines derived from adipose tissue (i.e. the so-called "adipokines" (Jung & Choi, 2014)). Furthermore, loss of muscle cells or muscle fibre atrophy, and reduction of the muscle to adipose tissue ratio in chronic inflammatory diseases such as CKD impairs this balance between IL6 and TNF-α and worsens the chronic inflammation (Petersen & Pedersen, 2005). Therefore, maintaining muscle mass and decreasing the mass of adipose tissue (especially visceral fat) is a very important goal in chronic inflammatory diseases such as CKD. For this reason, exercise therapy is regarded as increasingly important in CKD patients, not only to decrease frailty and increase muscle strength (Johansen & Lee, 2015), but also to reduce chronic inflammation (Viana *et al.,* 2014).

Another example of a muscle-derived cytokine is IL-15 which has been reported in muscle cells of different species (Argiles *et al.,* 2009). It was originally reported as a pro-inflammatory cytokine and was shown to have an anabolic effect on muscle mass by inducing differentiated myocytes to retain the muscle fibres and reducing the muscle protein break-down by down-regulation of ATP-Ubiquitin dependent pathways (Argiles *et al.,* 2009; Brandt & Pedersen, 2010).The role of this cytokine in enhancing skeletal muscle growth has also been reported by Quinn et al (2002): who found that the over-expression of IL-15 in the C2C12 cell line leads to hypertrophy (Quinn *et al.,* 2002). However, some of this earlier evidence of an anabolic effect in muscle was obtained *in vitro* and more recent *in vivo* studies have indicated a more complex role for muscle–derived IL-15, for example in regulating oxidative energy metabolism (Pistilli & Quinn, 2013) and suppressing accumulation of adipose tissue (Lacraz *et al.,* 2016).

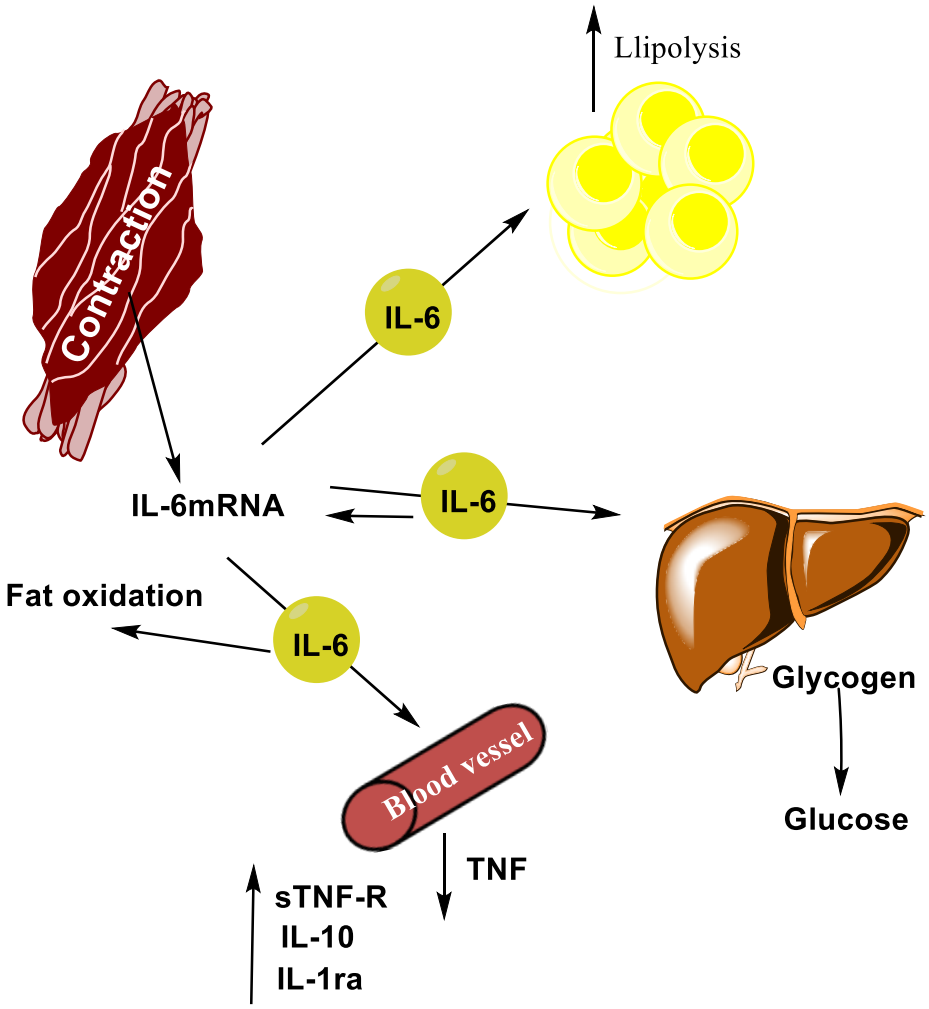


**Figure 1.3. Summary of anti-inflammatory effect of exercise.**

sTNF-R: Soluble tumour necrosis factor receptors, IL-1ra: Interleukin 1 receptor antagonist. The diagram is redrawn from (Petersen & Pedersen, 2005).

## 1.6 Anabolic signals in muscle

Anabolic signals in muscle are strongly dependent on the signalling pathways that increase protein synthesis, decrease protein degradation, and consequently increase muscle mass. Anabolic effects through decreased protein degradation are described below in Section 1.8.2. Increasing protein synthesis is performed through two processes, either increasing protein translation efficiency or increasing translation capacity (largely through ribosome biogenesis). A regulatory protein of central importance in this field is mTOR (mechanistic target of rapamycin). It is thought that signalling through mTOR is the major pathway that increases translation efficiency. However, the factors that induce both

translation efficiency and capacity are tightly coordinated (for example during muscle hypertrophy) (McCarthy & Esser, 2010; Nader *et al.,* 2005) and for that reason mTOR is also an important regulator of ribosome biogenesis (Mayer & Grummt, 2006).

Mechanistic target of rapamycin (mTOR) is a serine/threonine protein kinase which has homology with phosphatidylinositol kinase (Eunjung, 2009; Zheng *et al.,* 2016). mTOR is a precursor of two important signalling complexes, mTORC1 and mTORC2. mTORC1 comprises the proteins mTOR, Raptor, mLST, PRAS40 and Deptor (Limon & Fruman, 2012) and, unlike mTORC2, is inhibited by the immunosuppressive drug rapamycin. mTORC1 plays a major role in regulating metabolism, growth and proliferation of the cell by controlling protein translation through phosphorylation of its downstream targets - the ribosomal protein S6 kinase ($p70^{S6K1}$) and eukaryotic translation initiation factor 4E binding protein 1 (4E-BP1) (Figure 1.4).

Maintaining balance between protein synthesis and degradation (by interaction between anabolic or catabolic signals inside the cell) is partly the consequence of the net effect of hormones, growth factors and cytokines acting at the cell surface. Of particular importance as an extracellular anabolic signal acting on skeletal muscle cells is Insulin-like Growth Factor I (IGF-I) (Golberg *et al.,* 2014). Insulin and IGF-I are among the mTOR activators that can activate the mTORC1 pathway by binding to their receptors on the cell surface, resulting in activation of the receptor tyrosine kinases (RTKs) and inducing PI3K phosphorylation then Akt phosphorylation at Ser473 and Thr308. Akt phosphorylation results in mTORC1 activation (Golberg *et al.,* 2014), indirectly stimulating mTORC1 by phosphorylating TSC2, thereby activating the GTPase protein, Ras homolog enriched with brain (RHEB) (Figure 1.4) (Pasiakos, 2012).

In addition to anabolic hormones signalling through RTKs, nutrient supply is also an important regulator of mTORC1. Amino acids, especially L-leucine, can stimulate mTORC1 by an insulin independent pathway. Pharmacological inhibition of the insulin signal from its RTK through PI3K does not prevent mTORC1 activation by L-leucine (Pasiakos, 2012). A number of possible sensors of the L-leucine concentration inside the cell have been proposed which may then

be able to activate mTORC1. The enzyme Leucyl-tRNA synthetase (LRS), has been suggested to act as an L-leucine sensor which then acts on hVps34 (vacuolar protein sorting 34) which is a member of the Class 3 family of PI3 kinases upstream of mTORC1 (Figure 1.4). This then contributes to translocation of mTORC1 to the lysosome (Yoon *et al.,* 2016). Translocation of mTORC1 to the lysosome is the first step in activation of mTORC1 in response to amino acids. It is this lysosome-associated pool of mTORC1 which is regarded as the functionally active form of the mTOR kinase (Figure 1.4). Another L-leucine dependent mTORC1 activator is the Rag subfamily of Ras small GTPases which function as heterodimers and bind to Raptor. This Rag GTPase heterodimer is thought to be responsible for initiation of mTOR activation by combining with the Ragulator protein complex in the lysosome membrane which leads to Rag GTPase activation and then interaction with inactive mTORC1 in the cytosol via RAPTOR and localisation of mTORC1 to the surface of the lysosome (Taylor, 2014). This Rag-dependent mTORC1 translocation is stimulated by increasing intracellular amino acid concentration (Taylor, 2014), and this Rag-dependent process is currently regarded as the main mechanism whereby mTORC1 is activated by amino acids such as L-leucine.

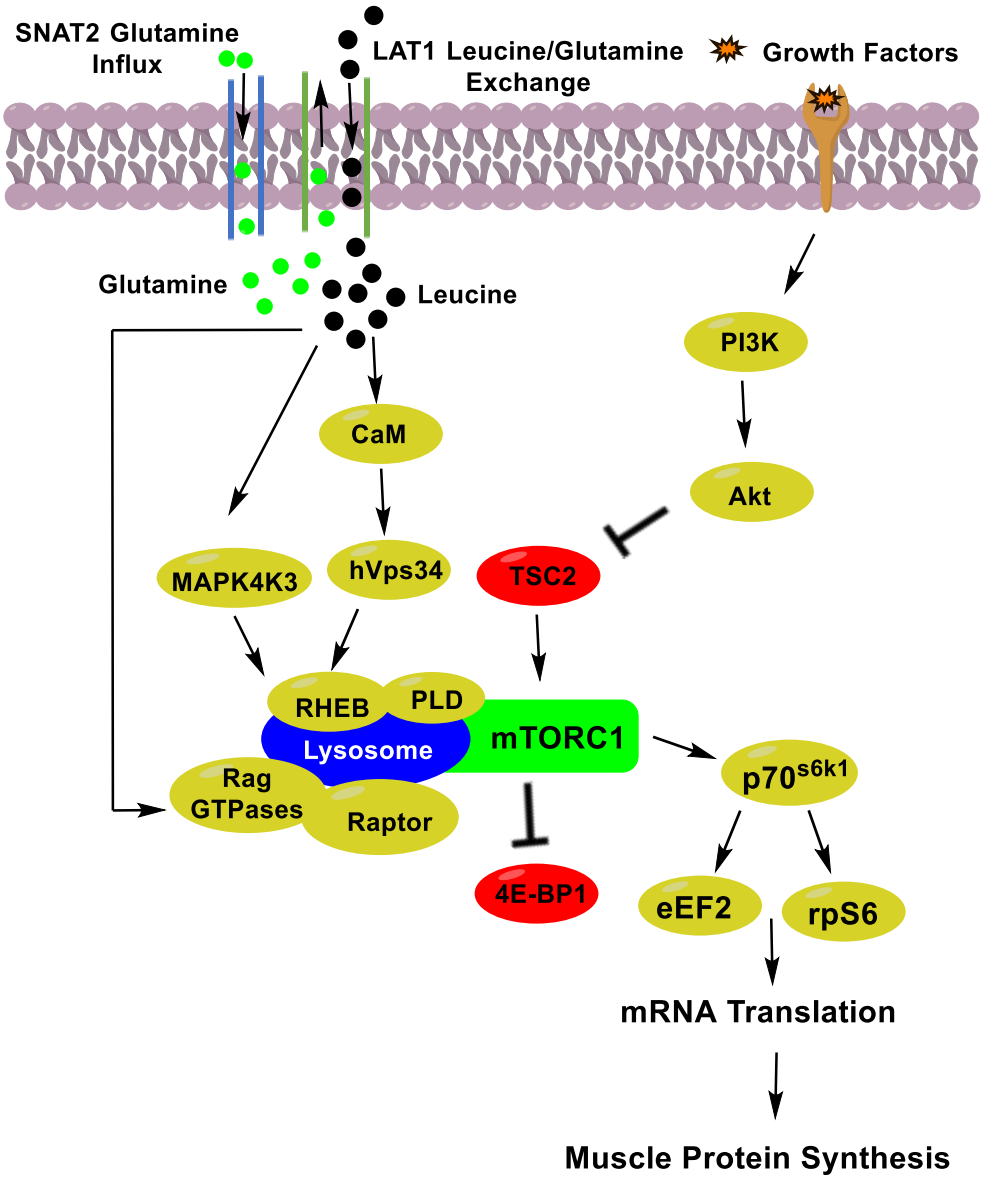


**Figure 1.4. A simplified diagram showing amino acid and growth factor mediated anabolic signals to mTORC1.**

The diagram is redrawn from (Pasiakos, 2012). Stimulators of muscle protein synthesis are depicted in yellow, whereas inhibitory proteins are depicted in red. Abbreviations: CaM, calcium/calmodulin; hVps34, human vacuolar protein sorting-34; PI3K, phosphatidylinositol 3-kinase; Akt, protein kinase B; TSC2, tuberous sclerosis complex; RHEB, Ras homolog enriched with brain; mTOR, mechanistic target of rapamycin; PLD, phospholipase D; 4E-BP1, eukaryotic initiation factor 4E-binding protein 1; $p70^{S6K1}$, 70-kDa ribosomal protein S6 kinase 1; eEF2, eukaryotic elongation factor 2; rpS6, ribosomal protein S6.

It has been suggested that some cells are able to sense changes in extracellular amino acid concentration (i.e. before the amino acids enter the cell) by means of a group of plasma membrane G protein-coupled receptors (GPCRs) which have a nutrient sensing element in their extracellular domain (Conigrave & Hampson, 2010). However, for amino acids such as L-leucine to activate mTORC1, they need to be located inside the cell; either in the cytosol or possibly within the lysosome. Amino acid transporter proteins in the plasma membrane or in the lysosomal membrane are therefore possible regulators of mTORC1 activity. In the plasma membrane, two important types of amino acid transporter which are involved in controlling muscle intracellular amino acid concentration are System A amino acid transporters of the SLC38 gene family (such as SLC38A2 (SNAT2)), and System L amino acid transporters which are heterodimers of proteins encoded by the SLC7 and SLC3 gene families (such as SLC7A5 (LAT1)/SLC3A2 (4F2hc)). (These are described in detail below in Section 1.11).

SLC38 family amino acid transporters have a well-established role in transporting amino acids across the plasma membrane from outside to inside the cell where they can activate mTORC1. However, presence of members of this family on the lysosome (such as human member 9 of the solute carrier family 38 (SLC38A9)) increases the possibility of their involvement in also activating mTORC1 at lysosomal level (Rebsamen *et al.,* 2015). SLC38A9 is a lysosomal amino acid transporter which has eleven transmembrane domains, with 119 amino acid residues, a cytosolic N-terminus and glycosylation sites in its transmembrane region (Wang *et al.,* 2015). It is highly glycosylated and (like mTORC1) has a role in regulating protein synthesis and cell proliferation as shown by the fact that silencing SLC38A9 leads to a decrease in cell growth and size. Evidence for the involvement of SLC38A9 in the protein complexes that regulate mTORC1 activation comes from experiments in which expression and immunoprecipitation of a tagged SLC38A9 fusion protein in HEK293 cells showed (by mass spectrometry analysis) that other regulatory proteins such as Ragulator-RAG GTPase are apparent binding partners of SLC38A9. siRNA silencing of SLC38A9 transporter led to disassociation of the other mTOR regulatory proteins from the lysosomal protein complex indicating the membership and interaction of SLC38A9 in the mTOR regulatory protein complex (Rebsamen *et al.,* 2015).

Furthermore, siRNA silencing of SCL38A9 in HEK 293T cells inhibited mTORC1 activation by amino acids (using ribosomal S6 kinase ($p70^{S6K1}$) phosphorylation downstream of mTORC1 as an indicator of mTORC1 activity (Figure 1.5)). It was concluded that SLC38A9 is a positive mTOR regulator like the other well-established regulators Ragulator, Rag and GTPase complexes (Wang *et al.,* 2015) and that it may serve as a sensor of L-arginine (Arg) concentration.

More generally it has been concluded that amino acid sensing that leads to mTORC1 activation is not only restricted to plasma membrane proteins or other extracellular sensors but can be sensed by amino acid transporters located on the lysosome surface. Apart from SLC38A9, the L-alanine/L-proline/glycine transporter SLC36A1 and the L-leucine transporter SLC7A5(LAT1)/SLC3A2 (4F2hc) have also been shown to associate with the lysosomal membrane and may play a role there in activating mTORC1 through an amino acid dependent mechanism (Goberdhan *et al.,* 2016; Jung *et al.,* 2015; Milkereit *et al.,* 2015) (Figure 1.5).

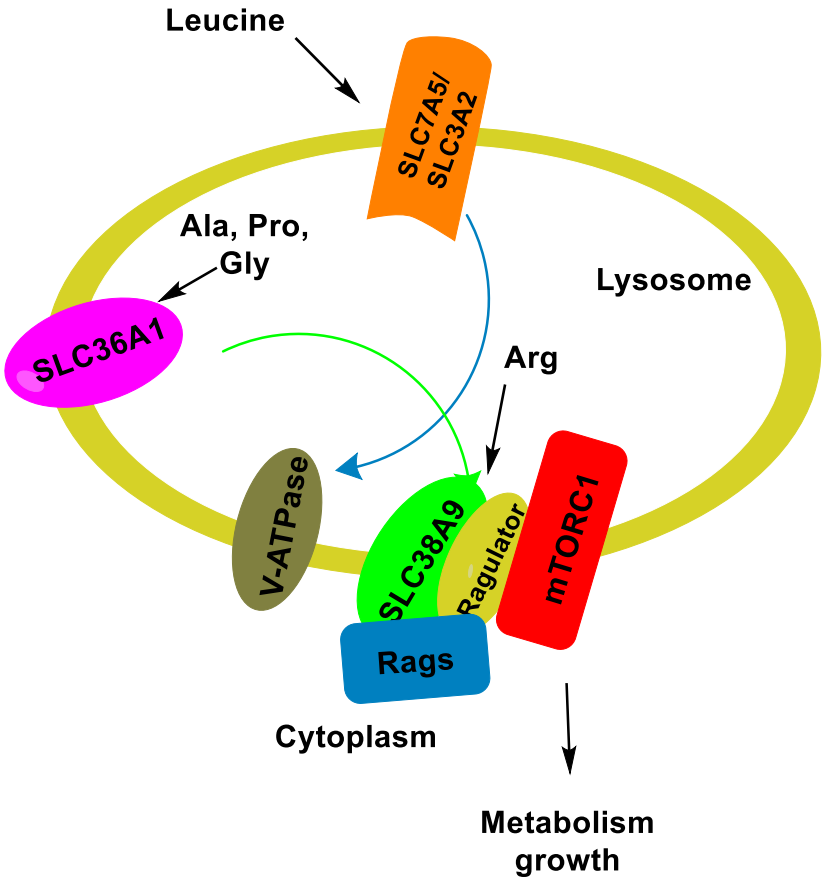


**Figure 1.5. Amino acid-dependent activation of mTORC1 through lysosome-associated amino acid transporters such as SLC38A9.**

The diagram is redrawn from (Goberdhan *et al.,* 2016), (Jung *et al.,* 2015) and (Milkereit *et al.,* 2015) V-ATPase denotes the vacuolar ATPase.

### 1.6.1 Anabolic resistance in skeletal muscle

Protein synthesis and building muscle is due to the body's response to protein synthesis stimuli and inability of the muscle to respond to these factors will result in anabolic resistance which advances with aging, mTOR signalling pathway is one of the central pathways with some of its downregulated targets for example ribosomal protein S6 kinase 1 (S6K1) that contribute to protein synthesis and is down regulated in elderly (Chalil *et al.,* 2015). As mentioned previously (Section 1.6), mTORC1 activation through growth factors or amino acids has an important role in protein synthesis, impairments in the mTORC1 pathway on the other hand thought to suppress protein synthesis. Controlling protein synthesis is vital for normal growth of the cell, there is evidence that hyper activation of mTOR lead to tissue hypertrophy causing abnormal growth for example tuberous sclerosis a

cell growth disorder in human cells which raised from mutations in the genes for the tuberous sclerosis complex proteins TSC1 or TSC2 the negative regulators of mTOR (Roux & Blenis, 2004; Wang & Proud, 2006). However, deficiency of amino acids such as Leucin or low energy status lead to mTOR impairment. In the process of protein translation, some factors which control initiation and elongation of the protein in response to growth factors such as insulin are partly depleted by rapamycin indicate the involvement of mTOR in protein synthesis through mRNA translation, eukaryotic elongation factors are among these factors (Wang & Proud, 2006). mTOR is activated directly by Rheb which lead to phosphorylation of p70S6, in turn induce cap-dependent translation and muscle protein synthesis therefore, controlling of translation initiation by mTOR is crucial in controlling muscle protein synthesis and inhibition of mTOR by rapamycin lead to decrease in translation and protein synthesis (You *et al.,* 2015). Furthermore, activation ribosomal proteins such as S6 by phosphorylation is linked to protein synthesis and cell growth and its inhibition by rapamycin again indicate the role of mTOR in protein synthesis (Roux & Blenis, 2004).

Skeletal muscle proteins are balanced by the ratio of protein synthesis and degradation which controlled by amino acids and growth factors, the elder population may be less efficient to utilise amino acids to build protein therefore the protein requirement will be higher with advancing of age which may be due to circulating inflammatory markers, this effect of amino acid on mTOR activation is short lasting between one to two hours after feeding. It has been shown that there is a relationship between muscle protein synthesis and inflammatory markers such as TNF-α, this cytokine can regulate mRNA translation and muscle protein synthesis by reducing mTOR phosphorylation (Breen & Phillips, 2011). There is also difference in the key protein synthesis regulators such as mTOR and its downstream target p70S6K availability between young and elder population which may contribute to the ability of muscle to sense the nutrient availability and building up protein (Burd *et al*., 2013).

## 1.7 Anabolic signals in response to exercise

As mentioned above, in normal muscle anabolic signals through mTORC1 control protein synthesis and hence play a major role in controlling muscle mass. The well documented anabolic effect of resistance exercise in humans might therefore be expected to be mediated in some way by more efficient activation of mTORC1, resulting in increased protein synthesis and muscle mass. Resistance exercise does facilitate mTORC1 translocation to the lysosome (Golberg *et al.,* 2014) and many of the beneficial effects of exercise in humans are thought to be mediated by signalling to mTOR (Watson & Baar, 2014). There is also evidence that the signal to mTORC1 in response to mechanical stimuli is PI3K mediated and then acts through phosphorylation of the 70-kDa ribosomal protein S6 kinase 1 ($p70^{S6K1}$), increasing muscle mass by increasing mRNA translation and subsequent anabolic effects. (Pasiakos, 2012). However, a study by Hornberger *et al.* (2004) showed activation of mTORC1 in response to mechanical stimuli independent of the PI3K pathway (Hornberger *et al.,* 2004). Their results suggested that $p70^{s6K1}$ can be phosphorylated when IGF and PI3K signalling pathways were blocked, which suggested that this pathway is not necessary for activation of anabolic signals in response to exercise or mechanical stimuli. This has been supported by *in vivo* studies which showed that mTORC1 activation in response to mechanical stimuli is not completely dependent on IGF1 and PI3K, because overexpression of Rheb in skeletal muscle is sufficient to induce muscle hypertrophy by a rapamycin-dependent pathway even without IGF-I and PI3K signalling (Goodman *et al.,* 2010; Spangenburg *et al.,* 2008). It was proposed that an alternative pathway for mechanical activation of mTORC1 was occurring through generation of the mTOR activator phosphatidic acid (Hornberger *et al.,* 2006).

Furthermore, while the above rapamycin-sensitive mechanism through mTORC1 may be true in resistance exercise, at least in mice it has been shown that in *endurance* exercise the resulting increases in muscle protein synthesis cannot be abolished by rapamycin and therefore seem to be occurring by a mechanism independent of mTORC1 activation (Philp *et al.,* 2015).

For exercise and mechanical stress to induce anabolic pathways such as mTORC1 there should be some mechanical sensor in the cell to transmit the

effect. However, it is not clear how this mechanical transduction signal to stimulate muscle protein synthesis is initiated (Pasiakos, 2012). There is evidence that mechanical stretch signals can be sensed through mechanosensitive ion channels (Tan & Lansman, 2014) generating mechanotransduction signals through Ca in the cytosol (Damm & Egli, 2014). There is also evidence that mechanotransduction can occur through sensing of mechanical stress in focal adhesions by Focal Adhesion Kinase (FAK) which binds to focal adhesions at the junction between the extracellular matrix, integrins and the cytoskeleton (Bell & Terentjev, 2017). There is also evidence that mechanotransduction may occur through intermediate filament proteins in the cytoskeleton (Palmisano *et al.,* 2015). Downstream from these Ca and FAK and intermediate filament signals it is thought that MAP kinase activation may have a role in muscle adaptation to exercise, because MAP kinases activate in response to exercise (Pasiakos, 2012). It has been reported that phosphorylation of the MAP kinases ERK1/2 (Extracellular signal-regulated kinases) on Thr202/Tyr204 increases in response to exercise (Drummond *et al.,* 2009). In humans, there was significant increase in ERK1/2 phosphorylation in response to resistance exercise compared with non–exercising controls (Moore *et al.,* 2011). Galpin et al, 2012 have also reported an increase in phosphorylation of the MAP kinases c-Jun NH2-terminal kinase (JNK), ERK 1/2 and p38 MAPK after 8 hours of exercise (Galpin *et al.,* 2012).

### 1.8 Muscle wasting (Cachexia)

Considerable confusion has arisen over the terminology of weight loss in chronic illness. The terms weight loss, muscle wasting, cachexia, malnutrition and disuse atrophy might all be applied to a patient with a chronic inflammatory illness such as CKD, and there is a tendency for the terms to be used interchangeably. However, whereas malnutrition is strictly muscle loss due to inadequate food intake which can in principle be reversed by nutritional intervention, and muscle disuse is muscle wasting of a group of muscles in the body because of inactivity or sedentary life style; muscle wasting or cachexia is irreversible loss of muscle, usually accompanied by chronic inflammation (Malavaki *et al.,* 2015; von Haehling & Anker, 2010). One detailed definition of cachexia, that has been proposed that is widely applicable is muscle wasting up to 5% within 12 months,

in the presence of a chronic condition, showing distinctive cachexia features such as fatigue, inflammation, loss of muscle strength and anaemia (von Haehling & Anker, 2010).

Cachexia is a multifactorial syndrome characterised by severe and rapid muscle wasting leading to weakness and impaired mobility in which nutritional intervention is not effective to reverse this muscle wasting. Decrease in protein synthesis and increase in protein degradation are dominant features in cachexia leading to decrease in muscle mass especially skeletal muscles (Müller *et al.,* 2010; Yoshida & Delafontaine, 2015). Cachexia is usually associated with increase in circulating inflammatory markers especially pro-inflammatory cytokines. Anorexia is another disorder accompanied by muscle wasting but should not be confused with cachexia because anorexia is primarily an eating disorder and unlike cachexia it is not characterised by inflammation (Müller *et al.,* 2010).

### 1.8.1 Occurrence and measurement of cachexia

Cachexia occurs in many chronic inflammatory diseases such as chronic heart failure (CHF), cancer, chronic obstructive pulmonary disease (COPD), chronic kidney disease (CKD) and sepsis (Müller *et al.,* 2010). Prevalence of cachexia is high and varies among these disease conditions, ranging from 5%-15% in advanced CHF or COPD to 60% to 80% in advanced cancer. The mortality rate is higher in patients with cachexia compared to non-cachectic patients with a similar diagnosis. Mortality associated with cachexia ranges from 10-15% per year in COPD, to 20-30% in chronic heart failure and CKD, to 80% in advanced cancer (Müller *et al.,* 2010; von Haehling & Anker, 2014). The burden of cachectic diseases is high on healthcare systems because the hospitalisation period is longer compare to non-cachexia disease (von Haehling & Anker, 2014). Cachexia is a growing syndrome worldwide and its prevalence is about 1% of the population globally. However, determining prevalence of cachexia is difficult worldwide owing to differences in the definition of cachexia applied in different studies, and technical problems such as the masking effect of obesity (von Haehling & Anker, 2010; von Haehling & Anker, 2014). To measure cachexia accurately in the presence of variable contributions from adipose tissue it is therefore important to use tools which accurately assess the amount of lean

tissue i.e. dual energy X-ray absorptiometry (DEXA), ultrasound, computed tomography (CT) and magnetic resonance imaging (MRI) (Greig & Jones, 2010) as outlined in Section 1.3 above.

### 1.8.2 Ubiquitin-proteasome pathway (UPP)

As increased muscle protein degradation is a major contributor to cachexia, it is important to understand the ubiquitin-proteasome pathway (UPP) which is the major pathway in mammalian cells for degradation of soluble proteins and some membrane proteins, including amino acid transporters (Rosario *et al.,* 2016). Ubiquitination is a post transcriptional modification: ubiquitin targeted proteins are susceptible to degradation by proteasomes. From initiation to complete degradation of the protein requires three ubiquitin-related enzymes E1, E2 and E3.

A protein targeted for ubiquitination is first ligated to the small (76 amino acids in humans) protein ubiquitin which makes it recognisable or susceptible for degradation by the UPP. The first step of ubiquitination involves combining the ubiquitin activating enzyme (E1) through a cysteine residue on its active site to the carboxyl terminus of ubiquitin through a high energy thioester bond in an ATP-dependent step. Then the ubiquitin is shifted to ubiquitin conjugases (E2) and conjugated to substrate by ubiquitin (E3) ligase through lysine residues on the substrate. E3 ligases occur in many isoforms each of which has the ability to recognise specific motifs and hence recognises a specific targeted protein. In skeletal muscle, the E3 ligases MuRF1 and MAFbx (also known as Atrogin-1) play an important role in protein degradation, and their expression may be up-regulated in cachexia (Watson *et al.,* 2013). Following attachment of an initial ubiquitin, more ubiquitins will attach to the first formed complex leading to formation of a poly-ubiquitinated protein which is then subjected to protein degradation by a proteasome (Figure 1.6) (Gong *et al.,* 2016a).

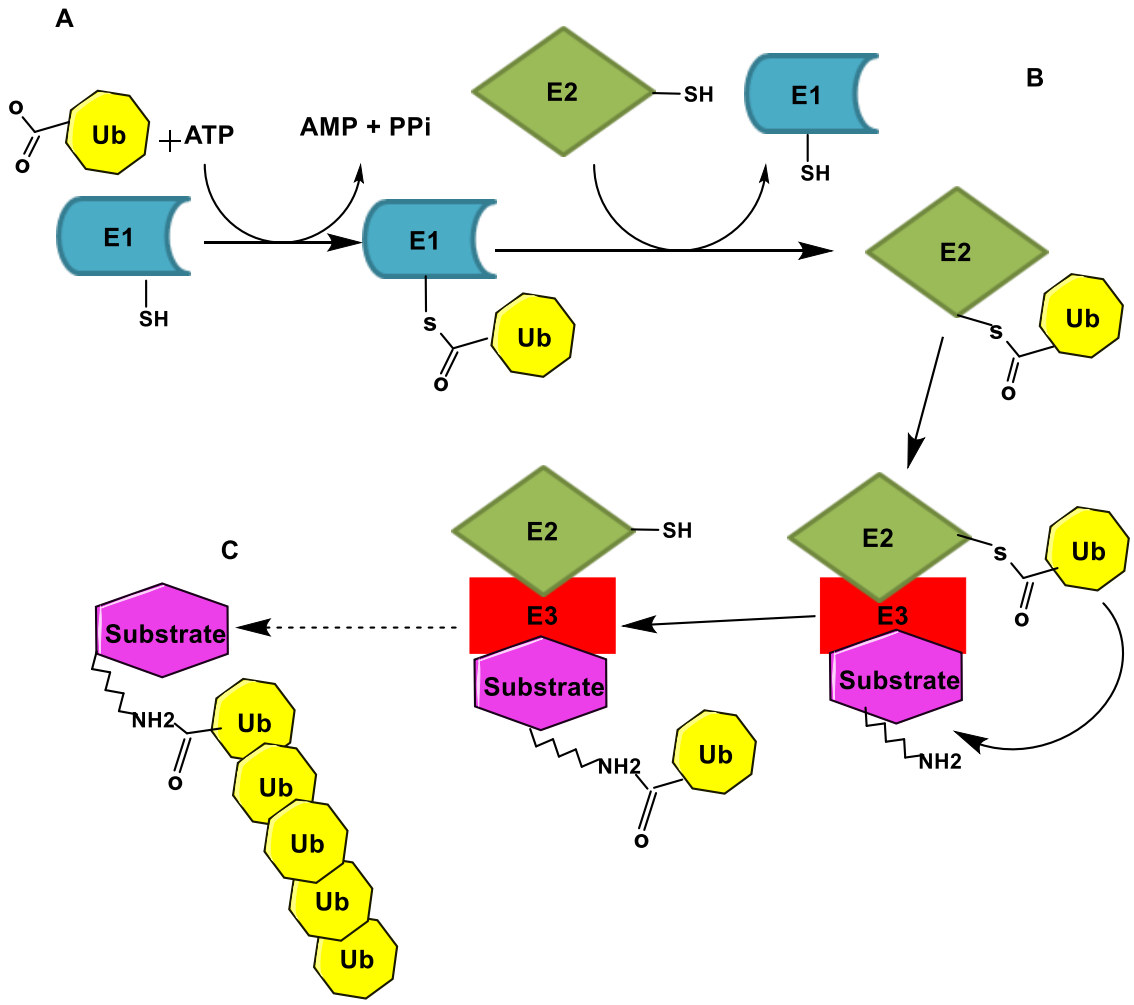


**Figure 1.6. Three steps of the ubiquitin-proteasome pathway (UPP) involved in substrate degradation.**

(A) Ubiquitin-activating enzymes (E1) form a thioester bond with ubiquitin in a reaction that requires ATP. (B) Ubiquitin is transferred to ubiquitin conjugases with which a new, high-energy thioester bond is formed. (C) Ubiquitin ligases (E3) provide substrate recognition and catalyse the covalent attachment of ubiquitin to the target substrate via an isopeptide bond. The polyubiquitinated substrate is then transferred to the 26S proteasome for degradation. The diagram is redrawn from (Gong *et al.,* 2016a).

Recognition of ubiquitinated protein by proteasomes is a complex process. This is due to the diversity and specificity of the UPP. Ubiquitin protein has seven lysine residues (K) (K6, K11, K27, K29, K33, K48, and K63) which make different chains or types of linkage. Ubiquitin also has the ability to form polyubiquitin chains from a similar ubiquitin linkage (homotypic) or from different linkages (heterotypic). This property of polyubiquitination is important for specific recognition of ubiquitinated proteins (Grice & Nathan, 2016). The 26S

proteasome is the key receptacle for the polyubiquitinated protein, which degrades the ubiquitinated substrate. 26S consists of proteolytic complex 20S and regulatory particle 19S. The substrate binds to the 19S regulatory complex which facilitates the entry of the substrate (by unfolding and transforming it) to the 20S chamber for degradation.

The UPP is very important in controlling and removing unwanted or misfolded proteins in the cell and preventing the adverse effects that would arise from accumulation of misfolded proteins. Dysfunction of the UPP leads to many disorders including neurological diseases such as Alzheimer's disease (AD), Amyotrophic Lateral Sclerosis (ALS), neuronal degeneration, remodelling and regeneration after spinal cord injury (SCI), and Parkinson's disease (PD) (Gong *et al.,* 2016a). However, excessive activation of the UPP may itself be pathological and this is an important mechanism of cachexia.

### 1.8.3 Mechanisms of cachexia in chronic diseases

There are a number of factors which contribute to the pathophysiology of cachexia. The process is not completely understood, but a number of studies indicate that pro-inflammatory cytokines play a major role in the onset and development of cachexia such as IL-6, IL-1, TNF-α and IFN-ɣ (Hall *et al.,* 2011a), particularly tumour necrosis factor alpha (TNF-α) (Kotler, 2000). CKD for example is characterised by high inflammatory cytokine concentrations, and acute phase protein responses e.g. high C-reactive protein (CRP) and low albumin level in circulation (Morley *et al.,* 2006). Pro-inflammatory cytokines serve as markers of inflammation, but they can also cause muscle wasting (Pecoits-Filho *et al.,* 2002).

In general, the cause of muscle wasting in many chronic inflammatory diseases such as CKD is increase in protein breakdown rather than inhibition of protein synthesis. A common feature of cachexia is increased protein degradation in skeletal muscle arising from activation of the UPP, with increased gene expression of E3 ubiquitin ligases MuRF1 and MAFbx/Atrogin-1 being used as a clear and convenient indicator of this activation (Watson *et al.,* 2013; Yoshida & Delafontaine, 2015). Inhibiting proteasomes has been shown to eliminate this excess protein degradation in CKD (Rom & Reznick, 2016).

As cachexia is commonly associated with chronic inflammation (Section 1.8), the pro-inflammatory cytokines listed above have been regarded as an important trigger for this UPP up-regulation. The pro-inflammatory cytokine TNF-α is one candidate, indeed the name cachectin was originally given to this cytokine because of its strong association with cachexia *in vivo*. It has been difficult to show direct stimulation by TNF-α of the UPP and protein degradation in skeletal muscle cells *in vitro,* suggesting that its effect may be indirect. However, TNF-α may directly induce muscle wasting via decrease in protein synthesis in CKD through activation of nuclear factor-kB (NF-kB) (Cheung *et al.,* 2010). In contrast IL-6 has been proposed as a cytokine that acts more directly on protein degradation in muscle to up-regulate the UPP (Zhang *et al.,* 2009a). The myokine myostatin also potently decreases the mass of skeletal muscle *in vivo*, and upregulation of Myostatin has been reported in many cachectic conditions, including CKD (Zhang *et al.,* 2009a).

It has also been shown that the circulating concentrations of catabolic hormones such as angiotensin II (Ang II) and glucocorticoid may increase in cachexia and induce muscle wasting by activation of the UPP. The glucocorticoid dexamethasone for example on administration to mice induces significant body weight loss and increased MAFbx/Atrogin-1 and MuRF-1 expression (Liu *et al.,* 2016).

However, as with TNF-α, some of these hormonal effects may not be directly on muscle cells. For example, in mice Ang II initially acts on liver to induce secretion of IL-6 and the acute phase protein Serum Amyloid A (SAA) which together act on skeletal muscle to increase protein degradation (Zhang *et al.,* 2009a). Glucocorticoid which is increased in muscle wasting conditions and activates the UPP (see Section 1.19) is another example of a hormone which may indirectly mediate the catabolic effect of other hormones (Yoshida & Delafontaine, 2015).

A common mechanism by which these cytokines and hormones may activate the UPP in skeletal muscle is through inhibition of the anabolic signalling that was outlined in Section 1.6. For example, even though Ang II may act partly by inducing reactive oxygen species (ROS) production in skeletal muscle cells, and decreasing ATP production by inhibiting AMPK activity, its main stimulatory

action on the UPP occurs by decreasing the anabolic pathway from IGF-I via PI3K/Akt (Yoshida & Delafontaine, 2015). Activation of Akt strongly suppresses transcription of the MAFbx/Atrogin-1 and MuRF-1 genes in skeletal muscle thus suppressing the UPP, and it is through inhibition of IGF-I/Akt signalling that IL-6 and SAA synergise to activate the UPP in mice treated with Ang II (Zhang *et al.,* 2009a). Similarly, glucocorticoid is well known to induce insulin resistance in muscle and thus to impair anabolic IGF-1 signalling through Akt (thus activating the UPP) and mTOR (thus impairing protein synthesis) (Liu *et al.,* 2016), leading to glucocorticoid-induced muscle atrophy (Section 1.19).

### 1.9 Metabolic acidosis as a cause of muscle wasting in CKD

An important cause of cachexia which applies particularly to CKD is metabolic acidosis. Protons are generated in the body as a by-product of protein catabolism (especially catabolism of sulphur amino acids which generates sulphuric acid) (Clapp & Bevington, 2011). 1mmol of hydrogen ions per Kg of body weight is generated per day. Excretion of this excess acid and maintaining the pH balance in extracellular fluid is an important function of the kidneys (Clapp & Bevington, 2011). The kidneys not only excrete the excess acid, but also generate and reabsorb bicarbonate (Kraut & Kurtz, 2005; Kraut & Madias, 2016). However, in CKD this regulation fails, resulting in metabolic acidosis (Chen & Abramowitz, 2014; Kalantar-Zadeh *et al.,* 2004) (Yang *et al.,* 2015), with arterial blood pH falling to less than 7.36 and serum bicarbonate level less than 22 mEq/L being considered as acidotic (Bobrow & Soothill, 1999).

Metabolic acidosis is common in CKD patients (Chen & Abramowitz, 2014; Watson *et al.,* 2013), its prevalence ranging between 2.3% to 13% in CKD stage 3 and 19% to 37% within CKD stage 4 (Kraut & Madias, 2016).

Metabolic acidosis has adverse effects on CKD patients because they frequently develop muscle wasting and osteoporosis in response to the acidosis (Kraut & Kurtz, 2005). Metabolic acidosis increases the rate of breakdown of muscle protein and impairs protein synthesis. Acidosis is thought to stimulate proteolysis through increasing the gene expression of components of this ubiquitin-proteasome system (Kraut & Kurtz, 2005). Metabolic acidosis in CKD patients on haemodialysis also decreases the intracellular free amino acid pool in muscle

(Bergstrom *et al.,* 1990) and a similar effect can be obtained *in vitro* in L6 rat skeletal muscle cells by exposing them to low extracellular pH which decreases the protein synthesis and impairs amino acid dependent signalling through mTORC1 (Evans *et al.,* 2007).

There is evidence that exercise may (through PI3K/Akt activation) decrease the rate of protein breakdown in CKD patients (Watson *et al.,* 2013). However, the exercise-induced acidosis may also worsen the situation because of the lactic acid that is produced during exercise (Watson *et al.,* 2013). Additional bicarbonate dose in exercising CKD patients may blunt the effect of exercise-induced acidosis through increasing the serum bicarbonate concentration and reducing fatigue (Watson *et al.,* 2013). Short term resistance exercise induces anabolic processes in CKD skeletal muscle cells, but this is less effective in long term endurance exercise. This may be partly because of depletion of free amino acids due to lactic acid production in endurance exercise (Bergstrom *et al.,* 1990; Watson *et al.,* 2013), but the effect of resistance exercise on intramuscular free amino acid concentrations is still unclear.

## 1.10 Possible pH sensors during acidosis and inflammation in mammalian cells

The molecular basis of the depletion of free amino acids in skeletal muscle described above during metabolic acidosis *in vivo* is not known. Acidic environment also triggers responses in many cell types, and may be associated with inflammation. Therefore, it is important to consider the sensor molecules which enable skeletal muscle cells and components of the immune system to sense low extracellular pH (Okajima, 2013).

### 1.10.1 G protein-coupled receptors (GPCRs)

GPCRs are membrane proteins, typically with seven hydrophobic transmembrane segments in common, but varying widely in their extracellular amino terminus and intracellular carboxyl terminus (Kobilka, 2007) (Figure 1.7). They have a role in many cell signalling pathways, including a recently suggested pH-sensing role in inflammation whereby, under the local hypoxic conditions in lymphatic and immune tissues during inflammation, GPCRs may sense the excess lactic acid that is produced by anaerobic glycolysis (Okajima, 2013; Yang

*et al.,* 2015). Examples of such GPCRs are GPR4 which is an endothelial proton sensor (Dong *et al.,* 2013) and ovarian cancer G-protein-coupled receptor 1 (OGR1) (Figure 1.8) (Vanek *et al.,* 2003) which is strongly activated at low pH (6.8), through protonation of its extracellular histidine residues. OGR1 loses its pH sensitivity after mutation of these histidine residues (Vanek *et al.,* 2003; Yang *et al.,* 2015) and is a widely expressed pH sensor in mammalian tissues. However, there is currently no evidence that such GPCRs play a role in pH sensing in the catabolic effects of metabolic acidosis in skeletal muscle.

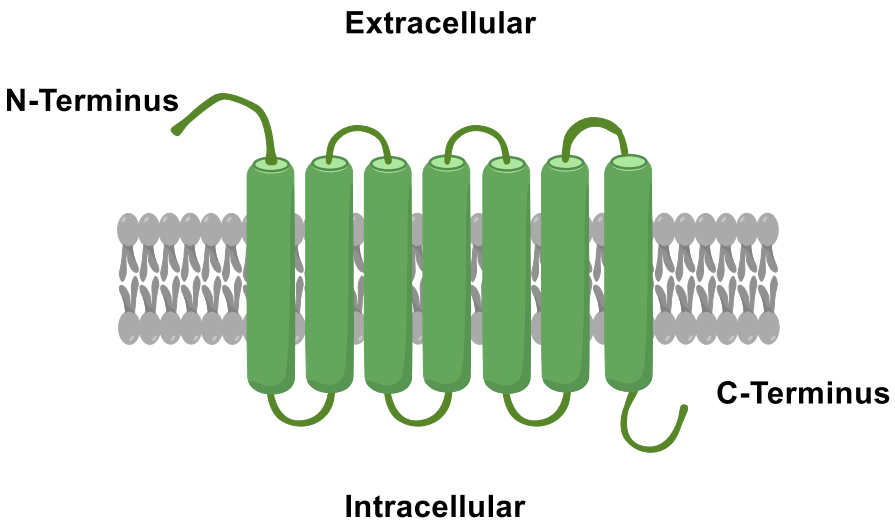


**Figure 1.7. General schematic structure of G protein-coupled receptors (GPCRs)**

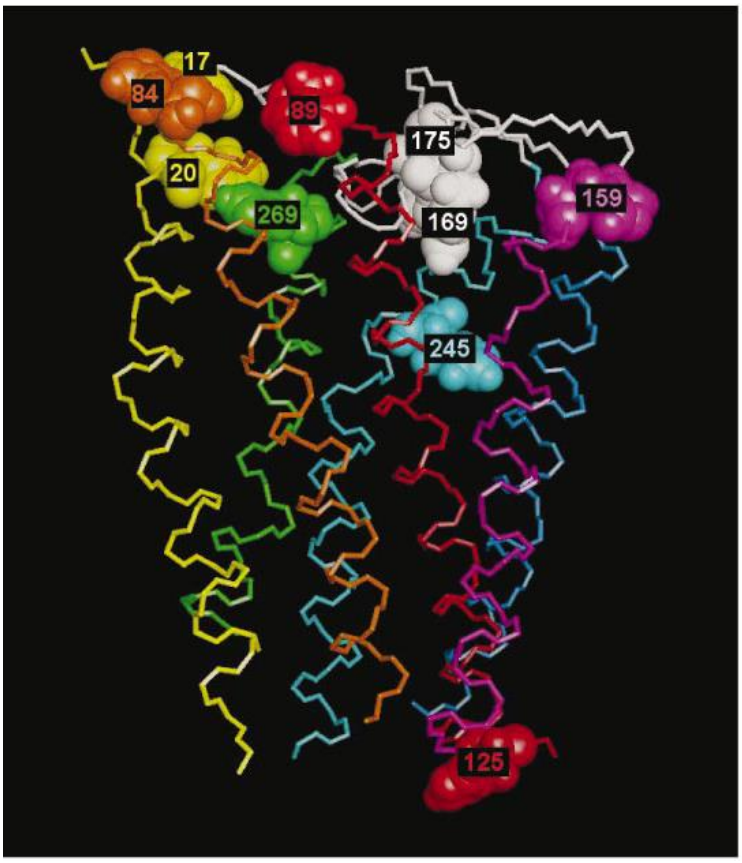


**Figure 1.8. Model of the backbone of the OGR1 protein with all histidine residues highlighted.**
**The diagram is taken from (Vanek *et al.,* 2003).**

### 1.10.2 Complement system proteins

As noted above, sites of inflammation may be acidotic. Conversely acidosis (at physiologically attainable pH values of ~ 7.1) may also induce inflammation by activating complement proteins, with production of inflammatory chemoattractant activation products such as the anaphylatoxins C3a and C5a (Sonntag *et al.,* 1998). Low extracellular pH can also induce C5 and C6 complement protein activation, ultimately leading to formation of lytic complex (C5b-9) (Lardner, 2001). This activation may arise as a result of cross-talk between the coagulation system and complement, with low pH first activating the Contact system (Kenawy *et al.,* 2015). For example, accumulation of both coagulation Factor XII and activation of C3a and C5a have been demonstrated together in response to acidic environment (Emeis *et al.,* 1998).

Whether such acid-induced complement activation could occur in acidotic skeletal muscle and play a role in acidosis-induced cachexia is currently

unknown. However, recent work from this laboratory has shown that low pH (7.1) can increase expression of the complement alternative pathway activator protein properdin in cultured C2C12 mouse skeletal muscle cells (Ghaderi-Najafabadi, M-unpublished observations), consistent with evidence elsewhere that acidosis can induce membrane attack complex formation through activation of the alternative pathway (Lardner, 2001).

### 1.11 Amino acid transporters

Some plasma membrane amino acid transporters are highly pH sensitive and are consequently potential pH sensors. System A and System N are two important groups of active $Na^+$ dependent plasma membrane amino acid transporters, which are members of the SLC38 gene family and are strongly inhibited by physiologically relevant low pH values (~ 7.1) in the surrounding extracellular environment (Baird *et al.,* 2006). In view of the potential importance of these transporters in regulating amino acid availability to mTORC1 (Figure 1.4), this provides a possible direct mechanism by which metabolic acidosis might impair protein synthesis.

Amino acid transporters are differentiated into so-called “Systems” according to their preferred amino acid substrates, regulatory mechanisms, and tissue and organ specificity (Hyde *et al.,* 2003; Palacn *et al.,* 1998). For example, $Na^+$ dependent active transporters of small neutral amino acids which are inhibited by low pH and which preferentially transport L-alanine or L-glutamine as their substrates are classed as System A and System N respectively. A further hallmark of System A transporters is that they carry non-metabolisable N-methylated synthetic substrates such as N-methyl-aminoisobutyric acid (MeAIB) (Bröer, 2014). In contrast System L transporters are usually $Na^+$ independent passive amino acid exchangers which preferentially transport essential amino acids with bulky side chains, especially L-leucine (Kim *et al.,* 2004).

In addition to being classified into “Systems”, these transporters are also classified into Solute Carrier (SLC) gene families according to sequence homology between the genes that encode them. Transporters within one family have at least 20% similarity in their DNA sequence (Hediger *et al.,* 2013). These are large gene families within the human genome, which include 52 separate

families and 395 transporter genes (Hediger *et al.,* 2013). SLC transporter genes have a numerical classification beginning with the root SLC gene family number, followed by a number for the specific solute carrier. For example, the System A transporter within SLC gene family 38 which is the subject of this thesis is designated SLC38A2.

### 1.11.1 Sodium-coupled neutral amino acid transporters (SNATs)

The eleven transporters of the SLC38 gene family are also known as Sodium-coupled Neutral Amino acid Transporters (SNATs) and are listed in Table 1.1 (Bröer, 2014). They are all $Na^+$ dependent and utilise a trans-membrane $Na^+$ gradient to transport amino acids against their concentration gradients (Bröer, 2014; Mackenzie & Erickson, 2004). As noted above, these amino acid transporters are divided into two groups known as System A and System N transporters according to the type of amino acids they transport. System A was originally thought to comprise SNAT1, SNAT2 and SNAT4, and these are functionally similar in their response to environmental changes and hormones (Palacn *et al.,* 1998). However, SNAT8 and SNAT10 have also more recently been demonstrated to be System A transporters (Hägglund *et al.,* 2015; Hellsten *et al.,* 2017). SNAT2 is the most widely expressed transporter of the group, being present in almost all tissues that have been screened to date (Mackenzie & Erickson, 2004). System A accepts a broader range of amino acid substrates than System N, transporting small neutral L-amino acids (such as alanine, asparagine, cysteine, glutamine, glycine, methionine, and serine) as well as its paradigm substrate N-methyl-aminoisobutyric acid (MeAIB) (Bröer, 2014).

System N comprises SNAT3, SNAT5 and SNAT7, with SNAT7 having been recently characterised as the principal L-glutamine exporter in the lysosomal membrane (Verdon *et al.,* 2017). In this respect, it resembles the lysosomal transporter SNAT9 (SLC38A9) which has the unusual property of transporting a charged amino acid (L-arginine) as its preferred substrate – as noted above in (Section 1.6, Figure 1.5). The narrower range of L-amino acids transported on System N includes asparagine, histidine and glutamine.

System N amino acid transporters can also be distinguished from System A transporters by their amino acid transport mechanism (Figure 1.9). System A has

a simpler transport mechanism by which an amino acid is transported into the cell against its concentration gradient, coupled with $Na^+$. System N however has a more complex transport mechanism in which, in addition to symport of one amino acid accompanied by one $Na^+$ into the cell, one $H^+$ is transported out of the cell (Bröer, 2014).

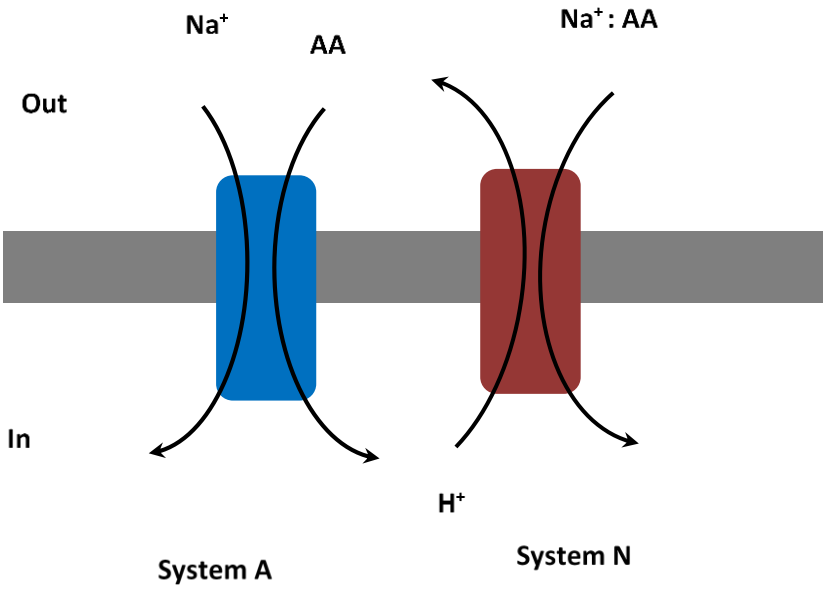


**Figure 1.9. Schematic representation of the System A and System N amino acid transport mechanisms.**

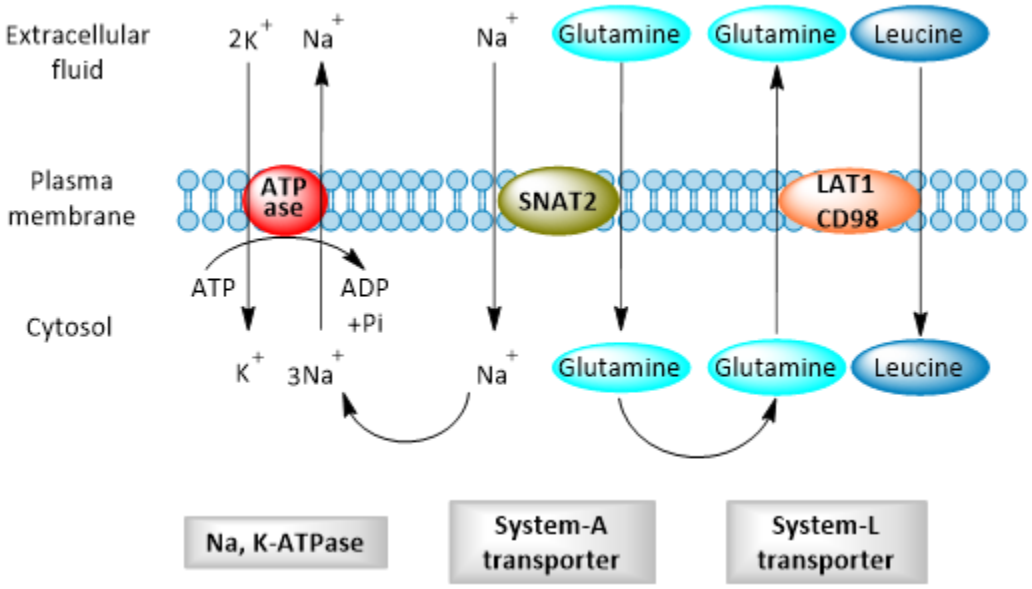


**Figure 1.10. Schematic diagram showing functional coupling between the SNAT2/ LAT1 transport systems.**

A primary active transporter (Na, K-ATPase), a secondary active System A amino acid transporter (SNAT2, SLC38A2), and a tertiary active System L amino acid transporter (the LAT1/CD98, SLC7A5/SLC3A2 heterodimer) are coupled to perform active accumulation of L-leucine inside the cell. The diagram is taken from ((Beltran, 2017) PhD thesis, University of Leicester) using original material from (Hundal & Taylor, 2009), (Baird et al., 2009).

It is important to note that SNAT transporters do not carry L-leucine, the most potent activator of mTORC1 (Section 1.11). However, SNAT transporters (especially SNAT2) do play an important role in controlling the cytosolic L-leucine concentration that acts on mTORC1. L-leucine is directly transported across the plasma membrane on System L amino acid transporters, such as the hetero-dimer LAT1/CD98 (SLC7A5/SLC3A2). These System L transporters are passive transporters which can usually only exchange amino acids across a biological membrane. However, they are also able to co-ordinate with a secondary active transporter such as SNAT2 to exchange the amino acid L-glutamine with L-leucine (Figure 1.10) (Hundal & Taylor, 2009). In this way L-leucine can be pumped into the cell against its concentration gradient, by using the L-glutamine gradient that has been built up by active transport through SNAT2. Consequently SNAT2 indirectly controls the L-leucine concentration in the cell and hence has a role in activating mTORC1 (Evans *et al.,* 2007; Rosario *et al.,* 2016).

**Table 1.1. Members and properties of the SLC38 family in the human genome.**

Taken from (Bröer, 2014). “Length” denotes the number of amino acid residues in the relevant transporter protein in hum

| Gene Name | Protein Name | Alias | Mechanism | Substrate specificity | Function | Expression profile | Length |
|---|---|---|---|---|---|---|---|
| SLC38A1 | SNAT1 | GlnT, SAT1, ATA1, SA2, NAT2 | S:1$Na^+$ | (G),A,S,C,N,Q,H,(M) | System A | Ubiquitous | 486 |
| SLC38A2 | SNAT2 | SAT2, ATA2, SA1 | S:1$Na^+$ | G,P,A,S,C,N,Q,H,M | System A | Ubiquitous | 505 |
| SLC38A3 | SNAT3 | SN1, NAT | S:1$Na^+$/A:1$H^+$ | Q,N,H | System N | Eye, liver, brain, pancreas | 503 |
| SLC38A4 | SNAT4 | ATA3, NAT3, SAT3, PAAT | S:1$Na^+$ | G,(P),A,S,C,N,(M), R, K | System A | Liver, bladder | 546 |
| SLC38A5 | SNAT5 | SN2 | S:1$Na^+$/A:1$H^+$ | Q,N,H,A,S | System N | Mouth, cervix, bladder, bone, intestine, kidney, oesophagus, lung, eye | 471 |
| SLC38A6 | SNAT6 | | | Unknown | | Oesophagus, cervix, mouth, lung, kidney, muscle | 520 |
| SLC38A7 | SNAT7 | | $Na^+$ dependent | Q,N,A,H,S | System N | Ubiquitous | 461 |
| SLC38A8 | SNAT8 | | | Unknown | | Testis | 434 |
| SLC38A9 | SNAT9 | | | Unknown | | Parathyroid, testis, adrenal gland, thyroid | 560 |
| SLC38A10 | SNAT10 | | | Unknown | | Ubiquitous | 1118 |
| SLC38A11 | SNAT11 | | | Unknown | | Spleen, eye, bone marrow, pharynx | 405 |

*A* antiport, *S* symport

### 1.11.2 SLC38A2 amino acid transporter (SNAT2)

SNAT2 is thought to be the main active transporter of small neutral amino acids (especially L-glutamine) in skeletal muscle cells, including *in vitro* models such as the L6 rat skeletal muscle cell line: other transporters are regarded as less important, either because they are expressed at low level or because L-glutamine is not their substrate (Evans *et al.,* 2007). SNAT2 is highly sensitive to extracellular pH change (Baird *et al.,* 2006). It is therefore a likely that, at least *in vitro,* it plays a role mediating the catabolic (protein wasting) effect of metabolic acidosis on skeletal muscle cells (Evans *et al.,* 2007).

There is no crystal structure available for SNAT2, but from hydropathy analysis it has been proposed that SNAT2 consists of eleven transmembrane domains with an intracellular N terminus and an extracellular C-terminus (Mackenzie & Erickson, 2004) (Figure 1.11). It is thought that the pH sensitivity is partly due to the presence of a histidine residue in the extracellular C-terminus of the transporter, because the histidine-modifying agent DEPC (diethyl pyrocarbonate) significantly reduces SNAT2 pH sensitivity, and mutation of this terminal histidine, replacing it with alanine, markedly decreased pH sensitivity (Baird *et al.,* 2006). It has also been suggested that protonation of the transporter leads to a defect in $Na^+$ binding, as the $H^+$ will compete with $Na^+$ on a cation binding site, resulting in impaired $Na^+$-dependent amino acid transport (Chaudhry *et al.,* 2002).

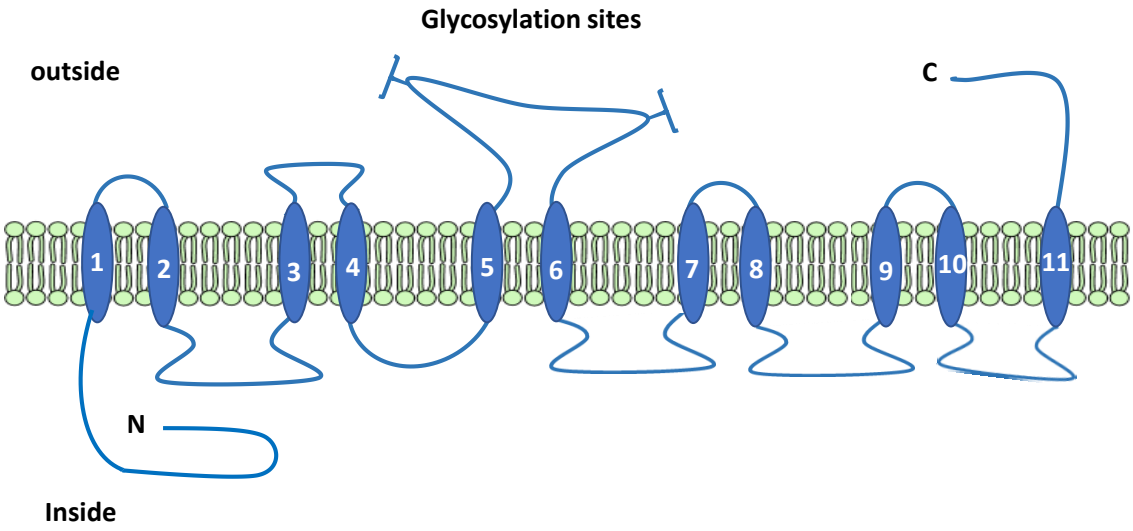


**Figure 1.11. Proposed structure of SNAT2.**

**Sodium-Coupled Neutral Amino Acid Transporter (SNAT2) (SLC38A2) adapted from (Zhang et al., 2009b).**

## 1.12 Functional importance of SNAT2 in skeletal muscle cells

It has been suggested that, in view of the dependence of anabolic signalling in skeletal muscle on the availability of free amino acids (see Figure 1.4), the transport of amino acids is important for maintaining protein content in skeletal muscle cells and hence muscle mass (Dickinson & Rasmussen, 2013). For example, in the rat L6 skeletal muscle cell line, pharmacological competitive inhibition of SNAT2 with MeAIB or siRNA silencing of SNAT2 expression significantly depleted intracellular free amino acids (including L-leucine) and impaired mTORC1 signalling, resulting in impaired global protein synthesis (Evans *et al.,* 2007). A similar response was observed on exposing the cells to a low extracellular pH of 7.1 to model metabolic acidosis, consistent with the intramuscular free amino acid depletion reported *in vivo* in acidotic haemodialysis patients (Bergstrom *et al.,* 1990). siRNA silencing of SNAT2 also significantly impaired signalling through PI3K and Akt, resulting in activation of protein degradation (Evans *et al.,* 2008). A similar response was again observed on exposing the cells to low extracellular pH to model acidosis, suggesting that, at least in this culture model, SNAT2 may mediate a UPP dependent protein degradation response to acidosis that is similar to that observed in CKD patients and acidotic rats *in vivo*. It has also been suggested that *in vivo* SNAT2 may

have a role in mediating anabolic responses in muscle through mTOR, because SNAT2 mRNA expression increases in response to essential amino acids and after exercise, accompanying the observed increase in global protein synthesis (Bröer, 2014; Taylor, 2014). A recent investigation by Wendowski et al (2017) also reported a decrease in expression of the SNAT2 and LAT1 transporter proteins in the muscle of aged mice in a model of sarcopenia, without affecting the transporter mRNA level, and this decline of these amino acid transporters was more marked in fast twitch muscle fibres compared to slow-twitch muscle fibres (Wendowski *et al.,* 2017). However, direct demonstration of the importance of SNAT2 *in vivo* (e.g. in a transgenic knock-out model) has not been performed.

The studies described above showed by siRNA silencing of SNAT2 expression in L6 cells that two important signalling pathways (which are involved in stimulating protein synthesis and suppressing proteolysis) are dependent on the presence of SNAT2 i.e. the mTORC1 pathway and the PI3K/Akt pathway respectively (Evans *et al.,* 2007; Evans *et al.,* 2008). While part of the effect on mTORC1 may be through an indirect effect of SNAT2 in maintaining the L-Leu concentration ((Evans *et al.,* 2007) and Figure 1.10), L-Leu is not directly transported by SNAT2. A role for directly transported SNAT2 amino acid substrates in signalling to protein metabolism is therefore possible. Studies in other tissues such as liver, and in quail myoblasts, have shown that mTORC1 (or its downstream substrates) can be activated by L-Methionine (L-Met) (Stubbs *et al.,* 2002; Tesseraud *et al.,* 2003), which can be transported directly by SNAT2 (Yao *et al.,* 2000). Preliminary results from this laboratory have also suggested that L-Met transported on SNAT2 may have a direct stimulatory effect on mTORC1 in L6 cells (JR Brown, N Abbasian, M Ghaderi-Najafabadi & A. Bevington, unpublished observations).

### 1.13 Regulation of SNAT2

The physiological importance of SNAT2 is also suggested by the significant number of mechanisms that exist to control its expression, activity and degradation. System A transporters such as SNAT2 are the main hormonally responsive amino acid transporters in mammalian cells (McGivan & Pastor-Anglada, 1994): in particular, like the GLUT4 glucose transporter, in skeletal muscle cells SNAT2 is strongly upregulated by insulin by translocation of the

SNAT2 protein from an intracellular pool to the plasma membrane (Hyde *et al.,* 2002). However, two important cellular stresses which lead to a particularly potent upregulation of transport activity, gene transcription and cellular redistribution for SNAT2 in many mammalian cell types are hyperosmotic stress and amino acid deprivation (Mackenzie & Erickson, 2004). When cells face hypertonicity or low amino acid availability SNAT2 is upregulated in two ways, either by increasing the recruitment of mature SNAT2 in the cell membrane or an increase in SNAT2 gene transcription (Kashiwagi *et al.,* 2009).

### 1.13.1 Osmotic stress and amino acid deprivation

There is considerable evidence that both hyperosmotic shock and amino acid deprivation lead to SNAT2 activation and increased expression by mechanisms involving MAPK activation (Kashiwagi *et al.,* 2009). Hypertonicity increases phosphorylation of the MAPKs JNK, P38 and ERK1, 2 and amino acid deprivation has a similar effect on JNK and ERK1, 2 but not P38. Pharmacological inhibition of this phospho-activation of MAPKs blocks the adaptive responses of SNAT2. For example, under amino acid deprived conditions, inhibition of ERK activation with a specific inhibitor blocked the enhanced SNAT2 mRNA expression (López-Fontanals *et al.,* 2003).

One of the largest regulatory effects on the activity of SNAT2 transporters is the activation which occurs when cells are starved of extracellular amino acids. Amino acid deprivation (AAD) leads to a significant increase in SNAT2 activity (measured by uptake of the synthetic amino acid MeAIB) for example in L6 myotubes following only 4h incubation of the cell under AAD conditions (Nardi *et al.,* 2015). This upregulation occurs through increased expression of the SNAT2 gene (Gaccioli *et al.,* 2006; Hyde *et al.,* 2007), increased translation of SNAT2 mRNA (Gaccioli *et al.,* 2006) and increased translocation of the SNAT2 protein to the plasma membrane (Hyde *et al.,* 2007). Under AAD conditions, global protein synthesis in cells is decreased by suppressing translation of the majority of the cell's mRNAs by activation of the GCN2 pathway (general control non-derepressible 2) (Taylor, 2014; Zheng *et al.,* 2016) which adapts the cell to survive amino acid inadequacy and leads to phosphorylation and activation of the eIF2α kinases. (These kinases sense severe amino acid depletion by responding to the resulting increase in the concentration of uncharged tRNA

(Kilberg *et al.,* 2009)). However, at the same time there is an increase in transcription of genes encoding a smaller number of stress induced proteins such as activation transcription factor 4 (ATF4) and SNAT2 (Gaccioli *et al.,* 2006). SNAT2 activation by AAD has been reported in a number of studies (Hyde *et al.,* 2007; Kashiwagi *et al.,* 2009) but the molecular mechanism by which SNAT2 translation is activated was revealed by Palii et al., in 2004 who showed the presence of an amino acid response element (AARE) in the human and mouse SNAT2 gene located on intron one (Palii *et al.,* 2004). Furthermore, amino acid starvation decreases the activity of eIF4F by dephosphorylation of 4E-BP1 and eIF4F. Translation of most proteins requires recognition of the 5`-end of the mRNA and its m-7G-cap by eIF4F. Therefore, dephosphorylation of 4E-BP1 and eIF4F leads to decreased translation of these mRNAs. However, in AAD some proteins continue to be translated by a cap-independent mechanism because they have internal ribosome entry sites (IRES). SNAT2 is one of those mRNAs that translates efficiently by this cap-independent mechanism under AAD conditions because it possesses an IRES near its 5`end and this process is promoted by eIF2α phosphorylation which is activated under AAD conditions (Gaccioli *et al.,* 2006).

### 1.14 Transporter phosphorylation as a regulator of transporter activity

The observation that MAPK signalling is important in regulation of SNAT2 activation raises the question of whether this occurs through phosphorylation of the SNAT2 protein itself. Addition of a phosphate group to a target protein molecule by kinases and ATP can be crucial in regulation of many fundamental properties of that protein such as its degradation, translocation and activation (Stolarczyk *et al.,* 2011). This applies to transporters, including SNAT3 (SLC38A3) which is a well-documented example of an amino acid transporter whose expression is down regulated by phosphorylation in response to inflammatory cytokines IL-6 and TNF-α which induce its localisation in the nucleus and decrease cell surface expression (Bröer, 2014). Another example of transporter regulation by phosphorylation is the Serotonin transporter which plays an important role in neurotransmission. Regulation of this transporter is mediated by phosphorylation through threonine residues by a cGMP stimulated

mechanism, and experimental mutation of these threonine residues leads to inactivation of the transporter (Ramamoorthy *et al.,* 2007).

## 1.15 Evidence for a Role for Protein Phosphorylation in the Regulation of SNAT2

SNAT2 activation also depends on Ser/Thr phosphorylation events mediated by MAP kinases (Hyde *et al.,* 2007), although it is unclear whether these kinases are acting directly on SNAT2 or on regulatory protein(s) upstream of SNAT2. In L6 skeletal muscle cells SNAT2 is also activated when there is stimulation of the insulin receptor (Hyde *et al.,* 2001) or related receptor tyrosine kinases (RTKs). This suggests that both Ser/Thr phosphorylation events and Tyr phosphorylation events upstream of SNAT2, or on the SNAT2 protein itself, are important in activating the transporter.

Online databases of protein mass spectrometry suggest that, at least for human SNAT2 in HeLa cells stimulated with Epidermal Growth Factor (EGF), phosphorylation can occur on several Ser/Thr and Tyrosine residues (Table 1.2). It is not known whether these phosphorylations have any functional effects, but a cluster of such sites occurs in the N-terminal cytoplasmic tail of human SNAT2 (Figure 1.12). This includes a possible MAPK phosphorylation site (Sheridan *et al.,* 2008) at residue 12; and most of these Ser and Tyr residues are conserved in rat SNAT2 (Figure 1.12).

**Table 1.2. Evidence of post-translational modification of SNAT2.**

(Sodium-coupled neutral amino acid transporter 2) taken from http://www.biosino.org/SysPTM/

| Protein ID | Gene Name | Species | PTM Type | PTM Subtype | Position in Protein | Sites AA | Source Type |
|---|---|---|---|---|---|---|---|
| Q96QD8 | SLC38A2 | Homo sapiens (Human) | Phosphorylation | O-Phosphorylation | 469 | S | SysPTM-A;SysPTM-B |
| Q96QD8 | SLC38A2 | Homo sapiens (Human) | Ubiquitination | | 38 | K | SysPTM-A;SysPTM-B |
| Q96QD8 | SLC38A2 | Homo sapiens (Human) | Phosphorylation | O-Phosphorylation | 18 | S | SysPTM-A;SysPTM-B |
| Q96QD8 | SLC38A2 | Homo sapiens (Human) | Phosphorylation | O-Phosphorylation | 10 | S | SysPTM-A;SysPTM-B |
| Q96QD8 | SLC38A2 | Homo sapiens (Human) | Phosphorylation | O-Phosphorylation | 12 | S | SysPTM-A;SysPTM-B |
| Q96QD8 | SLC38A2 | Homo sapiens (Human) | Phosphorylation | O-Phosphorylation | 41 | Y | SysPTM-A;SysPTM-B |
| Q96QD8 | SLC38A2 | Homo sapiens (Human) | Phosphorylation | O-Phosphorylation | 39 | S | SysPTM-A;SysPTM-B |
| Q96QD8 | SLC38A2 | Homo sapiens (Human) | Ubiquitination | | 33 | K | SysPTM-A;SysPTM-B |
| Q96QD8 | SLC38A2 | Homo sapiens (Human) | Phosphorylation | O-Phosphorylation | 21 | S | SysPTM-A;SysPTM-B |
| Q96QD8 | SLC38A2 | Homo sapiens (Human) | Phosphorylation | O-Phosphorylation | 151 | S | SysPTM-A |
| Q96QD8 | SLC38A2 | Homo sapiens (Human) | Ubiquitination | | 59 | K | SysPTM-A;SysPTM-B |
| Q96QD8 | SLC38A2 | Homo sapiens (Human) | Phosphorylation | O-Phosphorylation | 55 | S | SysPTM-A;SysPTM-B |
| Q96QD8 | SLC38A2 | Homo sapiens (Human) | Ubiquitination | | 60 | K | SysPTM-A;SysPTM-B |
| Q96QD8 | SLC38A2 | Homo sapiens (Human) | Phosphorylation | O-Phosphorylation | 20 | Y | SysPTM-A;SysPTM-B |
| Q96QD8 | SLC38A2 | Homo sapiens (Human) | Phosphorylation | O-Phosphorylation | 22 | S | SysPTM-A;SysPTM-B |
| Q96QD8 | SLC38A2 | Homo sapiens (Human) | Phosphorylation | O-Phosphorylation | 153 | S | SysPTM-A |
| Q96QD8 | SLC38A2 | Homo sapiens (Human) | Phosphorylation | O-Phosphorylation | 28 | Y | SysPTM-A;SysPTM-B |
| Q96QD8 | SLC38A2 | Homo sapiens (Human) | Phosphorylation | O-Phosphorylation | 30 | Y | SysPTM-A |
| Q96QD8 | SLC38A2 | Homo sapiens (Human) | Phosphorylation | O-Phosphorylation | 19 | S | SysPTM-A;SysPTM-B |
| Q96QD8 | SLC38A2 | Homo sapiens (Human) | Phosphorylation | O-Phosphorylation | 221 | T | SysPTM-A |
| Q96QD8 | SLC38A2 | Homo sapiens (Human) | Ubiquitination | | 140 | K | SysPTM-A |
| Q96QD8 | SLC38A2 | Homo sapiens (Human) | Phosphorylation | O-Phosphorylation | 17 | S | SysPTM-A;SysPTM-B |
| Q96QD8 | SLC38A2 | Homo sapiens (Human) | Phosphorylation | O-Phosphorylation | 24 | S | SysPTM-A;SysPTM-B |
| Q96QD8 | SLC38A2 | Homo sapiens (Human) | Phosphorylation | O-Phosphorylation | 220 | Y | SysPTM-A |
| Q96QD8 | SLC38A2 | Homo sapiens (Human) | Ubiquitination | | 3 | K | SysPTM-A;SysPTM-B |
| Q96QD8 | SLC38A2 | Homo sapiens (Human) | Phosphorylation | O-Phosphorylation | 217 | Y | SysPTM-A |
| Q96QD8 | SLC38A2 | Homo sapiens (Human) | Acetylation | | 1 | M | SysPTM-B |
| Q96QD8 | SLC38A2 | Homo sapiens (Human) | Phosphorylation | | 29 | S | SysPTM-B |
| Q96QD8 | SLC38A2 | Homo sapiens (Human) | Ubiquitination | | 2 | K | SysPTM-B |

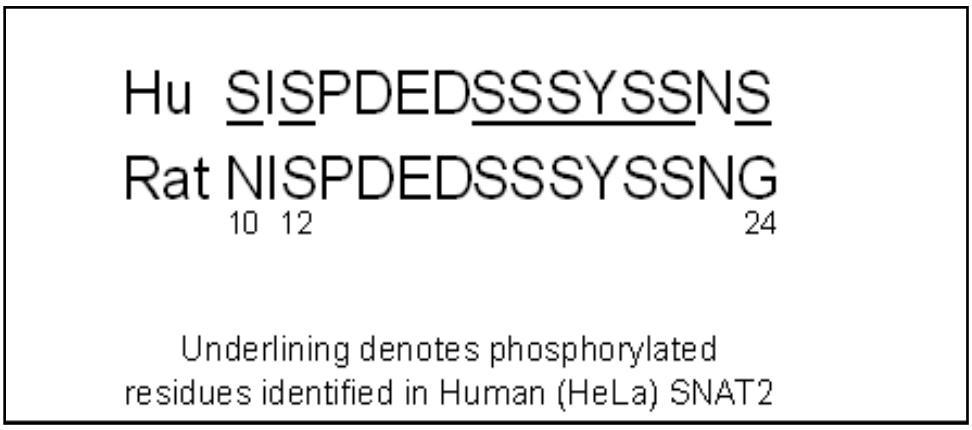


**Figure 1.12. Amino acid residues 10-24 of SNAT2 (SLC38A2) Potential phosphorylation sites in the cytoplasmic tail of SNAT2.**

Phosphorylated residues identified in human SNAT2 are taken from www.humanproteinpedia.org/cell_line_expression?HPRD_ID=05535&exp_id.

### 1.16 Glucocorticoids and sensing of acidosis

A study from this laboratory by (Watson *et al.,* 2013) showed that there was depletion in free amino acid concentrations in skeletal muscle biopsies from exercising CKD patients, probably due to lactic acid production during exercise. This lactic acid production is transient i.e. ceasing when exercise ceases. However, low amino acid level was detected 24h after the exercise had ceased (Watson *et al.,* 2013). Treatment with additional bicarbonate blunted this effect, suggesting that transient acidosis was also having a more prolonged effect on amino acid levels and that an initial transient fall in extracellular pH was then leading to a secondary and more prolonged signal which (like acidosis) was leading to depletion of intramuscular amino acids, perhaps through inhibition of SNAT2. This secondary signal might be due to glucocorticoid levels increasing in response to acidosis, an effect which has been well documented in humans (Buehlmeier *et al.,* 2016; Maurer *et al.,* 2003). There is also evidence from studies in rats that acidosis alone may not be sufficient to generate long term muscle wasting *in vivo*. In rats, metabolic acidosis fails to increase protein degradation in muscle if the animals' adrenal glands have been removed, but the stimulation of protein degradation by acidosis is restored if the rats are given glucocorticoid (May *et al.,* 1986).

An elevated level of glucocorticoid has been reported in patients with chronic kidney disease, which might be worsening their catabolic state (Kraut & Kurtz, 2005; Rosman *et al.,* 1982). Glucocorticoid secretion has been shown to increase both in rats and humans during metabolic acidosis (Maurer *et al.,* 2003; May *et al.,* 1986). It has therefore been suggested that glucocorticoid can generate its effect in combination with acidosis *in vivo* but that glucocorticoid or acidosis alone cannot induce significant muscle wasting separately (Garibotto *et al.,* 2010; Wang & Mitch, 2013). Increased circulating glucocorticoid is reported in many stress-induced conditions such as cachexia, metabolic acidosis and sepsis which cause muscle wasting (Schakman *et al.,* 2013). Glucocorticoid is thought to be a candidate cachectic hormone because blocking or removing its receptor reduce muscle atrophy. The effect of glucocorticoid on muscle to induce wasting is specific to certain type of muscle fibres: it acts mostly on Type II muscle fibres, but with little or no effect on Type I fibres which means that the effect of GC is

different in different muscle types according to their fibre type dominancy (Schakman *et al.,* 2013).

In view of the effect of metabolic acidosis on muscle cells in CKD – leading to amino acid depletion and impaired protein synthesis and increased protein breakdown as discussed above (Watson *et al.,* 2013); the pH sensitive System A amino acid transporter SNAT2 seems a likely contributor to these pathological effects. A particular feature of these transporters (Yao *et al.,* 2000) (Fig.1.11) which makes them of considerable interest in cachexia research, is that the transporters can be regulated or affected by environmental and hormonal change, in turn regulating the concentration of their amino acid substrates inside cells (Evans *et al.,* 2007). The response of muscle *in vivo* to glucocorticoid in the presence of acid that was described above leads to the important question of whether glucocorticoid (like low pH) may in turn inhibit System A/SNAT2.

For such effects to be understood, it is necessary first to consider in detail the biology of glucocorticoids.

## 1.17 Glucocorticoids

### 1.17.1 Regulation of glucocorticoid secretion

Glucocorticoids (GC) are steroid hormones secreted by the cortex of the adrenal gland located above each kidney. A number of corticosteroids exert glucocorticoid biological activity, but the main naturally occurring glucocorticoid in humans is cortisol (also known as hydrocortisone), whereas the main glucocorticoid in rat is corticosterone. They are stress-induced hormones that regulate many body functions and homeostasis by acting on the majority of tissues and organs in the body. GC synthesis and action is regulated through a negative feedback loop by the pituitary and hypothalamus (Figure 1.13) (Oakley & Cidlowski, 2013). GC secretion induced by a stress signal triggers the hypothalamus to secrete corticotropin releasing hormone (CRH) which in turn induces secretion of adrenocorticotropic hormone (ACTH) by the anterior pituitary gland and ACTH acts on the adrenal cortex to secrete GC (Oakley & Cidlowski, 2013). GC then exerts a negative feedback effect on CRH and ACTH secretion (Figure 1.13).

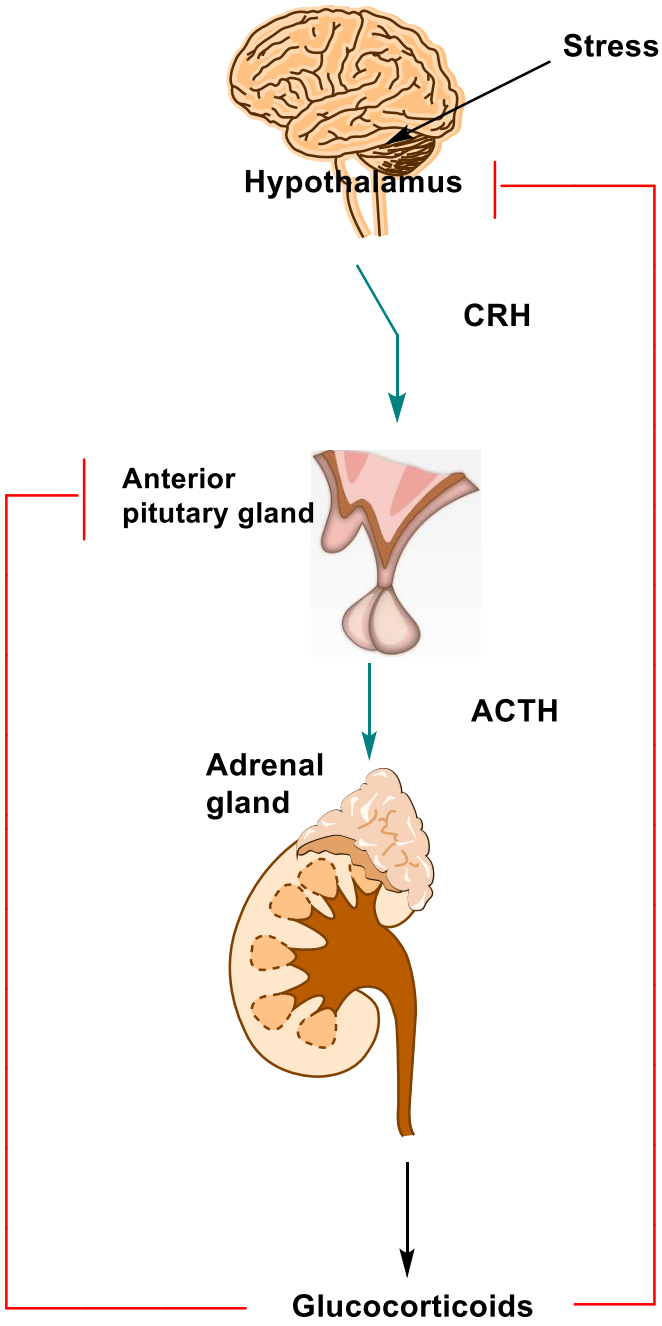


**Figure 1.13. Glucocorticoid hormone secretion and regulation.**

**The diagram is redrawn from (Oakley & Cidlowski, 2013).**

Glucocorticoid is regulated by a negative feedback loop, it acts on hypothalamus and pituitary gland which control the production and secretion of GC secretion induced by a stress signal triggers the hypothalamus to secrete corticotropin releasing hormone (CRH) which in turn induces secretion of adrenocorticotropic hormone (ACTH) by the anterior pituitary gland and ACTH acts on the adrenal cortex to secrete GC. GC then exerts a negative feedback effect on CRH and ACTH secretion.

### 1.17.2 Clinical use of GC

Synthetic GC is used as anti-inflammatory treatment for many inflammatory and immune diseases such as autoimmune disease, asthma, multiple sclerosis and rheumatoid arthritis. Furthermore, GC is used to prevent organ rejection in organ transplanted patients. For this reason, it is probably one of the world's most widely prescribed treatments. However, GC has many adverse side effects ranging from muscle wasting, to insulin resistance, to development of GC resistance, especially in patients with long term steroid treatment (Heitzer *et al.,* 2007; Oakley & Cidlowski, 2013). Exogenous GC can also reduce bone formation which may be partly due to reduction in calcium absorption and this osteoporosis effect of GC will become more obvious with long term treatment (Klein, 2015). Endogenous GC can also exert profound effects in a number of conditions such as inflammation, pituitary gland tumours or even some catabolic conditions such as diabetes and metabolic acidosis (Klein, 2015). Therefore, preventing or reducing the side effects of GC is very import, and this requires investigating the molecular and cellular mechanisms of GC action (Oakley & Cidlowski, 2013).

### 1.17.3 Mechanisms of GC action

#### 1.17.3.1 Classical mechanisms

The classical mechanism of glucocorticoid action in the cell is through glucocorticoid receptors (GR), which are members of the nuclear receptor superfamily. GR consists of three domains: an N-terminal transactivation domain (NTD), a central DNA-binding domain (DBD), and a C-terminal ligand binding domain (LBD). DBD is responsible for binding to a specific DNA target region on a target gene, called a glucocorticoid-responsive element (GRE) to initiate transcription of genes that are activated by GC, with the aid of the NTD (Oakley & Cidlowski, 2013). However, if GC binds to a negative GRE (nGRE) this will lead to gene suppression (Figure 1.14). GR induces its action by binding its GC ligand and the resulting complex then translocate to the nucleus and activation or deactivation of specific gene expression then occurs by transcription of these genes. GC may control as much as 10-20% of the human genome (Oakley & Cidlowski, 2013). The response of the human body to GC varies between cell types but can be very specific in a given cell type due to the diversity of GR isoforms that can be expressed in each cell. Consequently, the effect of GC may

differ within the same tissue or organ or among individuals (Oakley & Cidlowski, 2013).

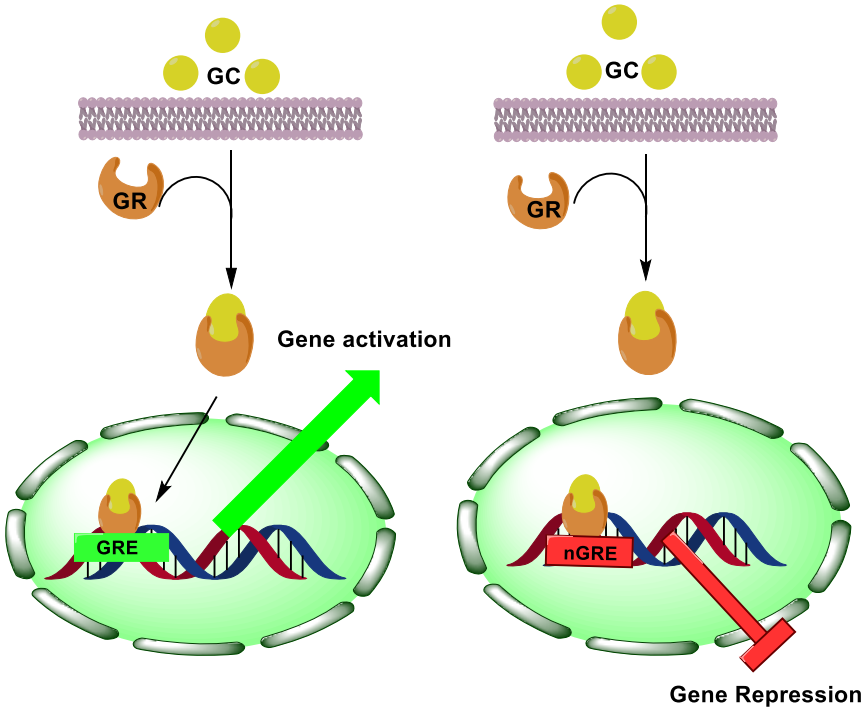


**Figure 1.14. Schematic representation of the classical mechanism of glucocorticoid action.**

The diagram is redrawn from (Oakley & Cidlowski, 2013). Glucocorticoid binding with glucocorticoid receptor lead to either activation and expression of certain gene by acting on glucocorticoid-responsive element (GRE) or repressing others through negative glucocorticoid-responsive element (nGRE).

### 1.17.3.2 Non-classical mechanisms

In the above classical or ligand-dependent mechanism of GC action, the biological response may occur over minutes or (more commonly) hours. However, sometimes the effect of GC is very quick, within seconds which does not require the classical receptor activation, translocation and gene expression. This is called the non-classic or non-genomic action of GC (Oakley & Cidlowski, 2013). Activation of some non-receptor tyrosine kinases e.g. c-Src, can exert GC effects through a non-genomic mechanism through a number of different downstream signalling pathways in the cell such as PI3K, Akt and MAPK. (Oakley & Cidlowski, 2013). For example, incubating C2C12 myotubes with the glucocorticoid dexamethasone (DEX) can induce ATP depletion and glucose

uptake after exposure to electric pulse stimulation in a non-genomic or GR-independent manner. This can be demonstrated by showing that inhibition of GR has no effect on the DEX-induced glucose uptake. Furthermore, the enzyme AMPK is activated during muscle contraction through phosphorylation of AMPK. Treating C2C12 myotubes with DEX significantly decreased this effect, and again inhibiting GR could not eliminate the DEX effect on AMPK phosphorylation (Gong *et al.,* 2016b).

### 1.18 Glucocorticoid sensitive kinases

In addition to the mechanisms described above, GC signals may feed into protein phosphorylation signalling pathways by altering gene expression of protein kinases.

One important example of such a kinase is Serum and Glucocorticoid regulated kinase-1 (SGK-1) which is widely expressed in mammalian tissues. For example, GCs induce SGK-1 expression in rat kidney, increasing both SGK1 mRNA and protein. The SGK-1 response to glucocorticoid at transcriptional level is mediated by a glucocorticoid response element (GRE) in the promotor region of the SGK-1 gene. Rat bilateral adrenalectomy results in significant decrease in SGK-1 expression detected by Western blot and immunohistochemistry, and the level of SGK-1 expression was returned to basal level by administration of dexamethasone for one week (Rosa *et al.,* 2003). Similarly, human SGK-1 mRNA has been shown to be induced after incubating a number of human cell lines with synthetic glucocorticoid dexamethasone. (Náray-Fejes-Tóth *et al.,* 2000). However, the physiological effects of SGK-1 induction differ significantly between cell types (Menon & He, 2016).

A second GC-responsive kinase is Liver Kinase B1 (LKB1). The direct effect of GC on this kinase has been shown to be a decrease in LKB1 mRNA in HEK293 cells *in vitro* (Lützner *et al.,* 2012) and a decrease in the kinase activity *in vitro* in rat prefrontal cortical astrocytes (Yuan *et al.,* 2016).This is the serine/threonine kinase which performs phospho-activation of the key energy status sensor AMP-activated protein kinase (AMPK) in most tissues (Mihaylova & Shaw, 2011). AMPK is activated and phosphorylated by LKB1 when the AMP concentration rises and AMP binds to AMPK. Activated AMPK down-regulates anabolic

pathways and stimulates catabolic pathways to maintain energy status. This is of importance in global protein metabolism (for example in muscle) because activated AMPK can inhibit mTORC1 by direct phosphorylation of TSC2 and Raptor, thus decreasing the ATP consumption that occurs during the process of translation (Mihaylova & Shaw, 2011).

### 1.19 Glucocorticoid and the Ubiquitin-Proteasome Pathways (UPP).

Glucocorticoids can induce net protein wasting in skeletal muscle and hence promote muscle wasting. However, the way in which they do this is complex. Firstly, the action of GCs on skeletal muscle varies according to the disease condition and the muscle type; fast-twitch muscle responding more to GC than slow-twitch muscle because it contains more glucocorticoid receptors (Klein, 2015). Secondly, the biochemical mechanism of GCs' action on the UPP is complex: GCs may induce protein wasting by increasing proteolysis and decreasing protein synthesis (Lfberg *et al.,* 2002) and through inhibiting the insulin-induced anabolic signalling. Through the classical GC-receptor interaction mechanism, GCs can increase transcription of genes encoding components of the UPP, including the E2 ubiquitin conjugating enzyme and E3 ligases such as MAFbx/Atrogin-1 and MuRF-1 and sub-units of the proteasomes themselves (Schakman *et al.,* 2013). GCs also induce insulin resistance, inhibiting the anabolic signal from insulin/IGF-I through RTKs and insulin receptor substrate 1 (IRS1) to PI3K/Akt, thus indirectly increasing E3 ligase expression and activating the UPP as was described for other catabolic stimuli in Section 1.8.3 above (Zheng *et al.,* 2010). GCs impose this insulin resistance in several ways, for example by increasing degradation of IRS-1 (Schakman *et al.,* 2013) and by increasing expression of P85α, the regulatory subunit of PI3K (Schakman *et al.,* 2013).

However not all GC responsive signalling pathways are catabolic: in skeletal muscle it has recently been shown that SGK-1 is anabolic (Luo *et al.,* 2016). Partly this occurs through inhibition of transcription factors such as FoxO3a which are involved in up-regulating transcription of E3 ligases. In a mouse SGK-1-knockout model there was increased expression of E3 ligases MAFbx/Atrogin1 and MuRF1 and subsequent increase in muscle loss. This may be of relevance to cachexia in CKD because decreased SGK-1 expression has been reported in

muscle in a mouse CKD model compared to healthy controls (Luo *et al.,* 2016). However, this is not necessarily a consequence of direct action of GCs on SGK-1. This kinase is also a downstream target of PI3K and insulin signalling and its low activity in CKD may be a response to inflammatory cytokines rather than GCs (Luo *et al.,* 2016).

**1.20 Glucocorticoid and UPP effects on System A transporters and SNAT2.**

It has also been suggested that the catabolic effect of GCs in muscle might occur through inhibiting amino acid transport into the cell resulting in decreased protein synthesis (Schakman *et al.,* 2013), possibly through inhibition of System A transporters and SNAT2 as suggested at the end of Section 1.16. At present, there is little direct published evidence of such inhibition, indeed GC acutely up-regulates total System A amino acid transport in hepatocytes (McGivan & Pastor-Anglada, 1994).

Even though there are no published reports of GCs down-regulating System A or SNAT2, there is evidence that the UPP (which may be activated by GCs) is sometimes involved in SNAT2 degradation. It has been shown that inhibiting proteasomes with the specific proteasome inhibitor MG132 significantly increased SNAT2 transport activity (i.e. MeAIB uptake) in adipocytes and preadipocytes; and proteasome inhibition also increased GFP-tagged SNAT2 expression detected by Western blots and GFP imaging in these cell lines. When the tagged SNAT2 was immunoprecipitated, it showed enhanced ubiquitination, mediated by the Ubiquitin E3 ligase Nedd4-2 (Hatanaka *et al.,* 2006).

It is well documented that amino acid deprivation (AAD) increases SNAT2 activity and protein abundance in cells. Nardi et al. (2015) showed this increase in SNAT2 activity and protein abundance in L6 myotubes and interestingly they detect two bands, one about 60KDa (i.e. the mature and highly glycosylated SNAT2 protein) and a lighter band about 40KDa – possibly recently synthesised and under-glycosylated immature SNAT2 protein. *In vitro* deglycosylation led to disappearance of the heavier band more rapidly than the lighter one (Nardi *et al.,* 2015). Furthermore, expression of V5-tagged SNAT2 in HeLa cells was enhanced under AAD conditions but the abundance of the protein (especially the immature form of the protein) was further enhanced when the cells were treated

with MG132, suggesting that the immature (possibly intracellular pool of the protein) was preferentially degraded through the UPP (Nardi *et al.,* 2015).

The *in vivo* observations described in Section 1.16 of apparent synergism between metabolic acidosis and glucocorticoid in activation of skeletal muscle protein degradation lead to the important question of whether glucocorticoid (like low pH) may inhibit System A/SNAT2 transporters. Preliminary experiments in this laboratory using L6 skeletal muscle cells treated for 4h with the glucocorticoid dexamethasone (Clapp, 2010) (PhD thesis, University of Loughborough) have suggested that the glucocorticoid Dexamethasone can inhibit System A transporter activity in L6-G8C6 cells (Clapp, 2010). A major aim of the work described in this thesis was therefore to investigate this effect in greater detail.

### 1.21 The *in vitro* model of skeletal muscle used in this project

For *in vitro* studies, intact *ex vivo* muscle preparations can be used, isolated from rat or mouse. For example, Hornberger and colleagues (2004) used an *ex-vivo* mechanical stimulator which is a refined myograph system (Kent Scientific, Torrington, CT, U.S.A.) (Hornberger *et al.,* 2004). However, one of the important factors to be considered in such *in vitro* preparations of isolated skeletal muscle is hypoxia which may occur in these non-perfused preparations. One way to minimise this problem is by using small bundles of mouse muscle fibres. This is a highly effective model, but the micro-dissection required for these preparations is extremely laborious (Wendowski *et al.,* 2017).

Another cell culture model used in skeletal muscle studies is human myotubes. This is an excellent system because it is very close to human skeletal muscle *in vivo,* but donor to donor variation introduces variation into the studies. The origin of these myotubes is satellites cells which are in quiescent state in adult skeletal muscle and activated in response to injury and muscle growth. They can be isolated by two methods, enzymatic digestion and cell migration (Aas *et al.,* 2013). They have the ability to transform to multinucleated myotubes *in vitro* and this model has been used extensively for many years. However, its use is not without limitation. For example, their glucose uptake capability is lower compared to muscle *in vivo.* This may be because of low expression of GLUT4 which is more highly expressed in Type 1 fibres than Type 2. Furthermore, there are

differences in gene expression between biopsies and cultured myotubes, most of the genes that have been studied show higher expression in biopsies rather than cultured cells. Unlike immortal cell lines, there is limited and variable capacity of human myotubes to grow, differentiate and undergo passaging. Their morphology, metabolic capacity and the ability to fuse to form myotubes will decline gradually with increased passage number (Aas *et al.,* 2013). It has been reported previously that human skeletal muscle myotubes are incapable of spontaneous contraction unless it they are stimulated by neuronal contacts. Similar observations of spontaneous contraction have been reported in rodent cell cultures by Guo and colleagues (Guo *et al.,* 2014).

For this reason, myotubes grown from immortalised myoblast cell lines e.g. L6 and C2C12 are still extensively used. C2C12 is a mouse myoblast which is used widely and successfully in research (Philp *et al.,* 2010; Philp *et al.,* 2011). However, C2C12 myotubes have been found to give rapid acidification of the culture medium which limits their use in studies of acidosis-induced protein degradation (Bevington *et al.,* 1998). The L6 sub-clone L6-G8C5 was found to give lower rates of acidification (Bevington *et al.,* 1998). Very highly differentiated L6-G8C5 myotubes can be obtained by pre-treatment with IGF-1 and retinoic acid (Elsner *et al.,* 1998). However, these were not used in the present study as previous work from this laboratory (Pickering *et al.,* 2003) has shown that they may give limited response to some catabolic stimuli and show poor adherence to the culture vessels. Therefore, spontaneously fused L6-G8C5 myotubes were used in the present study. Another reason for using L6-G8C5 is that it has been shown previously in this laboratory that the predominant isoform of System A amino acid transporter that is expressed is SNAT2 (Evans, 2009). Therefore, in the transport experiments on this cell line that are described in this thesis, the terms “System A transporter activity” and “SNAT2 transporter activity” are taken to mean the same thing.

## 1.22 Thesis hypothesis

The hypothesis to be tested in this thesis is that the synthetic glucocorticoid dexamethasone inhibits and down-regulates the System A amino acid transporter SNAT2 in rat L6 skeletal muscle cells (sub-clone G8C5) and, as a consequence of this, exerts functionally significant downstream effects on protein metabolism in these cells.

## 1.23 Aims of the project

The specific aims of this study were to investigate 3 important aspects of the biology of SNAT2 which are relevant to its possible role in maintaining muscle protein mass and hence (indirectly) to its role in influencing inflammation during acidosis and cachexia:

- To determine how glucocorticoid and amino acid depletion influence SNAT2 activity in the cultured L6-G8C5 rat skeletal muscle cell model.
- To determine the role of modification of the SNAT2 protein (including possible SNAT2 phosphorylation or SNAT2 degradation) in these effects, and
- To determine the way(s) in which the altered SNAT2 activity may signal to and act upon protein metabolism.

# Chapter 2 Materials and methods

## 2.1 General materials and reagents

Throughout the thesis, unless otherwise stated, all the reagents and chemicals used, including the molecular grade reagents, were purchased form Sigma. Sterile consumables for tissue culture were obtained as follows: Petri dishes and 35 mm diameter 6-wells were purchased from Thermo scientific; 96 well plates from Sarstedt; and 25cm$^2$ flasks and 22mm diameter 12-well plates were purchased from Corning (non-pyrogenic sterile polystyrene) and from Corning Costar respectively.

## 2.2 Cell culture models

### 2.2.1 L6 cells

L6-G8C5 is a sub-clone of the rat skeletal muscle cell line L6 (Yaffe, 1968) which has a strong tendency to fuse spontaneously to form myotubes when cultured in low serum medium (Elsner *et al.,* 1998). Stocks were obtained from ECACC (European Collection of Animal Cell Cultures) (ref. 9212111) and were used at passage number (5-20). L6-G8C5 were selected for this study because they have been used previously in this laboratory (Bevington *et al.,* 1998; Bevington *et al.,* 2001; Bevington *et al.,* 2002; Evans *et al.,* 2007; Evans *et al.,* 2008; Pickering *et al.,* 2003) and by others in research to study the effect of different experimental manipulations (including acidosis and glucocorticoid) on global protein metabolism in muscle. It is a well characterised skeletal muscle cell model, is easy to culture, and the results from previous studies in this laboratory showed that, among System A amino acid transporters, Sodium-coupled Neutral Amino acid Transporter 2 (SNAT2, SLC38A2) is the most strongly expressed type in L6-G8C5 cells and is consequently the focus of this project (Evans, 2009).

### 2.2.2 L6-cells, maintenance and passaging

The cells were plated in 9cm Petri dishes at $10\times10^4$ cells/ml in Growth Medium (GM), comprising Dulbecco's Modified Eagle Medium (DMEM-Life Technologies 11880-028) (Appendix A.1), which contains 5mM D-glucose and added pyruvate, supplemented with 10mg Phenol Red/L (Sigma-P5530), 100U/ml Penicillin G, 100µg/ml Streptomycin, 2mM L-glutamine and 10% v/v heat inactivated batch-tested foetal bovine serum (FBS). The cells were grown in a culture incubator at 37°C under humidified air, 5% $CO_2$ until they reached ~80% confluence, at which stage they were passaged. For passaging the GM was aspirated and each Petri rinsed with 5ml of (1x) Hank's Balanced Salt Solution (HBSS, Life Technologies-1754651) (Appendix A.4) and then incubated with 2ml of (1x) Trypsin-EDTA (T/E) (Invitrogen 25300) for 10min in 37°C in the culture incubator to detach the cells from the Petri. The cells were then re-suspended in 10ml of the GM described above and centrifuged at 500g for 5 minutes. After centrifugation, the supernatant was discarded, the cell pellet was re-suspended in another 10ml of GM, and the suspension counted using a haemocytometer and plated at $10x10^4$ cells/9cm Petri dish in 15ml of GM for maintaining stock cells.

### 2.2.3 Preparing L6 myoblasts for experiments and experimental test media

Unfused L6 myoblasts were used in some experiments (without prior fusion of the cells to form myotubes) by seeding at a plating density of $4.5x10^4$ cells/$cm^2$ in vessels of the required size containing the GM described in Section 2.2.2 at 0.2ml per $cm^2$ of culture area.

The basal medium that was used to make up the experimental test media was Minimum Essential Medium (MEM) (Invitrogen 21090-022) (Appendix A.3) supplemented with 100U/ml Penicillin G, 100µg/ml Streptomycin, and 2mM L-glutamine. If serum was required in the test media, 2% v/v heat-inactivated Dialysed Foetal Bovine Serum (DFBS, Invitrogen ref 26400) was used. In amino acid deprived experiments, MEM without amino acids, comprising Earle's Balanced Salt Solution ((EBSS-Invitrogen 24020) (Appendix A.5) +1% v/v MEM Vitamins was used.

Under a 5% $CO_2$ atmosphere, MEM has a pH of about 7.25. Therefore, unless otherwise stated, all experimental incubations were performed at the physiological pH of 7.4 by adding an extra 8mM $NaHCO_3$ to the medium.

Other variations in the experimental test media are described in the figure legends in the results chapters.

### 2.2.4 L6-myotube formation

For the experiments in which differentiated myotubes were required, the L6 myoblasts were cultured in GM at the plating density mentioned in Section 2.2.2. (Figure 2.1.A), but after 72 hours the serum content of the medium was reduced to 2%. The GM was aspirated and the ~70-80% confluent cultures were incubated in Minimum Essential Medium (MEM) (Invitrogen 21090-022) supplemented with 100U/ml Penicillin G, 100µg/ml Streptomycin, 2mM L-glutamine and 2% v/v heat inactivated foetal bovine serum (FBS) to induce fusion and myotube formation. Fresh medium (the 2% FBS in MEM described above) was added to the cells every two days. By day 8 the myotubes were ready for experimental incubations (Figure 2.1.B). More complete fusion can be achieved by prolonged incubation, but this may lead to myotube detachment and partial necrosis of the cultures (Elsner *et al.,* 1998). More rapid additional fusion can be achieved by adding differentiation factors such as insulin-like growth factor I and glucocorticoid (Elsner et al. 1998) but they were not used, as previous experiments have shown that they may interfere with the experiments presented here (Pickering *et al.,* 2003).

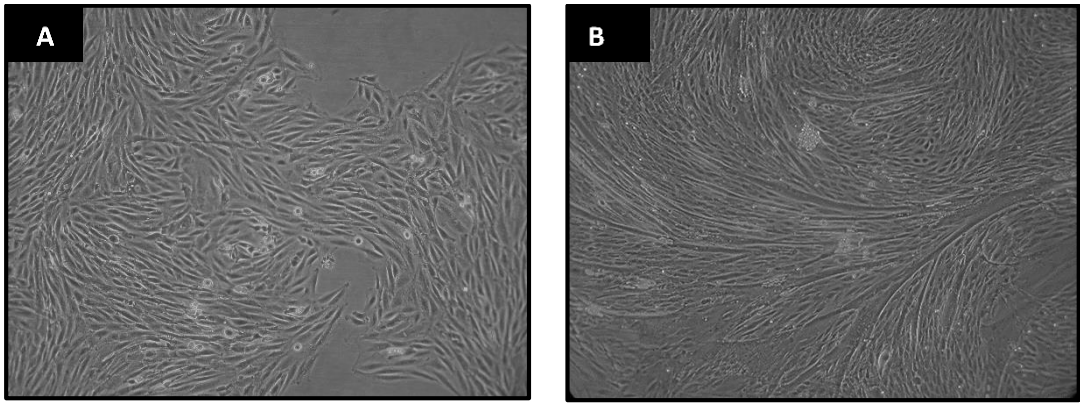


**Figure 2.1. Photograph of L6 cells.**

(A) Sub-confluent L6-G8C5 myoblasts after 3 days in Growth Medium with 10% v/v foetal bovine serum (FBS). (B) L6-G8C5 myotubes after incubating L6-myoblasts for another 3 days with 2% FBS in MEM, 100X magnification.

### 2.2.5 Immunohistochemistry

One of the most obvious characteristics of L6 myotubes is their multinucleate structure when the myoblasts differentiate to myotubes. To confirm multinuclear myotube formation, L6 myoblast cells were seeded in GM at $5x10^4$ cells per well on four well of an 8-chamber slide (Nunc-177445). After 72 hours the GM was replaced by 2% DFBS in MEM (Section 2.2.3) and the other 4 wells on the same slide were seeded at the same density as above for myoblasts to be ready at the same time as myotubes. After another 24h a fresh aliquot of 2% DFBS in MEM was added to myotube wells. On day 8 the medium was discarded, following the protocol for immunohistochemistry staining from:

http://www.abcam.com/protocols/immunocytochemistry-immunofluorescence-protocol, http://www.abcam.com/protocols/ihc-fixation-protocol

as follows. The wells were washed three times with 400µl per well of x1 Phosphate buffered saline (x1PBS) (Appendix B.9.1). The wells were then fixed for 20 minutes at room temperature by adding 400µl per well of fixation buffer (Appendix B.9.2) and the cells were permeabilized for 30 minutes at room temperature by adding 400µl per well of 0.5% Triton X100 (Sigma T-9284) in 1% PBS. A gasket and rubber seal were removed from the chamber slide. The cells were incubated for 1 hour with 100µl blocking buffer (5% Goat serum (Sigma-G6767) with 0.25% Triton X100 in x1 PBS). After blocking, the cells were washed three times with x1 PBS and incubated with the primary antibody overnight at 4°C (MY-32-Monoclonal Anti-Skeletal Myosin (Fast) Sigma-M4276) diluted 1:400 in the blocking buffer described above. (This antibody recognises skeletal muscle myosin heavy chain). After overnight incubation, the cells were washed three times, for 5 minutes each wash, with x1 PBS in a Coplin jar then incubated with the secondary antibody (Goat ant-mouse IgG Alexa fluor 555, Invitrogen-A21422) diluted 1:300 in blocking buffer, 100µl per well in the dark at room temperature for 2 hours. Three washes were then performed with x1 PBS in a Coplin jar in the dark after the secondary antibody incubation, and then incubated with DAPI (nuclear staining) for 5 minutes in the dark, followed by another three washes with x1 PBS and then mounting and examination using an inverted Olympus IX81 motorized microscope with a Scan^R screening platform and a Cell^R imaging station (Advanced Imaging Facility, University of Leicester) (Figure 2.2).

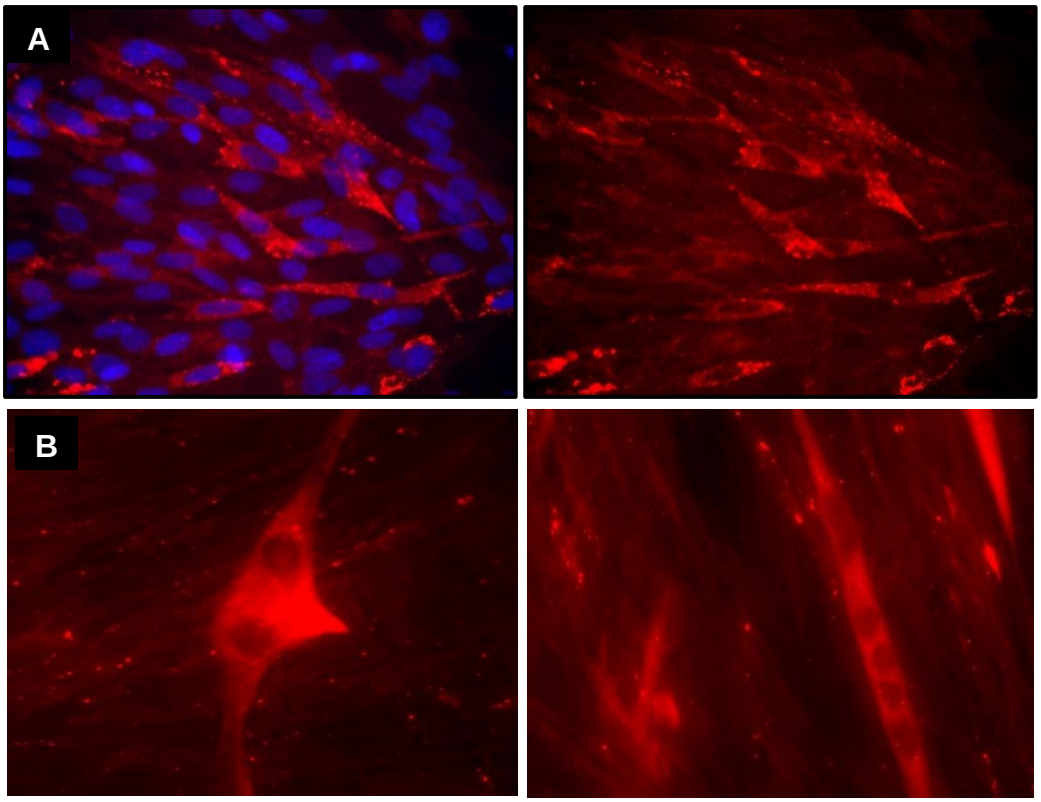


**Figure 2.2. Alexa Fluor® 555 immunofluorescence staining of skeletal muscle myosin heavy chain in L6 cells.**

L6 myoblasts (Day 4) (A) and L6 myotubes Alexa Fluor® 555 with nuclear stain DAPI (Day 8) (B). Magnification 20X. (Excitation max 555 nm; Emission max 580 nm).

### 2.2.6 L6 myoblast transfection

Unfused L6 myoblasts were used in transfection experiments including SNAT2 plasmid DNA and siRNA SNAT2 silencing. For SNAT2 plasmid DNA transfection, L6 myoblasts were plated at $8x10^4$ per 22mm well for plasmid DNA transfection and $10x10^4$ per 22mm well for siRNA transfection. Different transfection reagents were tested to optimise the SNAT2 plasmid DNA transfection efficiency: TransIT®-2020 (Mirus), calcium phosphate ProFection transfection system (Promega-E1200), and Effectene transfection reagent (QIAGEN-Cat No.301425) were used following manufacture's instructions. However, for siRNA silencing SNAT2, transfection with just the ProFection transfection system was found to be adequate.

### 2.2.7 Primary human skeletal myoblast culture

Normal human skeletal myoblasts from (Invitrogen-Cat no. A12555) were used to study the effect of DEX in human skeletal muscle cells and to compare the

effect with L6 cells, the cells were incubated in 1ml growth medium, made from 500ml of Ham's F-10 Nutrient Mix, (GlutaMAX-Gibco-41550-021) (Appendix A.9) supplemented with 100ml FBS, 100U/ml Penicillin G, 100µg/ml Streptomycin and 5ml Fungizone, in 22mm$^2$ 12-well plates for 48h (Figure 2.3A). Then the growth medium was discarded and 1ml of differentiation medium (DMEM, low glucose-Gibco-11885-084) (Appendix A.10) supplemented with 2% v/v horse serum (Gibco-16050-130) was added to each well and the cells were incubated for another 48h to induce myotube formation (Figure 2.3B).

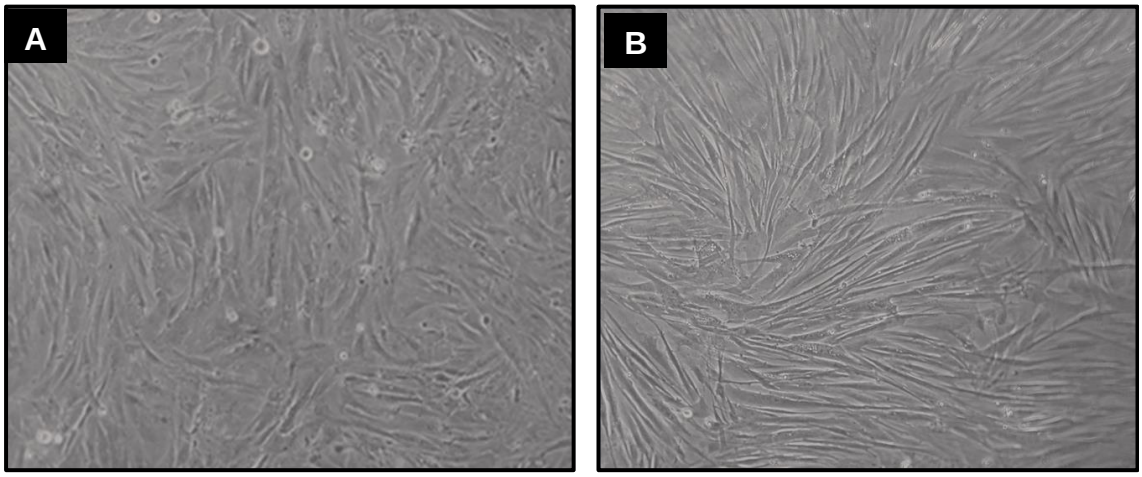


**Figure 2.3. Photograph of primary human skeletal muscle cells.**

(A) Myoblasts after 2 days in Growth Medium. (B) Primary human skeletal myotubes after incubating primary human myoblasts for another 2 days with differentiation medium, 100X magnification.

### 2.2.8 Human Embryonic Kidney cells (HEK-293A)

Human Embryonic Kidney cells (HEK293A) were used in this project as a vehicle to study tagged SNAT2 protein expression on a molecular level. HEK293A cells are a sub-clone of the Human Embryonic Kidney cell line (see below) which have flattened morphology and improved adherence on culture vessels. Stocks were obtained from Dr David Lodwick, Department of Cardiovascular Sciences, University of Leicester, and were used at passage number (3-21). The original HEK293 cells were a human embryonic kidney cell line which was transformed by exposing to sheared fragments of human adenovirus type 5 (Ad5) DNA. The history of the available HEK293 cells can be traced back to 1973 when they were first derived from a human embryo (ATCC accession number CRL-1573) (Lin *et al.,* 2014). HEK293 cells have been used frequently in research as a vehicle for transfection experiments because this is a very easy cell line to transfect with

high efficiency by using simple transfection reagents such as calcium phosphate (Thomas & Smart, 2005).

### 2.2.9 HEK293A cell passaging and media

The cells were grown in a growth medium based on high glucose DMEM (Sigma D6429) (Appendix A.2) supplemented with 100U/ml Penicillin G, 100µg/ml Streptomycin and 10% v/v heat inactivated foetal bovine serum (FBS). For propagation and maintenance of stock, the cells were plated at $10x10^4$ cells per 9cm Petri dish, and the cells were passaged when 70-80% confluent. For experiments, they were plated at $10x10^4$ cells / 2.2cm diameter 12-well in 1ml growth medium or $25x10^4$ cells / 3.5cm 6-well in 2ml growth medium (Zhang *et al.,* 2008).

## 2.3 Collagen coating plates for HEK293A cells

Collagen coated plates were used for all HEK293A cells experiments because collagen coating enhanced attachment of the cells to the plate. Bovine (Calf Skin) Collagen, Type I (1mg/ml or 0.1% w/v stock in 0.1M Acetic Acid) (Sigma C8919) was used to coat the wells. The collagen stock solution was diluted with sterile 0.1M Acetic Acid to 50µg/ml before use and applied at a density of $5µg/cm^2$. The culture plates were left in the culture hood with the lid off overnight. The following morning, they were rinsed three times with 0.40ml HBSS per 2.2cm well to remove any residual acetic acid, then the plates were kept at 4°C until used.

## 2.4 Bacterial transformation with SNAT2 plasmid DNA

### 2.4.1 SNAT2 cDNA constructs and cloning

The SNAT2 sequence derived from Human SLC38A2 ORF Shuttle Clone OCAAo5051E1145D (Source Biosciences) had previously been cloned by PROTEX (the University of Leicester Protein Expression Laboratory) (in collaboration with Dr EL Watson (ELW) & Dr TP Herbert (TPH)) into two mammalian expression vectors: pLEICS-29 and pLEICS-49 (Figure 2.3).The SNAT2 construct in pLEICS-29 was designed to express, under the control of an SV40 viral promoter, a SNAT2 protein with the following enhanced Green Fluorescent Protein (eGFP) tag/linker sequence at its C-terminus: EFMQSTVPRARDPPVAT-EGFP EFMQSTVPRARDPPVAT-EGFP.

The resulting 8257 bp plasmid construct (i.e. 6696 bp from the plasmid vector plus 1561 bp from the SNAT2 ORF Clone) and the eGFP-tagged SNAT2 fusion protein expressed from it are designated SNAT2-eGFP.The SNAT2 construct in pLEICS-49 was designed to express, under the control of an SV40 viral promoter, a SNAT2 protein with the following His4 3xFLAG (i.e. DYKDDDDK) tag/linker sequence at its C-terminus: TEV-2-His4-DYKDDDDKDYKDDDDKDYKDDDDK-GSEN. The resulting 9153bp plasmid construct (i.e. 7592 bp from the plasmid vector plus 1561bp from the SNAT2 ORF Clone) and the HisFLAG-tagged SNAT2 fusion protein expressed from it are designated SNAT2-HisFLAG. The corresponding empty (but ligated) pLEICS-29 and pLEICS-49 vectors (without the SNAT2 sequence) were also obtained from PROTEX and were used in mammalian transfection experiments to control for non-specific stress effects arising from plasmid transfection.

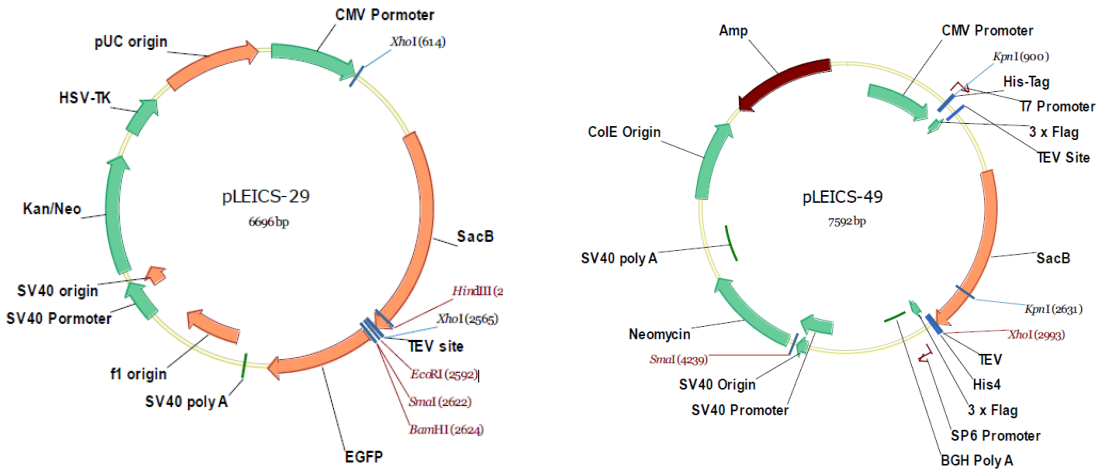


**Figure 2.4. Schematic diagrams of plasmid vectors used for SNAT2 cloning:**

pLEICS-29 (EGFP-tagged) and pLEICS-49 (HisFLAG tagged). Source of images: https://www2.le.ac.uk/colleges/medbiopsych/facilities-and-services/cbs/protein-and-dna-facility/protex/available-vectore/maps/view.

### 2.4.2 Bacterial transformation

A bacterial transformation procedure, using a heat shock protocol, was carried out to propagate the plasmids which were used in the transfection experiments. The competent cells used in the transformation procedure were One Shot® TOP10 Chemically Competent *E. coli* (C4040-Invitrogen) (kindly provided by Dr Karen Molyneux-Department of Infection, Immunity and Inflammation-University of Leicester). The competent cells were thawed on ice and 2µl of stock plasmid was added to the cells in a 0.5 ml tube and incubated on ice for 20 min, heat shocked by putting the tube in a water bath at 42°C for 1-2 min, and returned to ice for another 2 min. Then 300µl of Lennox Broth (LB) medium was added to the bacterial cells transformed with the plasmid and incubated at 37°C for 1 h and split onto two Petri dishes containing 25ml of LB agar with 100µg/ml antibiotic (Ampicillin for pLEICS-49 or Kanamycin for pLEICS-29) depending on the antibiotic resistance of the plasmid vector as shown in Figure 2.4. Plates were incubated in an incubator at 37°C overnight. Next day a single bacterial colony was transferred into 250 ml LB medium and incubated in a shaking incubator overnight at 37°C.

### 2.4.3 Plasmid purification

After overnight incubation, the plasmid was purified using a GeneJET$^{TM}$ Plasmid Maxiprep Kit-K0491 (Life technologies) by following the provided manufacture's protocol. Briefly, this involved centrifuging the content of the culture and suspending the pelleted bacterial cells in an SDS/alkaline lysis buffer to liberate plasmid DNA. The lysate was neutralized with SDS following the manufacturer's instructions to ensure re-annealing of plasmid DNA. Precipitated proteins and chromosomal DNA, cell debris and SDS precipitate were pelleted by centrifugation. The plasmid DNA in the supernatant was purified on a spin column and the adsorbed DNA was washed on the column and eluted with the manufacturer's Elution Buffer.

The purified plasmid was quantified by using a Thermo Scientific NANO DROP 1000 Spectrophotometer and stored at -20°C. The isolated plasmids were run out on a 2% agarose gel for 60 min at 100 volts (1µg DNA per lane) accompanied by a 1-10 kilo base ladder (NEB Ref #N3232) as a size marker, using a procedure similar to that in Section 2.12.4 below. The size of the plasmids was estimated

by visual comparison with the ladder and shown to agree with the sizes stated in Section 2.4.1 above. The presence of the human SNAT2 sequence in the constructs was confirmed by performing DNA sequencing, (Level 2 Sequencing, by the Protein and Nucleic Acid Chemistry Laboratory (PNACL), University of Leicester) using the purified SNAT2-eGFP and SNAT2-HisFLAG plasmid constructs as template. The sequencing data obtained is shown in Appendix C1-C4.

## 2.5 HEK293A transfection (Transient transfection)

For the transfection experiments, two transfection reagents were tested: TransIT®-2020 transfection reagent (Mirus) and calcium phosphate. In all transfection experiments, the concentration of cDNA applied to the mammalian cell cultures was approximately 2µg per 35mm culture well which is the recommended concentration for use with TransIT®-2020 Transfection Reagent (Mirus) for 35 mm 6-well plates. For experiments in which functional effects of tagged SNAT2 and empty control vector were being compared, the mass of plasmid DNA applied to the cultures was adjusted in proportion to the mass of the plasmids (Section 2.4.1) to ensure that a constant 0.36 pmol of plasmid was added per 35mm well.

### 2.5.1 Calcium phosphate transfection

The HEK293A cells were plated at 25 x $10^4$ cells / well in collagen coated Nunc 35mm 6-well plates in 2ml growth medium (Sigma-DMEM-D6429): after overnight incubation, the cells were transfected using calcium phosphate method as follows. With 2ml GM, the cells were transfected with the same molarity of either SNAT2-eGFP or GFP-empty vector. The transfection mix was prepared as shown in Table 2.1, SNAT2-eGFP or GFP-empty vector was mixed in 1.5ml tube with $CaCl_2$ and the volume was made up to 120µl with pharmacy grade water then mixed with 120µl of 2x HBSS by adding the content of both tubes to another tube using two pipettes at the same time to mix well. To each well 240µl of relevant transfection mixture was added dropwise and the culture vessel was rocked gently back and forth to distribute the mixture evenly over the cells. The cells were incubated with the transfection mixture for another 24h then the medium with the transfection mix was discarded and 2ml fresh GM was added per well and incubated for a further 24h before commencing experiments.

Judging from the resulting eGFP fluorescence, (obtained on the Scan^R/Cell^R imaging system (Section 2.2.5)) this gave high transfection efficiency as shown in Figure.4.2 and from the result of transport experiments (Chapter 4).

**Table 2.1. Calcium phosphate transfection mixture.**

| | **GFP-vector (p29) µl ×1 well** | | **SNAT2-eGFP (µl) ×1 well** | |
|---|---|---|---|---|
| | **Tube1 (µl)** | **Tube2 ×2HBS (µl)** | **Tube1 (µl)** | **Tube2 ×2HBS (µl)** |
| **cDNA** | 0.4 | 120 | 0.6 | 120 |
| **$CaCl_2$** | 15 | | 15 | |
| **Pharmacy water** | 104.6 | | 104.4 | |

### 2.5.2 TransIT®-2020 transfection

TransIT®-2020 transfection reagent (Mirus) is a very effective transfection reagent, serum compatible and with low toxicity which eliminates the need for changing media after transfection and the cells can be kept in the media with the transfection mix up to 48h. This transfection reagent was used in the GFP-Trap®_immunoprecipitation experiment of SNAT2-eGFP in which high transfection efficiency is crucial. Following manufacture's instructions, the transfection procedure was as follows. The HEK293A cells were plated at 25 x $10^4$ cells per well in collagen coated Nunc 35mm 6-well plates in 2ml growth medium (Sigma-DMEM-D6429) and incubated overnight. The transfection mixture was prepared by adding 20µl of Opti-MEM I Reduced-Serum Medium (Gibco-Life Technologies-Ref. 31985-062) in a sterile tube and 2µg per well SNAT2-eGFP or GFP-empty vector was added and mixed by gently pipetting. The TransIT®-2020 transfection reagent was pre-warmed to room temperature before use and 7µl was added to the diluted plasmid DNA then mixing again by pipetting. The tube was incubated at room temperature for 30 minutes to allow formation of transfection mix and added to the well dropwise. The tissue culture

vessel was gently rocked back and forth and side to side to allow even distribution of the transfection mix and the cells were incubated for 48h with the transfection mix before experiments.

### 2.6 Immunoprecipitation of GFP-SNAT2

In this procedure HEK293A cells were plated in collagen coated 9cm Petri dishes at 100 x $10^4$ cells / Petri in 10ml growth medium overnight. The cells were transfected at ~80% confluent with SNAT2-eGFP and GFP-empty vector using TransIT®-2020 transfection reagent. The GFP-Trap method used to isolate SNAT2-eGFP used GFP-Trap®_MA (Chromotek- gtma-20). Following the manufacture's instructions, 500µg of SNAT2-eGFP and GFP-empty vector as a control for the experiment was used. The GFP-Trap®_MA beads were washed twice by adding 25µl of beads to 500µl ice cold lysis buffer (Appendix B.6.1), vortexing and separating the beads again using a magnetic rack. The cell lysate was added to the magnetic beads after saving 50 µl (diluted cell lysate) then mixed beads and lysates were incubated in an end-over-end tumble mixer overnight at 4°C. Next day the beads were separated using a magnetic rack, 50 µl from the supernatant was saved for immunoblot analysis (cell lysate from first wash) and the rest was discarded. The beads were washed twice with 500µl lysis buffer and separated by a magnetic rack then the beads were resuspended in 50µl sample buffer (Appendix B.6.2) and boiled for 5 minutes on a heating block. The beads were separated again by magnetic rack and the supernatant was loaded on a 12% SDS gel. After the run completed, the gel was stained using RAPID stain reagent (Calbiochem. Cat no. 553215) then the stained SNAT2-eGFP and GFP-empty vector bands were cut and sent to the PNACL Proteomics facility in the University of Leicester for Mass Spectrometry analysis.

### 2.7 Fluorescence imaging and quantification

The fluorescence imaging was taken after transfecting the cells (HEK293A or L6 cells) using an inverted Olympus IX81 motorized microscope with a Scan^R screening platform and a Cell^R imaging station (Advanced Imaging Facility, University of Leicester). When it was required, the GFP intensity was measured and quantified using ImageJ software as described in:

https://sciencetechblog.com/2011/05/24/measuring-cell-fluorescence-using-imagej.

## 2.8 Protein measurement Assays

### 2.8.1 Lowry Protein Assay

The Lowry protein assay (Folin assay) (Lowry *et al.,* 1951) was used to measure the total protein content of cell lysates in transport activity experiments. BSA protein standards (Appendix B.4) made up at 0 to 500µg / ml in 0.5M NaOH were used to calibrate the protein content in the samples. For each assay, fresh Reagent C was prepared by mixing Reagent A and Reagent B (Appendix B.2 and B.3 respectively) with a ratio 50:1 (A: B v/v); and Ciocalteu's Folin Phenol reagent (Sigma F-9252) was diluted 2:1 v/v with ultra-pure water. To 50µl BSA standards or cell protein samples in 0.5M NaOH, 600µl of Reagent C was added and immediately vortexed. After exactly 10 min, then 60µl of the diluted Ciocalteu reagent was added and vortexed again, and then incubated for 30 min at room temperature. The OD at 650nm was read on a Titertek Multiskan Plus MKII spectrophotometer. The protein concentration in the samples was calculated from the optical density of the protein standards.

### 2.8.2 Bio-Rad detergent-compatible (DC) protein assay

As the Lysis Buffer (Appendix B.6.1) that was used to prepare cells for Western blotting (Section 2.11.3) contained detergent which interferes with the Lowry protein assay, to measure the protein content of cell lysates for Western blotting a Bio-Rad detergent-compatible (DC) protein assay kit (Bio-Rad 500-0113) was used. In this assay 5µl of cell lysate or standards (0-2000µg/ml BSA in 1% IGEPAL detergent) was added to 96 well plates in triplicate and 25µl of kit Reagent A - an alkaline copper tartrate solution (with 20µl of supplementary reagent S added to each ml of reagent) was added to each well then 200µl of Reagent B - a diluted Folin-like reagent, and incubated for 15 min at room temperature, and the absorbance was read at 750nm.The protein concentration in the samples was calculated from the optical density of the protein standards.

## 2.9 Transport activity assay ($^{14}$C MeAIB uptake measurement)

The activity of System A amino acid transporters in intact cell was assessed according to the amount of the selective System A substrate α-[1-$^{14}$C]-

methylaminoisobutyric acid (MeAIB) taken up by the cells in 5 minutes at room temperature. After incubating the cells on 22mm culture wells with appropriate experimental test media (depending on the purpose of experiment), the cells were rinsed twice with 1ml of Hepes-buffered saline (HBS) (Appendix A.8) then 500µl of HBS was added to each well. The transport experiment was started by adding a 10µl aliquot of α-[1-14C]-Methylaminoisobutyric acid (NEN-Du Pont NEC 671, 1.85MBq or 50µCi in 500ul of 0.01M HCl; about 50 pCi/pmol) to give a final concentration of 10µM in the culture well. In some culture wells 10mM unlabelled MeAIB (Sigma M-2383) was also present in the well as a negative control to assess non-specific binding. The plate was swirled to mix the $^{14}$C MeAIB with the medium, incubated at room temperature for exactly 5 minutes, and then immediately placed on a tray of ice to stop the transport. The medium was aspirated and the wells washed three times with 1ml of ice-cold 0.9% w/v NaCl followed by observing the cells under the microscope to check that they were still attached to the wells. The plates were then stored at -20°C until processed as described below.

### 2.9.1 Preparation of cell lysates for counting the radio-activity

After the transport activity incubation, cell lysates were prepared by scraping each well in 200µl 0.05M NaOH and transferring the scrapings into 1.5ml micro centrifuge tubes. The tubes were incubated in a water bath at 70°C for 30 min to digest the cells. From the cell digest, 110µl was added to 4ml of Ecoscint A scintillant (National diagnostics LS-273) then incubated in the dark for two hours at room temperature to allow chemiluminescence to decay, followed by counting with quench correction to determine disintegrations per minute (dpm) on an LKB 1219 liquid scintillation counter. The $^{14}$C-MeAIB dpm count in the non-specific binding control cultures was subtracted from the count in the other cultures to determine net $^{14}$C-MeAIB transport into the cells. The number of pmol transported was calculated from the $^{14}$C-MeAIB specific radio-activity of 50pCi/pmol or 110dpm/pmol stated by the manufacturer.

## 2.10 Total phosphoprotein tyrosine phosphatase (PTPase) catalytic activity assay

This assay was performed to measure the total phosphoprotein tyrosine phosphatase (PTPase) catalytic activity in L6 myotube cell lysates, using a

PTPase assay kit (Promega V2471) following manufacturer's instructions (summarised in Figure 2.5). Briefly, after experimental incubations in 22mm culture wells, myotubes were scraped in a pre-chilled 100µl aliquot of lysis buffer on ice (Appendix B.6.1). The cell lysates were cleaned to remove free inorganic phosphate (Pi - which is a potent phosphatase inhibitor) by passing each individual sample through a Sephadex® G-25 column. After cleaning, each sample was mixed with an equal volume of 100% glycerol. A 10µl aliquot of the cell lysate was then incubated with 5µl of the stock solution of phosphorylated peptide substrate (Tyr Phosphopeptide-1: END(pY)INASL, or Tyr Phosphopeptide-2: DADE(pY)LIPQQG) provided in the kit, or 5µl of ultra-pure water as a control, for 90 minutes at room temperature. After this incubation, 50µl of freshly made Malachite Green phosphate colour reagent was added then incubated for another 15 minutes at room temperature to allow colour development before reading the absorbance at 595nm using a MultiSKAN FC Thermo Scientific plate reader.

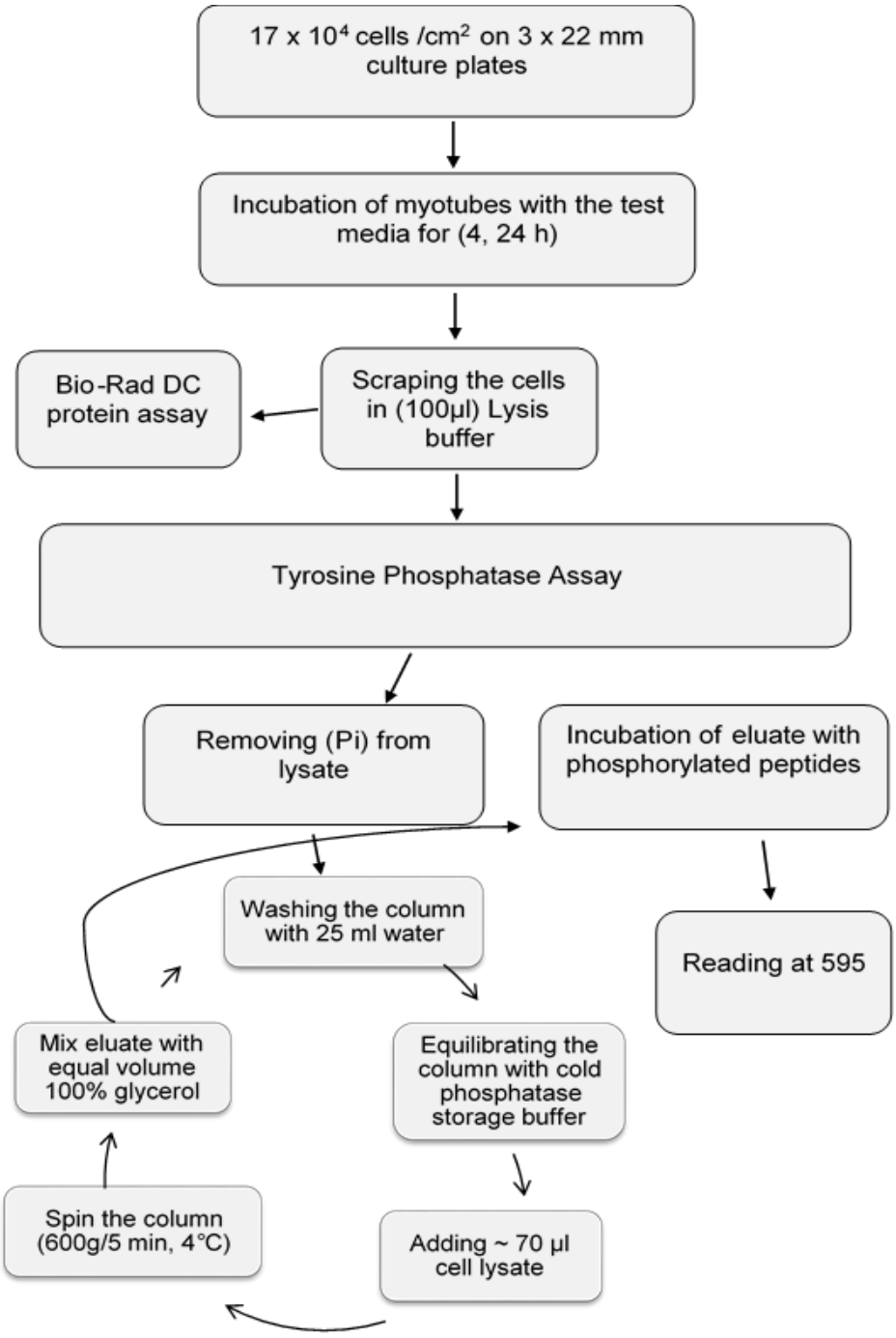


**Figure 2.5. Schematic diagram of procedure for total phosphoprotein tyrosine phosphatase catalytic activity measurement.**

## 2.11 Sodium Dodecyl Sulphate Polyacrylamide Gel Electrophoresis (SDS-PAGE)

### 2.11.1 Preparing the samples for SDS-PAGE

At the end of the experimental incubation, the culture plates were immediately put on ice and each 35mm well was scraped in 200µl of pre-chilled Lysis buffer (Appendix B.6.1). Each lysate was transferred to a 1.5ml micro centrifuge tube on ice and centrifuged on a refrigerated micro centrifuge at 13,000 rpm for 10 minutes at 4°C to remove insoluble debris. A Bio-Rad DC protein assay was carried out (Section 2.8.2) to determine the amount of cell lysate required to deliver 30µg of protein. The calculated amount of lysate was mixed with the same volume of SDS-reducing sample buffer (Appendix B.6.2) and heated on a heating block (Grant QBT2) at 100°C for 5 minutes.

### 2.11.2 Running the gel

Discontinuous Laemmli gels (Laemmli 1970) (1.5mm thick with 12% polyacrylamide in the resolving gel) were placed in an electrophoresis tank with running buffer (Appendix B.6.5) and the samples prepared in Section 2.11.1 were loaded into the sample wells, with molecular weight standards (Full-Range Rainbow MW Markers 10-250kDa, Fisher Ref 11580684) in one lane. The electrophoresis was run on a Bio-Rad Mini-Protean® system at 200 volts until the bromophenol blue dye front approached the end of the gel.

### 2.11.3 Western blotting

The proteins that had been separated by SDS-PAGE were blotted onto a 0.45µm nitrocellulose membrane (Fisher Ref 10773485) in a wet transfer cell in transfer buffer (Appendix B.6.4) at 80 volts for two hours in the presence of an ice block with continuous stirring to keep the transfer cool. The membranes were washed with x1 Tris-buffered Saline with 0.5% Tween 20 (TTBS) three times and blocked with 5% w/v milk powder in x1 TTBS for one hour, followed by three washes with x1 TTBS and overnight incubation at 4°C on a rocker with the primary antibodies shown in Table 2.2. After incubation with the primary antibody, three further washes were then carried out with x1 TTBS, and the membranes were then incubated with the secondary antibody shown in Table 2.2 for two hours at room temperature to detect the primary antibody. The membranes were then washed with x1 TTBS three times, 10 minutes per wash, and chemiluminescence on the

membranes was generated using an ECL kit (Thermo Scientific-34080) with detection of the fluorescence using Kodak BioMax Light film or ChemiDoc™ Touch Imaging System. The positions of the bands were compared with the molecular weight standards to confirm the size of the detected proteins.

### 2.11.4 Quantification and data analysis

Using digital images of the membrane taken as described above, the bands were quantified and analysed using Image Lab ™ software.

**Table 2.2 details of antibodies**

| Antibody Against | Source | Ref/lot No. | Dilution | Diluted in | Block-ing agent | Secondary Antibody |
|---|---|---|---|---|---|---|
| **$P^{Ser473}$-AKT** | NEB | D9E | 1:1000 | TTBS | 5%Milk powder | R |
| **Total AKT** | NEB | 9272 | 1:1000 | TTBS | 5% Milk powder | R |
| **GFP** | Cell Signaling | 2956 | 1:1000 | 5% w/v BSA in TTBS | 5% Milk powder | R |
| **β-Actin** | Abcam | Ab6276 | 1:10,000 | TTBS | 5% Milk powder | M |
| **$P^{Ser235/236}$ rpS6** | Cell Signaling | 2211/11 | 1:1000 | TTBS | 5% Milk powder | R |
| **Total rpS6** | Cell Signaling | 2217 | 1:1000 | TTBS | 5% Milk powder | R |
| **$P^{Thr172}$AMPK** | Cell Signaling | 2535/4 | 1:1000 | 5% w/v BSA in TTBS | 5% Milk powder | R |
| **AMPK** | Cell Signaling | 2532/19 | 1:1000 | 5% w/v BSA | 5% Milk powder | R |
| **$P^{Thr202}$-ERK1/ $P^{Tyr204}$-ERK2** | Cell Signaling | 9101 | 1:1000 | 5% w/v BSA | 5% Milk powder | R |
| **Total-ERK2** | Cell Signaling | 9108 | 1:2000 | 5% w/v BSA | 5% Milk powder | R |
| **P $^{Thr183/Tyr185}$ JNK** | Promega | V7931/7 | 1:4000 | 5% w/v BSA | 5% BSA | R |
| **Total JNK2** | Cell Signaling | 9258 | 1:4000 | 5% w/v BSA | 5% Milk powder | R |
| **P $^{Thr180/Tyr182}$p38** | Promrga | V121A/7 | 1:1000 | 5% w/v BSA | 5% BSA | R |
| **Total p38** | Cell Signallig | 9217S | 1:1000 | 5% w/v BSA | 5% Milk powder | M |

R: HRP conjugated Goat anti Rabbit IgG (1:1000) (Dako P0448)
M: HRP conjugated Goat anti Mouse IgG (1:1000) (Dako P0260)

## 2.12 RNA techniques

### 2.12.1 PCR primer design and optimisation

Rat SNAT2 and rat Cyclophilin primers were a gift from Dr Emma Watson, Department of Infection, Immunity & Inflammation. University of Leicester and had previously been optimised and their sequences checked (Clapp, 2010). Primers for rat protein tyrosine phosphatase 1B (PTP1B) (RGD reference RGD:61965; NCBI reference NM_012637.2) were designed using https://www.ncbi.nlm.nih.gov/tools/primer-blast/index.cgi?LINK_LOC=BlastNoResAd then optimised for the best annealing temperature by running the PCR amplification (Section 2.12.3.2) at four different annealing temperatures (52°C, 58°C, 59°C and 60°C) followed by agarose gel electrophoresis of the PCR amplification products as described in Section 2.12.4. The most intense signal on the gel was obtained using 59°C. The primer efficiency was determined by measuring the slope of a standard curve which was obtained by plotting $C_T$ (Figure 2.6) (measured as described in Section 2.12.3.2) versus amount of serially diluted cDNA using seven descending concentrations of the cDNA (1:5 dilution) The efficiency was 96.25%.

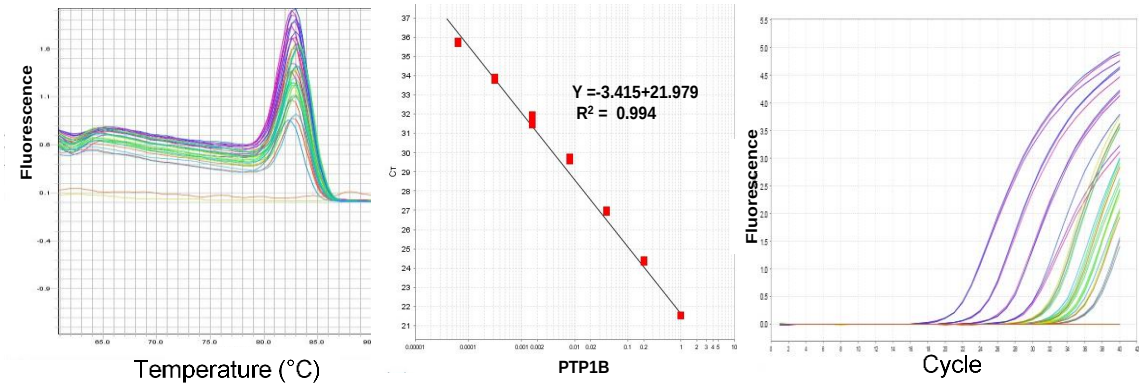


**Figure 2.6. Standard curve, amplification and melt curve of PTP1B amplicon.**

The primer efficiency was determined by measuring the slope of a standard curve which was obtained by plotting $C_T$ versus amount of serially diluted cDNA using seven descending concentrations of the cDNA (1:5 dilution) of eight serial dilutions. The efficiency was 96.25%.

### 2.12.2 PCR amplicon sequencing

The qPCR product obtained using the PTP1B primers following PCR amplification (Section 2.12.3.2) was isolated by running out the amplicon on a 1% agarose gel (Section 2.12.4) and visualised under UV light from a trans-

illuminator. Then the band was cut out with a scalpel and placed in a pre-weighed tube to determine the weight of gel that had been sampled. The amplicon was purified from the gel using a QIAquick® Gel extraction kit (Qiagen-28706) following the manufacturer's instructions. Three volumes of buffer QG (provided with the kit) were added to one volume of gel (assuming that 100mg of gel is ~ 100µl). The tube was incubated at 50°C using a heating block for 10 min or until the gel slice dissolved completely, with vortexing for 2-3 min if required. After that one volume of isopropanol was added to the tube and mixed by vortexing. The sample was transferred to a QIAquick spin column and the column placed in a 2ml collection tube and spun for 1 min to bond the DNA to the column. The flow through was discarded and the column was put back in the collection tube and 500µl of buffer QG was added to the column and centrifuged for one minute. After discarding the flow through, the DNA on the QG column was washed with 750µl buffer PE and centrifuging again for 2 minutes. Finally, the column was placed in a clean 1.5ml centrifuge tube and 50µl of buffer EB (10µM Tris.HCl, pH 8.5) was added to the column and incubated for 1 min at room temperature and centrifuged for 1 min. The eluted DNA was quantified using a Nano-Drop 1000 V3.71 spectrophotometer. To check that the DNA had been eluted intact, an aliquot of the cleaned qPCR product was run out on a 4% low melting point agarose gel. The remaining cleaned sample was then sent to the Protein and Nucleic Acid Chemistry Laboratory (PNACL), University of Leicester for sequencing (3730 sequencer, Applied Biosystems, Warrington, UK). The resulting sequence was checked on NCBI BLAST and showed 98% identity to the predicted amplicon.

### 2.12.3 L6 myotube RNA extraction

RNA was extracted from L6 myotubes using Trizol® reagent (Life Technologies 15596) - 1.5ml per 25cm$^2$ flask or 600µl per 35mm culture well. The cells were incubated in Trizol at room temperature for 5 minutes and the resulting cell digest was transferred into autoclaved screw capped 2ml polypropylene tubes, to which 200µl of Molecular Biology grade chloroform (Sigma-302432) per ml of Trizol extract was added. The tubes were vortexed thoroughly and then were centrifuged at 13,000 rpm for 15 minutes at 4°C on a micro centrifuge. The upper clear phase which contained RNA was transferred into another autoclaved 2ml tube. The RNA was precipitated by adding (750µl per 25cm$^2$ flask or 300 µl per

35mm well) of molecular biology grade isopropyl alcohol (propan-2-ol), vortexed gently and incubated at room temperature for 10 minutes to complete the precipitation. Next the tube was micro centrifuged at 10,000rpm for 10 minutes at 4°C. After centrifugation, a very faint RNA pellet was visible at the bottom of the tube. The isopropyl alcohol was decanted and the RNA pellet washed by adding 1ml of RNAase free 75% ethanol. The tube was vortexed gently and micro centrifuged at 10,000rpm for 10 minutes. Finally, the ethanol was discarded and the RNA pellet at the bottom of the tubes allowed to dry in air for 10 minutes. The RNA was then dissolved by adding 20µl of RNAase-free diethyl pyrocarbonate-treated (DEPC) water. The concentration of RNA was measured from the absorbance at 260nm on a Nano-Drop 1000 V3.71 spectrophotometer and the sample was stored at -80°C.

#### 2.12.3.1 Reverse transcription (RT) reaction (cDNA synthesis)

For the RT reaction, an AMV Reverse Transcription System (Promega A3500) was used to synthesise cDNA from the samples prepared in Section 2.12.3) following manufacturer's instructions. Samples were diluted to 0.5µg/µl with DEPC water and an RT master mix was prepared as described in Table 2.3. From the RT master mix 18µl was added into a thin wall PCR tube with a 2µl RNA sample (i.e. 1µg of total RNA per reaction). The tubes were placed on a PCR thermal cycler (Techne Genius, TC-3000X) on the following program:

- Cycle 1, Segment 1, 42°C, Hold Time (1h) for synthesis time.
- Segment 2, 99°C, Hold Time (5 min) for enzyme inactivation.
- Segment 3, 4°C, Hold Time (5 min) or leave over-night.

At the end the samples were stored at -20°C.

**Table 2.3. Reverse transcription master mix.**

| Component | Amount |
|---|---|
| $MgCl_2$, 25mM | 4µl |
| Reverse Transcription 10x Buffer | 2µl |
| dNTP Mixture, 10mM | 2µl |
| Recombinant RNasin Ribonuclease Inhibitor | 0.5µl |
| AMV Reverse Transcriptase | 0.75µl (15U) |
| $Oligo(dT)_{15}$ Primers | 1µl (0.5µg) |
| DEPC Water | 7.75µl |
| **Total** | **18.0µl** |

### 2.12.3.2 Quantitative real time- polymerase chain reaction (qPCR)

The qPCR reaction was performed by adding 1µl of the cDNA prepared in Section 2.12.3.1 to 24µl of a qPCR master mix. The master mix was made by mixing 12.5µl of Power SYBER®Green PCR Master Mix (Applied Biosystems; Cat No. 4367659) with 10.5µl of nuclease-free water, 0.5µl of Forward Primer and 0.5µl of Reverse Primer. (Details of primers used are in Table 2.5). Samples were then mixed by pipetting. Negative control samples were also prepared by adding 1µl of DEPC water in place of the cDNA in the mixture above. An Applied Biosystems 7500 Fast Real-Time PCR System was then used to perform Real-time PCR analysis by applying the following thermal cycling:

**Table 2.4. Real time QPCR thermal cycle.**

| Thermal cycle | | | | | | |
|---|---|---|---|---|---|---|
| Stage 1 | Stage 2 | Stage 3 | | Stage 4 | | |
| Reps 1 | Reps 1 | Reps 40 | | Reps 1 | | |
| 50°C | 95°C | 95°C | 60°C | 95°C | 60°C | 95°C |
| 2 min | 10 min | 15 sec | 1 min | 15 sec | 1 min | 15 sec |

The relative gene expression level was normalised to the corresponding Cyclophilin signal and the gene expression was represented as a fold change in relation to the control condition in the experiment (ΔΔCt) according to the following equation (Pfaffl, 2001):

$$\text{Ratio} = \frac{(E^{\text{Target}})^{\text{Delta CT Target (Control – Treatment)}}}{(E^{\text{Reference}})^{\text{Delta CT Reference (Control – Treatment)}}}$$

E = PCR efficiency and $C_T$ = comparative threshold value.

**Table 2.5. Primers used for qPCR.**

| Primer (Rat) | | Sequence | Length | Product size (bp) | NCBI Reference |
|---|---|---|---|---|---|
| PTP1B | F | TCGTCAGTGCAGGATCAGTG | 20 | 102 | NM_012637.2 |
| | R | CTCCAATGTGCGTTTGGGTG | 20 | | |
| SNAT2 | F | GCTCATTCTCCCATTGTCAC | 20 | 105 | NM_181090.2 |
| | R | TTGCAAATCACCACAATCAG | 20 | | |
| Cyclophilin | F | CACCGTGTTCTTCGACATC | 19 | 88 | NM_017101.1 |
| | R | TGCTGTCTTTGGAACTTTGTC | 21 | | |

### 2.12.4 Agarose gel electrophoresis of PCR amplicons

Agarose gel electrophoresis was performed using 1% agarose gels (Sigma-A9539) in 40mM Tris-Acetate, 1mM EDTA, pH 8.3 (1x TAE) and 0.3µg/ml Ethidium Bromide (Sigma E-1510). After the gel set it was placed in a buffer chamber filled with 1x TAE buffer (Fisher Bioreagent. Lot.110789). DNA samples (qPCR amplification products) were mixed with sample loading dye (Sigma-G2526) and loaded on the gel, accompanied by a DNA Size Marker Ladder (φX174 Hae III Digest) (Sigma D-0672). The gel was run at 100 volts until the dye front reached to the middle of the gel. Then the samples were visualised under UV illumination on a UV transluminator to confirm the size and relative intensity of the bands.

### 2.12.5 SNAT2 siRNA Silencing

SNAT2 silencing using siRNA was performed as described previously in this laboratory using a validated siRNA (Evans *et al* 2007, 2008). The custom-

synthesised siRNA oligonucleotides were provided by Eurogentec. The oligonucleotides were supplied in solution as ds siRNA in 50mM TRIS-HCl, 100mM NaCl, and pH 7.6 at a concentration of 100µM. The SNAT2 silencing siRNA (SIL) had a forward sequence of 5'-CUGACAUUCUCCUCCUCGUdTdT which was directed against base position 1095 onward in the SNAT2 gene sequence (Evans *et al.,* 2007; Evans *et al.,* 2008). To control for non-specific functional effects of siRNA transfection, scrambled SNAT2 (Scr) siRNA control was also used in parallel transfections containing the same overall base composition as for SNAT2 SIL but in randomised sequence (forward sequence 5'-CGCUCAACUCUACUUGUCCdTdT).

#### 2.12.5.1 SNAT2 siRNA transfection

L6 myoblasts were seeded at low density for these experiments because it has been shown previously in this laboratory that gene silencing by siRNA oligonucleotides is more effective in unfused myoblasts (Evans, 2009). L6 myoblasts was plated at 5 x $10^4$ per well on 2.2cm 12-wells, 10x$10^4$ per well on 3.5 cm 6-wells and 33 × $10^4$ per flask in 25$cm^2$ flasks in DMEM Growth Medium (Section 2.2.2). After overnight incubation, the Growth Medium was discarded and half the normal volume of fresh GM was added to the culture vessels and the cells were transfected with SNAT2 siRNA using a Profection Calcium Phosphate transfection kit (Promega E1200). Details of transfection mixture are shown in Table 2.6. The stock of pre-annealed siRNA oligonucleotide supplied by the manufacturer was diluted before use to 20µM by adding nuclease-free water. A transfection blank (T), containing transfection reagent only without oligonucleotides was used to detect any stress that may arise from transfection reagent. The content of Tube 1 and Tube 2 were mixed by pipetting and added to the culture well drop-wise:

60µl/2.2cm 12-well, 150µl/3.5cm 6-well and 395µl/25$cm^2$ flask.

The culture plate was then gently rocked backwards and forwards to ensure even distribution of transfection mixture over the cells. The final concentration of siRNA in the culture medium was 30nM: the cells were incubated in a culture incubator at 37°C for 16 hours then the medium was changed to double the normal volume of Growth Medium (i.e. 2ml per 2.2cm well, 4ml per 3.5cm well

and 13ml per 25cm$^2$ flask for another 24 hours. On day 4 this medium was aspirated and experimental incubations and measurements were performed.

**Table 2.6. siRNA transfection mixture for L6 transfection.**

| | Tube 1 | Tube 2 | | | |
|---|---|---|---|---|---|
| Transfection Mixture Label | 2×HBS * (µl) | 20µM Scr. SNAT2 siRNA (µl) | 20µM SIL SNAT2 siRNA (µl) | Nuclease-Free Water (µl) | 2M $CaCl_2$ (µl) |
| **T** | 310 | ---- | ---- | 271 | 39 |
| **Scr** | 310 | 7 | ---- | 264 | 39 |
| **SIL** | 310 | ---- | 7 | 264 | 39 |

*Hepes-buffered saline (Promega-E110A).

## 2.13 Measuring the intracellular free amino acids in HEK293A cells by high performance liquid chromatography (HPLC)

At the end of experimental incubations, the culture plate was placed on ice and the experimental medium was discarded and the cells rinsed three times with 2ml/3.5cm well of pre-chilled 0.9% w/v NaCl to remove the extracellular amino acids. The cells were then scraped in 150µl 0.3M Perchloric Acid (PCA). The cell scrapings were incubated on ice for 30 minutes to allow as much protein as possible to precipitate followed by centrifugation for 10 minutes using a Jouan CR422 centrifuge at 3000 x g at +4˚C. The precipitated proteins were dissolved in 1ml 0.5 NaOH and Lowry protein assay was performed as described above (Section 2.8.1). To neutralise the acid, the supernatant was mixed with an equal volume of Freon-Tri-octylamine Mixture (FTO) (pre-chilled on ice) which was prepared immediately before use by mixing 0.22ml of Tri-octylamine and 0.78ml of Freon. The tubes were vortexed vigorously for 60 seconds and quickly pulsed on a micro-centrifuge to separate the phases. Three layers were visible: the neutralised aqueous top phase was filtered using a 0.45 µm micro filter and stored at -80°C. The extracted intracellular amino acids in these samples were

measured on an Agilent 1100 high performance liquid chromatograph with a Zorbax Eclipse AAA column (4.6x75mm, 3.5μm) at 40°C with *o*-phthalaldehyde/3-mercaptopropionate/9-fluorenylmethylchloroformat precolumn derivatization and ultraviolet post-column detection. The amino acid concentration was normalised to the total protein content in the culture and presented as pmol of amino acid per mg of protein.

### 2.14 Statistical analysis

Unless stated otherwise, pooled data are presented from at least 3 independent experiments. Data were analysed using GraphPad Prism 7.0. Data normality was checked with the D'Agostino-Pearson normality test. Normally distributed data are presented as the mean ± SEM, and were analysed by Student's t-test or by repeated measures ANOVA, followed by Tukey's multiple comparisons test. Non-normally distributed data are presented as linked data curves for the individual experiments, and were analysed by Friedman's nonparametric repeated measures ANOVA, followed by Dunn's multiple comparison test.

# Chapter 3 Signals from glucocorticoid to SNAT2 in L6 skeletal muscle cells

## 3.1 Introduction

As explained previously (in Section 1.17), glucocorticoid (GC) is known for its anti-inflammatory effect as a drug or hormone and is widely used to treat different immunological disorders as an anti-inflammatory and immune suppressive agent, in asthma and many other diseases (Klein, 2015). However, GC either as a steroid-based treatment, or through increase in its endogenous level due to disease conditions, can cause muscle wasting (Klein, 2015). CKD patients are characterised by muscle wasting, and metabolic acidosis is one of the factors that enhances muscle protein degradation in this population (Kraut & Madias, 2016). *In vivo* studies in rat showed that presence of GC is essential for acidosis-induced protein degradation (May *et al.,* 1986). Furthermore, metabolic acidosis increases GC activity *in vivo* leading to amino acid degradation and protein turnover (Buehlmeier *et al.,* 2016). In earlier preliminary experiments in this laboratory, an inhibitory effect of the synthetic glucocorticoid Dexamethasone (DEX) seemed to occur on System A (SNAT2) amino acid transporter activity in L6 myotubes in the presence of 2% serum (Clapp, 2010) (PhD thesis, University of Loughborough). This is of interest because SNAT2 has been proposed as a potential sensor of metabolic acidosis (Section 1.11).

Therefore, the aims of the experiments in this chapter were:

- To investigate the effect of DEX on System A activity in L6-myotubes and the possible role of phosphorylation events in this effect.
- To investigate the possible role of the ubiquitin-proteasome pathway (UPP) in the regulation of System A (SNAT2) activity by DEX.

Dexamethasone was used in this project because it has a long biological half-life, and has been used previously to mimic the effect of glucocorticoids *in vivo* (Putney *et al.,* 1997; Zheng *et al.,* 2010), including effects on muscle protein degradation (May *et al.,* 1986).

## 3.2 Results

### 3.2.1 The effect of DEX on System A (SNAT2) transporter activity

Initial characterisation of the effect of DEX on System A transport in L6 myotubes in the presence of 2% serum was performed by incubating with DEX and comparing with control cultures incubated with DMSO vehicle only. This showed that DEX significantly inhibited transport activity, with optimum effect (about 60% decrease) observed after 4h of incubation (Figure 3.1) with a dose of 500nM DEX. As little as 5nM gave a statistically significant but smaller effect (Simms, 2013). Full differentiation of the cells to myotubes was not required, as a similar response was also observed with confluent unfused L6 myoblasts (Figure 3.2). Initial studies also showed that the effect was occurring through a classical glucocorticoid receptor, triggering transcriptional events (Section 1.17. 3.1) as it was blocked by the glucocorticoid receptor antagonist RU38486 and by the transcription inhibitor actinomycin D (Figure 3.3 A and B respectively). It was also observed that the effect of DEX was partly blunted by the broad-spectrum phosphatase inhibitor vanadate (100µM sodium orthovanadate) (Figure 3.4), possibly indicating that a phosphotyrosine protein phosphatase or an ATPase was involved. The significance of this observation in the role of protein phosphorylation signals in the action of DEX is considered in more detail in Section 3.2.3 below.

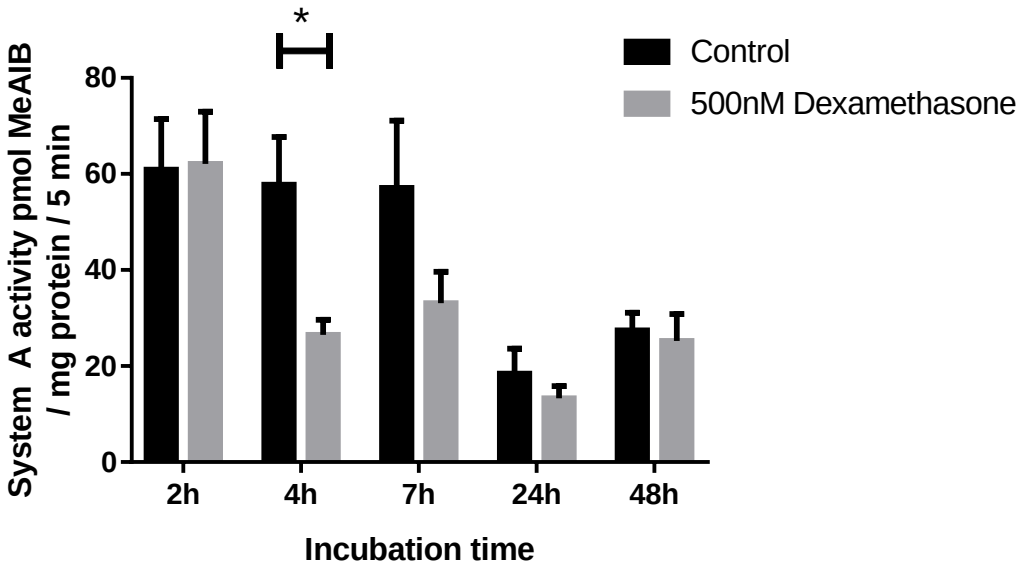


**Figure 3.1. Time course of the inhibitory effect of Dexamethasone on System A transport activity in L6-G8C5 myotubes.**

The cells were incubated in growth medium (DMEM with 10% serum) for 3 days, then on day 4 the medium was replaced by MEM + 2% serum, and on day 5 fresh MEM + 2% serum was added again for another three days to induce myotube formation. On day 8, myotube formation was confirmed by phase contrast microscopy and immunohistochemistry was performed as explained in Section (2.2.5). The cells were then incubated in test medium based on MEM with 2% dialysed serum (2% DFBS) with 500nM DEX, or Control medium (with DMSO vehicle at 0.0005% vol/vol) for the incubation times as shown. After incubation, System A transport activity was measured according to the amount of $^{14}C$ labelled MeAIB transported into the cells. The data are presented as Mean ± SEM from three independent experiments (n=3) independent experiments. * Denotes that the DEX condition is significantly different from the Control condition $P<0.05$.

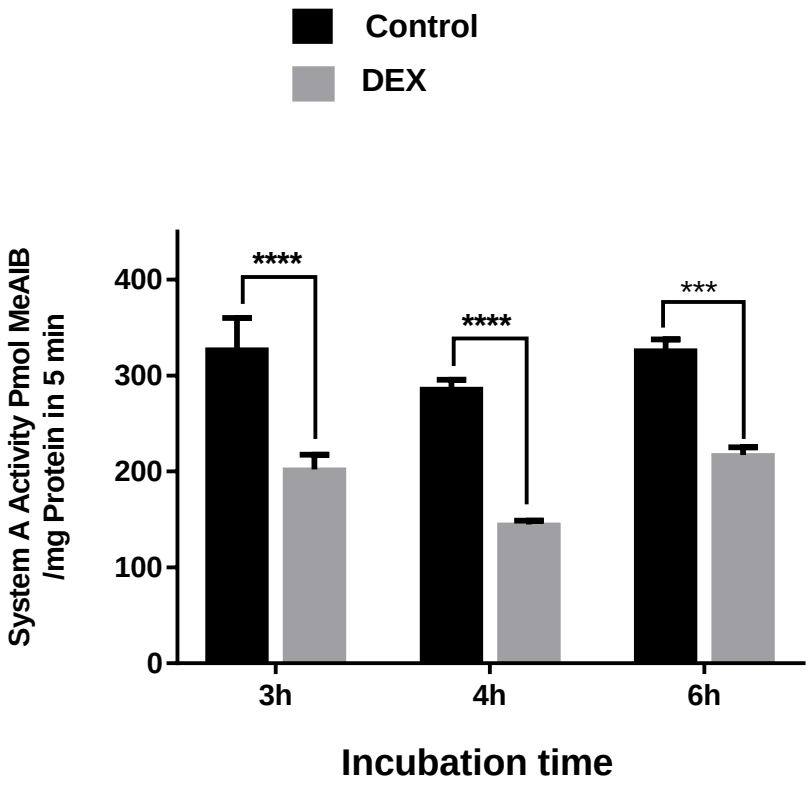


**Figure 3.2. The inhibitory effect of DEX on System A amino acid transporter activity in L6 myoblasts before fusion to myotubes.**

The cells were incubated under Control conditions (0.0005% vol/vol DMSO) or with 500nM DEX for 3h, 4h and 6h. The data are presented as Mean ± SEM of five independent experiments (n=5) with five replicate cultures in each experiment. **** P<0.0001, *** P=0.001 denotes DEX values which are significantly different from their Control condition

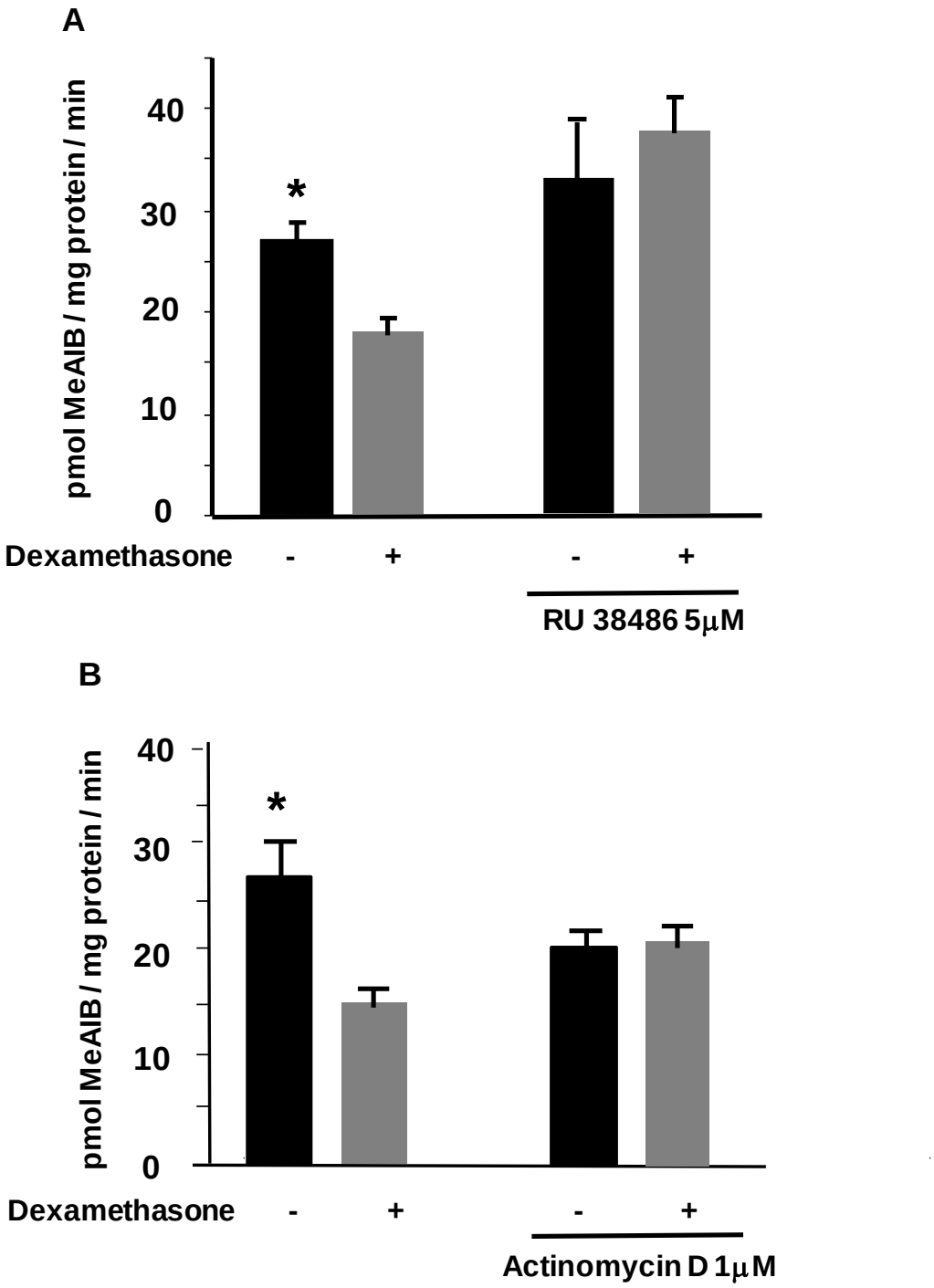


**Figure 3.3. The effect of Dexamethasone on SNAT2 transport activity in L6-myotubes depends on GC receptors and transcription.**

The cells were incubated with or without 500nM DEX for 4h. (A) Influence of 5μM glucocorticoid receptor antagonist RU38486 and (B) Effect of 1μM transcription inhibitor actinomycin D. The data are presented as Mean ± SEM of three independent experiments (n=3) (A) and four independent experiments (n=4) (B). *Denotes conditions are significantly different from DEX treated conditions alone $P< 0.05$.

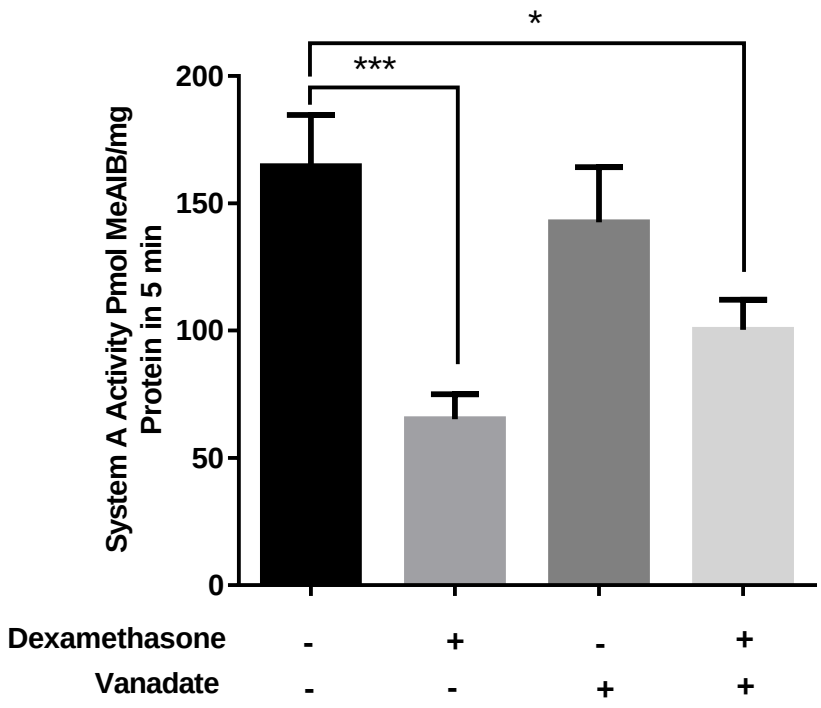


**Figure 3.4. Vanadate blunts the inhibitory effect of Dexamethasone in L6 myotubes.**

The cells were incubated for 4h under the experimental conditions shown in test medium based on MEM+2% dialysed serum (DFBS)): Control (0.0005% vol/vol DMSO); 500nM Dexamethasone; 100µM Sodium orthovanadate. The DMSO concentration was kept constant in all cultures. After incubation for 4h, System A transport activity was measured according to the amount of $^{14}C$ labelled MeAIB transported into the cells. Data are presented as Mean ± SEM. of seven independent experiments (n=7) (with five replicate culture wells for each treatment). *P<0.05, ***P< 0.001. In the presence of vanadate, the apparent inhibitory effect of Dexamethasone no longer reached statistical significance.

### 3.2.1.1 Serum withdrawal does not prevent the inhibitory effect of DEX on System A (SNAT2)

Dexamethasone might act on SNAT2 through two different pathways, first, directly on SNAT2 protein itself and second indirectly through a serum factor sending a glucocorticoid-inhibited insulin-like stimulatory signal to System A (Figure 3.5). For example GC is known to inhibit insulin-like anabolic signals in muscle cells, leading to muscle wasting (Schakman *et al.,* 2013), and SNAT2 is known to be the main insulin-stimulated amino acid transporter in mammalian cells (Section 1.13). To eliminate the contribution of the second pathway, in the present experiment the cells were incubated in serum-free media for 15h and the

effect of DEX and vanadate re-examined (Figure 3.6). The result showed the same gureinhibitory effect of DEX on SNAT2 as seen before with 2% serum (Figure 3.4) although the blunting effect of vanadate was less marked in serum-free media in comparison to 2% serum. The fact that under serum-free conditions DEX can still inhibit SNAT2 activity suggests that DEX may be exerting a relatively direct effect on SNAT2 activity, rather than acting indirectly by blunting a SNAT2-stimulating signal from an insulin-like factor in serum.

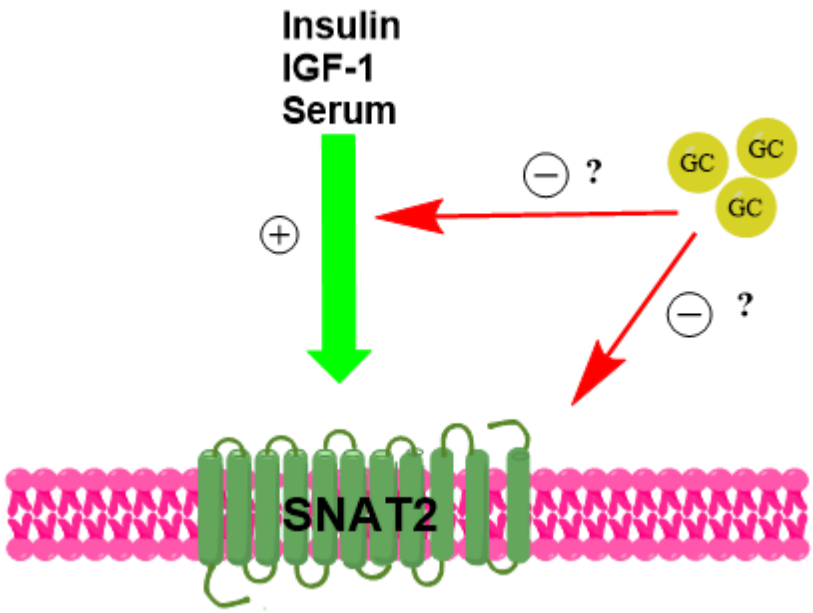


**Figure 3.5. A schematic diagram explaining the possible ways in which glucocorticoid may act on System A (SNAT2).**

In spite of this observation, 2% serum was used in all of the subsequent experiments as this was found to suppress the slight apoptosis that was observed in the cultures under serum-free conditions.

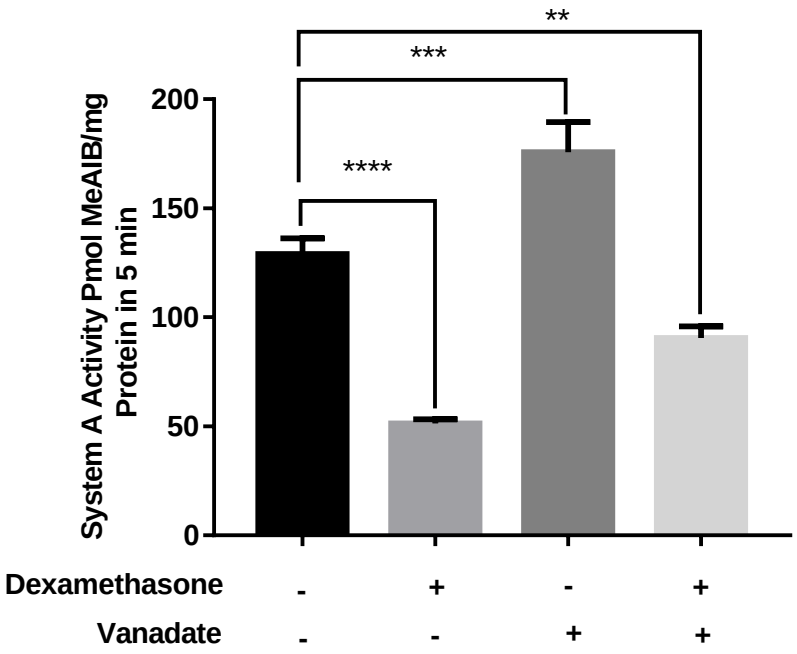


**Figure 3.6. Serum withdrawal does not prevent the inhibitory effect of DEX on System A activity in L6 myotubes.**

The cells were incubated in serum-free media (MEM) for 15h then the cells were rinsed with HBSS twice to remove the remaining serum from the cell layer. Cells were incubated for 4h under the experimental conditions shown: Control (0.0005% vol/vol DMSO)); 500nM Dexamethasone; 100µM Sodium orthovanadate and combination of both. The DMSO concentration was kept constant in all cultures. Data are presented as Mean ± SEM. of three independent experiments (n=3) (with five replicate culture wells for each treatment), **P<0.01, ***P<0.001 ****P< 0.0001.

A possible interpretation of the actinomycin D experiment (Figure 3.3B) is that DEX acts by inducing gene expression of a regulator of SNAT2 (e.g. an inhibitory protein kinase or an inhibitory phosphoprotein phosphatase). This may explain the apparent increase in System A activity in the presence of DEX when transcription is blocked with actinomycin D (Figure 3.3B). A series of inhibitor experiments was therefore performed to test this explanation.

### 3.2.2 Glucocorticoid-dependent protein kinase pathways

#### 3.2.2.1 Serum glucocorticoid–regulated kinase-1 (SGK-1)

Serum and Glucocorticoid-dependent Kinase 1 (SGK-1) (described in detail in Section 1.18) is a serine threonine kinase which shares sequence similarity with Akt and is regulated either by increasing its gene expression or phosphorylation of the protein by different mechanisms such as serum, glucocorticoid and growth factors for example transforming growth factor β (TGF-β) (Rosa *et al.,* 2003). In this experiment, the possibility of SGK-1 involvement in the inhibitory effect of DEX on System A amino acid activity was examined in L6 myotubes, as shown in Figure 3.7. The cells were incubated with a specific SGK-1 inhibitor for three different incubation times (4, 24 and 48h). However, under all of the conditions tested, SGK1 inhibitor had no blunting effect on DEX's action on System A activity – if anything at 4 and 24h it may have slightly enhanced it.

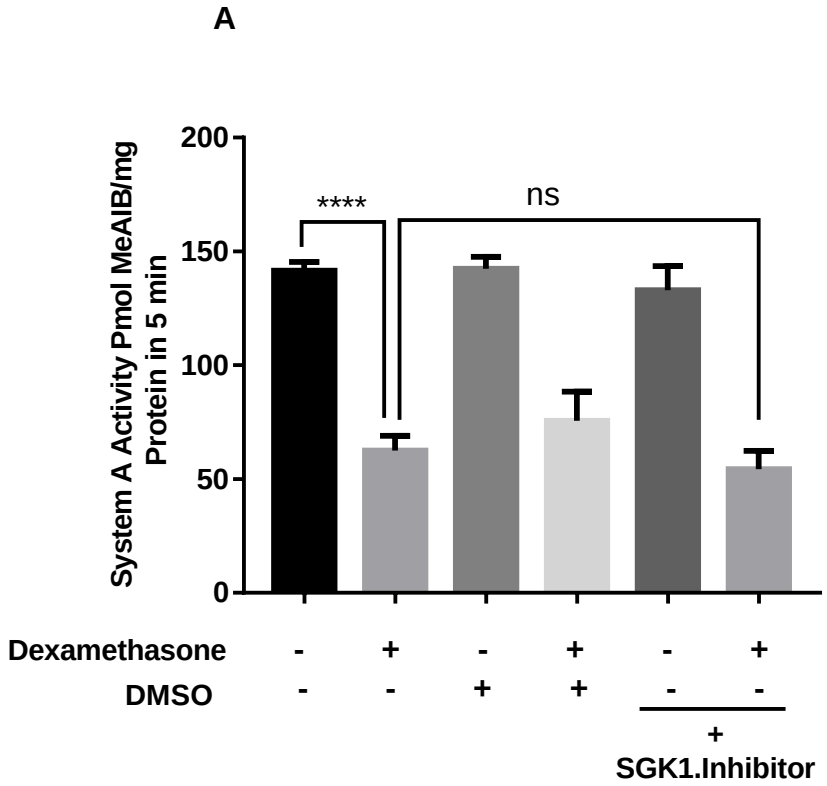

B

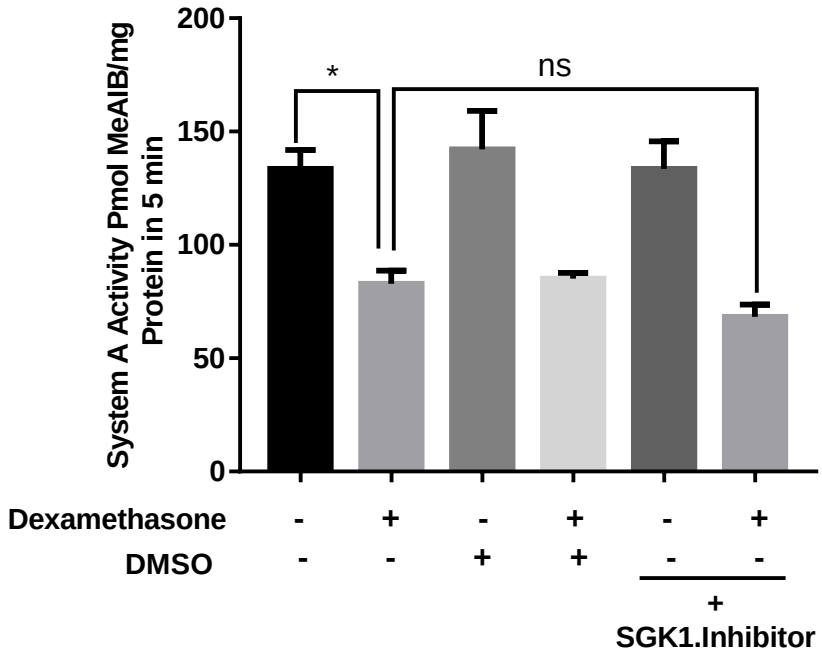
System A Activity Pmol MeAIB/mg Protein in 5 min
200
150
100
50
0
*
ns
Dexamethasone - + - + - +
DMSO - - + + - -
+
SGK1.Inhibitor

C

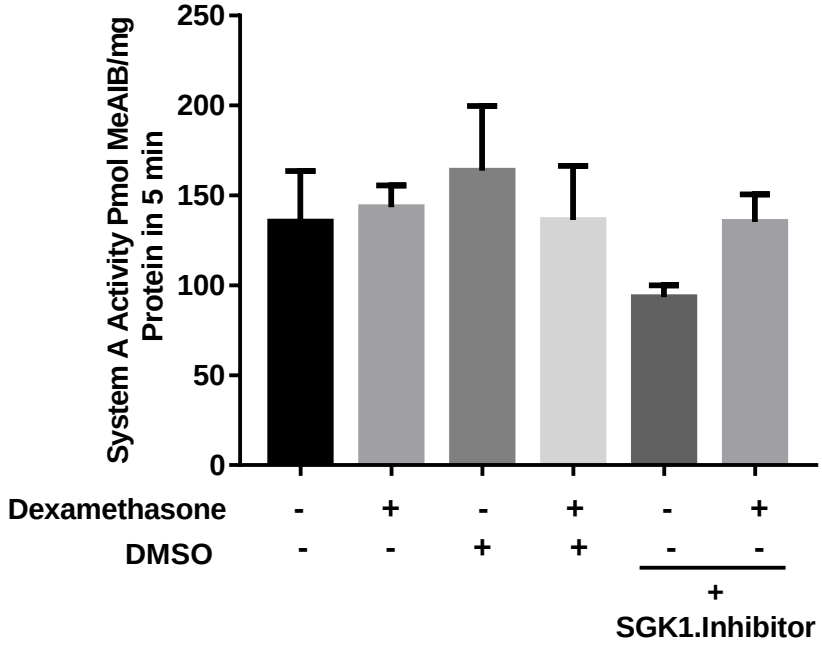
System A Activity Pmol MeAIB/mg Protein in 5 min
250
200
150
100
50
0
Dexamethasone - + - + - +
DMSO - - + + - -
+
SGK1.Inhibitor

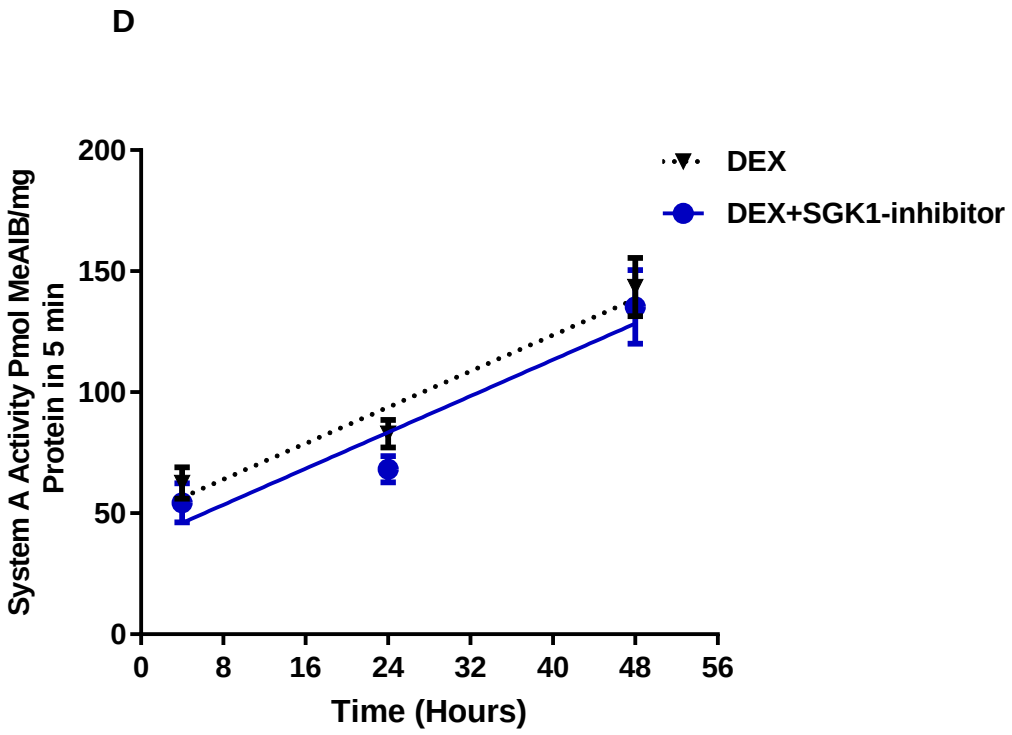


**Figure 3.7. An inhibitor of Serum and Glucocorticoid-dependent Kinase 1 (SGK-1) has no detectable effect on the inhibitory action of DEX.**

L6 myotubes were pre- incubated with a final concentration of 103nM of a specific Serum and Glucocorticoid-dependent Kinase 1 (SGK1) inhibitor (GSK650394-Sigma) or DMSO control for one hour in the culture incubator. Then the medium was discarded and replaced with the test media containing 500nM DEX or DMSO control with or without 103nM SGK1 inhibitor for another 4h (A), 24h (B) and 48h (C). Then the amino acid transport activity was measured by assaying MeAIB uptake by the cells. (D) shows a line graph of the effect of DEX with or without SGK1 inhibitor at three different time points (4,24,48h). The data are presented as Mean ± SEM of three independent experiment (n=3). * P<0.05, **** P< 0.0001, ns-statistically non-significant.

### 3.2.2.2 Glucocorticoid-dependent kinase LKB1 and AMP-activated protein kinase (AMPK)

A second GC-responsive kinase which might be involved in the action of DEX on System A / SNAT2 transport activity is Liver Kinase B1 (LKB1) which has been reported to be down-regulated by GC, as described in Section 1.18. No selective inhibitor of this kinase was available to allow testing of the involvement of LKB1 in the action of DEX on System A transport. However, as AMP-activated protein kinase (AMPK) is phosphorylated and activated by LKB1, if DEX acts by inhibiting LKB1 in L6 myotubes, this should lead to a decrease in phospho-activation of

AMPK. It should therefore be possible to use AMPK phosphorylation as a readout of DEX action on LKB1. As shown in Figure 3.8, phospho-activation of AMPK by the AMPK agonist AICAR as a positive control was readily detectable in L6 myotubes by immunoblotting with antibody against phosphorylated AMPK. However, DEX did not give the predicted decline in AMPK phosphorylation, and may have shown a statistically insignificant increase. A possible explanation is that the inhibition of System A transport by DEX (Figure 3.1) was reducing amino acid availability as fuels in the cells, thus activating AMPK phosphorylation and masking the expected inhibitory effect of DEX on AMPK phosphorylation. To test this, complete blockade of System A amino acid transport with 10mM MeAIB, or complete removal of amino acids from the culture medium were also tested (Figure 3.8). These also had no statistically significant effect on AMPK phosphorylation. It is therefore unlikely that a major effect of amino acid depletion was masking an inhibitory effect of DEX on LKB1 and AMPK phosphorylation in L6 myotubes.

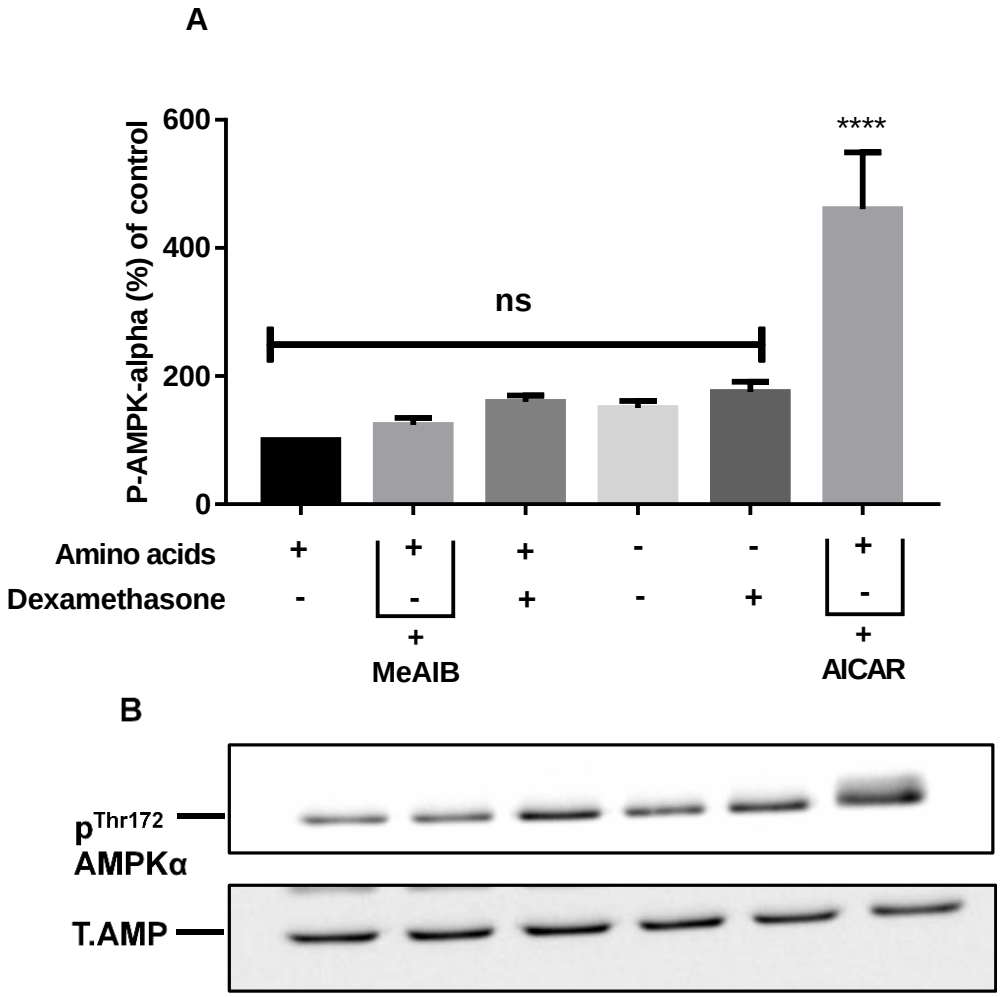


**Figure 3.8. Dexamethasone acting through LKB1 fails to inhibit AMPK-α phosphorylation (P-AMPK) in L6 myotubes.**

$P^{Thr172}$AMPK-α and total AMPK (T. AMPK) were detected by immunoblotting in lysates from L6 myotubes after incubation under the conditions shown for 4h: 500nM DEX with or without amino acids, 10mM MeAIB; and 750μM AICAR (Sigma A-9978) as a positive control. (A) Densitometry data are presented as Mean ± SEM of pooled data from six independent experiments (n=6). The P-AMPK-α signal is normalised for T-AMPK. (B) Shows a representative blot of $P^{Thr172}$AMPK (upper panel) and T-AMPK (lower panel). ****P<0.0001 compared with control cultures with amino acids and no AICAR. ns-statistically non-significant.

### 3.2.3 Glucocorticoid-dependent phosphoprotein phosphatases

#### 3.2.3.1 The effect of glucocorticoid (Dexamethasone) on Protein Tyrosine Phosphatase 1B (PTP1B) gene expression in L6 myotubes

In skeletal muscle *in vivo* glucocorticoid is reported to up-regulate mRNA encoding the enzyme Phosphoprotein Tyrosine Phosphatase 1B (PTP1B) about 2-fold (Almon *et al.,* 2005). As such enzymes are inhibited by vanadate, this may explain why inhibition of System A transport by DEX was partly blunted by vanadate in Figure 3.4. The effect of the conditions shown in Figure 3.4 on PTP1B gene expression was therefore investigated in Figure 3.9. It can be seen that DEX significantly up regulated the PTP1B gene expression but, as expected, Vanadate (which only acts directly on the phosphatase protein and not on gene transcription) had no significant effect. Although DEX showed a significant effect on PTP1B gene expression (Figure 3.9), incubating L6 myotubes with a specific PTP1B inhibitor for 4h did not show a significant effect on SNAT2 transport activity, nor did it blunt the DEX inhibitory effect (Figure 3.10). Furthermore, in this series of experiments, in contrast with the apparent effect seen in Figure 3.4, vanadate itself showed negligible blunting of the effect of DEX on System A transport (Figure 3.10).

A major role for DEX-induced up-regulation of phospho-tyrosine phosphatase activity in the cells was also excluded by directly assaying phospho-tyrosine phosphatase catalytic activity in cell lysates under these conditions. No increase in response to DEX was seen; indeed, a significant decrease was observed (Figure 3.11). Furthermore, Dephostatin, an alternative phospho-tyrosine phosphatase inhibitor, exerted no blunting action on the effect of DEX on System A transport (Figure 3.12), even though this has previously been reported to be an effective inhibitor in mammalian cells at the concentration used here (Thoroed *et al.,* 1999).

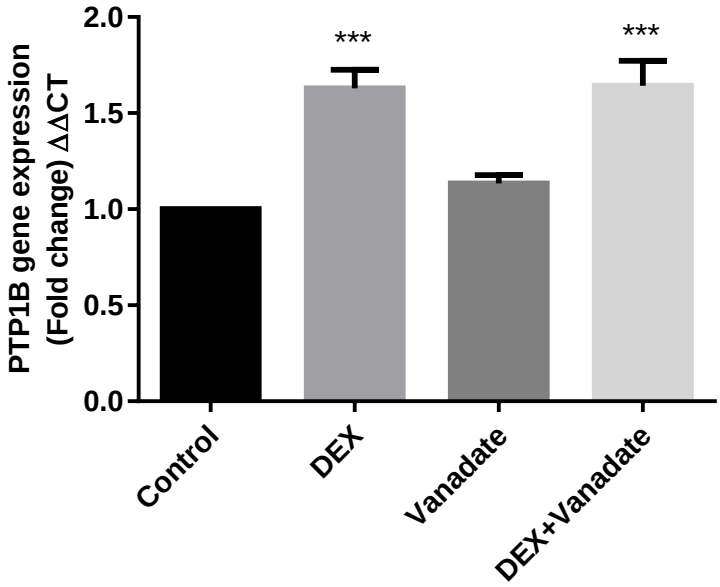


**Figure 3.9. The effect of Dexamethasone on Protein Tyrosine Phosphatase 1B (PTP1B) gene expression in L6-myotubes.**

Gene expression was assessed by RT-qPCR after 4h incubation in the culture incubator under the conditions shown: Control (DMSO control for DEX (0.0005% vol/vol)); DEX-500nM Dexamethasone; Vanadate-100µM Sodium orthovanadate; and 500nM Dexamethasone + 100µM Sodium orthovanadate. The data are expressed as ΔΔCT (ΔΔCT= PTP1B gene expression in the treated conditions in relation to the control condition). Gene expression of PTP1B is corrected for the housekeeping gene Cyclophilin. The data are presented as Mean ± SEM of four independent experiments (n=4) ***Denotes conditions differing significantly from Control, $P < 0.001$.

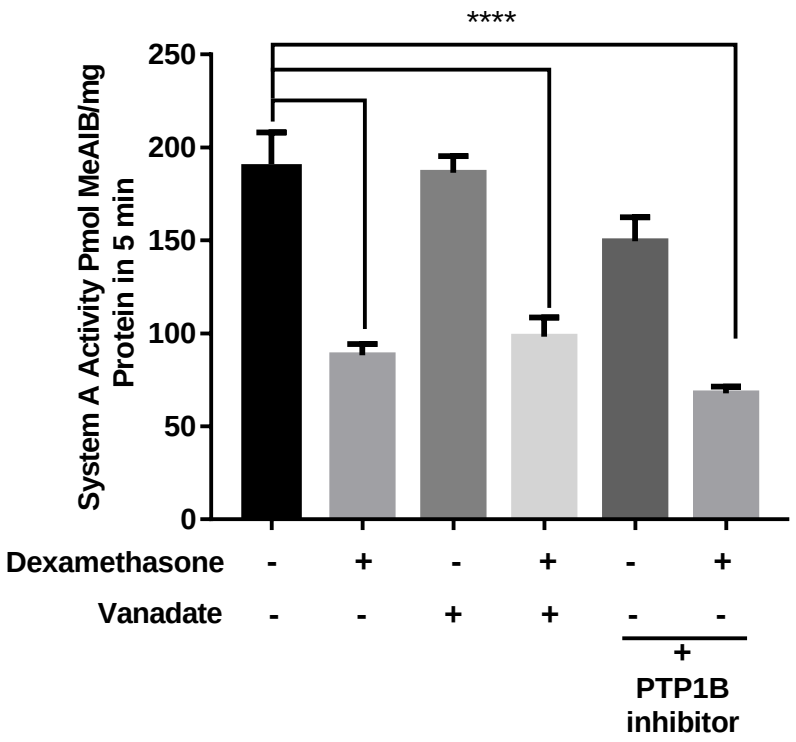


**Figure 3.10. The effect of a specific protein tyrosine phosphatase 1B (PTP1B) inhibitor on the inhibitory effect of Dexamethasone on System A amino acid transporter activity in L6 myotubes.**

L6-myotubes were incubated in the culture incubator with the test media under conditions shown for 4h: Control-(DMSO vehicle only, 2% DFBS MEM), DEX-500nM Dexamethasone, Vanadate-100μM Sodium orthovanadate, PTP1B inhibitor (20μM Calbiochem 539741). The data in this graph are presented as Mean ± SEM of three independent experiments (n=3) **** Denotes conditions differing significantly from Control, P<0.0001.

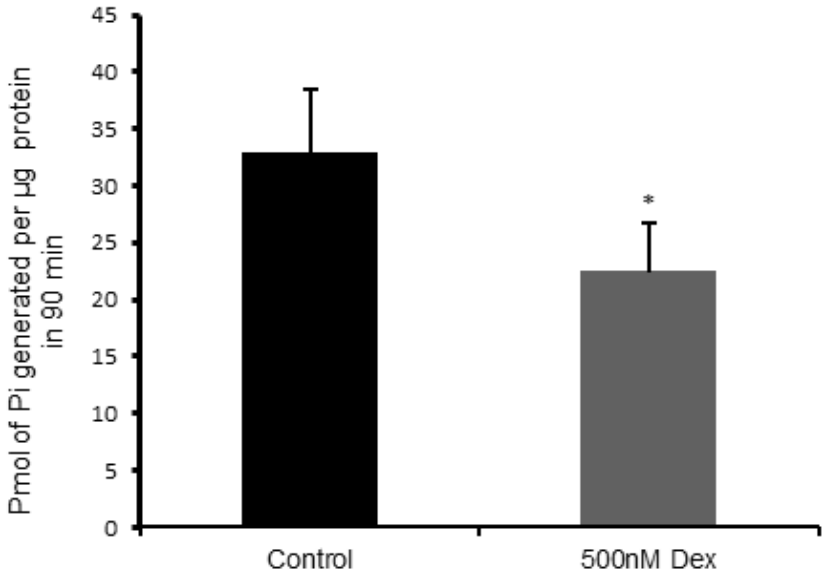


**Figure 3.11. Protein Tyrosine Phosphatase catalytic activity pmoles of Pi generated per µg cell protein in 90 min.**

The cells were incubated for 4h in the culture incubator under the conditions shown; Control (DMSO control for DEX 0.0005% vol/vol)); and 500nM Dexamethasone. The data are presented as Mean ± SEM of three independent experiments (n=3), Paired t analysis, *P<0.05.

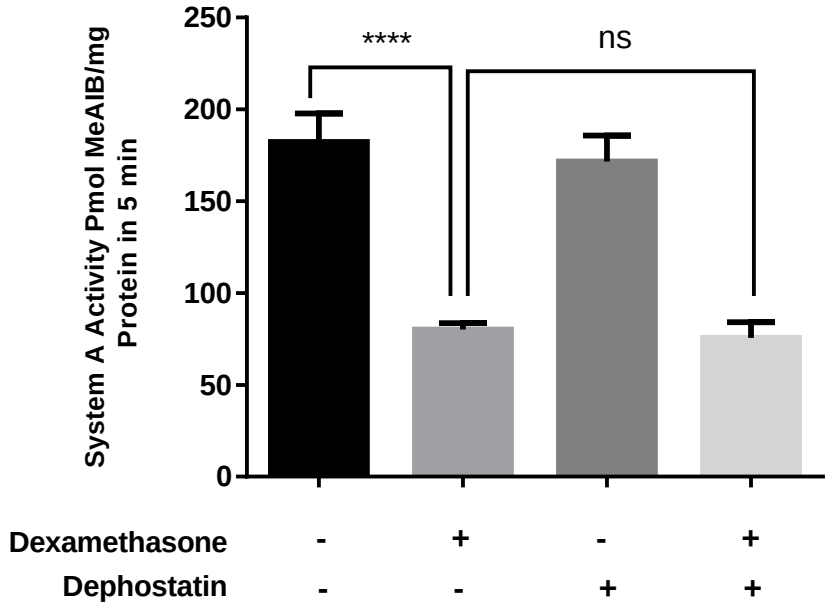


**Figure 3.12. The effect of a potent broad-spectrum protein tyrosine phosphatase inhibitor (Dephostatin) on the inhibitory effect of Dexamethasone on System A amino acid transporter activity in L6 myotubes.**

L6-myotubes were incubated with the test media of conditions shown in the culture incubator for 4h: Control (DMSO vehicle only); 500nM Dexamethasone; and 20µM Dephostatin. The data are expressed as Mean ± SEM of three independent experiments (n=3) **** P<0.0001, ns-statistically non-significant.

### 3.2.4 Serine-threonine phosphorylation events

#### 3.2.4.1 System A activity dependence on Mitogen-activated protein kinase (MAPK) in L6 myotubes

As even 100 µM Vanadate had not completely abolished the inhibitory effect of DEX in Figure 3.4 and gave negligible effect in Figures 3.6 and 3.10; and as human SNAT2 has been reported to be phosphorylated on Ser (S) residues, including a possible Mitogen-activated protein kinase (MAPK) phosphorylation site (Section 1.15), the possible involvement of such serine-threonine phosphorylation events in the action of DEX on SNAT2 was examined.

To confirm the importance of Mitogen-activated protein kinases (MAPK) in the regulation of System A (SNAT2) activity in these L6 myotube cultures, inhibitors of these pathways were applied: (SP600125 - JNK inhibitor; SB202190 - P38 inhibitor; and PD98059-MEK inhibitor) alone or in combination. In Figure 3.13, inhibition of JNK, P38 or all three pathways exerted a significant effect but the MEK inhibitor alone had no effect, possibly because, at the dose used here, it fails to block phospho-Erk activation in these cells (Simms, 2013).

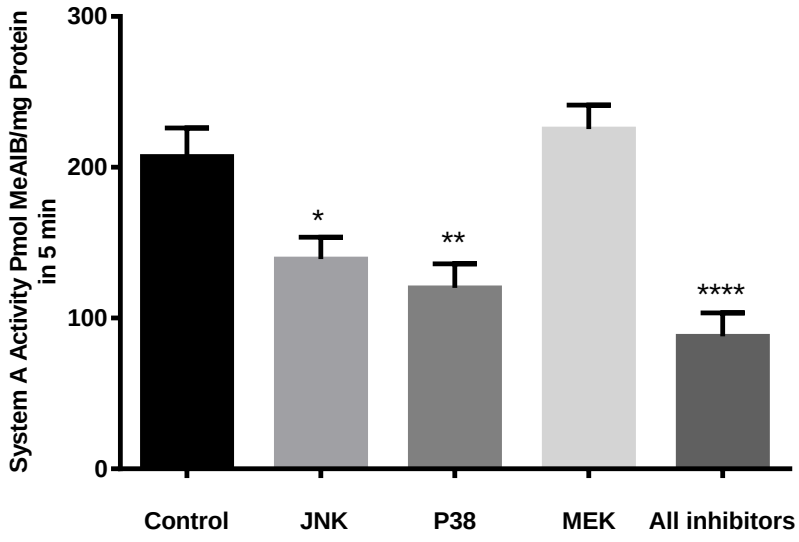


**Figure 3.13. The effect of Mitogen-activated protein kinase (MAPK) inhibitors on System A amino acid transporter activity in L6 myotubes**

The cells were incubated for 4h with the conditions shown: Control (DMSO vehicle only); JNK-10µM SP600125-JNK inhibitor; P38-5µM SB202190-P38 inhibitor; MEK-20µM PD98059-MEK inhibitor, and a combination of all inhibitors. Data are presented as Mean ± SEM. of three independent experiments (with 5 replicate culture wells for each treatment), *P<0.05, ** P<0.01, **** P<0.0001 versus Control.

#### 3.2.4.2 Effect of amino acid depletion on the inhibition of System A transport activity by DEX in L6 myotubes

The Ser/Thr (MAP) kinase JNK has been reported to play an important role in the dramatic up-regulation of SNAT2 that occurs in L6 myotubes on amino acid depletion (AAD) (Hyde *et al.,* 2007). If the inhibitory effect of DEX on SNAT2 activity occurs through inhibition of such MAPK signals and Ser/Thr phosphorylation events, amino acid starvation may blunt the inhibitory effect of DEX. An experiment was therefore performed to see whether SNAT2 activation by amino acid depletion (with its presumed accompanying JNK activation) could over-ride the inhibitory effect of DEX (Figure 3.14). The usual fractional inhibition of activity by DEX alone (i.e. 56% decrease) was observed in Figure 3.14. As predicted, in amino acid depleted cultures, the basal transport activity strongly increased, and the fractional inhibition by DEX under these conditions was less marked than usual (only 32%) (Figure 3.14) possibly indicating that amino acid depletion and DEX were acting through a common serine-threonine signalling pathway.

However, when the effect of a broad-spectrum phosphoprotein Ser/Thr phosphatase inhibitor (Fluoride) was tested on the inhibitory effect of DEX on System A (SNAT2) transporter activity (Figure 3.15), even though Fluoride alone inhibited SNAT2 activity (marginally significant, P = 0.0501), the usual ~ 50-60% inhibitory effect of DEX on SNAT2 activity was still observed without being significantly blunted.

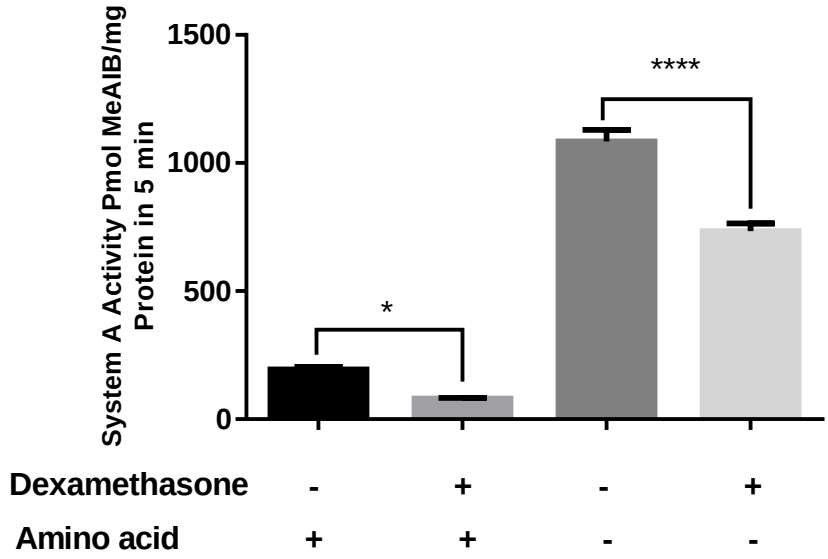


**Figure 3.14. The effect of amino acid depletion on the inhibitory effect of Dexamethasone on System A activity in L6 myotubes.**

System A amino acid transporter activity in L6 myotubes was measured after 4h incubation in the culture incubator under the conditions shown: Control (MEM with DMSO vehicle only); 500nM Dexamethasone; Amino acid starved ((Earle's Balanced Salts (EBSS)) +1% MEM Vitamins+1% Peni-Strep (100x) +2% DFBS, pH7.4). The bar graph values are presented as Mean ± SEM of three independent experiments (n=3) (with 5 replicate culture wells for each treatment), *P<0.05, **** P<0.0001.

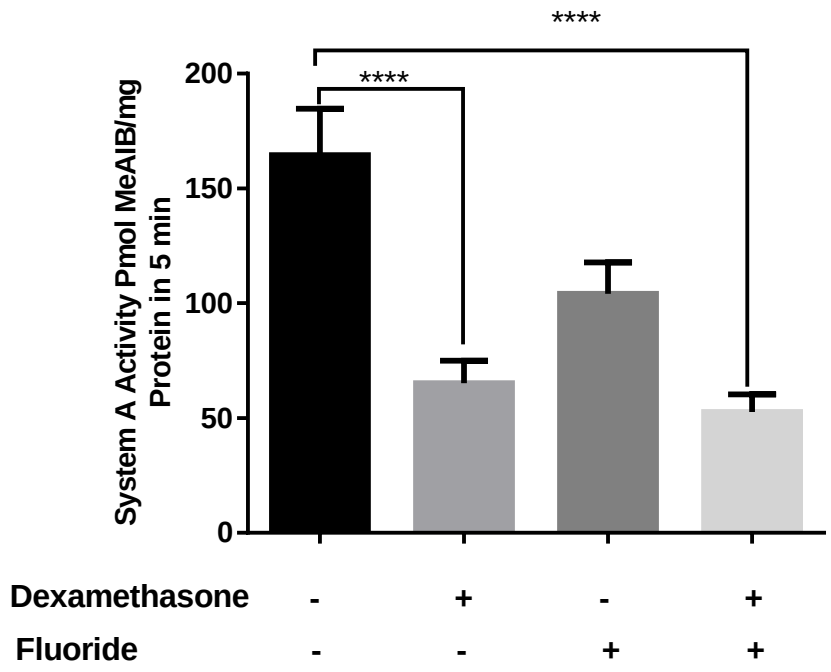


**Figure 3.15. The effect of Dexamethasone and Fluoride (a broad-spectrum Ser-Thr phosphatase inhibitor) on System A amino acid transporter activity in L6 myotubes.**

The cells were incubated with the conditions shown for 4h in the culture incubator: Control (DMSO vehicle only); 500nM Dexamethasone; and 1mM Sodium Fluoride. The data are expressed as Mean ± SEM of four independent experiments (n=4), **** P <0.0001. The apparent inhibitory effect of Fluoride alone is marginally significant (P=0.0501).

### 3.2.4.3 The combined effect of Vanadate and amino acid starvation) on the inhibitory effect of Glucocorticoid (Dexamethasone) on System A activity in L6 cells

The results from the experiments above imply that System A (SNAT2) activity in L6 myotubes and its inhibition by DEX involve signals that are partly inhibited by Vanadate and amino acid depletion (AAD), but that the inhibitory effects of Vanadate and AAD by themselves are incomplete and, in the case of Vanadate, very variable. Therefore, a further experiment was performed to investigate the combined effect of both Vanadate and AAD on the inhibitory action of Dexamethasone (DEX) on System A activity in L6 myotubes (Figure 3.16). Again, the inhibitory effect of DEX on System A activity was only partly blunted by Vanadate or AAD, when these conditions were applied separately (Figure 3.16). However, when these two manipulations were applied together, the inhibitory effect of DEX was completely abolished (Figure 3.16).

A possible interpretation of this result is that Vanadate is blunting DEX-induced signals through Tyr phosphorylation and that AAD is blunting DEX-induced signals through Ser/Thr phosphorylation, and that both sets of signals must be blocked together to prevent the action of DEX. If Vanadate is acting as a PTP1B phosphatase inhibitor (as suggested in Section 3.2.3.1), applying the specific PTP1B inhibitor Calbiochem 539741 along with AAD should also abolish the effect of DEX. In fact, the PTP1B inhibitor had no effect (with or without AAD) (Figure 3.17) confirming the conclusion reached at the end of Section 3.2.3.1, that Vanadate's action is unlikely to be an effect on Tyr phosphorylation.

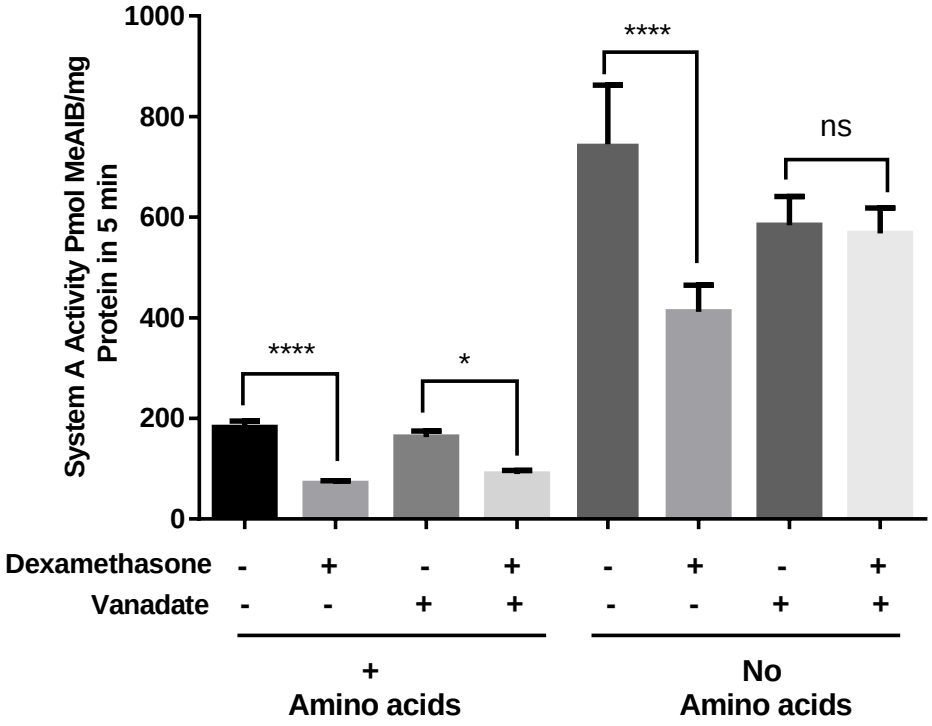


**Figure 3.16. The combined effect of Vanadate and amino acid depletion on the inhibitory effect of Dexamethasone on System A activity in L6 Myotubes.**

L6 myotubes were incubated for 4h in the culture incubator under the conditions shown: MEM with DMSO vehicle only was used as a control for the experimental conditions. Other cultures were treated with 500nM Dexamethasone; Vanadate-100µM Sodium orthovanadate; or amino acid depleted medium. Amino acid depleted medium was (Earle's Balanced Salt Solution (EBSS) +1% MEM Vitamins + 1% Peni-Strep (100x) + 2% DFBS, pH7.4). (The bar graph values are presented as Mean ± S.E. of three independent experiments (n=3) (with 5 replicate culture wells for each treatment). * P<0.05, **** P<0.0001, ns; statically non-significant.

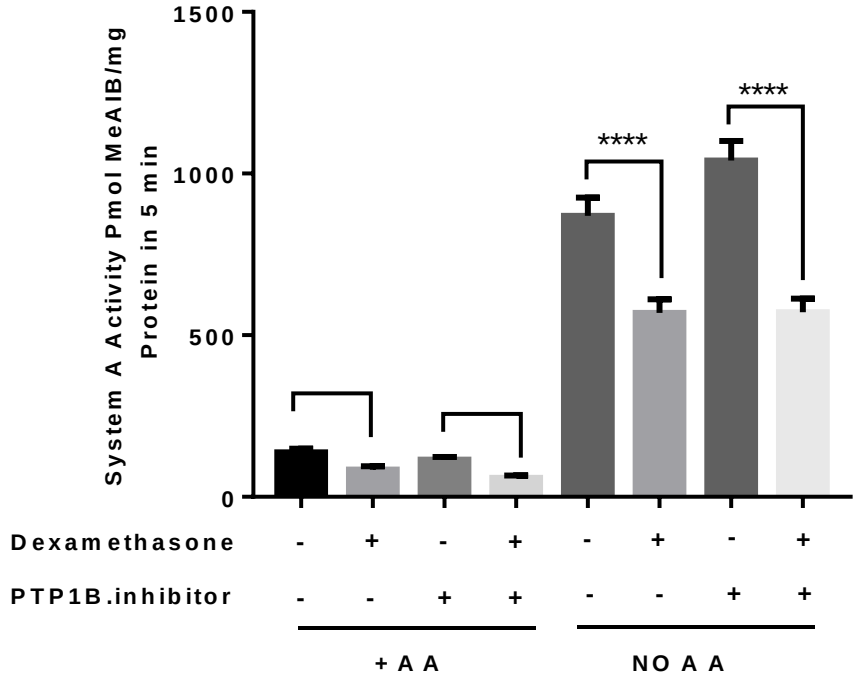


**Figure 3.17. The combined effect of a specific protein tyrosine phosphatase 1B (PTP1B) inhibitor and amino acid deprivation on the inhibitory effect of Dexamethasone on System A amino acid transporter activity in L6 myotubes.**

Myotubes were incubated for 4h in the culture incubator under the conditions shown: MEM with DMSO vehicle only was used as a control for the experimental conditions. Other cultures were treated with 500nM Dexamethasone; PTP1B inhibitor (20μM Calbiochem 539741) or amino acid depleted medium. Amino acid depleted medium was (Earle's Balanced Salt Solution (EBSS) +1% MEM Vitamins + 1% Peni-Strep (100x) + 2% DFBS, pH7.4). The data are presented as Mean ± SE of three independent experiments (n=3) with five culture well replicates per condition. No statistically significant effect of the PTP1B inhibitor was detected, **** $p<0.0001$.

### 3.2.5 Glucocorticoid effects on SNAT2 gene expression

#### 3.2.5.1 Involvement of glucocorticoid-dependent transcription events

A possible interpretation of the abolition of the effect of DEX on System A transport by actinomycin D in Figure 3.3B is that DEX binds to a negative GRE (glucocorticoid response element) on the SNAT2 gene itself, thus decreasing SNAT2 transcription and ultimately expression of the SNAT2 protein. The effect of Dexamethasone on SNAT2 mRNA level was therefore assessed by RT-qPCR analysis in L6 myotubes using SNAT2-specific primers and primers specific for Cyclophilin as a house keeping gene (Figure 3.18). Incubating L6 myotubes with 500nM DEX for four hours did not show any significant effect on SNAT2 mRNA level, suggesting that no direct effect of Dexamethasone had occurred on SNAT2 transcription. This absence of an effect on SNAT2 mRNA has also been confirmed by direct Northern blotting for SNAT2 mRNA in DEX-treated L6 myotube cultures (Clapp, 2010) (PhD thesis, Loughborough University).

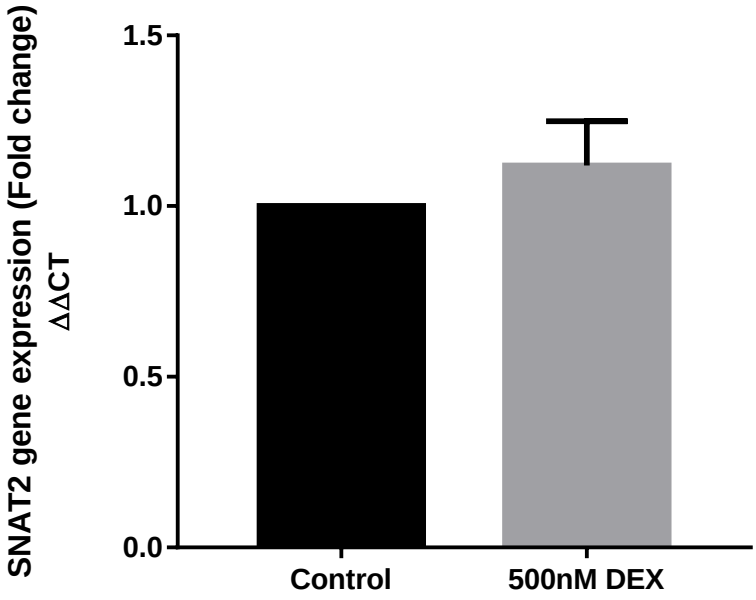


**Figure 3.18. Dexamethasone does not affect SNAT2 gene expression at mRNA level in L6 myotubes.**

The cells were incubated under the conditions shown in the graph for 4h. Cultures were incubated with DMSO vehicle (0.0005% vol/vol) (Control) or with 500nM DEX. The data are expressed as ΔΔCT (ΔΔCT= SNAT2 gene expression in the DEX treated condition in relation to the control condition). Gene expression of SNAT2 was corrected for variation in expression of the house-keeping gene Cyclophilin. The data are presented as Mean ± SEM (n=3).

#### 3.2.5.2 Glucocorticoid effects on expression of the SNAT2 protein

In spite of this lack of effect of DEX on SNAT2 gene expression at mRNA level, it is still possible that DEX could be inhibiting translation of the mRNA or increasing degradation of the SNAT2 protein. Membrane preparations were therefore isolated from L6 myotubes after incubation with 500nM DEX followed by immunoblotting of the membrane proteins with a specific anti-SNAT2 antibody that has been used previously in this laboratory Strong depletion of SNAT2 protein by DEX was observed, even though no statistically significant depletion was seen with two house-keeping membrane proteins, $\alpha$1-Na, K-ATPase and Annexin II (Evans *et al.,* 2007).

### 3.2.6 The effect of proteasome inhibition on regulation of SNAT2 activity by DEX in L6 myotubes

In spite of the absence of a DEX effect on SNAT2 mRNA (Figure 3.18), incubation with DEX significantly depleted SNAT2 protein in L6 myotubes assessed by immunoblotting with anti-SNAT2 antibody (Evans *et al.,* 2007), consistent with increased degradation of this transporter. If the inhibitory effect of DEX on SNAT2 transport activity is mediated by SNAT2 protein degradation through the ubiquitin proteasome pathway (UPP), it should be possible therefore to block it with the proteasome inhibitor MG132.

In adipocytes and pre-adipocytes, it has previously been reported that treating the cells for 4h with MG132 increases the amount of MeAIB intake as a measurement of System A (SNAT2) transport activity (Hatanaka *et al.,* 2006). This is thought to arise from decreased degradation of SNAT2 protein, resulting in accumulation of the active transporter protein.

It has been known in this laboratory for many years that incubation with MG132 does *not* increase System A (SNAT2) transporter activity in L6 myotubes. It was therefore thought to be unlikely that the effect of DEX on System A transport was mediated by DEX-induced up-regulation of the UPP. This was confirmed in Figure 3.19 in which, in the absence of DEX, MG132 again failed to increase transport activity, indeed it seemed to decrease it. However, when the effect of MG132 was measured in the presence of DEX, it was found that this inhibitor significantly

blunted the inhibitory effect of DEX on System A (SNAT2) transporter activity in the L6 myotubes, reducing the effect by more than 70% (Figure 3.19) and suggesting an important role for the UPP in the action of DEX on SNAT2.

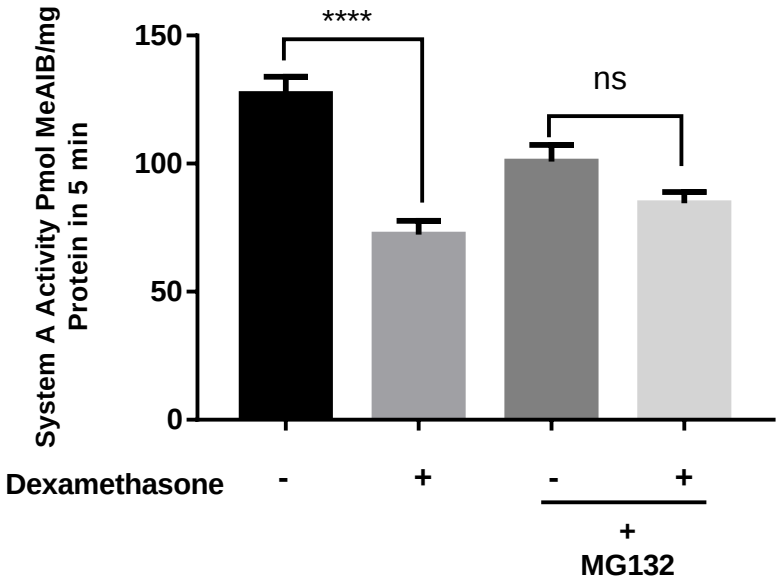


**Figure 3.19. The effect of proteasome inhibitor (MG132) on the inhibitory effect of dexamethasone in L6 myotubes.**

The cells were incubated with the test media shown for 4h. Control cultures were incubated only with DMSO vehicle (0.0005% vol/vol). Other cultures were incubated with 500nM DEX, and/or 10µM MG132. The graph is presented as Mean ± SEM of pooled data of four independent experiments (n=4) and five replicate values for each condition in each experiment. **** denotes statistically significant difference from the control P<0.0001 and ns denotes-statistically non-significant.

## 3.3 Discussion

### 3.3.1 SNAT2 degradation and the Ubiquitin-proteasome Pathway (UPP)

The data presented in this chapter have shown that the inhibitory effect of DEX on System A (SNAT2) transporter activity is weakly blunted by vanadate or by amino acid depletion (AAD), but completely abolished by vanadate and AAD in combination, or by blockade of transcription with actinomycin D. However, the effect of DEX on transport is not apparently blunted by more specific phosphotyrosine phosphatase inhibitors, or by the phospho-serine-threonine phosphatase inhibitor fluoride; nor was there any evidence that the effect was mediated by the SGK1 or LKB1 glucocorticoid-dependent protein kinase pathways. The experiments did however demonstrate a marked DEX-induced decline in SNAT2 protein content, and significant blunting of the effect of DEX on transport when protein degradation through the UPP was blocked with the proteasome inhibitor MG132.

In addition to inhibiting phosphotyrosine phosphatases, vanadate is also a potent inhibitor of proteasomes; and there is evidence that amino acid depletion also strongly impairs the degradation of the SNAT2 protein (Nardi *et al.,* 2015). Membrane proteins are usually degraded by lysosomes, but some membrane proteins such as amino acid transporters are degraded by proteasomes (Hatanaka *et al.,* 2006). There is evidence that SNAT2 is one of the membrane proteins that is degraded in this way in some cell types such as adipocytes (Hatanaka *et al.,* 2006; Nardi *et al.,* 2015). A possible explanation for the observations in this chapter therefore is that DEX activates degradation of the SNAT2 protein through the well-documented transcription dependent up-regulation by glucocorticoid of the ubiquitin-proteasome pathway (UPP) (as described in Section 1.19). GCs induce protein degradation by activating UPP components, either enhancing protein ubiquitination and conjugation through E2 ubiquitin conjugating enzyme, and E3 ligase enzymes such as Atrogen-1 and MuRF-1; or by increasing proteasome activity by increasing gene expression of proteasome sub-units, leading to direct protein degradation (Schakman *et al.,* 2013).

E3 ligases are important in ubiquitination of specific proteins identified by each specific E3 ligase. For example, there is evidence that SNAT2 is degraded

through Nedd4-2 E3 ligase in CHO cells, indicated by a decrease in SNAT2 transport activity when the cells are co-transfected with SNAT2 and Nedd4-2 (Hatanaka *et al.,* 2006). Furthermore, Nedd4-2 silencing increases SNAT2 amino acid transport in some cell types e.g. trophoblasts (Rosario *et al.,* 2016); and in adipocytes and pre-adipocytes, proteasome inhibition with MG132 increases System A (SNAT2) transport activity (Hatanaka *et al.,* 2006). It is not known however why MG132 fails to increase the basal System A transport rate (in the absence of DEX) in L6 myotubes (Figure 3.19).

### 3.3.2 Further experiments on the SNAT2 protein

Contrary to the original hypothesis, in this chapter manoeuvres that are reported to alter both Tyr phosphorylation and Ser/Thr phosphorylation showed no clear and unambiguous effects on the inhibition of System A/SNAT2 transporter activity by DEX. To characterise further the effect of DEX on SNAT2, and signals downstream from SNAT2 that might regulate global protein metabolism – for example through amino acid effects on mTORC1, it would be helpful to study the SNAT2 protein itself and alter its level of expression in the cell. Working with intact L6 cells alone gives no information on this. Furthermore, no additional characterisation of the effect of DEX on the endogenous SNAT2 protein was performed in this project by SNAT2 immunoblotting in L6 myotubes (as in (Evans *et al.,* 2007)) because of the cumbersome nature of these experiments. The apparently low protein copy number of SNAT2 in L6 cells means that isolated membrane preparations are needed to concentrate the samples before immunoblotting, and the SNAT2 protein is quite unstable even in lysis buffers prepared with cocktails of protease inhibitors.

For this reason, an alternative strategy was used to test the hypothesis that DEX acts by stimulating proteasome-dependent catabolism of SNAT2 protein. i.e. cloning and expression of tagged SNAT2 constructs in readily transfected HEK 293A cells. A further advantage of this approach is that it might allow isolation of the tagged SNAT2 protein thus assisting direct detection of post-translational modification of the protein, such as phosphorylation.

Such molecular cloning and expression experiments are described in the next chapter.

# Chapter 4 Cloning and expression of SNAT2 in HEK293A and L6 myoblasts

## 4.1 Cloning and expression of SNAT2 in HEK293A and strategy for expression and characterisation of tagged SNAT2 proteins

To provide a molecular system in which to study the SNAT2 protein and its regulation and possible phosphorylation, SNAT2 plasmid DNA incorporating enhanced Green Fluorescent Protein (eGFP) and His-FLAG tags were transfected into Human Embryonic Kidney cells (HEK293A) This was done to express tagged SNAT2 in a form in which it is readily detected and isolated (e.g. with anti-GFP antibodies) to allow study of changes in expression of tagged protein and whether phosphorylated isoforms of the protein can be detected. HEK293A cells were used for initial experiments because they are readily transfected and have been used in many studies as a vehicle for transfection (Thomas & Smart, 2005).

Initial objectives in these experiments were:

- To determine optimum transfection conditions under which expression of SNAT2-eGFP could be detected by fluorescence microscopy.
- To determine whether expression of a functioning System A transporter could be detected in transfected HEK293A cultures by assaying $^{14}$C-MeAIB transport and, if so, whether it was regulated by amino acid deprivation (AAD) and DEX as in L6 cells.
- To determine whether expression of epitope-tagged SNAT2 could be detected by immunoblotting.

## 4.2 Results

### 4.2.1 Basal System A activity in non-transfected (wild type) Human Embryonic Kidney (HEK293A) cells.

As a starting point in HEK293A experiments, the basal System A transporter activity was assayed under the conditions that had previously been studied in L6 cells. When HEK293A cells were incubated with 500nM DEX or amino acid deprived (AAD) medium for four hours, clear up-regulation of transport activity was observed in response to AAD (Figure 4.1A) suggesting that some of the System A regulatory mechanisms previously reported in L6 cells (Hyde *et al.,* 2007) are also present in HEK293A. The inhibitory effect of DEX however was almost undetectable in HEK293A cells (Figure 4.1A) and, more surprisingly, it was found that the inhibitory effect of DEX was also undetectable in myotubes grown from human skeletal muscle (Figure 4.1B).

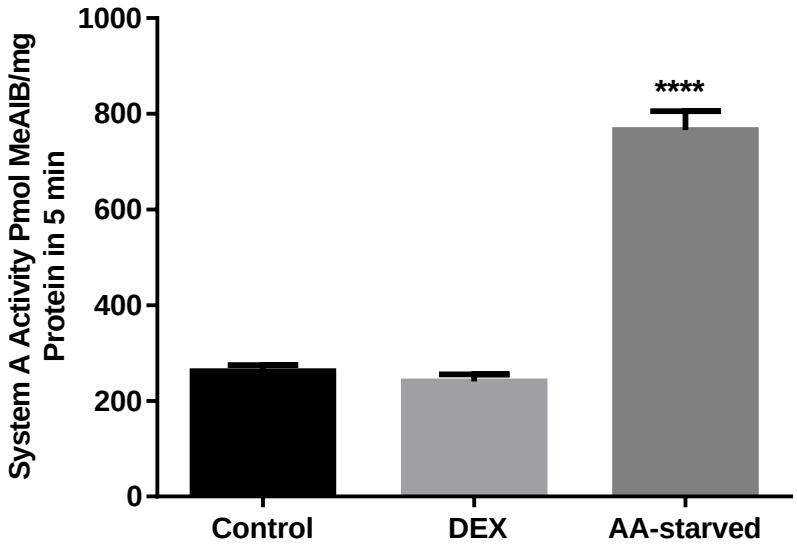


**Figure 4.1A. Amino acid deprivation (AAD) increases System A activity in HEK293A cells.**

Basal System A amino acid transporter activity in HEK293A cells (wild type) was measured after 4h incubation under control condition (DMSO vehicle only), in the presence of 500nM Dexamethasone (DEX), and AAD (EBSS + MEM Vitamins + Peni-Strep + 2% vol/vol DFBS, pH 7.4) as described in Section 2.2.3. The bar graph values are presented as Mean ± SEM. of three independent experiments (n=3) (with 5 replicate culture wells for each treatment). Incubating the cells with AAD medium induces significant increase in System A transport activity. **** denotes condition significantly different from control condition, P<0.0001.

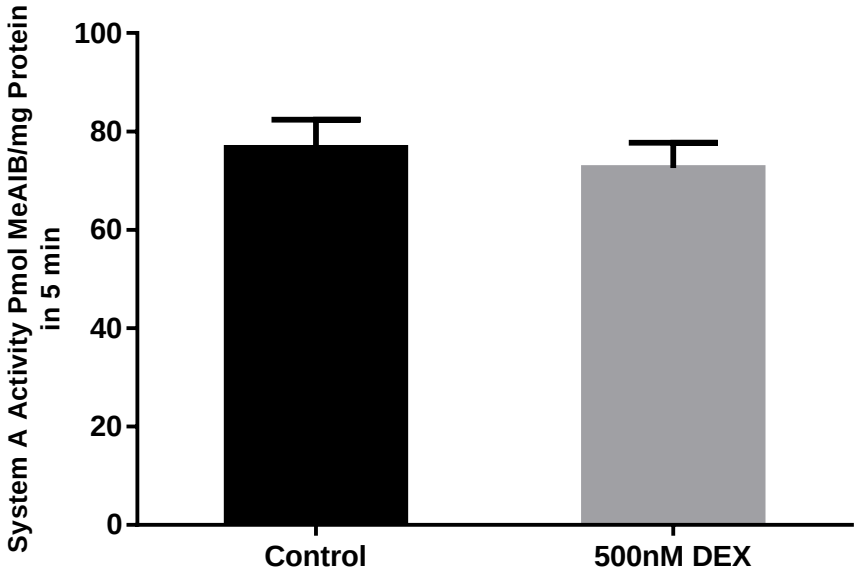


**Figure 4.1B. The effect of 500nM Dexamethasone on System A amino acid transporter activity in human myotubes.**

Human skeletal myoblasts were incubated in 1ml of growth medium for 48h then the cells were put in differentiation medium (Section 2.2.7) for another 48h to form myotubes After myotube formation the cells were incubated under the conditions shown for 4h; Control (DMSO vehicle only); or 500nM Dexamethasone, followed immediately by assay of transport activity (Section 2.9). Pooled data from 4 independent experiments are shown (n=4) (Paired t analysis, P = 0.3852).

### 4.2.2 Expression of SNAT2-eGFP in HEK293A cells

Fluorescence imaging detected significant apparent expression of the SNAT2-eGFP construct when it had been transfected into HEK293A cells (Figure 4.2) at a plasmid DNA concentration of 1µg/22mm well. This high apparent transfection efficiency was obtained using TransIT-2020 (Mirus-MIR 5400) following the manufacturer's protocol, and this same DNA concentration was used for all subsequent experiments. When the same concentration of SNAT2-eGFP construct was applied using the calcium phosphate transfection method, the same high transfection efficiency was observed. System A transport activity was assayed in such calcium phosphate transfected cultures to determine whether the expressed protein was a functionally active transporter. In the transfected cultures (Figure 4.3) a clear 5-fold increase in activity was detected. In contrast, control cultures transfected with pLEICS-29-GFP-tagged ligated empty vector showed no significant change in transport activity (Figure 4.3). However, the normal up-regulation of transport induced by amino acid deprivation (AAD) was

not observed in SNAT2-eGFP transfected cultures which were already expressing a high level of transport activity (Figure 4.3), nor did the expressed SNAT2-eGFP transport activity show a significant inhibitory response to 500nM DEX (Figure 4.4).

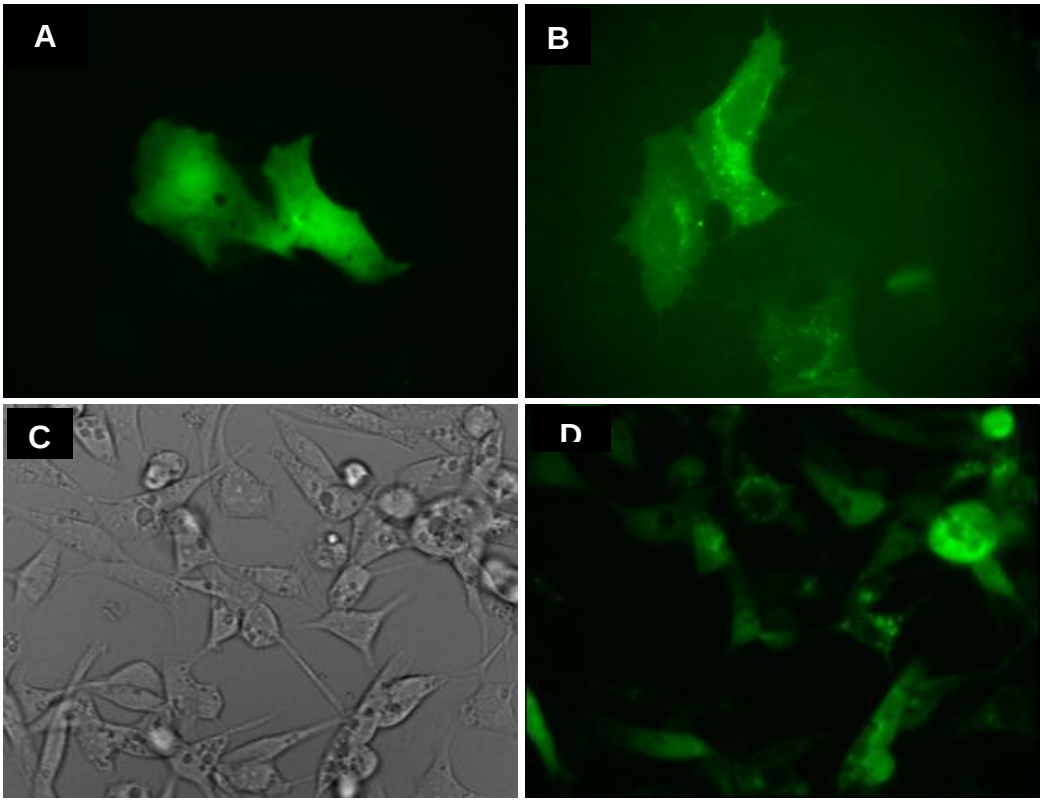


**Figure 4.2. Fluorescence images of Human Embryonic Kidney cells (HEK293A).**

(A) Transfected with 0.8µg/22mm well ligated empty GFP vector (pLEICS-29); (B and D) transfected with (1µg/22mm well) SNAT2-eGFP DNA. Note that the empty vector and SNAT2-eGFP are equi-molar. Cultures were examined 48h after transfection using 40X objectives (A, B) and 20X objectives (C, D) on an Olympus Scan^R/Cell^R microscope (with GFP (470/22) filter). For comparison, image (C) shows the same cells as in (D) by phase contrast microscopy.

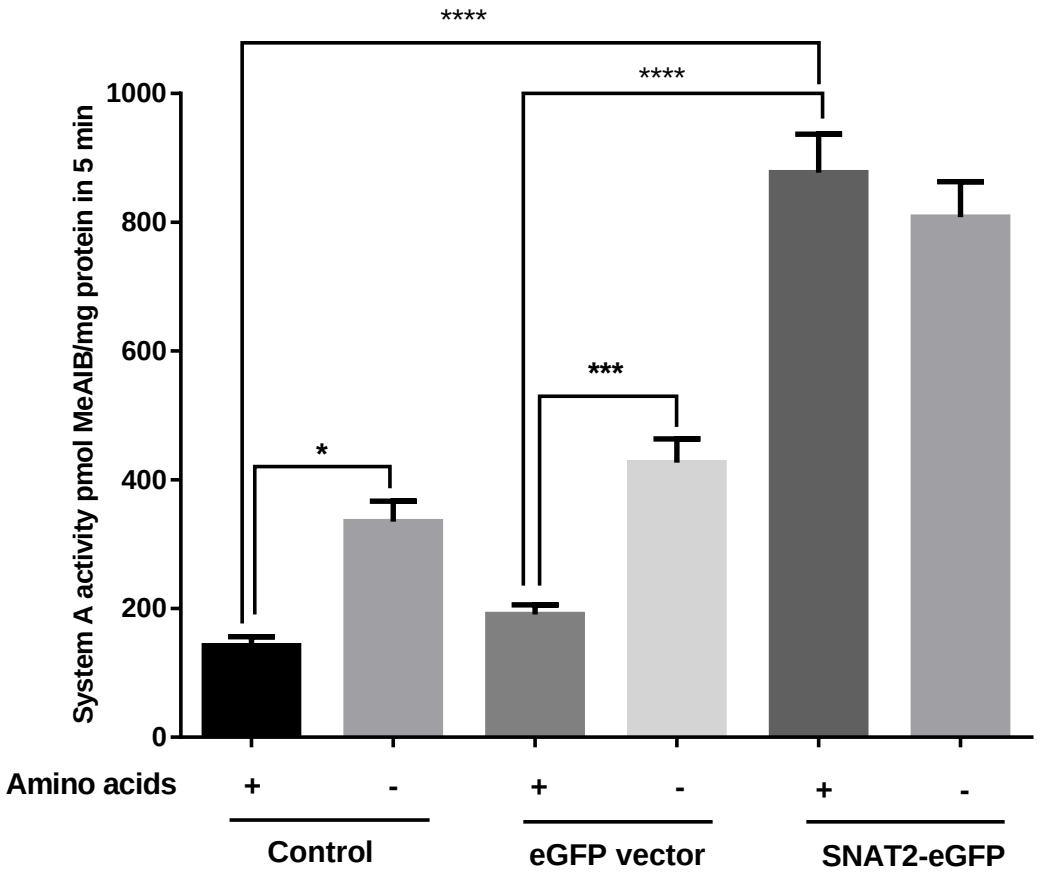


**Figure 4.3. SNAT2 over expression increases System A activity in HEK293A cells.**

Transfecting the cells with 1µg/22mm well SNAT2-eGFP plasmid for 24h significantly increased System A transport activity in this cell line. eGFP vector at 0.8 µg/22mm well did not affect the transport activity, which was similar to wild type (control) which was assayed after incubating the cells for 4h with or without AA in the media. The amino acid-deprived medium was (EBSS + MEM Vitamins + Peni-Strep + 2% vol/vol DFBS, pH 7.4). The bar graph values are presented as Mean ± SEM of three independent experiments (n=3), *P<0.05, ***P<0.001, ****P<0.0001.

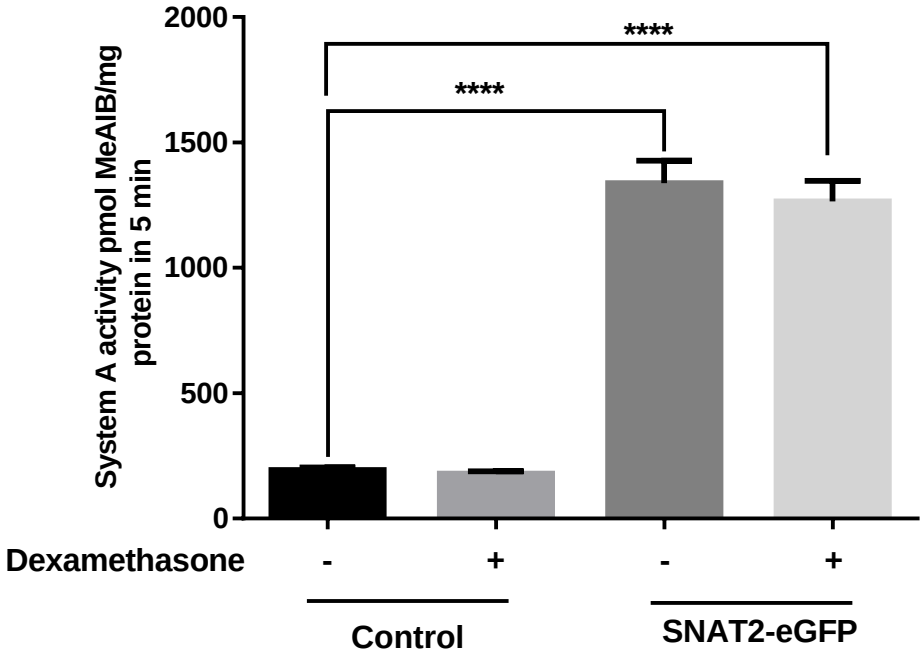


**Figure 4.4. Dexamethasone does not inhibit System A activity in transfected HEK293A cells.**

Incubating the cells with 500nM DEX for 4h had no significant inhibitory effect on System A activity in this cell line, neither in the control cells (wild type) nor in the SNAT2-eGFP over-expressing cells (transfected with 1µg/22mm well SNAT2-eGFP plasmid). The medium for the control cells contained the vehicle for DEX (i.e. 5.4 x $10^{-4}$ % vol/vol DMSO)). The bar graph values are presented as Mean ± SEM of three independent experiments (n=3). **** Denotes conditions differing significantly from Control, P<0.0001.

### 4.2.3 Expression of SNAT2-eGFP in L6 myoblasts

To determine whether these effects could be confirmed in cultured skeletal muscle cells, an attempt was also made to express the same SNAT2-eGFP construct in L6 cells. Unfused L6 myoblasts were transfected as described in Section 2.2.6 with the SNAT2-eGFP plasmid or the empty eGFP-vector at two different plasmid DNA concentrations. As shown in Figure 4.5, fluorescence imaging detected SNAT2-eGFP expression in L6 myoblasts at both plasmid DNA concentrations tested. There was a statistically significant stimulatory effect on System A transport activity ($^{14}$C-MeAIB uptake) in the cells transfected with 0.3µg SNAT2-eGFP DNA per 22mm well when compared with cells transfected with empty vector, both in medium with normal amino acid concentrations and (unlike HEK293A cells) under AAD conditions (Figure 4.6A and B respectively). However, this stimulation was too small relative to the basal transport activity to

allow the response of the transfected SNAT2-eGFP to DEX to be determined reliably. Transfection with SNAT2-HisFLAG also failed to give an increase in transport activity when compared with the un transfected Control cultures (Figure 4.6). The remaining experiments in this chapter therefore used tagged SNAT2 expressed in HEK293A cells.

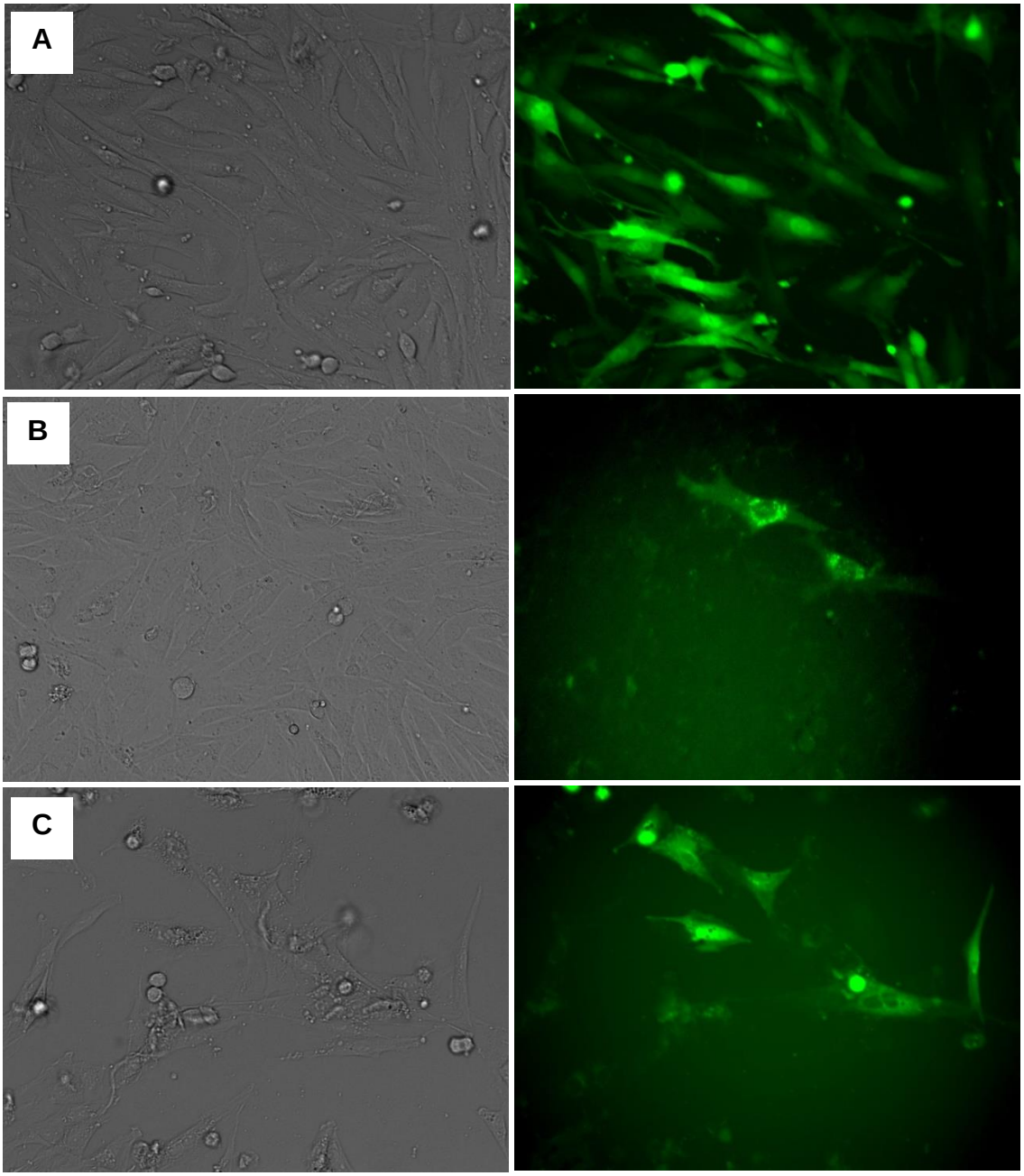


**Figure 4.5. Fluorescence microscopy imaging of transfected L6 myoblasts.**

with (A) 0.3µg of eGFP vector per 22mm well, and two concentrations of SNAT2-eGFP plasmid DNA (B) 0.3µg and (C) 0.5µg. Left: Bright field images and right: corresponding eGFP fluorescence (470/22 filter, 40X objective on Olympus Scan^R/Cell^R microscope).

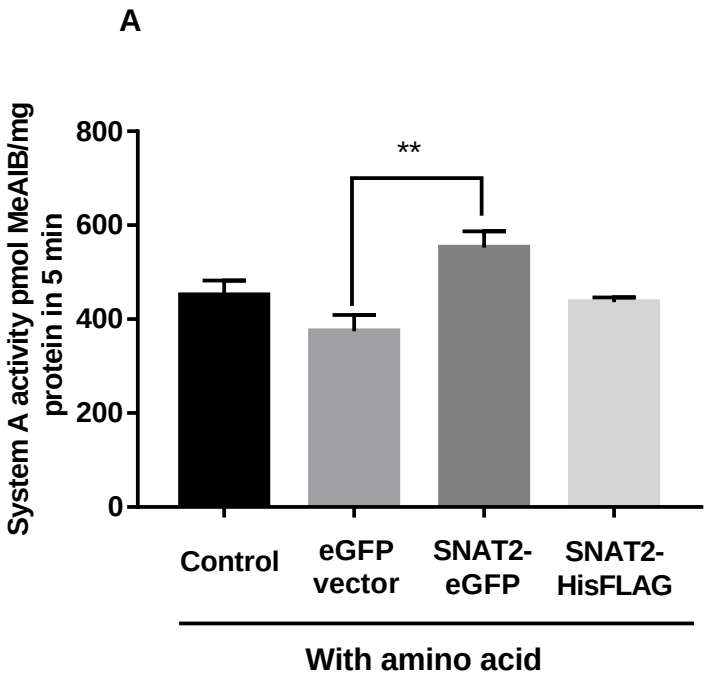
A
System A activity pmol MeAIB/mg protein in 5 min
800
600
400
200
0
**
Control
eGFP vector
SNAT2-eGFP
SNAT2-HisFLAG
With amino acid

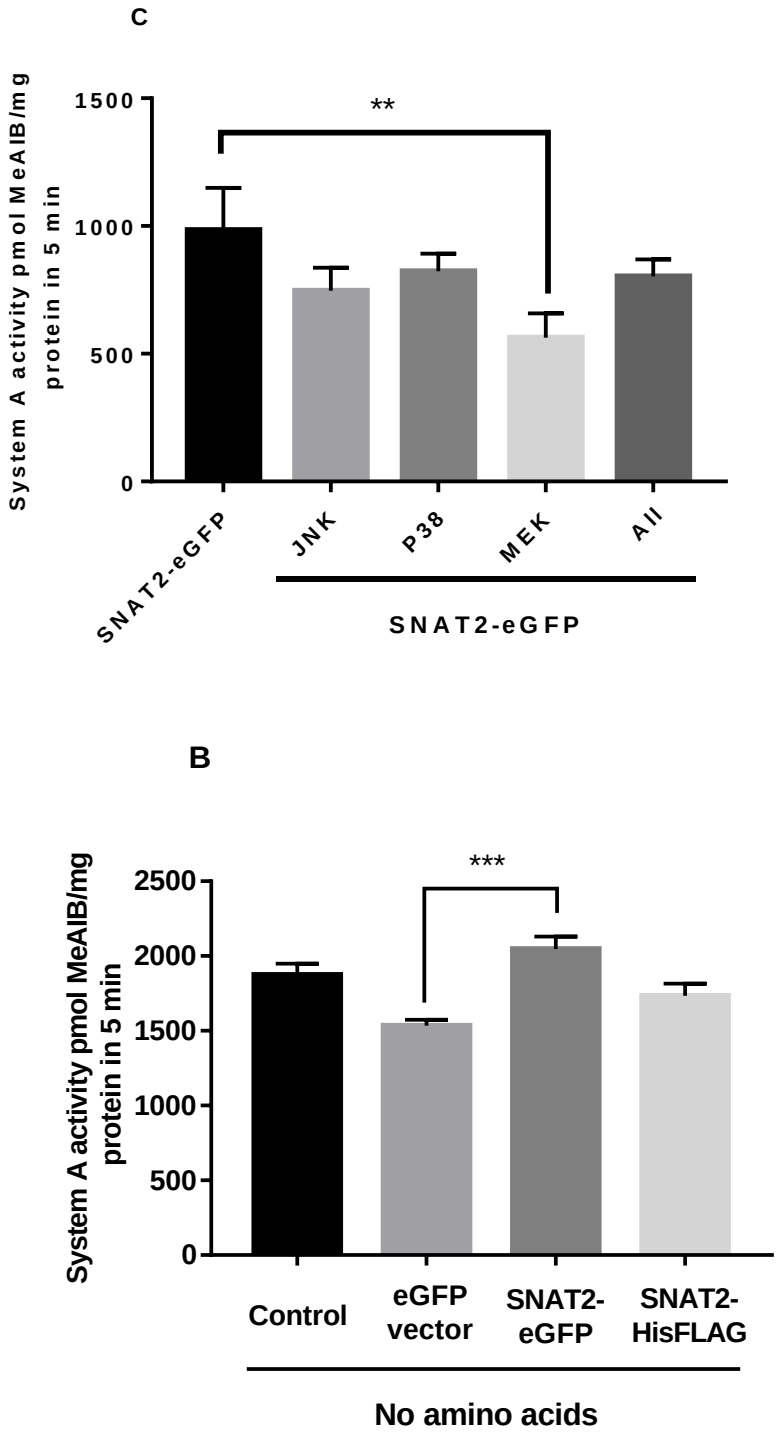


**Figure 4.6. SNAT2-eGFP expression increases System A transport activity in L6 myoblasts.**

L6 myoblasts were cultured for 24h prior to transfection with 0.3µg plasmid DNA of either eGFP vector, SNAT2-eGFP or SNAT2-HisFLAG per 22mm well using Effectene transfection reagent. The cells were incubated with the transfection mixture for a further 24h then the cells were incubated for 4h in media with amino acids (MEM + 2% serum) (A) or in AAD media (EBSS+MEM Vitamins+1% Peni-Strep (100x) + 2% DFBS, pH 7.4) (B). SNAT2-eGFP expressing cells showed a small but significant increase in transport activity compared to eGFP vector transfected cells. The data are presented as Mean ± SEM of pooled data of three independent experiments (n=3). **P<0.01, ***P<0.001.

### 4.2.4 Characterisation of System A amino acid transporter activity in HEK293A cells transfected with SNAT2-eGFP and SNAT2-HisFLAG constructs

A possible explanation for the lack of response of expressed SNAT2-eGFP activity in HEK293A cells to amino acid deprivation (Figure 4.3) and to DEX (Figure 4.4) is that the presence of a C-terminal tag domain in the protein seriously disturbs the normal regulation of the transporter. This would be expected to be particularly a problem for the normal inhibition of transporter activity by low extracellular pH that is thought to be sensed largely through the C-terminal His residue of SNAT2 (Baird *et al.,* 2006). However, when the pH-dependence of the over-expressed SNAT2-eGFP transport activity was assayed, the usual strong pH dependence was observed (Figure 4.7A). A statistically significant pH dependence was also observed in the basal System A transport activity of non-transfected HEK293A cells. However, when the basal data were plotted on the same vertical scale as for the transfected cells (Figure 4.7B), it could be seen that this basal pH sensitivity made a negligible contribution to the pH sensitivity of the transfected cells in Figure 4.7A.

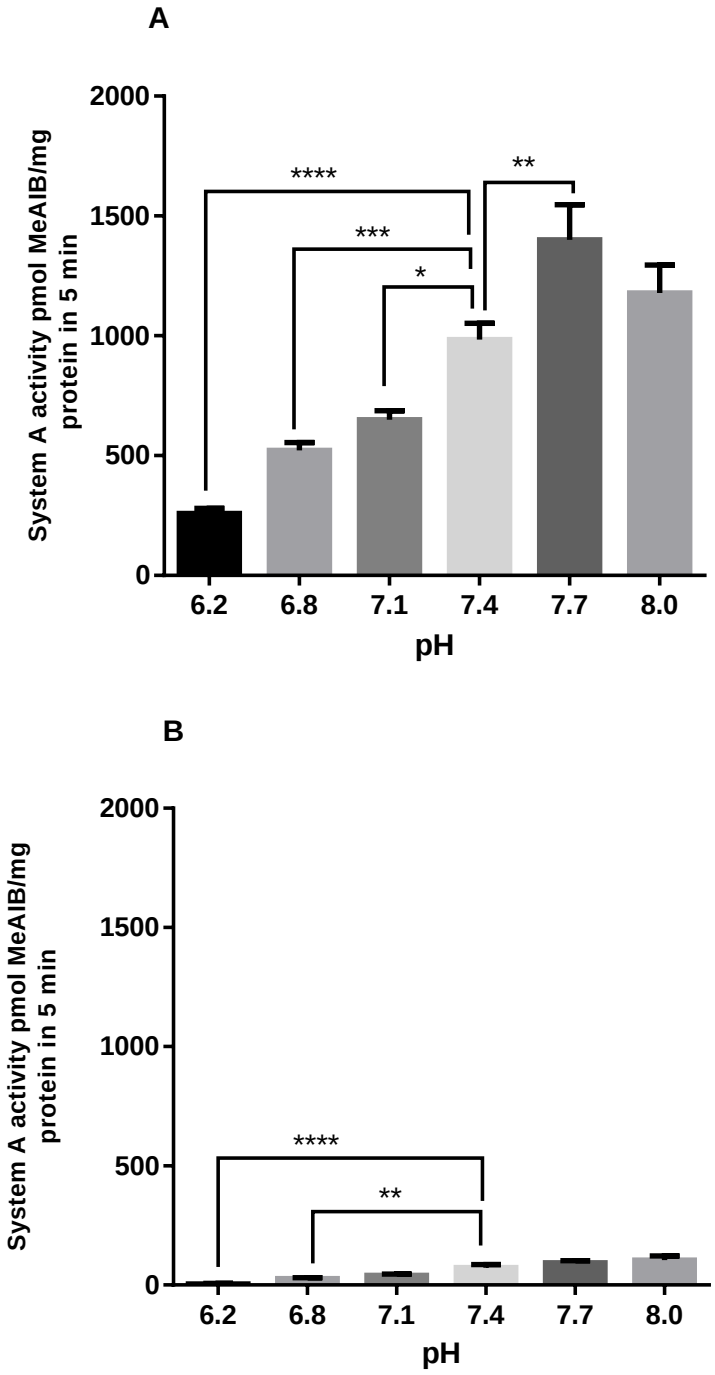


**Figure 4.7. The effect of variation of extracellular pH during the transport assay on System A amino acid transporter activity in HEK293A cells.**

(A) HEK293A cells were plated (as described in Methods) and transfected after 24h with 1µg SNAT2-eGFP plasmid DNA per 22mm well, the medium was changed to fresh growth medium 24h after transfection. The cells were then incubated in serum-free medium for another 24h prior to the performing the transport experiment in Hepes-buffered Saline (HBS) (Appendix A.8). (B) Control (wild type) cultures were cultured as in (A) for the same incubation time and then subjected to the transport assay at the pH values shown. To aid comparison, the transport data are plotted on the same vertical scale as in (A). The cells were incubated in HBS at the specified pH for 5 min only during the transport experiment. The data are presented as Mean ± SEM of three independent experiments (n=3) (with five replicate culture wells for each treatment), *P<0.05, **P<0.01, ***P<0.001, ****P<0.0001 versus the pH 7.4 control cultures.

An apparent increase in System A amino acid transporter activity was also expressed in HEK293A cells that had been transfected with SNAT2-HisFLAG plasmid, when compared with ligated empty vector (Figure 4.8A). However, the magnitude of this expressed activity was small in some experiments (see Figure 4.9). Furthermore, when the pH sensitivity of the expressed SNAT2-HisFLAG activity was calculated by subtracting the activity assayed at the same pH in parallel cultures transfected with the empty vector, only weak residual pH sensitivity was detected (Figure 4.8B), suggesting that the presence of the C-terminal HisFLAG tag may impair the normal pH sensitivity of the transporter.

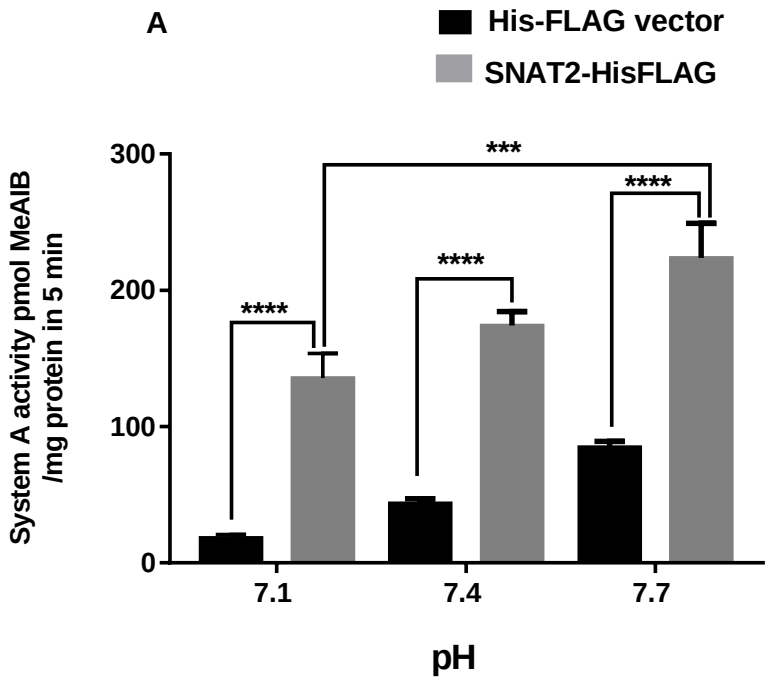

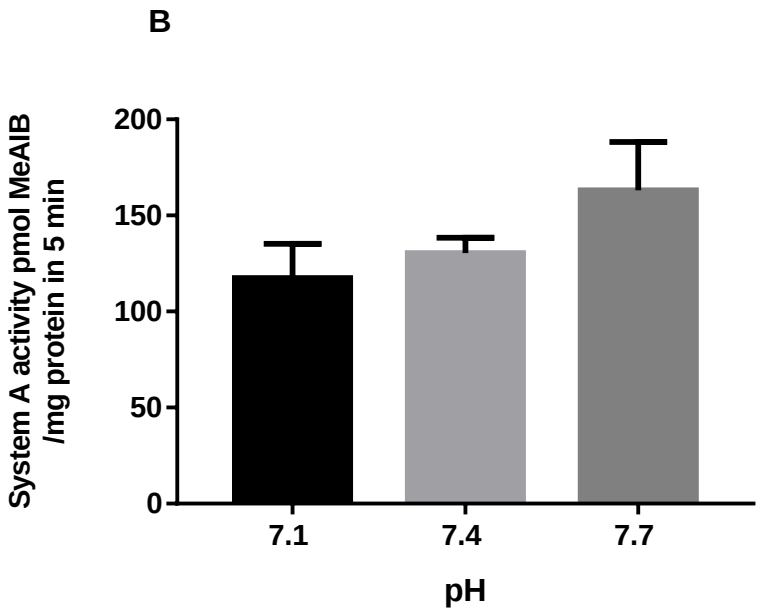


**Figure 4.8. The effect of variation of extracellular pH during the transport assay on System A amino acid transporter (SNAT2) activity in HEK293A cells.**

The cells were transfected with 1µg per 22mm well SNAT2-HisFLAG plasmid or empty HisFLAG-Vector. (A) Cells were incubated in serum-free media for 24 h prior to transport experiments then the cells were incubated in a medium (HBS) (Appendix A.8) with the different pH values shown in the graph. The data are presented as Mean ± SEM of three independent experiments (n=3) (with 5 replicate culture wells for each treatment). ****p<0.0001. (B) Transport activity in SNAT2-HisFLAG-transfected cultures after subtraction of activity in the corresponding empty HisFLAG vector control cultures show no statistically significant pH sensitivity. (pH 7.1 versus pH 7.7 cultures, P =0.1508).

It was also found that the usual up-regulation of System A transporter activity by amino acid deprivation in HEK293A cells was not observed in cultures transfected with SNAT2-HisFLAG plasmid (Figure 4.9).

In view of these apparent problems with the expressed HisFLAG-tagged SNAT2 fusion protein (Figure 4.8B and Figure 4.9), it was not used for further studies in this thesis.

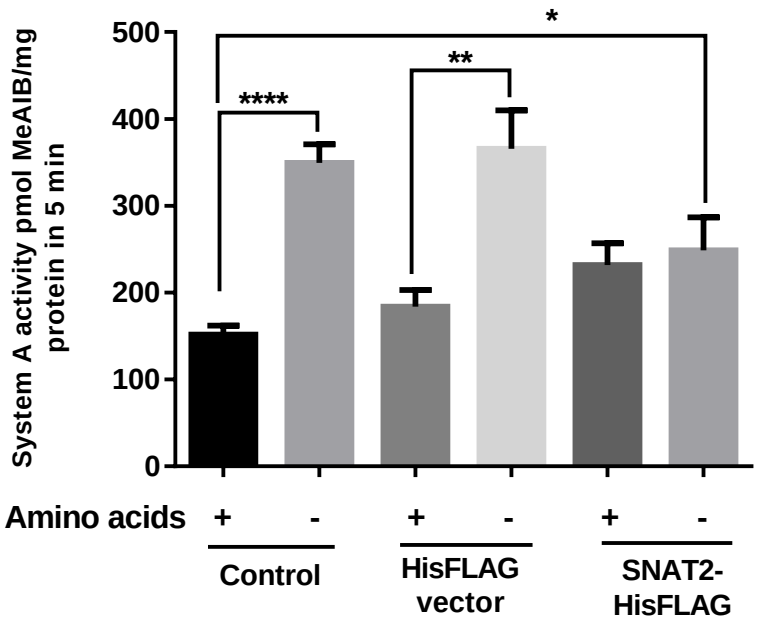


**Figure 4.9. Amino acid deprivation (AAD) does not increase System A transport activity in HEK293A cells expressing SNAT2-HisFLAG.**

The usual increase in System A activity was observed in control (wild type) and HisFLAG vector transfected cells after 4h. Transfecting the cells with 1µg SNAT2-HisFLAG did not activate System A activity under AAD conditions (EBSS + MEM Vitamins + Peni-Strep + 2% vol/vol DFBS, pH 7.4) at the same incubation time. The bar graph values are presented as Mean ± S.E. of three independent experiments (n=3) (with 5 replicate culture wells for each treatment). * Denotes conditions differing significantly from Control (*P<0.05, **P<0.01****P<0.0001. The apparent decline between SNAT2-HisFLAG and HisFLAG vector under AAD conditions was not statistically significant (P = 0.090).

### 4.2.5 MAPK dependence

As MAP kinases (MAPKs) are physiologically important regulators of System A amino acid transporters, including SNAT2 (Kashiwagi *et al.,* 2009), and as the dependence of System A transport activity on MAPKs had already been confirmed in L6 myotubes in Chapter 3 (Figure 3.13), the effect of MAPK inhibition on the System A activity of SNAT2-eGFP transfected HEK293A cells was investigated (Figure 4.10) to determine whether similar kinase regulation of SNAT2 occurred in HEK293A cells, as in L6 cells. Transfecting HEK293A cells with SNAT2-eGFP and treating the cells with MAPK inhibitors showed significant inhibitory effects on System A transporter activity, especially when MEK inhibitor (50µM) was used (Cerioni *et al.,* 2003; Newton *et al.,* 2000) and when a combination of all 3 MAPK inhibitors was applied (Figure 4.10A). From Figure 4.10B a clear dependence on the individual MAPK inhibitors was also observed

when the basal System A transport activity of non-transfected HEK293A cells was studied, and complete inhibition was seen when all inhibitors were combined. However, (as in Figure 4.7) this basal effect of MAPK inhibition was not large enough to account for the effect of MAPK inhibition in the transfected cells in Figure 4.10A. When the basal activity was subtracted to show the net activity arising from SNAT2-eGFP transfection (Figure 4.10C), a statistically significant inhibitory effect was still seen with the MEK inhibitor, suggesting that phosphorylation events downstream from the MEK/Erk pathway can regulate SNAT2-eGFP.

These experiments did not show however whether direct phosphorylation of the SNAT2-eGFP fusion protein was involved in these effects. The fusion protein was therefore further characterised by immunoblotting and by immunoprecipitation in an attempt to determine whether direct phosphorylation occurs.

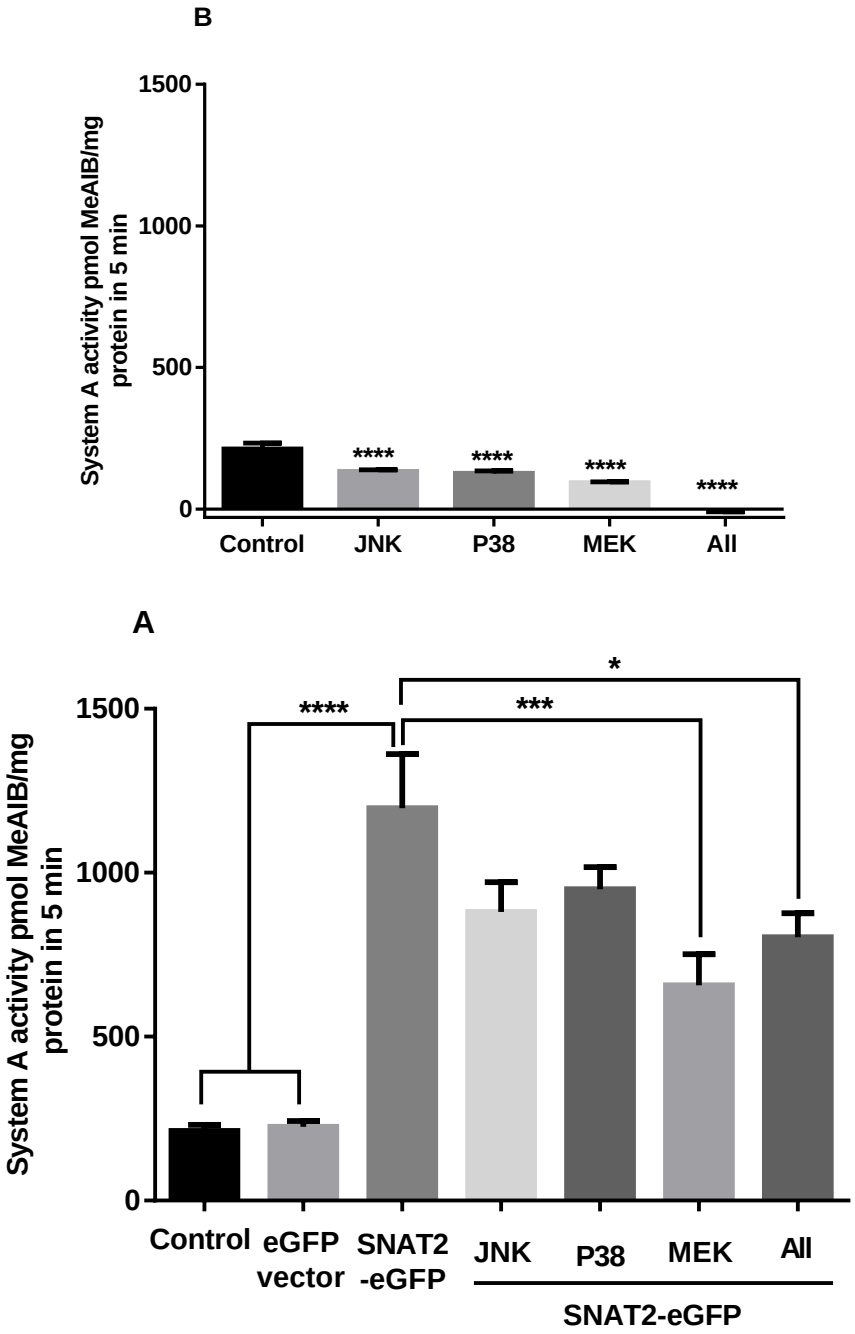
B
System A activity pmol MeAIB/mg protein in 5 min
1500
1000
500
0
****
****
****
****
Control
JNK
P38
MEK
All
A
System A activity pmol MeAIB/mg protein in 5 min
1500
1000
500
0
****
***
*
Control
eGFP vector
SNAT2 -eGFP
JNK
P38
MEK
All
SNAT2-eGFP

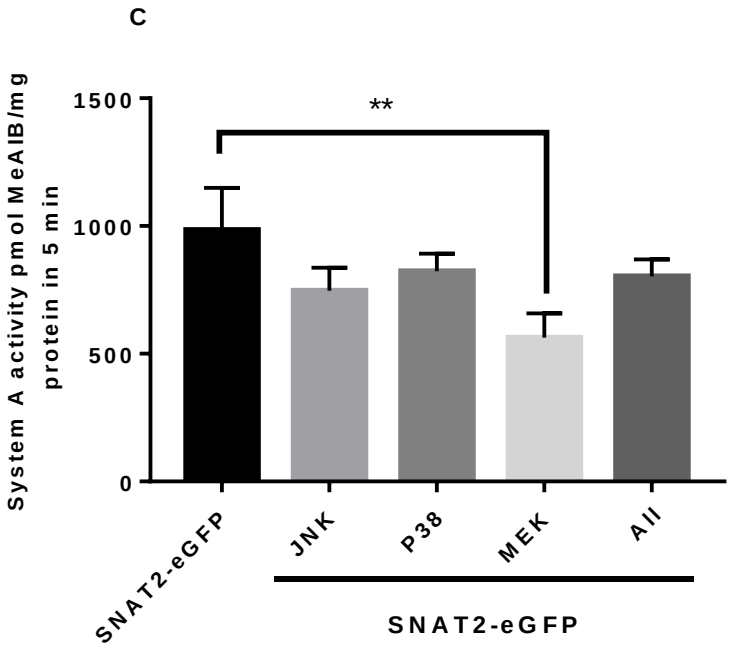


**Figure 4.10. Mitogen-activated protein kinase (MAPK) inhibitors inhibit System A activity in HEK293A cells.**

(A) HEK293A cells were plated (as described in Methods) and transfected after 24h with 1µg SNAT2-eGFP plasmid DNA per 22mm well. The medium was changed to fresh growth medium 24h after transfection. On the day of the experiment the cells were incubated with three different MAPK inhibitors, 10µM SP600125 - JNK inhibitor; 5µM SB202190 - P38 inhibitor; 50µM PD98059 - MEK inhibitor; "All" denotes all inhibitors combined. *P<0.05, ***P<0.001, ****P<0.0001 (n=3). (B) The same inhibitors applied to wild type HEK293A cells. Transport activity measured with each individual inhibitor or all inhibitors combined was compared with Control cultures without inhibitor ****P<0.0001 (n=3). (C) Net transport activity in SNAT2-eGFP-transfected cultures (A) after subtraction of activity in the corresponding non-transfected control cultures (B) **P<0.01. The data are presented as Mean ± SEM of three independent experiments (n=3).

### 4.2.6 Detection of intact SNAT2-eGFP protein in HEK293A cells by immunoblotting: the effects of amino acid deprivation; and of Alkaline Phosphatase treatment of lysates

As an alternative to System A activity assay, anti-GFP antibody was used for Western blotting as a semi-quantitative measurement of expression of the SNAT2-eGFP construct. The aim of this experiment was also to determine the effect of amino acid deprivation on eGFP-tagged SNAT2 protein expression (Fig.4.11A), and to test the effect of protein de-phosphorylation by incubating the cell lysates with Alkaline Phosphatase (50U/ml) for 30 min at $37^0$C before performing the immunoblotting (Fig.4.11B).

In this experiment, immuno-blotting with anti-GFP antibody detected more than one band (see Discussion): a light band at ~80kDa (the size expected for the SNAT2-eGFP fusion protein i.e. 56kDa SNAT2 plus 27kDa eGFP), with a heavier band at ~100kDa. An additional band at ~25kDa possibly arose from free eGFP released by proteolysis of the fusion protein (Figure 4.11). No such bands were observed in non-transfected HEK293A lysates (data not shown). Similar approximately 80 and 100kDa bands have been reported previously in anti-GFP immunoblots of SNAT2-eGFP transfected cells (Hatanaka *et al.,* 2006).

De-phosphorylation of proteins in the lysates by incubation with Alkaline Phosphatase at 37$^{o}$C for 30 min caused no detectable mobility shift in the suspected SNAT2-eGFP light band, but it did enhance the intensity of the light band relative to that seen with Alkaline Phosphatase Vehicle as a control (Figure 4.11B), possibly indicating that de-phosphorylation of the lighter form of SNAT2 (or de-phosphorylation of an associated protein such as a protease) inhibits SNAT2 proteolysis in lysates.

In contrast to the lack of effect of amino acid deprivation that was seen on transport activity in Figure 4.3, amino acid deprivation did up-regulate expression of the SNAT2-eGFP fusion protein in the immunoblots in Figure 4.11A, possibly because the total SNAT2-eGFP protein pool in the cell increases but the plasma membrane is saturated with these proteins in SNAT2-eGFP transfected cells and no further increase can be induced in that plasma membrane pool (i.e. the $^{14}$C-MeAIB transporting pool) by amino acid deprivation.

The apparent heavy (100kDa) GFP-tagged band detected in Figure 4.11 (which may be a glycosylated isoform of SNAT2 (Nardi *et al.,* 2015)) showed no statistically significant dependence on AAD or Alkaline Phosphatase treatment (Figure 4.11C). However, the heavy/light band ratio declined significantly in response to AAD and declined even further on Alkaline Phosphatase treatment (Figure 4.11D).

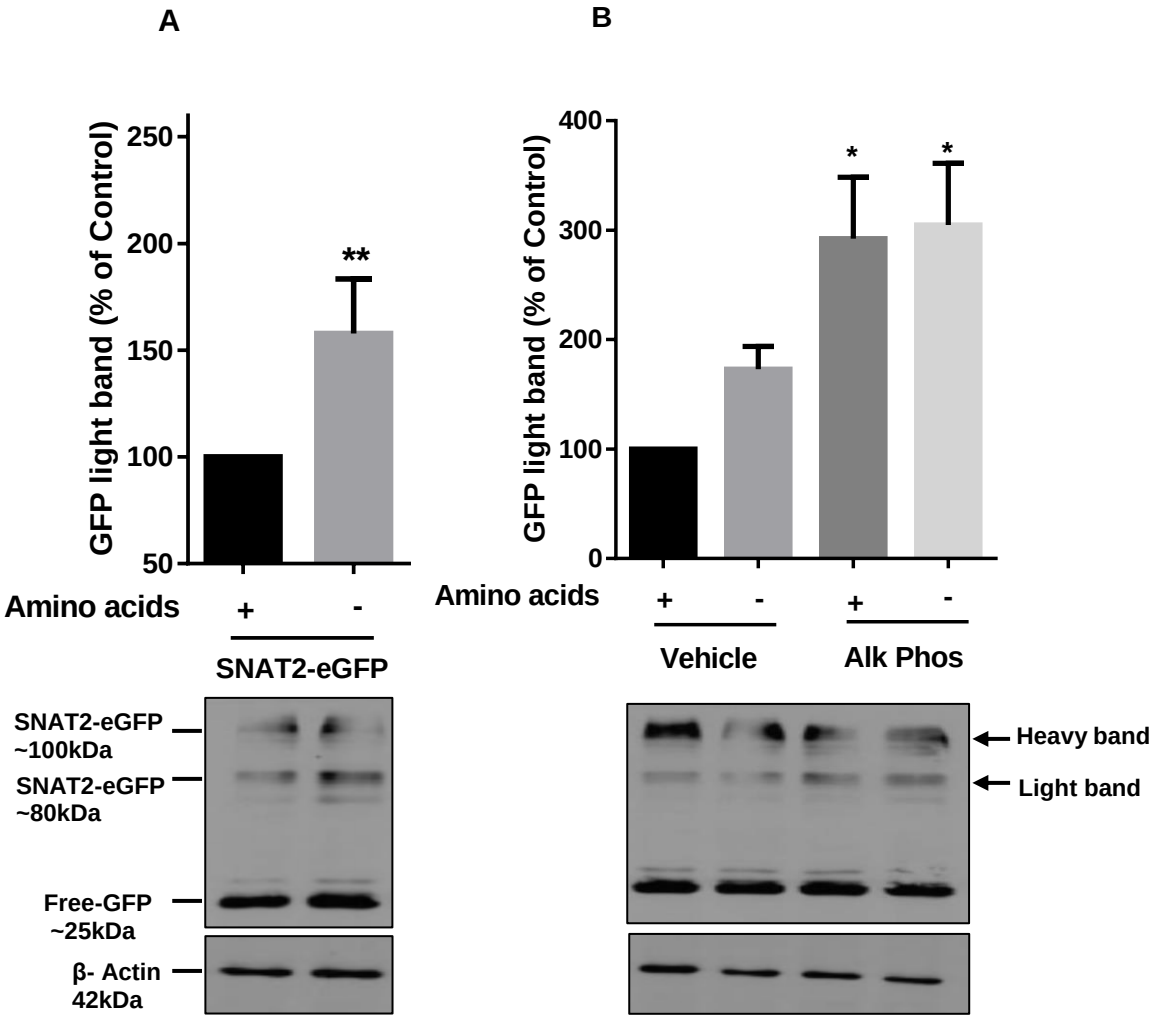
A
B
GFP light band (% of Control)
250
200
150
100
50
**
Amino acids
+
-
SNAT2-eGFP
SNAT2-eGFP
~100kDa
SNAT2-eGFP
~80kDa
Free-GFP
~25kDa
β- Actin
42kDa
GFP light band (% of Control)
400
300
200
100
0
*
*
Amino acids
+
-
+
-
Vehicle
Alk Phos
Heavy band
Light band

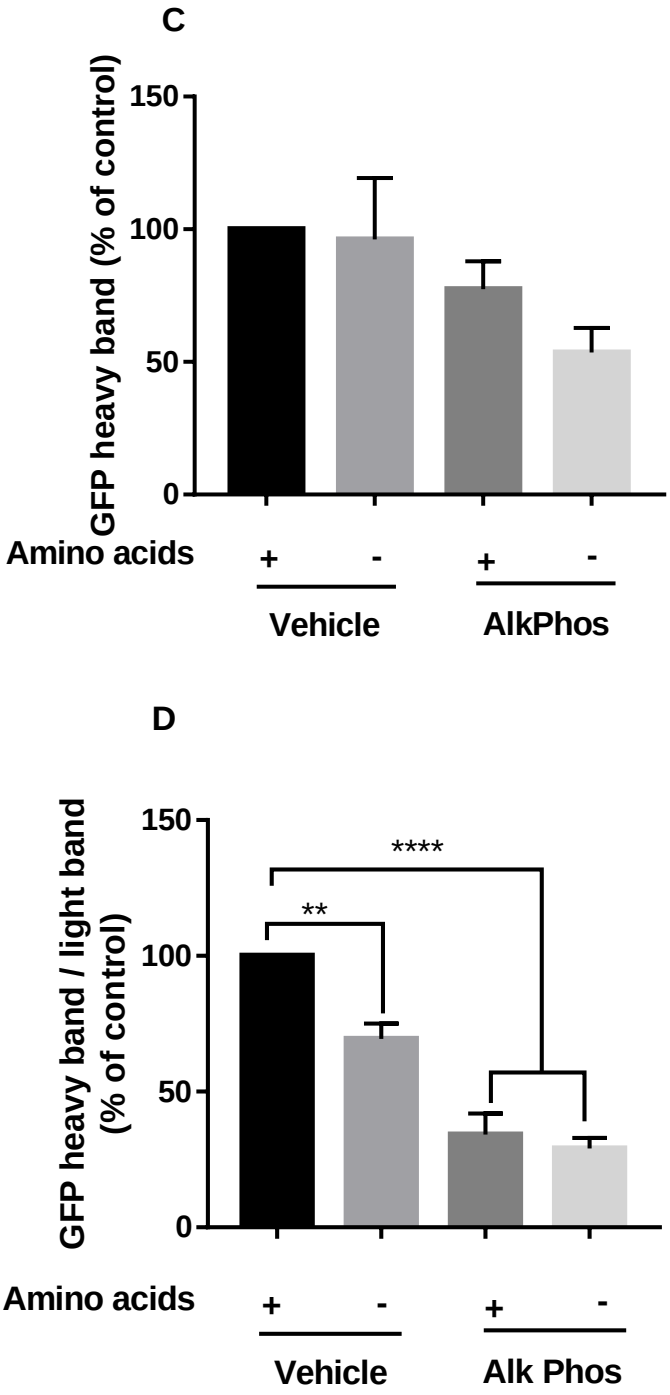


**Figure 4.11. Amino acid deprivation increases SNAT2-eGFP protein expression detected by anti-GFP immunoblotting.**

(A) Incubating HEK293A cells (transfected with 2µg SNAT2-eGFP cDNA per 35mm well) for 4h in amino acid deprived medium showed a significant increase in SNAT2 protein expression. The cells were rinsed three times with 2ml HBSS to remove any extracellular amino acids then incubated in MEM with 2% vol/vol DFBS or in medium without amino acids (EBSS + MEM Vitamins + Peni-Strep + 2% DFBS, pH 7.4). Densitometry is shown for six independent experiments (n=6) accompanied by a representative blot, **P<0.01. (B - D) The cells were incubated with or without amino acids then scraped in 200µl lysis buffer and the lysates were treated with either Alkaline Phosphatase Vehicle (50mM KCl, 10mM Tris-HCl pH 8.2, 1mM $MgCl_2$,

0.1mM $ZnCl_2$, 50% Glycerol) or Alkaline Phosphatase (50U/ml) and warmed at 37°C for 30 min in a culture incubator (n=3). The black arrows indicate the bands that were quantified: (B) shows densitometry of the light band accompanied by a representative blot, *p<0.05. (C) Shows densitometry quantification of the heavy band, and (D) densitometry analysis of the heavy / light ratio. Data are presented as a percentage of the control (Alk.Phos. vehicle treated cells with amino acids) (n=3). **P<0.01, ****P<0.0001.

### 4.2.7 Immunoprecipitation of SNAT2-eGFP protein

In an attempt to detect directly phosphorylation of SNAT2, the SNAT2-eGFP fusion protein was isolated by immunoprecipitation using the GFP-Trap method following by mass spectrometry analysis of the isolated protein. To maximise the yield of the protein, SNAT2-eGFP transfected cells were amino acid starved for 4h to up-regulate expression of the protein (as in Figure 4.11). The isolated GFP-trapped protein was sent to the PNACL proteomics facility at the University of Leicester for peptide identification and detection of possible phosphorylation sites.

Initial analysis of the GFP-trapped proteins by SDS-PAGE (Lane D1 in Figure 4.12A) yielded results consistent with the immunoblots in Figure 4.11 i.e. a band of approximately the molecular weight expected for the fusion protein (~80 kDa), a heavier band of about 100kDa and a protein of ~25 kDa (the size expected for free eGFP) (Fig 4.12A). Mass spectrometry of the 80kDa band detected SNAT2 peptides but the peptides that were detected only covered 10% of the human SNAT2 amino acid sequence (Figure 4.12B) and only contained 2 of the 20 phosphorylation sites that were reported in human SNAT2 in a preliminary mass spectrometry screen (Proteinpedia, see bibliography for the link). Partly for that reason no phospho-peptides were detected.

The presence of free eGFP in GFP-trapped SNAT2-eGFP cell lysates (Figure 4.12A) suggested that proteolysis of SNAT2-eGFP had occurred. Furthermore, a previous study (Nardi *et al.,* 2015) had reported degradation of newly synthesised SNAT2 through the ubiquitin-proteasome pathway (UPP), and the data in Figure 3.19 had suggested a role for the UPP in regulation of System A activity and SNAT2 in L6 myotubes. The same GFP-trap procedure was therefore repeated but with incubation of the SNAT2-eGFP-transfected cells during the 4h amino acid deprivation period with 10µM proteasome inhibitor MG132. SDS-PAGE analysis of the resulting GFP-trapped proteins now detected bands above about

70kDa, but no obvious free GFP band at 29 kDa (Lane D2 in Figure 4.12C). The GFP-trapped protein bands were again isolated from the SDS gel. The bands denoted B1 and B2 at ~ 100 and ~70-80 KDa (the expected size for SNAT2-eGFP) (Figure 4.12C) were both confirmed by proteomics to contain SNAT2-eGFP (Appendix D), but this time the peptides detected showed improved coverage (18% of the human SNAT2 amino acid sequence – Figure 4.12D) and contained more of the amino acid residues that had previously been reported as phosphorylation sites, including the closely spaced sequence of such sites SSSYSS that are shown in Figure 1.12 at residues 17-22 ( Proteinpedia, see bibliography for the link). In spite of this, no phosphopeptides were detected (Figure 4.12D).

**A**

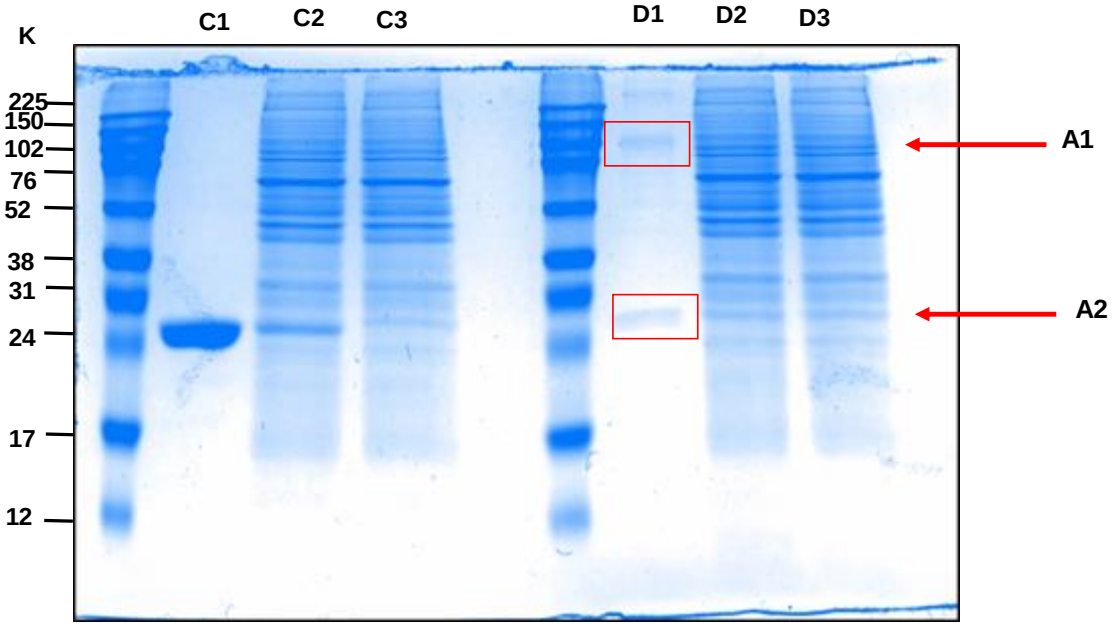


**C1: GFP vector**
**C2: Diluted cell lysate**
**C3: Cell lysate from the 1st wash**
**D1: SNAT2-eGFP**
**D2: Diluted cell lysate**
**D3: Cell lysate from the 1st wash**

**B**

Nominal mass ($M_r$): **56359; Calculated pI value: 8.08**
Matched peptides shown in **Bold Red**

```
   1 MKKAEMGRFN ISPDEDSSSY SSNSDFNYSY PTKQAALKSH YADVDPENQN
  51 FLLESNLGKK KYETEFHPGT TSFGMSVFNL SNAIVGSGIL GLSYAMANTG
 101 IALFIILLTF VSIFSLYSVH LLLKTANEGG SLLYEQLGYK AFGLVGKLAA
 151 SGSITMQNIG AMSSYLFIVK YELPLVIQAL TNIEDKTGLW YLNGNYLVLL
 201 VSLVVILPLS LFRNLGYLGY TSGLSLLCMV FFLIVVICKK FQVPCPVEAA
 251 LIINETINTT LTQPTALVPA LSHNVTENDS CRPHYFIFNS QTVYAVPILI
 301 FSFVCHPAVL PIYEELKDRS RRRMMNVSKI SFFAMFLMYL LAALFGYLTF
 351 YEHVESELLH TYSSILGTDI LLLIVRLAVL MAVTLTVPVV IFPIRSSVTH
 401 LLCASKDFSW WRHSLITVSI LAFTNLLVIF VPTIRDIFGF IGASAASMLI
 451 FILPSAFYIK LVKKEPMKSV QKIGALFFLL SGVLVMTGSM ALIVLDWVHN
 501 APGGGH
```

**Match to: Homo sapiens Sodium-coupled neutral amino acid transporter 2**

**C**

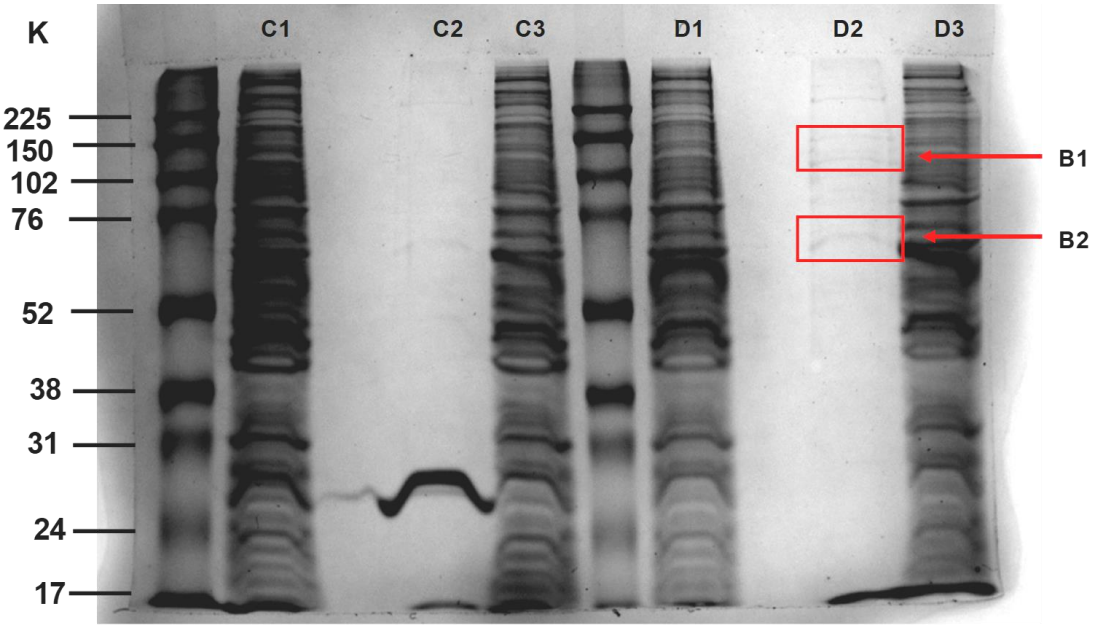


**C1: Diluted cell lysate**
**C2: GFP-vector**
**C3: Cell lysate from the 1st wash**
**D1: Diluted cell lysate**
**D2: SNAT2-eGFP+MG132**
**D3: Cell lysate from the 1st wash**

**D**

Nominal mass ($M_r$): **56332**; Calculated pI value: **8.08**

Matched peptides shown in **Bold Red**

```
   1 MKKAEMGRFS ISPDEDSSSY SSNSDFNYSY PTKQAALKSH YADVDPENQN
  51 FLLESNLGKK KYETEFHPGT TSFGMSVFNL SNAIVGSGIL GLSYAMANTG
 101 IALFIILLTF VSIFSLYSVH LLLKTANEGG SLLYEQLGYK AFGLVGKLAA
 151 SGSITMQNIG AMSSYLFIVK YELPLVIQAL TNIEDKTGLW YLNGNYLVLL
 201 VSLVVILPLS LFRNLGYLGY TSGLSLLCMV FFLIVVICKK FQVPCPVEAA
 251 LIINETINTT LTQPTALVPA LSHNVTENDS CRPHYFIFNS QTVYAVPILI
 301 FSFVCHPAVL PIYEELKDRS RRRMMNVSKI SFFAMFLMYL LAALFGYLTF
 351 YEHVESELLH TYSSILGTDI LLLIVRLAVL MAVTLTVPVV IFPIRSSVTH
 401 LLCASKDFSW WRHSLITVSI LAFTNLLVIF VPTIRDIFGF IGASAASMLI
 451 FILPSAFYIK LVKKEPMKSV QKIGALFFLL SGVLVMTGSM ALIVLDWVHN
 501 APGGGH
```

**Match to: Homo sapiens Sodium-coupled neutral amino acid transporter 2**

**Figure 4.12. (A) SDS-PAGE gel showing the GFP-Trapped SNAT2-eGFP bands and other protein fractions obtained using the GFP-Trapping method (Section 2.6).**

The gel was stained using RAPID stain reagent (Calbiochem. Cat.no. 553215) followed by excision of the bands (A1 and A2) followed by proteomic analysis by mass spectrometry. The A1 band was confirmed as SNAT2-eGFP and A2 as GFP protein. HEK293A cells were incubated in amino acid-deprived medium for 4h before preparation of lysates. (B) Peptide sequence homology with SNAT2 (shown in red bold letters) identified by Mascot database search of data from the A1 band. (C) SDS-PAGE gel of samples prepared by the same method as in A but the cells were incubated in amino acid-deprived medium with 10μM MG132 for 4h before preparation of lysates. Bands B1and B2 were both confirmed as SNAT2-eGFP by proteomic analysis by mass spectrometry. (D) Peptide sequence homology with SNAT2 (shown in underlined red bold letters) identified by Mascot database search of data from the B1 band, A similar result was obtained from the B2 band (result not shown).

### 4.2.8 The Effect of DEX on intracellular GFP fluorescence intensity in SNAT2-eGFP transfected HEK293A cells

The data above suggest that the SNAT2-eGFP fusion protein is expressed mainly intact in HEK293A cells, and shows physiological responses to pH and MAPK inhibitors that are similar to those for wild-type SNAT2 (Baird *et al.,* 2006; Kashiwagi *et al.,* 2009). However, the expressed SNAT2-eGFP does not show the normal up-regulation of its transporter activity in response to amino acid deprivation (Figure 4.3) nor the down-regulation of its activity in response to DEX (Figure 4.4) that were seen in L6 myotubes in Chapter 3. It has previously been proposed that the SNAT2 protein occurs in cells in at least 2 pools: a newly synthesised (probably immature) intracellular pool with a lower molecular weight

close to the 56kDa predicted from the mRNA sequence, and a heavier glycosylated and functionally mature form that performs amino acid transport in the plasma membrane (Nardi *et al.,* 2015). The lower molecular weight form has been reported to be preferentially degraded through the ubiquitin-proteasome pathway (Nardi *et al.,* 2015). It is possible therefore that some of the regulatory effects on SNAT2 previously suggested in L6 myotubes in Chapter 3 (e.g. DEX-induced degradation through the ubiquitin-proteasome pathway) may be observed more readily in the newly synthesised intracellular SNAT2-eGFP pool inside transfected HEK293A cells, but not in the functionally active (i.e. amino acid transporting) pool in the plasma membrane.

To test this possibility, HEK293A cells transfected with SNAT2-eGFP were incubated for 4h with 500nM DEX (with or without the proteasome inhibitor MG132) exactly as in the L6 myotube experiment in Figure 3.19 but, instead of measuring System A transport activity, SNAT2-eGFP fluorescence was quantified. The results are shown in Fig 4.13. A significant decrease in fluorescence was observed with DEX, and a partial blunting of this decrease was seen in the presence of MG132. This was similar to the effects on System A transport activity in L6 myotubes in Figure 3.19 and consistent with the hypothesis that DEX down-regulates the SNAT2 protein at least partly by degradation through the Ubiquitin Proteasome Pathway.

**A**

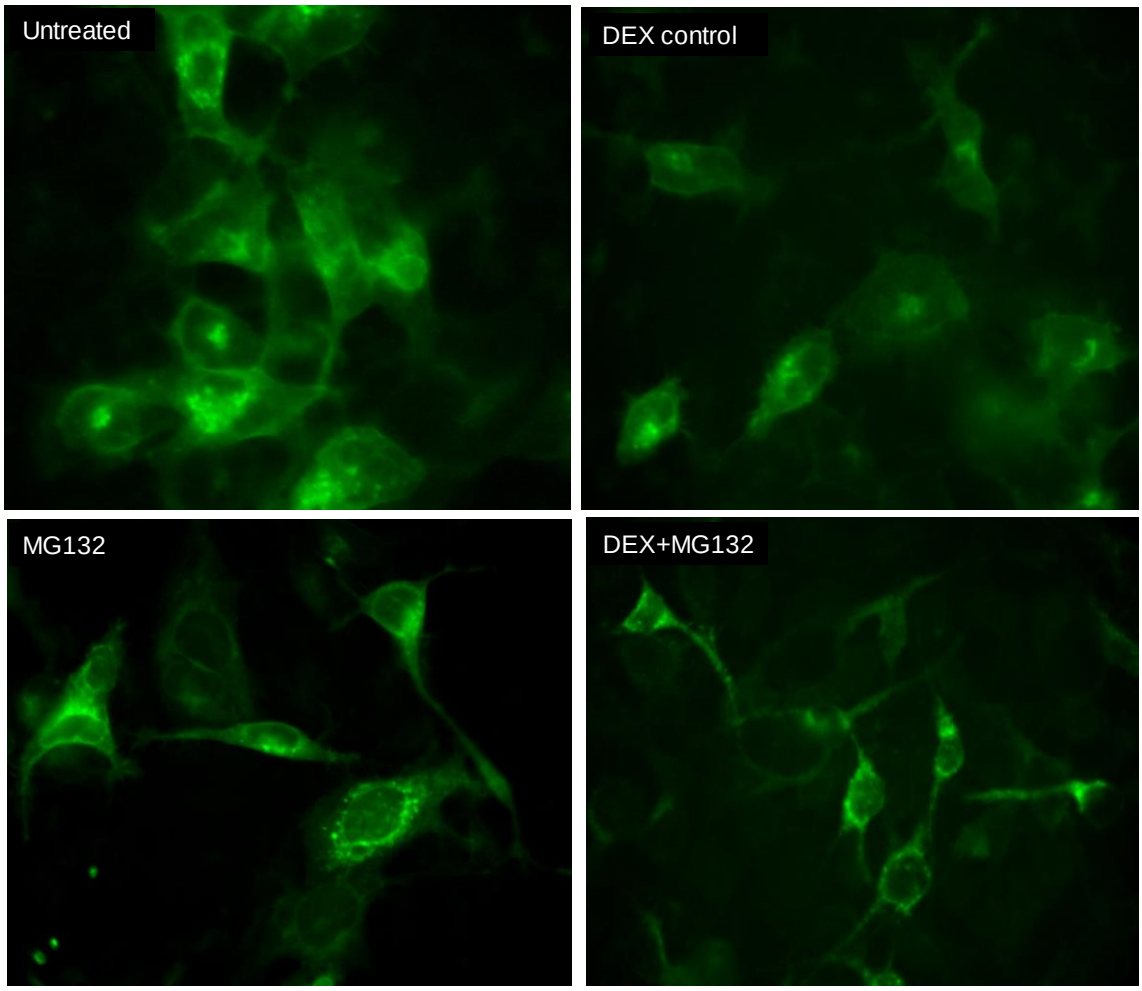

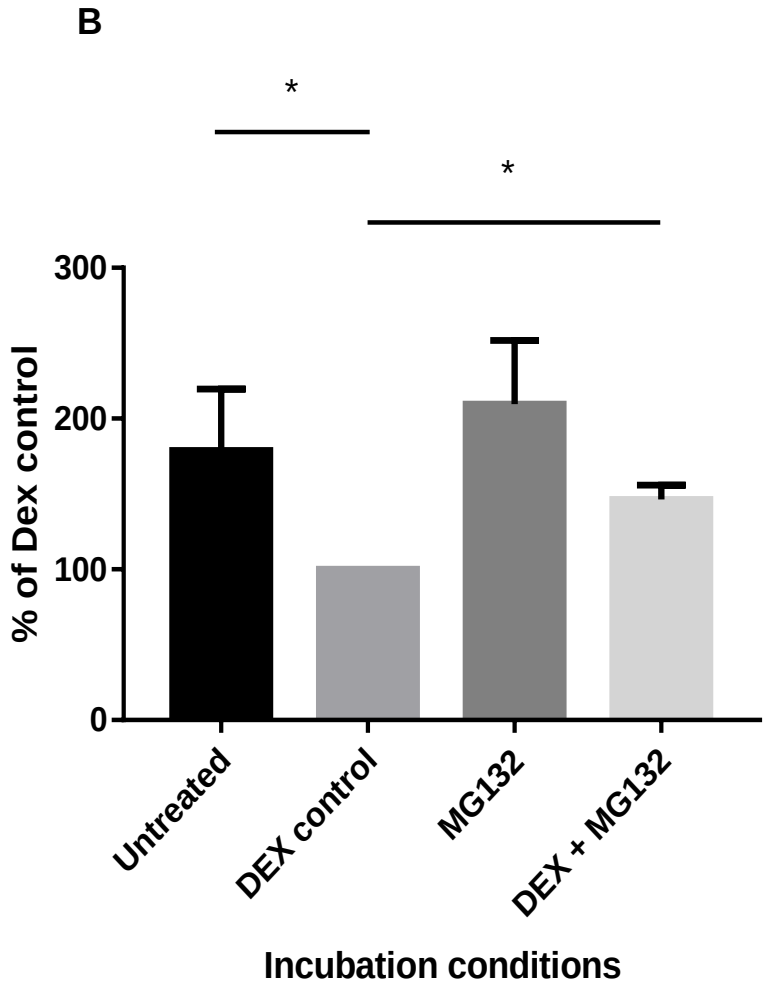


**Figure 4.13. Dexamethasone decreases the GFP fluorescence intensity in SNAT2-eGFP transfected HEK293A cells.**

HEK293A cells were transfected with 2µg SNAT2-eGFP construct per 35mm well for 24h then the cells were incubated with 500nM DEX with or without 10µM proteasome inhibitor MG132 for 4h. Images were taken by using an inverted Olympus IX81 motorized microscope with a Scan^R screening platform and a Cell^R imaging station (Advanced Imaging Facility, University of Leicester). (A) Shows representative fluorescence images for each experimental condition 40X. (B) Shows fluorescence intensity data pooled from eight independent experiments (n=8) from analysis of approximately 17 cell images under each experimental condition in each experiment. The GFP fluorescence was quantified using ImageJ software. *P<0.05.

## 4.3 Discussion

### 4.3.1 Expression of SNAT2-eGFP in HEK293A cells leads to a functioning System A amino acid transporter

The characterisation experiments in this chapter showed that expression of SNAT2-eGFP in HEK293A cells leads to expression of a fusion-protein (tagged amino acid transporter) with properties similar to those previously reported for the amino acid transporter SNAT2 in (for example) L6 cells (Baird *et al.,* 2006; Bröer, 2014; Hatanaka *et al.,* 2006; Kashiwagi *et al.,* 2009; Nardi *et al.,* 2015).These properties included:

- Ability to transport the System A substrate MeAIB (Figure 4.3)
- Inhibition of the transport by low pH (Figure 4.7A)
- Dependence of the transport on MAP kinases (Figure 4.10A, C)
- Approximate mass predicted from the mass of SNAT2 + eGFP (Figure 4.11A)
- Expected amino acid sequence in peptides detected by mass spectrometry (Figure 4.12D)
- Up-regulation of the protein by AAD (Figure 4.11A)
- Down-regulation of the protein by DEX (Figure 4.13)

It was surprising that the over-expressed SNAT2-eGFP was strongly pH sensitive. The eGFP tag is at the C-terminal His residue which is reported to be the main pH-sensing site in the molecule (Baird *et al.,* 2006) and this might have been expected to block pH-sensing. However, lysates of these SNAT2-eGFP transfected cells were found to contain high concentrations of free eGFP in addition to the predicted fusion protein (Figure 4.11) suggesting that some of the fusion proteins had been cleaved. If this cleavage occurred selectively at the coupling site between SNAT2 and eGFP in the intact cells before lysate preparation, it may have been the pH sensitive transport activity of the resulting free SNAT2 which was detected in Figure 4.7. This explanation is unlikely however because the amino acid sequence that couples SNAT2 to eGFP in the SNAT2-eGFP fusion protein that is expressed from SNAT2 cDNA in the pLEICS-

29 expression vector is designed to be resistant to the proteases in mammalian cells. For example, when the human LAT1 (slc7a5) amino acid transporter was recently expressed in this laboratory using the same expression vector (with the same coupling sequence) and the same HEK293A cells, the intact LAT1-eGFP fusion protein, but no detectable free eGFP, was detected in lysates prepared and immunoblotted by the method described here (Violeta Diez Beltran, PhD thesis, University of Leicester, June 2017). It therefore seems more likely that the free eGFP detected in Figure 4.11 was produced by rapid degradation of the SNAT2 sequence of the SNAT2-eGFP fusion protein, either in the intact cells, or later in the lysates.

This fusion protein model of SNAT2 showed at least 2 limitations when compared with the data in Chapter 3: its transport activity did not rise in response to AAD and it did not fall in response to DEX. However total protein expression did respond as expected to AAD and DEX, suggesting that translocation of the fusion protein to the plasma membrane was limiting these expected effects on transport.

### 4.3.2 Isoforms of SNAT2 and SNAT2-eGFP

Published immunoblots of endogenous wild-type SNAT2 in lysates or membrane preparations from L6 cells, using antibody against the cytoplasmic tail of SNAT2, detect a band at ~55kDa (the size of the SNAT2 protein predicted from the cDNA sequence), usually accompanied by a heavier band of ~70-80kDa (possibly glycosylated isoform(s)) and a lighter band ~ 40kDa, probably arising from rapid SNAT2 degradation that occurs even in cell lysates containing protease inhibitors (Evans *et al.,* 2008; Hyde *et al.,* 2007). Repeated freeze-thaw of lysates also leads to loss of the 55kDa band, again suggesting rapid SNAT2 degradation (A. Bevington, personal communication).

Apparent high and low molecular weight forms of SNAT2-eGFP were also detected here both by anti-GFP immuno-blotting (Figure 4.11) and by GFP-trapping (Figure 4.12), in agreement with previously reported 80 and 100kDa bands in anti-GFP immunoblots of SNAT2-eGFP transfected 3T3-L1 cells (Hatanaka *et al.,* 2006). The molecular weight of the heavier GFP-trapped band was higher than expected for SNAT2-eGFP, but mass spectrometry of the excised band showed the presence of SNAT2 peptides (Figure 4.12B and 4.12D)

suggesting that this arose from a heavy (possibly glycosylated) isoform of SNAT2 (as proposed by Nardi et al, 2015) rather than from non-specific binding of anti-GFP antibody to another protein.

### 4.3.3 Up-regulation of the SNAT2-eGFP protein by AAD

Amino acid deprivation increased SNAT2-eGFP protein expression in the anti-GFP Western blotting shown in Figure 4.11A. This is consistent with the up-regulation of the SNAT2 protein that is observed in response to AAD in L6 cells (Hyde *et al.,* 2007; Nardi *et al.,* 2015). There are two possible mechanisms through which AAD can increase SNAT2-eGFP expression. Firstly, through an increase in SNAT2 gene transcription (Hyde *et al.,* 2007) and *de novo* SNAT2 protein synthesis; or secondly through decreased degradation (stabilisation of the protein) (Hyde *et al.,* 2007). The first possibility is not applicable here because the SNAT2-eGFP construct transfected into HEK293A cells does not contain the amino acid responsive upstream regulatory region of the human SNAT2 gene and transcription was controlled instead by an SV40 promoter (Section 2.4.1). Therefore, decreased SNAT2 protein degradation during AAD seems more likely to be the explanation (Nardi *et al.,* 2015). Such degradation through the UPP is thought to act mainly on the newly synthesised intracellular pool of SNAT2 which has a lower molecular weight than the mature pool transporting amino acid in the plasma membrane (Nardi *et al.,* 2015).This is consistent with the present immunoblotting data (Figure 4.11) in which AAD increased the light SNAT2-eGFP band but not the heavy band.

### 4.3.4 Phosphorylation of the SNAT2-eGFP protein

Even though MAP kinase activation is thought to be involved in the up-regulation of SNAT2 during amino acid deprivation (Hyde *et al.,* 2007), no mobility shift of the SNAT2-eGFP protein was observed on amino acid deprivation (suggesting that there was no large-scale phosphorylation of the fusion protein). Similarly, treatment with alkaline phosphatase (AP) also did not induce a shift, even though AP did alter band intensity (Figure 4.11) suggesting an effect of protein dephosphorylation on SNAT2-eGFP stability in HEK293A cell lysates. This experiment gave no information however on the protein(s) that were phosphorylated.

No phosphopeptides were detected in the mass spectrometry analysis of GFP-trapped SNAT2-eGFP. This might have arisen because of technical limitations in the sample preparation which led to loss of post-translational modifications to SNAT2. For example, no evidence of other post-translational modifications to SNAT2 was observed in the peptide fragments detected by mass spectrometry (e.g. glycosylation and ubiquitination) even though glycosylated and ubiquitinated SNAT2-eGFP almost certainly occurred in the HEK293A cells used here (Figure 4.11, 4.12 and 4.13). The peptides detected also covered only part of the SNAT2 amino acid sequence so phosphorylation sites may have been missed.

## 4.4 Conclusion

In the experiments described in this chapter it was possible to express an eGFP-tagged molecular clone of SNAT2 and partly characterise and isolate the resulting tagged SNAT2 protein. It was also possible to show by fluorescence imaging with SNAT2-eGFP transfected HEK293A cells that the resulting SNAT2-eGFP protein is depleted in cells treated with DEX, through a pathway that is at least partly dependent on the ubiquitin proteasome pathway.

The functional importance of these regulatory effects on SNAT2 in signalling to global protein synthesis and global protein degradation is the subject of the next chapter.

# Chapter 5 Functionally important signals from SNAT2 to global protein metabolism

## 5.1 Unsolved problems in SNAT2 signalling

The effects of glucocorticoid on the activity and protein expression of SNAT2 transporters that were shown in Chapters 3 and 4 would be of little biological significance if changes in the activity of this transporter had no functional effect. The overall aim of this chapter therefore is to provide further understanding of the functional effects of this transporter that might arise from changes in activity and protein expression of SNAT2.

In addition to amino acid-dependent signalling to mTORC1 (Evans *et al.,* 2007), SNAT2 inhibition (by low pH) or siRNA silencing of SNAT2 expression in L6 cells has also been shown to inhibit Akt (Evans *et al.,* 2008). In L6 cells, this coupling between SNAT2 inhibition and Akt has been shown to explain the stimulation of global protein degradation that occurs in response to low pH (acidosis). However, this coupling between SNAT2 and Akt does not occur through amino acids and cannot be mimicked by blocking amino acid transport through SNAT2 with 10mM MeAIB (Evans *et al.,* 2008).

To assess the biological importance of the effects on System A/SNAT2 activity that were observed in the two previous chapters, it is important to understand how changes in SNAT2 expression and activity affect availability of amino acids in cells and potentially anabolic signals to global protein metabolism. Even though it has been shown previously that ***inhibition*** or siRNA silencing of SNAT2 in L6 cells impairs anabolic signals to protein metabolism through mTORC1 and PI3K/Akt (Evans *et al.,* 2007; Evans *et al.,* 2008), the corresponding effect(s) on other major growth signalling pathways such as Ras/Raf/MEK/Erk is still unclear. Furthermore, the possibility of ***stimulation*** of these signalling pathways through over-expression of SNAT2 has not been demonstrated, nor is it fully understood how this amino acid transporter signals to mTORC1 and PI3K/Akt. For example, even though it is well established that the branched chain amino acid L-leucine is a major regulator of mTORC1 in mammalian cells (Kim *et al.,* 2004), it is not certain that L-leucine accounts for all of the effect of SNAT2 on mTORC1 in L6-

G8C5 cells. L-leucine is a poor substrate for SNAT2 and, even though inhibition or silencing of SNAT2 in L6-G8C5 cells leads to depletion of intracellular L-leucine (Evans *et al.,* 2007), this occurs ***indirectly*** through coupling of SNAT2 to System L amino acid transporters (Hundal & Taylor, 2009; Rosario *et al.,* 2016). The possibility that SNAT2 signals to mTORC1 more directly through an amino acid that is transported directly by SNAT2 (i.e. a SNAT2 substrate) has not been investigated. For example, it has been reported previously that the essential amino acid L-methionine (L-Met) which is a good substrate for SNAT2 (Yao *et al.,* 2000) can stimulate mTORC1 in animal cells (Shigemitsu *et al.,* 1999; Stubbs *et al.,* 2002).

The experiments in this chapter therefore had 4 main aims:

- To confirm and extend previous work in L6-G8C5 cells (Evans *et al.,* 2007; Evans *et al.,* 2008), which had shown that siRNA silencing of SNAT2 significantly impairs mTORC1 and Akt signalling
- To determine the effect of SNAT2 over-expression in HEK293A cells on mTORC1 and Akt signalling; and on intracellular free amino acid concentrations.
- To test the hypothesis that transport of a single SNAT2 amino acid substrate (i.e. L-Met) into cells through SNAT2 can be sufficient to induce a detectable activation of the amino acid-sensing mTORC1 pathway (using downstream phosphorylation of ribosomal protein S6 (rpS6) as a sensitive read-out of mTORC1 activation).
- To determine whether the observed inhibition or down-regulation of SNAT2 by DEX in L6 cells that was observed in Chapter 3 has significant corresponding effects on protein anabolic signalling to Akt.

## 5.2 Results

### 5.2.1 The effect of siRNA silencing of SNAT2 on growth signalling in L6-G8C5 cells

Silencing of SNAT2 expression in L6-G8C5 myoblasts using the same SNAT2-silencing double-stranded siRNA oligonucleotides (SIL) and scrambled control sequence (Scr) that were described previously (Evans *et al.,* 2007; Evans *et al.,* 2008) led to significant depletion of SNAT2 mRNA (Figure 5.1A) and inhibition of System A transport activity (Figure 5.1B). As reported previously (Evans *et al.,* 2007; Evans *et al.,* 2008), this also led to significant inhibition of rpS6 phosphorylation downstream from mTORC1 (Figure 5.2) and Akt phosphorylation (Figure 5.3). For comparison, Erk phosphorylation was also studied (as an indicator of effects on the other major growth signalling pathway downstream of receptor tyrosine kinases (i.e. Ras/Raf/MEK/Erk) (McCubrey *et al.,* 2007).This was strongly inhibited by SNAT2 silencing (Figure 5.4). As SNAT2 itself was shown in Chapters 3 and 4 to be dependent on MAP kinase signalling, the other two arms of the MAP kinase signalling pathways (P38 and JNK) were also examined. While SNAT2 silencing had no significant effect on P38 phosphorylation (Figure 5.5A), a significant inhibitory effect was seen on JNK phosphorylation (Figure 5.5B).

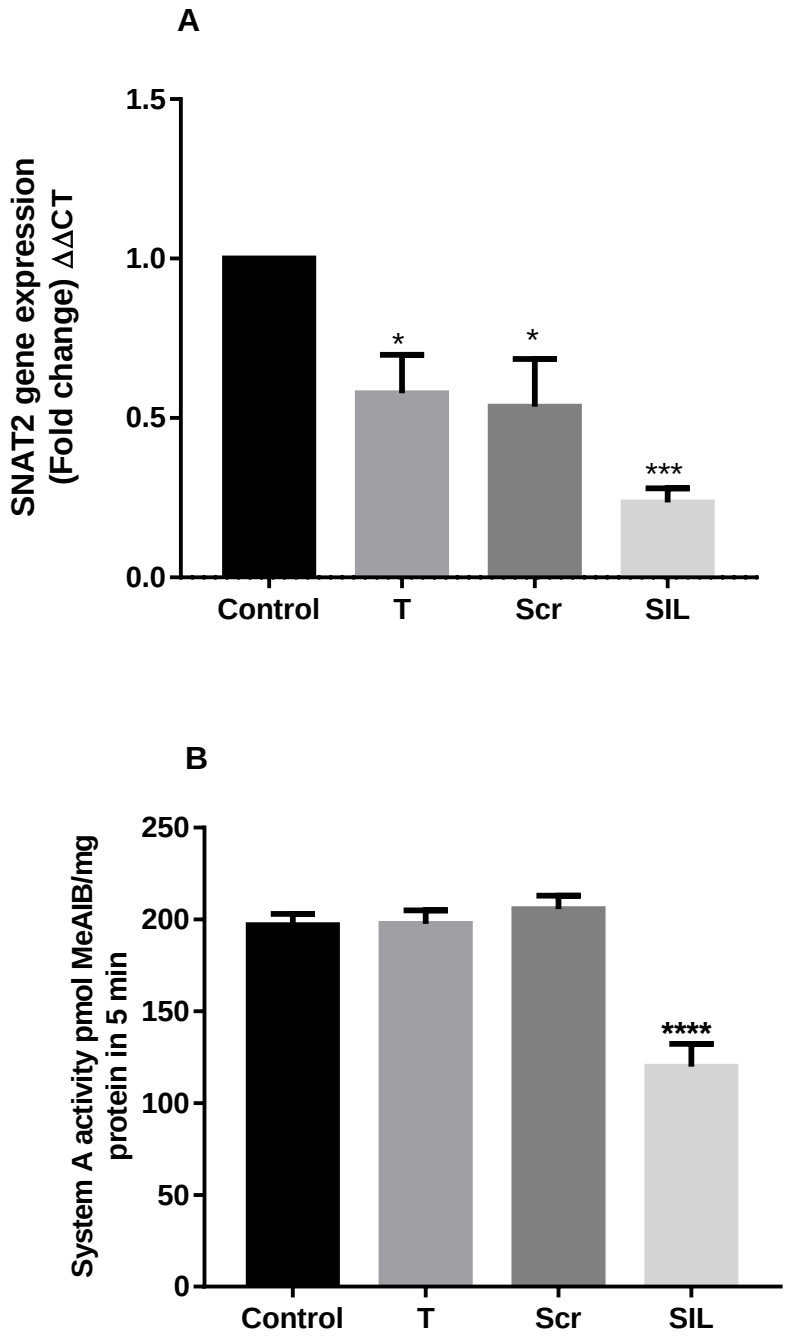


**Figure 5.1. Silencing of SNAT2 in L6 myoblasts leads to significant depletion of SNAT2 mRNA and SNAT2 transport activity.**

L6 myoblasts were cultured in DMEM growth medium for 24h then the medium was aspirated and replaced with half of the usual volume of growth medium and treated with 30nM scrambled control siRNA (Scr), silencing anti-SNAT2 siRNA (SIL) or Transfection reagent alone (T) using (ProFection® Mammalian Transfection System-Calcium Phosphate, Cat. #E1200). The non-transfected cells (shown here as "Control" were used as an additional negative control in the experiment. The cells were left with the transfection mix for 16h then the medium with the transfection mix was aspirated and replaced with double the normal volume of the usual growth medium for another 24h before commencing the experiment. (A) SNAT2 mRNA was measured by RT-qPCR using SNAT2 primers and Cyclophilin as a house-keeping gene. The data are expressed as ΔΔCT (ΔΔCT= SNAT2 gene expression in the treated conditions in relation to the

control condition). Gene expression of SNAT2 is corrected for variation in expression of the housekeeping gene Cyclophilin. The data are presented as Mean ± SEM of four independent experiments (n=4) * P<0.05, *** P< 0.001 versus Control. (B) SNAT2 transport activity was measured according to the amount of $^{14}$C-MeAIB transported into the cell: significant reduction in SNAT2 transport activity was observed in the SNAT2 silenced condition (SIL) compared to scrambled SNAT2 (Scr) and Transfection reagent only (T). The data are presented as Mean ± SEM of three independent experiments (n=3). **** P<0.0001.

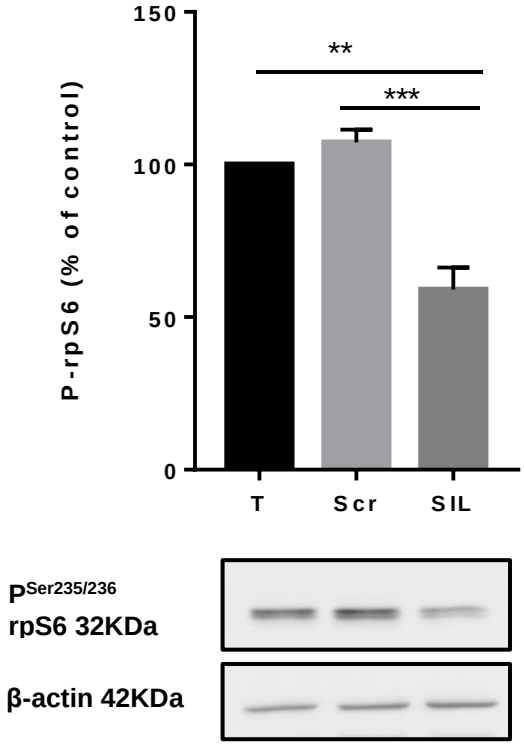


**Figure 5.2. SNAT2 siRNA silencing significantly decreases rpS6 phosphorylation in L6 myoblasts.**

L6 myoblasts were cultured in DMEM growth medium for 24h then the medium was aspirated and replaced with half of the usual growth medium and transfected with 30nM scrambled control siRNA (Scr), silencing anti-SNAT2 siRNA (SIL) or Transfection reagent only as a control using (ProFection® Mammalian Transfection System-Calcium Phosphate, Promega Cat. #E1200). The cells were left with the transfection mix for 16h then the medium with the transfection mix was aspirated and replaced with a double volume of the usual growth medium for another 24h before commencing the experiment. The cells were incubated in a test medium (MEM with 2% DFBS) for 2h then cell lysates were prepared for Western blots. The membrane was probed for P-rpS6 antibody and β-actin as a loading control. Data are presented as densitometry quantification of three independent experiments (n=3) and representative blots of P-rpS6 and β-actin are shown. ** P<0.01, *** P< 0.001.

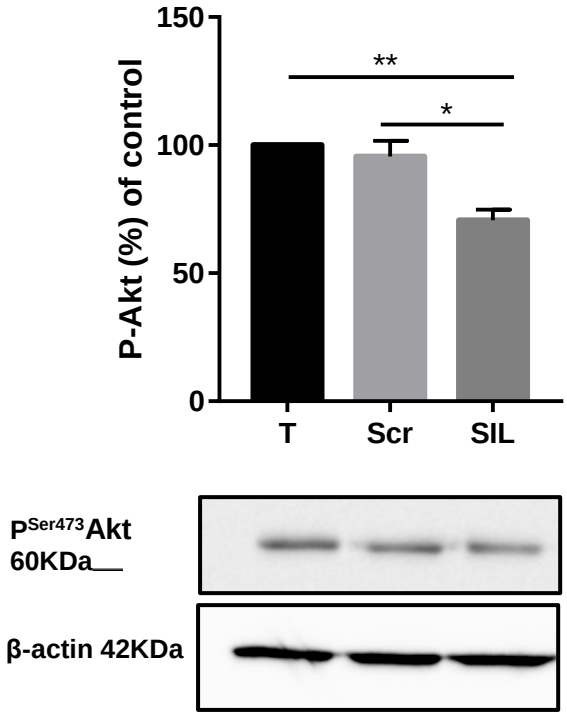


**Figure 5.3. SNAT2 siRNA silencing significantly decreases Akt phosphorylation in L6 myoblasts.**

L6 myoblasts were cultured in DMEM growth medium for 24h then the medium was aspirated and replaced with half of the usual volume of growth medium and transfected with 30nM scrambled control siRNA (Scr), silencing anti-SNAT2 siRNA (SIL) or Transfection reagent only (T) as a control using (ProFection® Mammalian Transfection System-Calcium Phosphate, Promega Cat. #E1200). The cells were left with the transfection mix for 16h then the medium with the transfection mix was aspirated and replaced with double the normal volume of the usual growth medium for another 24h before commencing the experiment. The cells were incubated in a test medium (MEM with 2% DFBS) for 2h then cell lysates were prepared for Western blots. The membrane was probed for P-Akt antibody and β-actin as a loading control. Data are presented as densitometry quantification from three independent experiments (n=3) and representative blots of P-Akt and β-actin. *P<0.05; ** P<0.01.

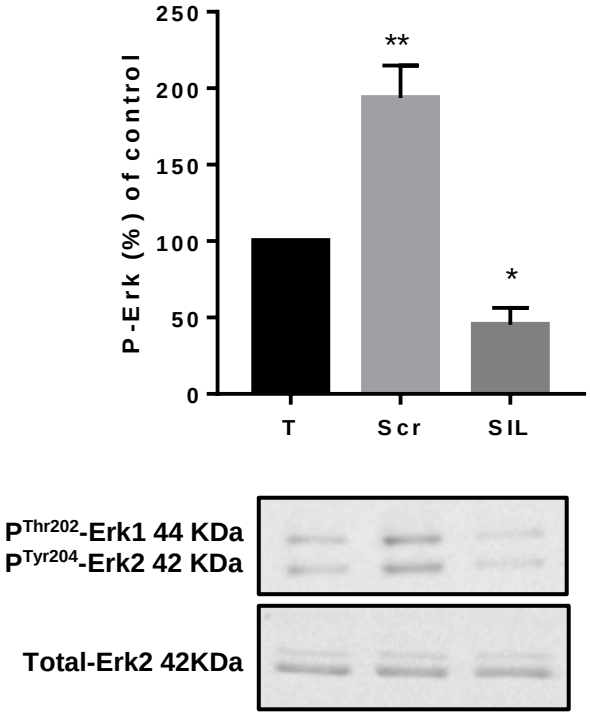


**Figure 5.4. Erk phosphorylation decreases after siRNA silencing of SNAT2 in L6 myoblasts.**

L6 myoblasts were cultured in DMEM growth medium for 24h then the medium was aspirated and replaced with half of the usual volume of growth medium and transfected with 30nM scrambled control siRNA (Scr), silencing anti-SNAT2 siRNA (SIL) or Transfection reagent only (T) as a control using (ProFection® Mammalian Transfection System-Calcium Phosphate, Promega Cat. #E1200). The cells were left with the transfection mix for 16h then the medium with the transfection mix was aspirated and replaced with double the normal volume of the usual growth medium for another 24h before commencing the experiment. The cells were incubated in a test medium (MEM with 2% DFBS) for 2h then cell lysates were prepared for Western blots. The membrane was probed with P-Erk antibody and total Erk2 antibody as a loading control. Data are presented as densitometry quantification of four independent experiments (n=4) and representative blots of P-Erk and Erk2 are shown. ** $P<0.01$, * $P<0.05$ versus control "T".

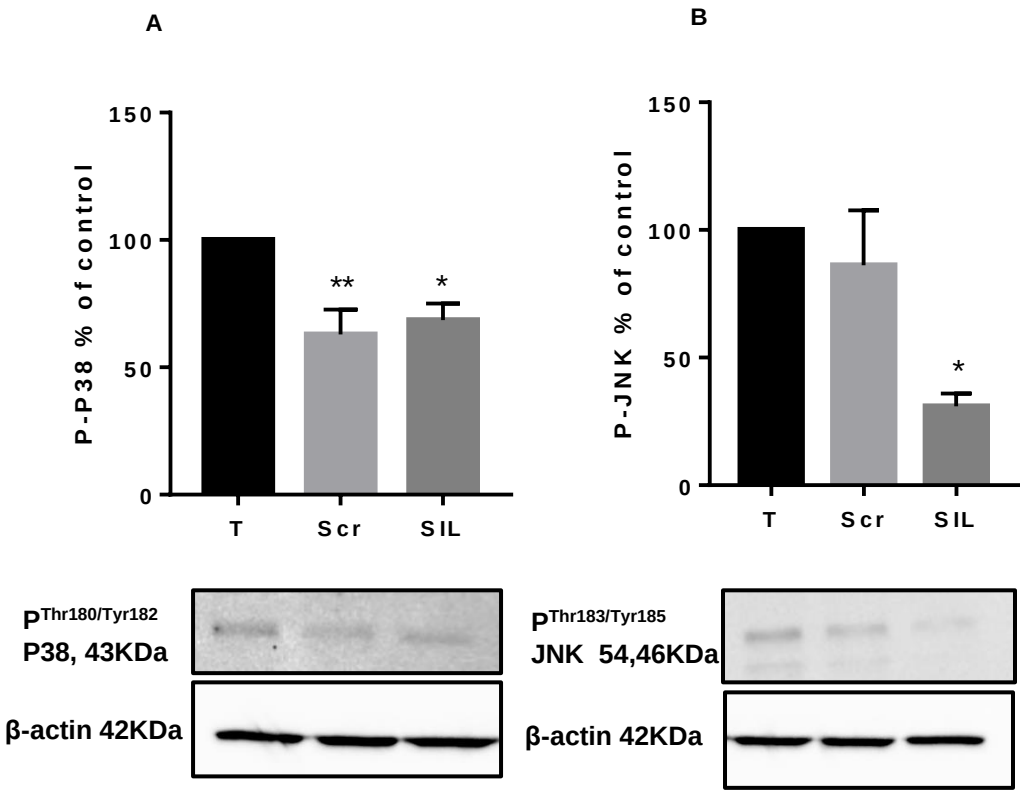


**Figure 5.5. SNAT2 silencing significantly decreases JNK phosphorylation in L6 myoblasts but has no effect on P38 phosphorylation.**

L6 myoblasts were cultured in DMEM growth medium for 24h then the medium was aspirated and replaced with half of the usual volume of growth medium and transfected with 30nM scrambled control siRNA (Scr), silencing anti-SNAT2 siRNA (SIL) or Transfection reagent only (T) as a control using (ProFection® Mammalian Transfection System-Calcium Phosphate, Cat. #E1200). The cells were left with the transfection mix for 16h then the medium with the transfection mix was aspirated and replaced with double the normal volume of the usual growth medium for another 24h before commencing the experiment. The cells were incubated in a test medium (MEM with 2% DFBS) for 2h then cell lysates were prepared for Western blots. (A) Represents densitometry quantification of three independent experiment (n=3) in which the membrane was probed for P-P38, and β-actin as a house keeping protein with representative blots of each antibody. (B) Represents densitometry quantification of three independent experiments (n=3) in which the membrane was probed for P-JNK and β-actin as a house keeping protein with representative blots of each antibody. The data are presented as Mean ± SEM, ** P<0.01, * P<0.05 versus control "T".

### 5.2.2 The effect of over-expression of SNAT2 on mTORC1 in HEK293A cells

As it was not possible to transfect L6-G8C5 cells efficiently with SNAT2-eGFP plasmid DNA (Chapter 4), in this experiment the effect of SNAT2 over expression on mTORC1 was studied by transfecting HEK293A cells and assessing mTORC1 activation by detecting the downstream rpS6 phosphorylation. As can be seen in Figure 5.6, SNAT2-eGFP transfected cells showed high P-rS6 signal on Western blots compared with control (non-transfected) cultures, and the effect of SNAT2 over expression was decreased by adding 10mM MeAIB as a selective System A substrate to compete out physiological amino acid influx through SNAT2. The transfection process itself (shown in the eGFP empty vector controls) also had a detectable but very variable stimulatory effect on rpS6 phosphorylation. However, this did not reach statistical significance and was lower than that observed in the SNAT2-eGFP cultures in all 4 independent experiments (paired comparison, P = 0.043).

Even though this supported the conclusion from Figure 5.2 that SNAT2 expression was activating mTORC1, in these short experiments there was no detectable growth effect of SNAT2 over-expression on the total protein content of the HEK293A cells (Figure 5.7). In contrast to the effect of siRNA silencing of SNAT2 in L6 myoblasts on total protein content (Table 4 in (Evans *et al.,* 2007)) and growth signalling (Figure 5.2 – 5.4); SNAT2-eGFP over-expression in HEK293A cells also had no detectable effect on Akt phosphorylation (Figure 5.8) or on Erk phosphorylation (Figure 5.9) (see Discussion).

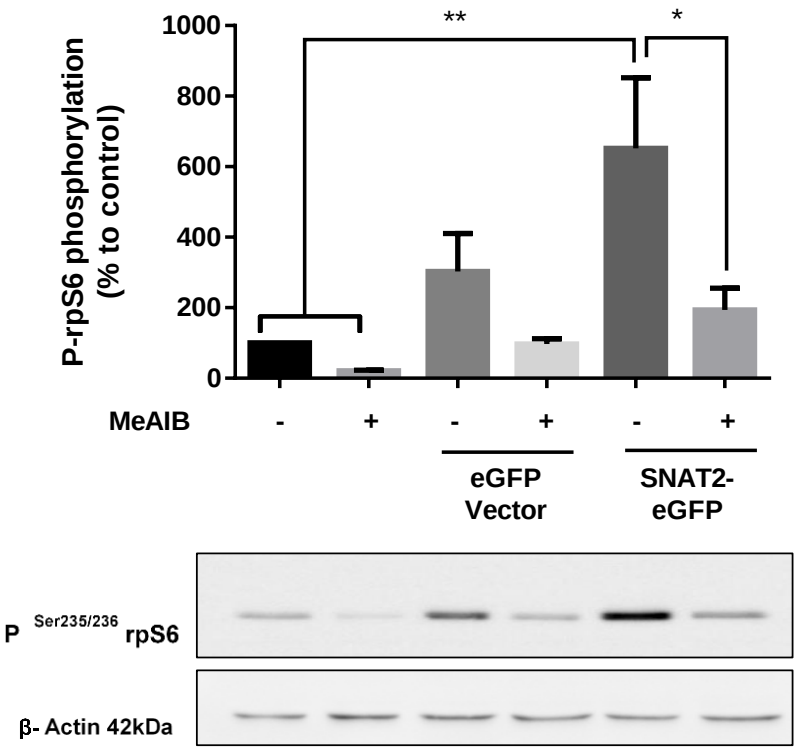


**Figure 5.6. Over expression of SNAT2-eGFP increases P-rpS6 in HEK293A cells.**

The cells were transfected with either 2µg SNAT2-eGFP plasmid DNA or 1.6µg GFP-vector per 35mm well 48h before the experiment. After this incubation time, the cells were washed three times with 2ml HBSS per well, then 2ml of appropriate test medium was added per well (with or without 10mM MeAIB) for 2 hours (as shown in the graph). Cell lysates were then prepared and subjected to immunoblotting, and the membrane was probed for P-Ser235/236 rpS6 and re-probed for β actin as a loading control. The result is expressed as Mean ± SEM of pooled data from four independent experiments (n=4) (upper panel) and the lower panel shows representative blots of the experiment. * P<0.05, ** P<0.01.

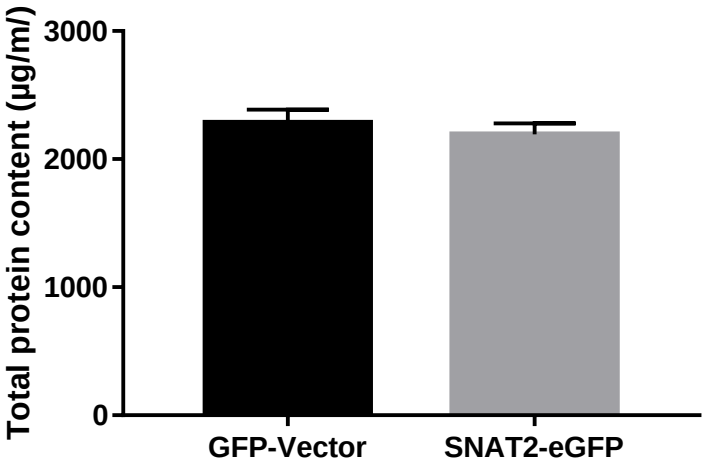


**Figure 5.7**. **Absence of a growth effect on total protein content in SNAT2-eGFP transfected HEK293A cells compared with GFP-vector control cultures.**

The total protein content in each well was measured using the BioRAD assay in the experiments presented in Figure 5.6 above.

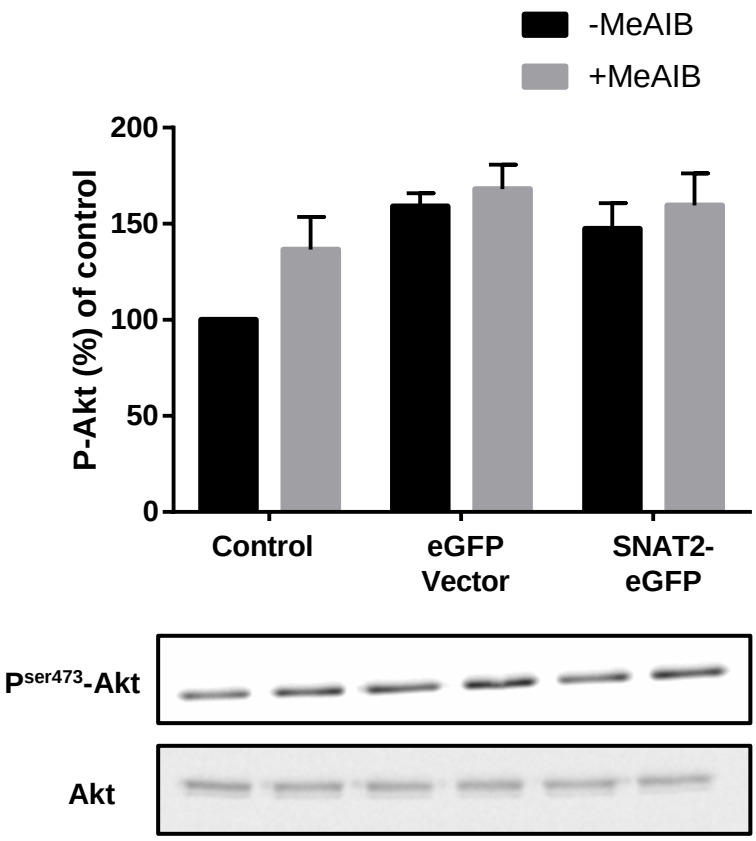


**Figure 5.8. SNAT2-eGFP over-expression does not affect Akt phosphorylation in HEK293A cells.**

The cells were transfected with either 2µg SNAT2-eGFP plasmid DNA or 1.6µg GFP vector per 35mm well 48h before the experiment. After this incubation time, the cells were washed three times with 2ml HBSS per well, then 2 ml of appropriate test medium was added per well (with or without 10mM MeAIB) for 2 hours (as shown in the graph). Cell lysates were then prepared and subjected to immunoblotting, and the membrane was probed for P-Ser$^{473}$-Akt and re-probed for total Akt as a loading control. The result is expressed as Mean ± SEM of pooled data from five independent experiments (n=5) (upper panel) and the lower panel shows representative blots of the experiment.

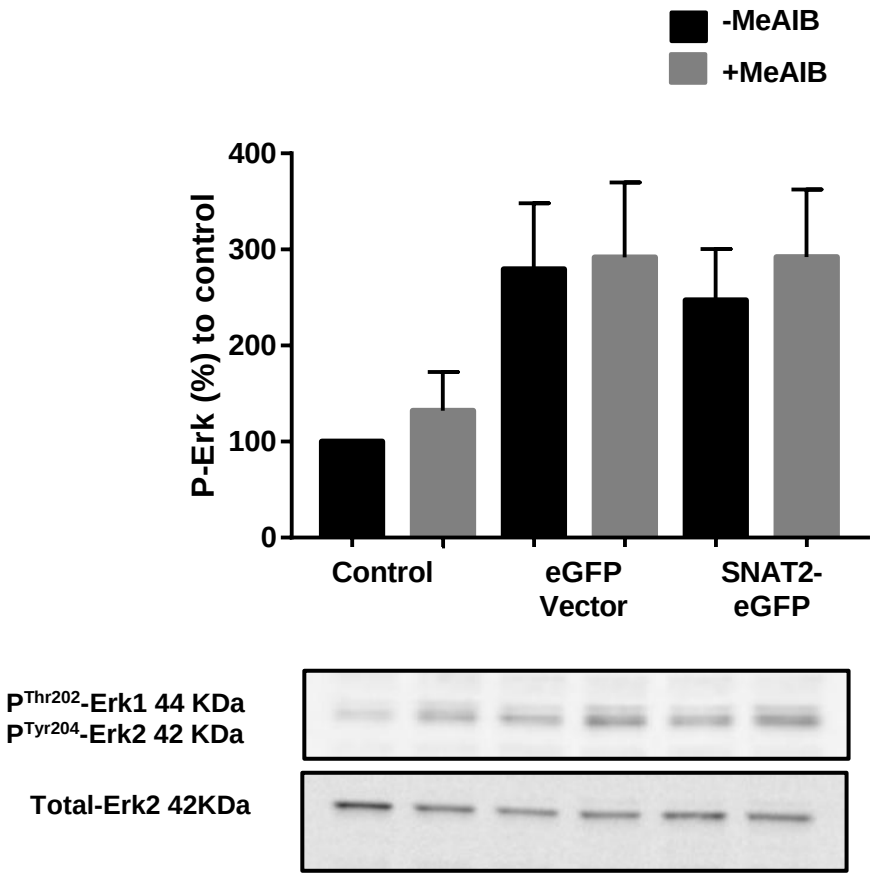


**Figure 5.9. Over-expression of SNAT2-eGFP does not affect ERK signalling in HEK293A cells.**

The cells were transfected with 2µg SNAT2-eGFP plasmid DNA or 1.6µg GFP vector per 35mm well 48h before the experiment. After this incubation time, the cells were washed three times with 2ml HBSS per well, then 2 ml of appropriate test medium was added per well (with or without 10mM MeAIB) for 2 hours (as shown in the graph). Cell lysates were then prepared and subjected to immunoblotting, and the membrane was probed for P-Thr$^{202}$ Erk1 / P-Tyr$^{204}$ Erk2 and re-probed for total Erk2 as a loading control. The result is expressed as Mean ± SEM of pooled data from five different experiments (n=5) (upper panel) and the lower panel shows representative blots of the experiment.

### 5.2.3 The effect of SNAT2 over-expression in HEK293A cells on key intracellular free amino acid concentrations

It has previously been shown in L6 cells in complete MEM, in the presence of 2% serum, that blockade of amino acid transport through SNAT2 with a saturating dose (10mM) of MeAIB or siRNA silencing of SNAT2 significantly depletes a number of intracellular amino acids, including the suspected anabolic amino acid L-glutamine (L-Gln) and the essential amino acids L-leucine (L-Leu) and L-

methionine (L-Met). (Evans *et al.,* 2007). L-Met is the only essential amino acid that is directly and efficiently transported on SNAT2 (Yao *et al.,* 2000). In HEK293A cells transfected with SNAT2-eGFP, all amino acids were measured (Table 5.1) and significant elevation of these intracellular free amino acid concentrations was observed, including a clear elevation of L-Met (Figure 5.10).

**Table 5.1. Amino acid concentrations (pmol AA/mg protein) in HEK293A cells.**

| Amino acid | GFP-Vector | SNAT2-eGFP |
|---|---|---|
| L-Aspartate | 526.6 ± 353.7 | 693.1 ± 328.8 |
| L-Glutamate | 1585 ± 103.9 | 1361 ± 42.39 |
| L-Asparagine | 57.53 ± 40.73 | 42.39 ± 8.297 |
| L-Serine | 20.98 ± 7.358 | 21.71 ± 3.664 |
| L-Glutamine | 1732 ± 79.24 | 3397 ± 491.2* |
| L-Histidine | 56.23 ± 9.328 | 176.6 ± 25.53* |
| Glycine | 181.3 ± 125.8 | 64.76 ± 10.13 |
| L-Threonine | 532.9 ± 34.73 | 1100 ± 167.7 |
| L-Arginine | 108.4 ± 14.59 | 157.9 ± 21.08 |
| L-Alanine | 235.3 ± 64.49 | 360.6 ± 81.42 |
| L-Tyrosine | 76.17 ± 14.51 | 121.8 ± 19.3 |
| L-Cystine | 5.94 ± 2.798 | 26.02 ± 22.41 |
| L-Valine | 105.7 ± 7.233 | 213.3 ± 31.6* |
| L-Methionine | 29.29 ± 2.454 | 89.93 ± 14.68* |
| L-Norvaline | 122.5 ± 56.25 | 105.2 ± 42.97 |
| L-Tryptophan | 39.23 ± 22.5 | 23.66 ± 4.143 |
| L-Phenylalanine | 64.06 ± 7.395 | 124.6 ± 17.98* |
| L-Isoleucine | 94.69 ± 5.325 | 146.2 ± 30.27 |
| L-Leucine | 89.97 ± 9.206 | 199.8 ± 32.4* |
| L-Lysine | 54.57 ± 2.26 | 96.25 ± 23.5 |

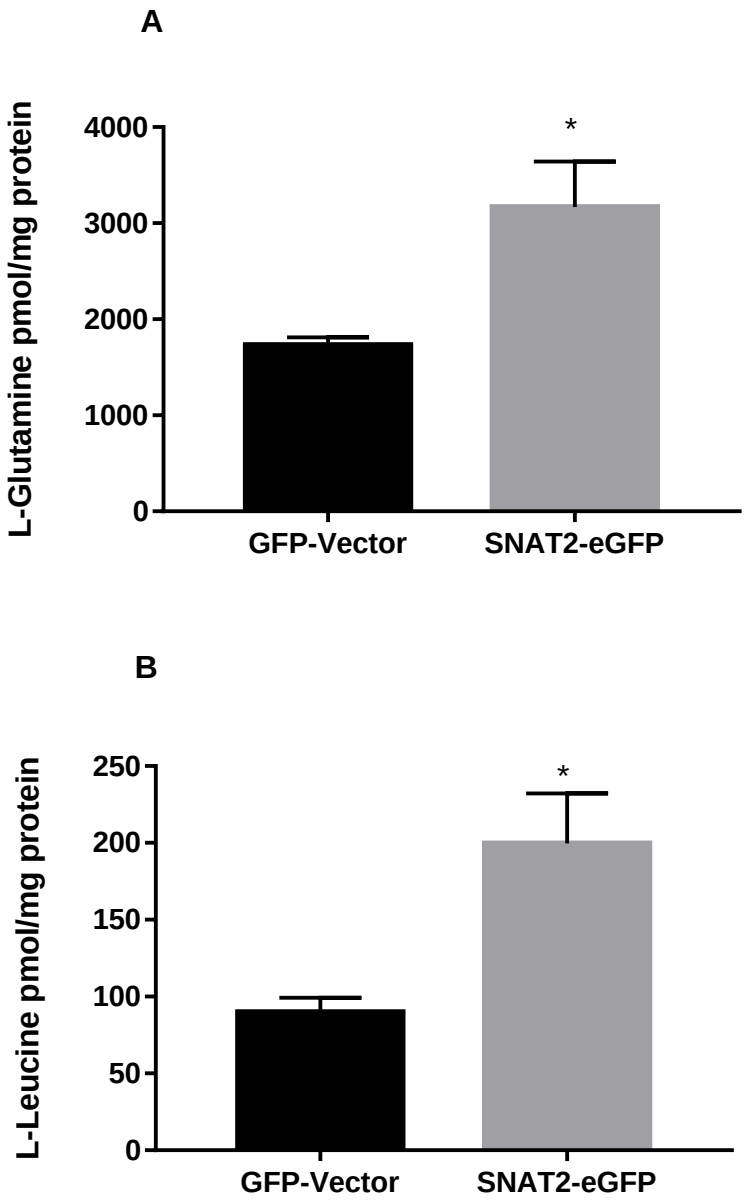
A
L-Glutamine pmol/mg protein
4000
3000
2000
1000
0
*
GFP-Vector
SNAT2-eGFP
B
L-Leucine pmol/mg protein
250
200
150
100
50
0
*
GFP-Vector
SNAT2-eGFP

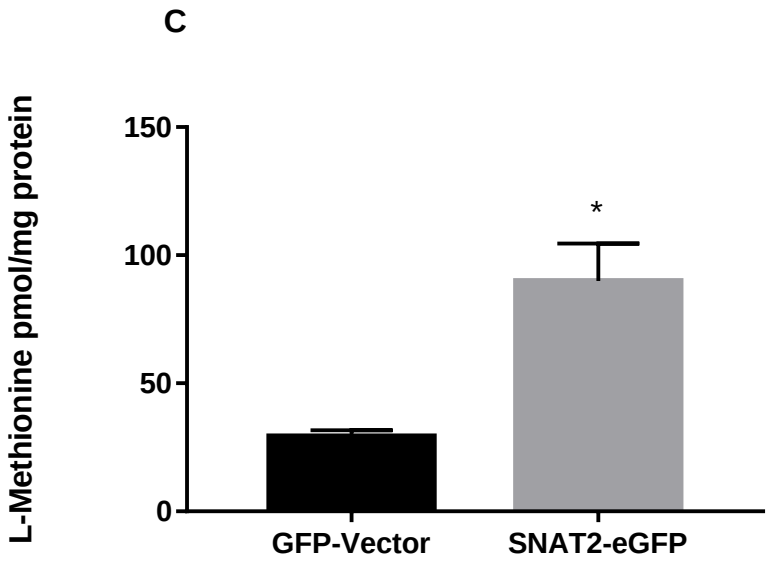


**Figure 5.10. Significant elevation of intracellular amino acid concentrations is obtained by over expression of SNAT2-eGFP in HEK293A cells.**

HEK293A cells were transfected with 2µg of SNAT2-eGFP plasmid DNA or 1.8µg GFP vector per 35mm well. The cells were rinsed with 2ml of HBSS three times to remove any extracellular amino acids in the media, then the cell lysates were prepared for HPLC analysis. Clear elevation of L-glutamine, L-leucine and L-methionine was detected in SNAT2-eGFP transfected cells in comparison to GFP vector transfected cells (A, B and C respectively). The concentration of the amino acids (pmol) was corrected for the total protein content (mg) per well. The data are presented as Mean ± SEM of four independent experiments (n=4). * P <0.05.

### 5.2.4 mTORC1 activation (rpS6 phosphorylation) can occur with a single SNAT2 substrate (L-Met) in L6 myotubes

It has also previously been shown in L6 cells that in MEM with its complete set of amino acids, in the presence of 2% serum, blockade of System A (mainly SNAT2) amino acid transport (by applying a saturating 10mM dose of MeAIB, or by siRNA silencing of SNAT2), significantly inhibits mTORC1 signalling assessed from rpS6 phosphorylation (Evans *et al.,* 2007). However, it is still unclear which amino acid(s) that are carried by SNAT2 are responsible for this effect on mTORC1.

In the present study, when all amino acids were omitted from the medium in cultures of L6 myotubes, significant inhibition of rpS6 phosphorylation was observed as expected (Figure 5.11). The remaining P-rpS6 signal was still readily detectable even in the absence of extracellular amino acids, because the

intracellular amino acid concentration in L6 myotubes does not fall to zero when amino acids are removed from the medium (Evans *et al.,* 2007).This baseline signal showed no further significant inhibition in response to 10mM MeAIB (Figure 5.11), confirming that the intracellular mTORC1 amino acid sensing mechanism (Section 1.6) is not blocked by MeAIB.

To determine whether the SNAT2 substrate L-Met is a possible contributor to mTORC1 activation in these cells, the concentration of L-Met was varied in the medium. When L-Met was the only amino acid in the medium, the intensity of rpS6 phosphorylation was found to be higher than in medium without amino acids (Figure 5.11). For example, the signal with 101μM L-Met alone in the medium was about 1/3 of the intensity observed with the complete amino acid mixture and it was inhibited by 10mM MeAIB, suggesting that L-Met transport through a System A transporter (possibly SNAT2) contributed to this effect. A further experiment (Figure 5.12A) was conducted to compare the effect of L-Met on rpS6 phosphorylation with the effect of L-Leu alone – i.e. the amino acid which is regarded as the most important stimulator of mTORC1 (Section 1.6). When L-Met and L-Leu were added alone here at their usual concentration in MEM (101μM and 396μM respectively) they both stimulated P-rpS6, but surprisingly the effect of L-Leu was no larger than that of L-Met (Figure 5.12A).

When L-Met alone was removed from the medium, this decreased the P-rpS6 signal by about 30% compared with MEM with all amino acids. As expected, this was similar to the decrease observed when System A/SNAT2 transport was blocked with 10mM MeAIB in medium with L-Met (Figure 5.12B). However, MeAIB still inhibited P-rpS6 signalling even in MEM without L-Met, showing that, while L-Met transport through SNAT2 may contribute to SNAT2's stimulatory effect on mTORC1, it cannot be the full explanation.

To test more selectively the role of SNAT2 in the action of L-Met on rpS6 phosphorylation, SNAT2 expression was silenced using siRNA (Figure 5.13). However, under these conditions, no statistically significant stimulation of P-rpS6 by L-Met was observed, possibly because the transfection agent was blunting the action of L-Met.

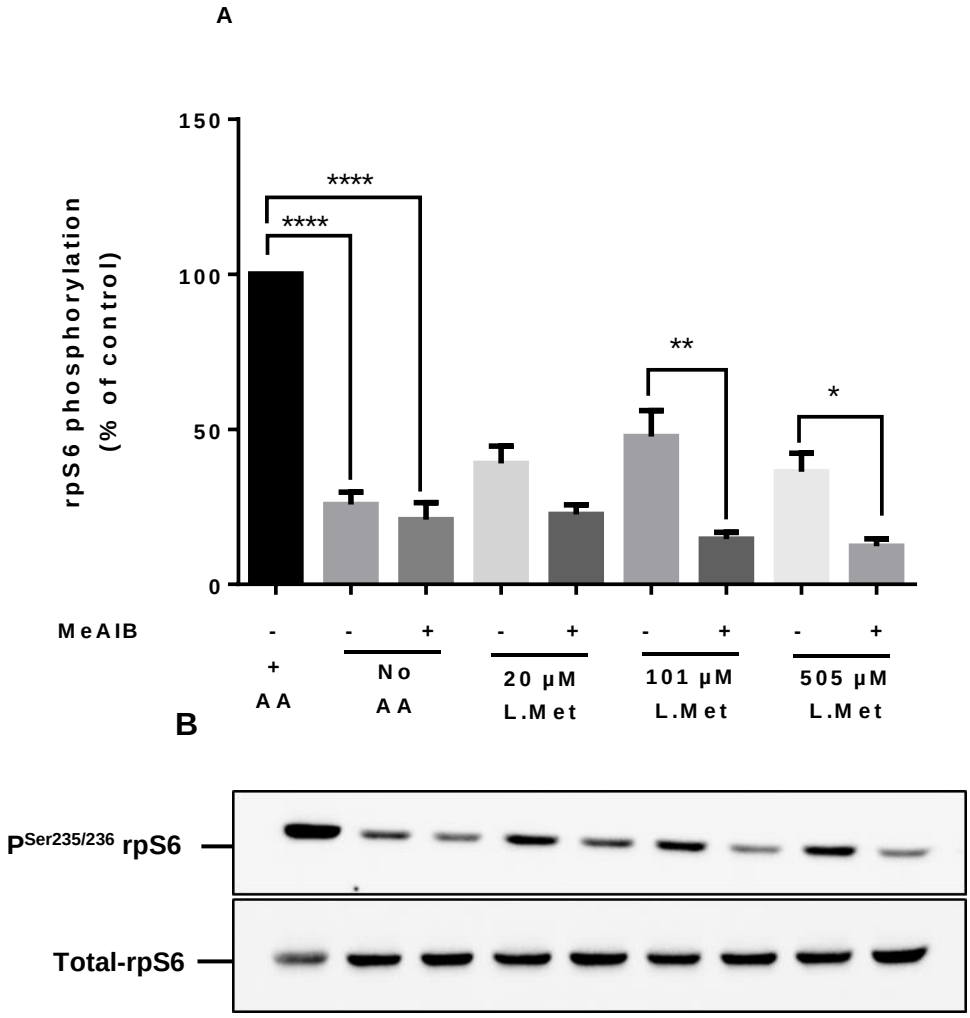


**Figure 5.11. The effect of a single amino acid (L-methionine, L-Met) on mTORC1 activation (rpS6 phosphorylation) in L6 myotubes.**

The cells were washed three times with 2ml HBSS per 35mm culture to remove extracellular amino acids before adding the test media. Cells were then incubated under the conditions shown for 2h: +AA; MEM with 2% DFBS, No AA; ((EBSS) +1% MEM Vitamins+1% Peni-Strep (100x) + 2% DFBS, pH7.4); with or without 10mM MeAIB and different concentrations of L.Met. (A) Represents the quantification by densitometry of four independent experiments (n=4) with two replicates of the same condition in each experiment. The graph is presented as Mean ± SEM.*P<0.05, **P<0.01, ****P<0.0001. (B) Representative blots of P-rpS6 (upper panel) and Total-rpS6 (lower panel).

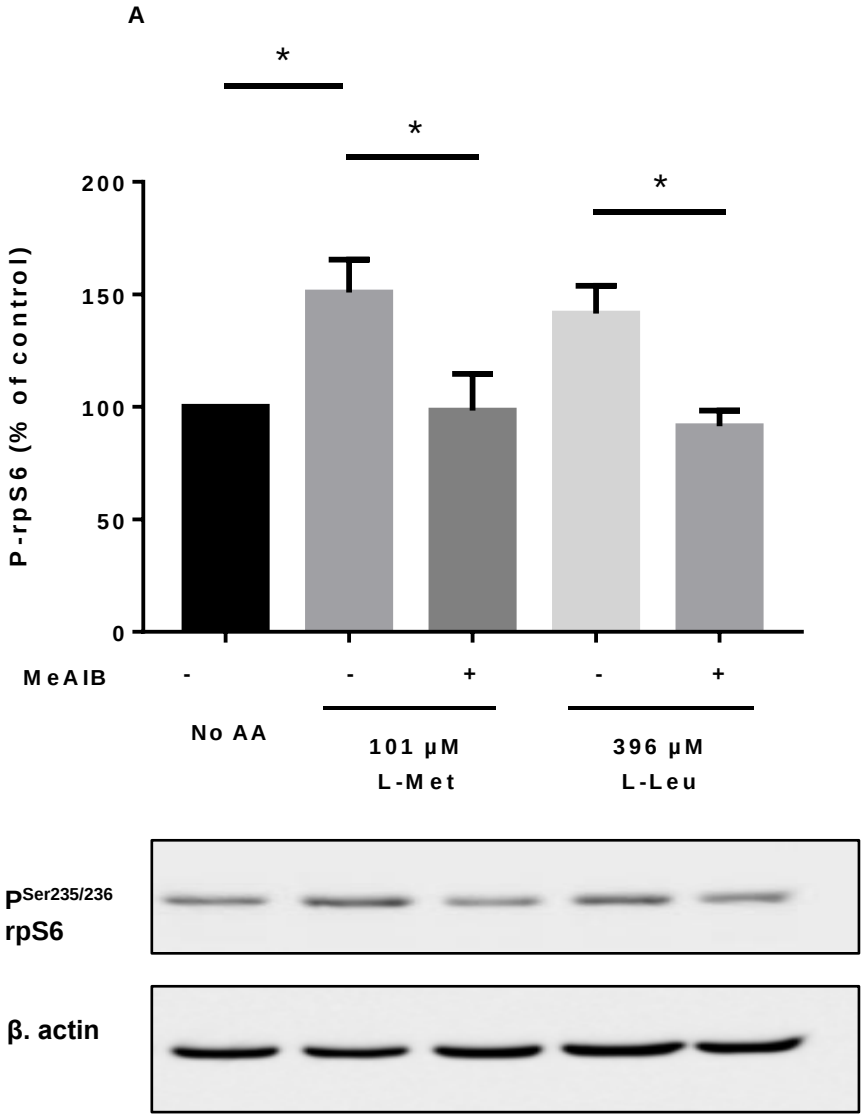
A
*
*
*
200
150
100
50
0
P-rpS6 (% of control)
MeAIB
-
-
+
-
+
No AA
101 µM
L-Met
396 µM
L-Leu
PSer235/236
rpS6
β. actin

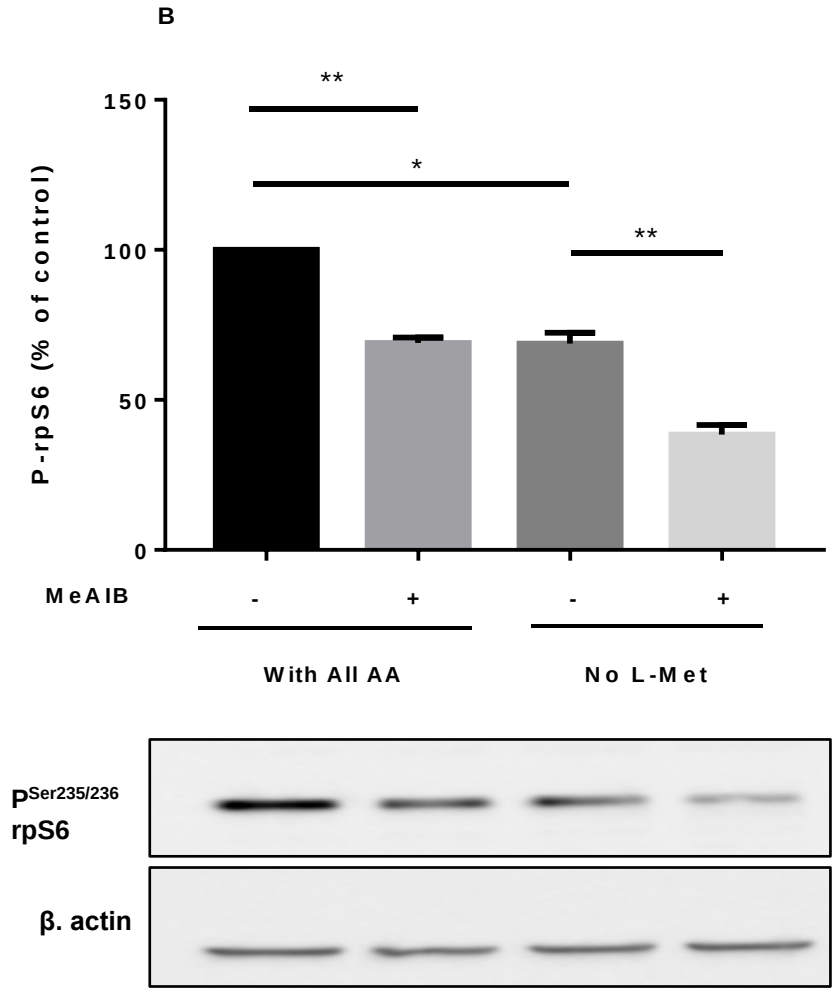


**Figure 5.12. The effect of (A) single amino acids (L-methionine, L-Met) or (L-leucine, L-Leu) and (B) L-Met withdrawal on mTORC1 activation (rpS6 phosphorylation) in L6 myotubes.**

The cells were washed three times with 2ml HBSS per 35mm culture to remove extracellular amino acids before adding the test media. Cells were then incubated under the conditions shown for 2h. (A) No AA; ((EBSS) +1% MEM Vitamins+1% Peni-Strep (100x) + 2% DFBS, pH7.4); with or without 10mM MeAIB, L-Met or L-Leu. (B) MEM with or without 101μM L-Met + 2% DFBS with or without 10mM MeAIB. Bar charts represent densitometry quantification of four independent experiments (n=4) in (A) and n=3 in (B), with two replicates of the same condition in each experiment. The graphs are presented as Mean ± SEM.*P<0.05, ** P<0.01. Representative blots of P-rpS6 (upper panel) and β-actin (lower panel) are shown under each bar graph.

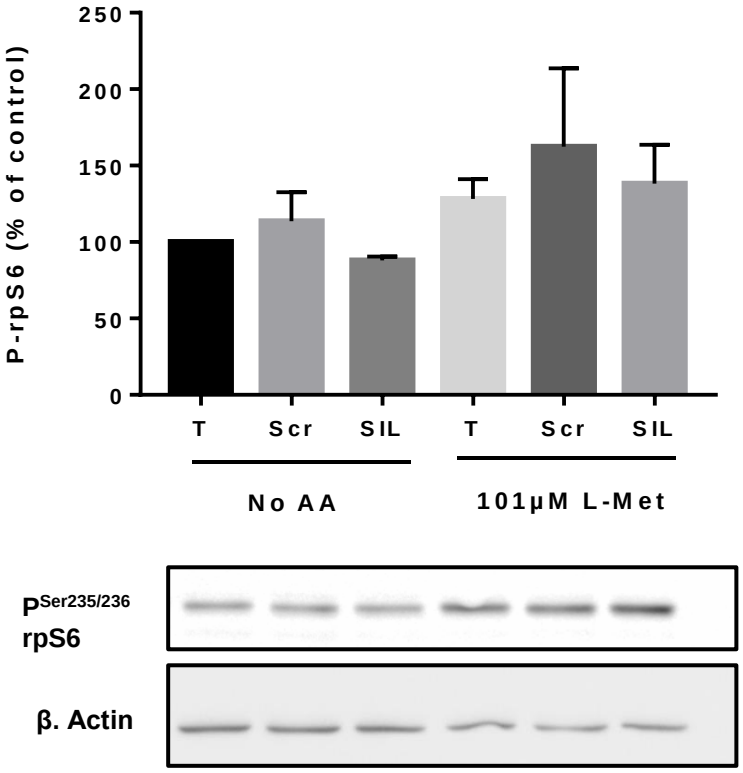


**Figure 5.13**. **Effect of SNAT2 siRNA silencing on the action of L-Met on rpS6 phosphorylation in L6 myoblasts.**

The cells were transfected with either scrambled SNAT2 (Scr) or SNAT2-silencing siRNA and transfection reagent as a control for 16h (as in the legend to Figure 5.1) then the medium containing transfection mix was replaced by double the usual volume of fresh GM for another 24h, The cells were incubated in a test medium either with no amino acids (No AA) or containing a single amino acid (L.Met) (101µM). Data are presented as Mean ± SEM of three independent experiments (n=3). The graph shows densitometry analysis of the experiment with representative blots of P-rpS6, and β-actin as a loading control. No statistically significant effects were observed.

### 5.2.5 The functional significance of the DEX effect on SNAT2: coupling to protein kinase B (Akt) phosphorylation

Finally, if the inhibition or down-regulation of SNAT2 by DEX in L6-G8C5 cells that had been investigated in Chapters 3 and 4 is functionally important, it should lead to a significant corresponding effect on protein anabolic signalling. In skeletal muscle cells, Akt is an important regulator of protein degradation, and inhibition of Akt strongly activates protein catabolism and is a major contributor to cachexia (Wang & Mitch, 2013). In view of the significant signalling effects associated with SNAT2 in the experiments above, an attempt was therefore made to determine whether the down-regulation of SNAT2 by DEX can (as shown previously for the inhibition of SNAT2 by acidosis (Evans *et al.,* 2008)), lead to impaired Akt phosphorylation.

In L6-G8C5 cells, a low pH of 7.1 has previously been shown (Evans *et al.,* 2008) to inhibit SNAT2 transport activity by ~ 50% resulting in decreased Akt phosphorylation and increased protein degradation. If the similar (~60%) inhibition of SNAT2 activity by DEX (Chapter 3) is biologically important, it should also exert an inhibitory effect on Akt similar in magnitude to that seen at pH 7.1. The results (Figure 5.14) showed that, as predicted, DEX can significantly reduce phospho-Akt in comparison to the control condition (DMSO vehicle only), giving an effect similar in magnitude to that seen with low pH (Figure 5.14). This suggests that, at least in L6-G8C5 myotubes, DEX sends a protein catabolic signal via P-Akt similar in size to that induced by metabolic acidosis (Evans *et al.,* 2008).

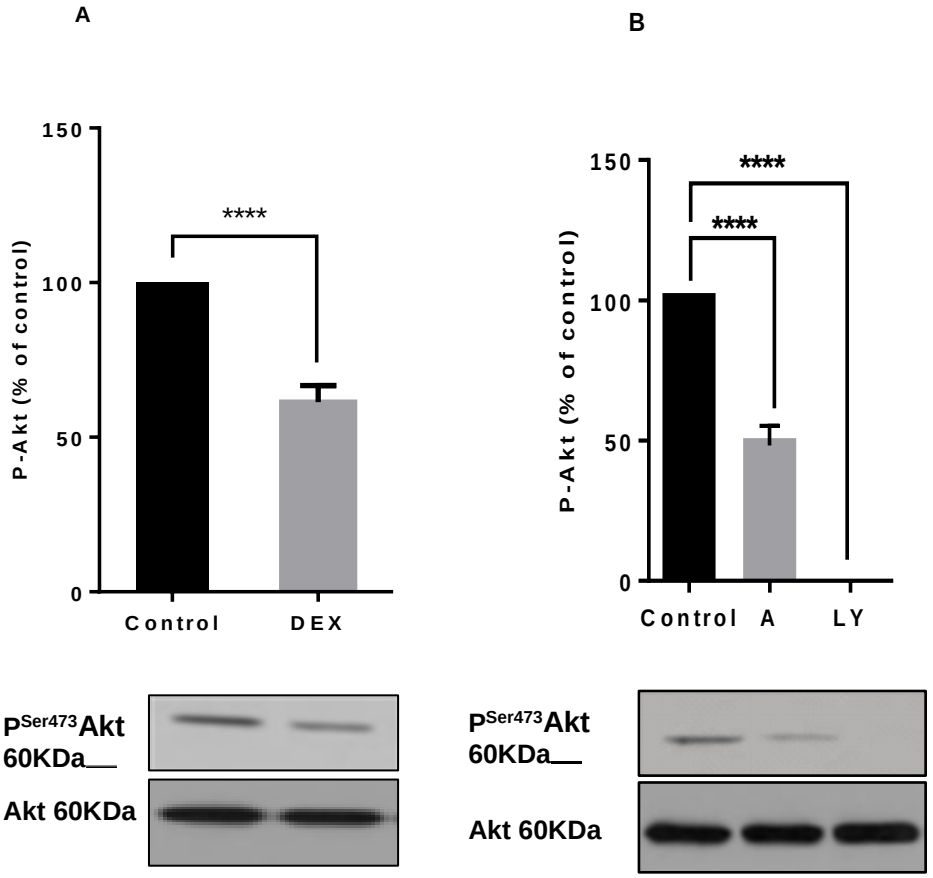


**Figure 5.14. Dexamethasone significantly reduces Akt phosphorylation, similar to the effect of acidic pH in L6 myotubes.**

In this experiment, the effect of acute treatment with DEX on Akt phosphorylation was determined by immunoblotting with antibodies specific for P-Ser$^{473}$-Akt and Total Akt. L6-myotubes were treated with 500nM Dexamethasone for 4h (A); and the effect was compared with that of acidified medium (pH: 7.1). PI-3-kinase inhibitor 2-(4-morpholinyl)-8-phenyl-4H-1-benzopyran-4-one (LY294002, 50µM) was used to inhibit downstream Akt as a negative control. L6 myoblasts were plated on 35mm 6-well plates in 2ml of Growth Medium (DMEM), and myotube formation was induced by incubating the cells with MEM + 2% serum 48 h after plating the cells. Myotubes were incubated with different MEM test media for 4h, Control (DMSO vehicle only); DEX-500nM Dexamethasone (B) The effect of acid on Akt in L6 myotubes. A-acidified MEM test medium (pH: 7.1); Control medium pH 7.4. LY denotes 50µM PI-3-kinase inhibitor. The data represent pooled densitometry quantification of five independent experiments and a representative immunoblot of one of the experiments. Both experiments (A) and (B) were run in parallel. Immunoblots of five independent experiments (n=5) were scanned and analysed by densitometry, and the phosphorylated Akt results presented as a percentage of the signal intensity under control conditions (DMSO vehicle only). **** Denotes conditions differing significantly from Control, $P<0.0001$.

## 5.3 Discussion

### 5.3.1 SNAT2 siRNA silencing impairs anabolic and MAPK signalling pathways in L6 myoblasts.

The first aim of the experiments presented in this chapter was to confirm and extend previous work in L6-G8C5 cells which had shown that siRNA silencing of SNAT2 significantly impairs important anabolic signals to mTORC1 and rpS6, and to PI3K and Akt (Evans *et al.,* 2007; Evans *et al.,* 2008). The experiments conducted here in L6 myoblasts showed that effective siRNA silencing of SNAT2 decreased SNAT2 mRNA expression and System A transport activity (Figure 5.1A and 5.1B respectively). In addition to the expected inhibition of rpS6 and Akt phosphorylation, this also led to novel inhibitory effects on the MAP kinases Erk and JNK, but not P38. This is potentially important for two reasons. Firstly, when combined with the observations in Chapter 3 and 4 that MAPK inhibition inhibits SNAT2, this observation that SNAT2 silencing inhibits MAPKs suggests that conditions might exist in which SNAT2 and MAPK kinases activate each other in a positive feedback loop. Secondly, MAPK activation is thought to be an important process in mechanotransduction signalling, for example in the response of skeletal muscle to exercise. This suggests that in future it may be of interest to investigate whether SNAT2 inhibition by acidosis or glucocorticoid, or SNAT2 activation for example by IGF-I, may modulate the response of skeletal muscle cells to mechanical stress or (*in vivo*) to exercise.

### 5.3.2 SNAT2 over expression in HEK293A cells

As expected from the SNAT2 silencing experiments in L6 cells, SNAT2 over-expression in HEK293A cells seemed to exert the opposite effect and raised free amino acid concentrations in the cells and stimulated P-rpS6, again suggesting an important functional effect of SNAT2 on mTORC1. This occurred even though the baseline concentrations of free amino acids (expressed per mg of cell protein) in HEK293A cells are about 40 times lower than in L6 myoblasts (Fig 5.10 and Evans 2007).

In contrast to the effect of siRNA silencing of SNAT2 in L6-G8C5 cells, SNAT2-eGFP over-expression in HEK293A had no detectable effect on Akt phosphorylation or on Erk phosphorylation. The reason for this is unknown but both of these signalling pathways are thought to be amino acid independent

(supported here by the observation that the amino acid transport antagonist MeAIB had no effect on Akt and Erk signalling in Figures 5.8 and 5.9 respectively). A possible interpretation is that in L6-G8C5 cells SNAT2 acts on Akt and Erk through some form of protein-protein interaction which was impaired by the C-terminal eGFP tag on the SNAT2-eGFP fusion protein when it was expressed in HEK293A cells. It would therefore be interesting in future experiments to compare the effect on these signalling pathways of over-expressing untagged SNAT2.

In some experiments, an apparent non-specific stimulatory effect of the empty eGFP vector was seen on P-rpS6 (Fig 5.6). This was variable and did not reach statistical significance, and there was no corresponding effect of the empty vector on baseline System A transport activity in the experiments shown in Chapter 4. However, some stimulation of P-Akt and P-Erk may also have occurred with the vector control in Figures 5.8 and 5.9. This may arisen from a stress effect on the cells caused by the transient transfection process itself. Therefore, to avoid such transient transfection problems in future, a stably transfected HEK or L6 cell line may be required in signalling experiments of this type.

### 5.3.3 The amino acid signal from SNAT2 to mTORC1

The observed activation of mTORC1 by SNAT2 suggests that the transporter is signalling to mTORC1 through its effects on intracellular free amino acid concentrations. L-Leu is regarded as a key mTORC1 regulator but is not directly transported by SNAT2. SNAT2 inhibition by MeAIB has been reported by Pinilla *et al.* (2011) to decrease intracellular L-Leu. This is probably an indirect effect through the exchange that SNAT2 substrates have with System L essential amino acids as shown in Figure 1.10 and Section 1.11.1. The experiments described in this chapter suggest however that at least one amino acid that is directly transported on SNAT2 may also have a role in signalling to mTORC1. A detectable activation of rpS6 phosphorylation was observed in L6 myotubes when only one amino acid (L-Met) was present in the culture medium (Figure 5.11 and 5.12) and this was decreased by incubating with MeAIB, a System A competitive substrate, suggesting that SNAT2 was involved.

Interestingly, even though L-Leu *withdrawal* from culture medium strongly inhibits mTORC1 signalling in most mammalian cells (Section 1.6), *addition* of L-Leu alone had no more effect than L-Met in stimulating P-rpS6 in Figure 5.12A. The reason for this is unknown. It is also unclear why MeAIB inhibited P-rpS6 activation by L-Leu in Figure 5.12. L-Leu is not a substrate for SNAT2, and MeAIB is not a substrate for L-Leu transporters such as LAT1, so it would not be expected that MeAIB would compete for L-Leu transport.

To investigate further the role of L-Met in signalling from SNAT2 to mTORC1, stable and efficient silencing of SNAT2 is needed. However, as siRNA transfection seemed to blunt the effect of L-Met (Figure 5.13) it was not possible to test this directly by the transient SNAT2 silencing method that was used here.

### 5.3.4 Protein degradation and the DEX effect.

Glucocorticoid is a cause of muscle wasting, for example the well-documented muscle atrophy that accompanies glucocorticoid excess in humans (Schakman *et al.,* 2013). However, the mechanisms by which GC stimulates protein degradation and UPP activation are not fully understood. High doses of GC lead to UPP activation by increasing ubiquitin and proteasome mRNA expression (Hu et al., 2009). However, because there is no GRE on the promotors of these genes, the mechanism is uncertain. It is also known that prolonged (24h) stimulation of L6 myotubes with DEX can up-regulate E3 ligase expression in L6 myotubes (Castillero *et al.,* 2013; Menconi *et al.,* 2008).

The effect observed in Figure 5.14 is of interest as a possible more rapid (4 hour) mechanism for DEX signalling to protein degradation via Akt. A non-genomic mechanism of GC action has been proposed, by which high GC concentrations decrease Akt phosphorylation by interaction of the GR with the P58 subunit of PI3K (Thomas & Mitch, 2013). However, it is known that the ~ 50% inhibition of SNAT2 by pH 7.1 or by partial SNAT2 siRNA silencing leads to impaired Akt phosphorylation ((Evans *et al.,* 2008) and Figure 5.3), and the similar degree of SNAT2 inhibition by DEX (Chapter 3) was shown here in Figure 5.14 to be associated with the expected similar degree of important of Akt phosphorylation,

suggesting that SNAT2 also plays a significant role in the signal from DEX through Akt to UPP.

# Chapter 6 General Discussion and Future Work

## 6.1 General discussion

### 6.1.1 Trafficking of SNAT2 within cells and the response to DEX

Even though a lot remains to be learned about the regulation of the SNAT2 transporter protein and its trafficking between different SNAT2 pools within cells, the results presented in this thesis seem to be consistent with a model of SNAT2 compartmentation that has been proposed by Nardi et al (Nardi *et al.,* 2015) (Figure 6.1). The immunoblotting and GFP trapping experiments in Chapter 4 detected a heavy and a light isoform of eGFP-tagged SNAT2, consistent with two isoforms of the transporter – possibly a light (newly synthesised form) and a heavier (strongly glycosylated) form which might be the mature transporter protein in the plasma membrane (Figure 6.1). The data from Chapters 3 and 4, showing an apparent blunting by the proteasome inhibitor MG132 of the effects of DEX, suggesting that DEX acts, at least partly, by increasing degradation of SNAT2 protein through the UPP. In HEK293A cells over-expressing SNAT2-eGFP, DEX decreased the fluorescing intracellular pool of SNAT2-eGFP (Figure 4.13) but had no significant effect on the System A activity of the transporter in the plasma membrane. This suggests that DEX may act selectively in these cells to increase degradation of the light (intracellular) pool of SNAT2 i.e. similar to the selective degradation of light SNAT2 stimulated by free fatty acids in the study by Nardi et al (2015). The mechanism of degradation of heavy SNAT2 is unknown, but might be through endocytosis and fusion with lysosomes as shown in Figure 6.1.

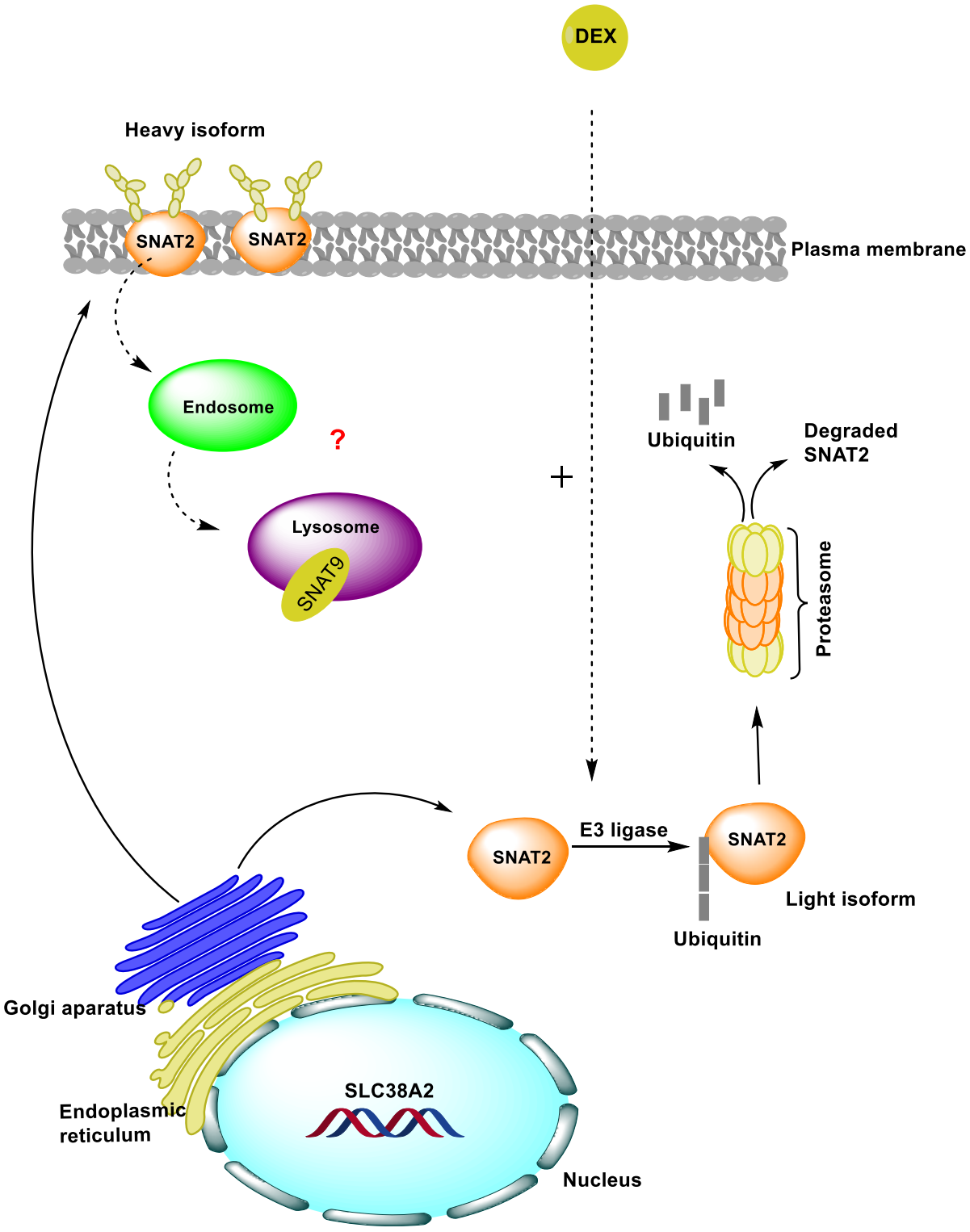


**Figure 6.1. Possible pathways for trafficking of SNAT2 protein in L6 and HEK293A cells (adapted from (Nardi *et al.*, 2015)).**

It seems likely that, even though SNAT2-eGFP is strongly expressed in HEK293A cells and is translocated to the plasma membrane where it increases System A transport activity, this translocation is an important limiting factor and means that regulatory effects on the newly synthesised intracellular SNAT2-eGFP pool (for example by DEX) are not always expressed in the active plasma membrane pool. A similar apparent limiting effect of translocation to the plasma membrane may also have occurred when SNAT2-eGFP transfection was attempted in L6 myoblasts. It is not known whether the down-regulation of the intracellular pool of SNAT2 by DEX without a significant effect on the plasma membrane (MeAIB transporting pool) can occur in other cell types apart from HEK293A. However, in future experiments, it would be interesting to find out whether this explains the failure of human myotubes to show down-regulation of System A transport activity in response to DEX (Figure 4.1B), even though DEX has a clear inhibitory effect on System A transport in L6 myotubes (Chapter 3). This variation in response to DEX by different muscle cell lines might arise because they were derived from different fibre types, with L6-G8C5 myotubes perhaps behaving (and staining in Figure 2.2) more like Type II or fast twitch muscle fibres which are known to be more responsive to GC (Gupta & Gupta, 2013).

### 6.1.2 Links between SNAT2 and other SNAT transporters

Evans et al (2007 and 2008) concluded that SNAT2 is the dominant active neutral amino acid transporter in L6-G8C5 cells, because SNAT2 silencing had significant effects on intracellular free amino acid concentrations and on amino acid signalling to mTORC1. SNAT2 silencing also impaired Akt signalling, apparently through an amino acid-independent pathway (Evans *et al.,* 2008). These apparent signalling effects of SNAT2 were confirmed in the present study, and significant effects of SNAT2 siRNA silencing were also shown on MAPK's i.e. JNK phosphorylation (Figure 5.5). Screening of SNAT transporter expression in L6-G8C5 myoblasts by RT-PCR showed strong expression of SNAT2 mRNA but only weak expression of SNAT1, 3, 4 and 5 (Evans *et al.,* 2007). A similar conclusion was reached in L6 myotubes (Hyde *et al.,* 2001). However, it should not be concluded from the above that SNAT2 is the only functionally important

active Na-linked neutral amino acid transporter in skeletal muscle cells – or even in L6 cells. For example, in Chapter 5 (Figure 5.11) it was shown that culture medium containing only L-Met can detectably stimulate rpS6 phosphorylation and that this effect is blunted by the System A competitive inhibitor MeAIB, suggesting that the L-Met effect depends on a System A transporter. However, because of technical problems during the attempted siRNA silencing of SNAT2 in these L-Met experiments (Figure 5.13), it was not possible to prove that SNAT2 was the most important L-Met transporter. In the amino acid-depleted medium (containing only extracellular L-Met) shown in Figure 5.13, some other System A-type SNAT transporter capable of carrying L-Met might have been up-regulated. Therefore, in future work, testing the expression of other SNATs may be of interest, although it should be noted that System L transporters can also efficiently carry L-Met (Eunjung, 2009).

Another important SLC38 transporter which was not considered in the earlier work of Evans et al (2007 and 2008) is SLC38A9 (SNAT9) which, in principle, might be inhibited by MeAIB and might sense L-Met. Its substrate specificity is not fully understood (Goberdhan *et al.,* 2016; Wang *et al.,* 2015), and it is located on the lysosome. Its amino acid sensitivity is mediated by its cytoplasmic tail. (Goberdhan *et al.,* 2016; Jung *et al.,* 2015), and it is part of the Rag-Ragulator amino acid sensing machinery involved in activating mTORC1.

## 6.2 Future work on phosphorylation of SNAT2.

At the start of this project, it was thought that the transport activity of the SNAT2 protein in the plasma membrane of L6 cells might be activated by phosphorylation of the transporter by MAP kinases or by receptor tyrosine kinase stimulated by autocrine IGF-I; possibly at one of the cluster of Ser and Tyr phosphorylation sites that had previously been reported near the cytoplasmic N-terminus of the protein (Section 1.15). By this model, phosphorylation might activate System A amino acid transport by promoting translocation of SNAT2 into the plasma membrane or inhibition of its internalisation and degradation. This would be consistent with the observations that insulin and IGF-I activate SNAT2, and that amino acid deprivation (a known activator of MAP kinases) strongly up-regulates SNAT2 (Section 1.13). It was also thought that DEX might down-regulate transport by inducing transcription of a phosphoprotein phosphatase such as PTP1B which might reduce phosphorylation of the transporter.

The experiments in this thesis failed to support this model for the following reasons:

- Even though the PTPase inhibitor vanadate variably blunted the effect of DEX on System A (SNAT2) transport in L6 cells, other PTPase inhibitors did not.
- GFP-trapping of GFP-tagged SNAT2 expressed in HEK293A cells followed by mass spectrometry failed to detect SNAT2 phosphopeptides
- Dephosphorylation (by incubation with Alkaline Phosphatase) of lysates from HEK293A cells expressing SNAT2-eGFP did not enhance SNAT2-eGFP proteolysis. On the contrary, dephosphorylation was associated with apparent stabilisation of the protein, (although it was also uncertain whether this Alkaline Phosphatase effect was a direct effect on phosphorylated SNAT2 or on some other phosphoprotein(s)).

Instead of phosphorylation of SNAT2 being an important factor, experiments with the proteasome inhibitor MG132 (Figures 3.20 and 4.13) suggested that proteolysis of SNAT2 through the UPP might be a more relevant mediator of the action of DEX on SNAT2.

However, this experimental evidence does not completely rule out a role for SNAT2 phosphorylation in the regulation of the transporter. The mass spectrometry data obtained here on GFP-trapped SNAT2 was incomplete and only covered a small part of the full amino acid sequence. For that reason, phosphorylation sites may have been missed. Also, even though there is no evidence that phosphorylation stabilises the SNAT2 protein, it is possible that phosphorylation might *de*-stabilise it, promoting proteolysis - as has been described for the closely related transporter SNAT3 (also known as SN1 (SLC38a3)). It has been shown that Protein Kinase C (PKC) directly phosphorylates SNAT3 on Ser52 in its N-terminal cytoplasmic tail, thus targeting it for degradation (Nissen-Meyer & Chaudhry, 2013). There is no evidence yet that any PKC isoform regulates SNAT2, but a potential PKC phosphorylation site has been suggested at Ser320 of rat SNAT2, which is thought to be in the third cytoplasmic loop of the protein (Yao *et al.,* 2000). SNAT2 destabilisation by phosphorylation might also explain the apparent increased stability of the light form of SNAT2-eGFP in Alkaline Phosphatase-treated lysates in Figure 4.11. For that reason experiments like those described for SNAT3 (Nissen-Meyer & Chaudhry, 2013) might be a useful way to investigate further the molecular mechanism of the effects that were described in this thesis, for example site-directed mutagenesis of SNAT2-eGFP at suspected phosphorylation sites (a) to see the functional effects of this in intact cells e.g. on System A transport activity, and (b) to see whether this alters the stabilising effect of Alkaline Phosphatase on SNAT2-eGFP in lysates as in Figure 4.11.

If an important regulatory phosphorylation on SNAT2 controlling its degradation can be found, it may be relevant to muscle wasting *in vivo* in view of recent evidence that the loss of SNAT2 protein in mouse fast twitch muscle in sarcopaenia cannot be explained by declining SNAT2 transcription (Wendowski *et al.,* 2017), possibly because there is increased degradation of the transporter, stimulated by the increased glucocorticoid secretion that is thought to contribute to sarcopaenia in fast twitch fibres (Sakuma & Yamaguchi, 2012). This effect of age on SNAT2 was reversed by treating muscle fibres with a physiological concentration (~2nM) of the anabolic steroid dihydrotestosterone (Wendowski *et*

*al.,* 2017). This raises the interesting possibility that the molecular mechanism of the effect of DEX that was studied in this thesis may also be the site at which anabolic steroids exert a therapeutic effect.

# Appendixes

## Appendix A: Culture medium and Test medium

### A.1 DMEM (Invitrogen 11880-028)

| Components | Molecular Weight | Concentration (mg/L) | mM |
|---|---|---|---|
| **Amino Acids** | | | |
| **Glycine** | 75.0 | 30.0 | 0.4 |
| **L-Arginine hydrochloride** | 211.0 | 84.0 | 0.39810428 |
| **L-Cystine 2HCl** | 313.0 | 63.0 | 0.20127796 |
| **L-Histidine hydrochloride-H2O** | 210.0 | 42.0 | 0.2 |
| **L-Isoleucine** | 131.0 | 105.0 | 0.8015267 |
| **L-Leucine** | 131.0 | 105.0 | 0.8015267 |
| **L-Lysine hydrochloride** | 183.0 | 146.0 | 0.7978142 |
| **L-Methionine** | 149.0 | 30.0 | 0.20134228 |
| **L-Phenylalanine** | 165.0 | 66.0 | 0.4 |
| **L-Serine** | 105.0 | 42.0 | 0.4 |
| **L-Threonine** | 119.0 | 95.0 | 0.79831934 |
| **L-Tryptophan** | 204.0 | 16.0 | 0.078431375 |
| **L-Tyrosine** | 181.0 | 72.0 | 0.39779004 |
| **L-Valine** | 117.0 | 94.0 | 0.8034188 |
| **Vitamins** | | | |
| | 140.0 | 4.0 | 0.028571429 |
| **D-Calcium pantothenate** | 477.0 | 4.0 | 0.008385744 |
| **Folic Acid** | 441.0 | 4.0 | 0.009070295 |
| **Niacinamide** | 122.0 | 4.0 | 0.032786883 |
| **Pyridoxine hydrochloride** | 206.0 | 4.0 | 0.019417476 |
| **Riboflavin** | 376.0 | 0.4 | 0.0010638298 |
| **Thiamine hydrochloride** | 337.0 | 4.0 | 0.011869436 |
| **i-Inositol** | 180.0 | 7.2 | 0.04 |
| **Inorganic Salts** | | | |

| | | | |
|---|---|---|---|
| **Calcium Chloride (CaCl2-2H2O)** | 147.0 | 264.0 | 1.7959183 |
| **Ferric Nitrate (Fe(NO3)3"9H2O)** | 404.0 | 0.1 | 2.4752476E-4 |
| **Magnesium Sulfate (MgSO4-7H2O)** | 246.0 | 200.0 | 0.8130081 |
| **Potassium Chloride (KCl)** | 75.0 | 400.0 | 5.3333335 |
| **Sodium Bicarbonate (NaHCO3)** | 84.0 | 3700.0 | 44.04762 |
| **Sodium Chloride (NaCl)** | 58.0 | 6400.0 | 110.344826 |
| **Sodium Phosphate monobasic (NaH2PO4-2H2O)** | 154.0 | 141.0 | 0.91558444 |
| **Other Components** | | | |
| **D-Glucose (Dextrose)** | 180.0 | 1000.0 | 5.5555553 |
| **Sodium Pyruvate** | 110.0 | 110.0 | 1.0 |

URL: http://www.lifetechnologies.com/uk/en/home/technical-resources/media-formulation.183.html Last accessed 18/12/2015.

## A.2 DMEM- high glucose (Sigma-D6429)

| Components | (1×) Concentration g/L |
|---|---|
| **Inorganic Salts** | |
| Calcium Chloride (CaCl2-2H2O) | 0.2 |
| Ferric Nitrate (Fe(NO3)3"9H2O) | 0.0001 |
| Magnesium Sulfate (MgSO4) | 0.09767 |
| Potassium Chloride (KCl) | 0.4 |
| Sodium Bicarbonate (NaHCO3) | 3.7 |
| Sodium Chloride (NaCl) | 6.4 |
| Sodium Phosphate monobasic (NaH2PO4-2H2O) | 0.109 |
| **Amino Acids** | |
| L-Arginine. HCl | 0.084 |
| L-Cysteine 2HCl | 0.0626 |
| L-Glutamine | 0.584 |
| Glycine | 0.03 |

| | |
|---|---|
| L-Histidine. HCl .H2O | 0.042 |
| L-Isoleucine | 0.105 |
| L-Leucine | 0.105 |
| L-Lysine. HCl | 0.146 |
| L-Methionine | 0.03 |
| L-Phenylalanine | 0.066 |
| L-Serine | 0.042 |
| L-Threonine | 0.095 |
| L-Tryptophan | 0.016 |
| L-Tyrosine. 2Na. 2H2O | 0.10379 |
| L-Valine | 0.094 |
| **Vitamins** | |
| Choline Chloride | 0.004 |
| Folic Acid | 0.004 |
| myo-Inositol | 0.0072 |
| Niacinamide | 0.004 |
| D-Pantothenic Acid. ½Ca | 0.004 |
| Pyridoxine. HCl | 0.00404 |
| Riboflavin | 0.0004 |
| **Other** | |
| D-Glucose | 4.5 |
| Phenol Red. Na | 0.0159 |
| Pyruvic Acid. Na | 0.11 |

URL: Modified from: https://www.sigmaaldrich.com/content/dam/sigma-aldrich/docs/Sigma/Formulation/d6429for.pdf Last accessed 13/1/2016.

## A.3 MEM (Invitrogen 21090-022)

| Components | Molecular Weight | Concentration (mg/L) | mM |
|---|---|---|---|
| **Amino Acids** | | | |
| **L-Arginine hydrochloride** | 211.0 | 126.0 | 0.5971564 |
| **L-Cystine** | 240.0 | 24.0 | 0.1 |
| **L-Histidine hydrochloride-H2O** | 210.0 | 42.0 | 0.2 |
| **L-Isoleucine** | 131.0 | 52.0 | 0.39694658 |
| **L-Leucine** | 131.0 | 52.0 | 0.39694658 |
| **L-Lysine hydrochloride** | 183.0 | 73.0 | 0.3989071 |
| **L-Methionine** | 149.0 | 15.0 | 0.10067114 |
| **L-Phenylalanine** | 165.0 | 32.0 | 0.19393939 |
| **L-Threonine** | 119.0 | 48.0 | 0.40336135 |
| **L-Tryptophan** | 204.0 | 10.0 | 0.04901961 |
| **L-Tyrosine** | 181.0 | 36.0 | 0.19889502 |
| **L-Valine** | 117.0 | 46.0 | 0.3931624 |
| **Vitamins** | | | |
| **Choline chloride** | 140.0 | 1.0 | 0.007142857 |
| **D-Calcium pantothenate** | 477.0 | 1.0 | 0.002096436 |
| **Folic Acid** | 441.0 | 1.0 | 0.0022675737 |
| **Niacinamide** | 122.0 | 1.0 | 0.008196721 |
| **Pyridoxal hydrochloride** | 204.0 | 1.0 | 0.004901961 |
| **Riboflavin** | 376.0 | 0.1 | 2.6595744E-4 |
| **Thiamine hydrochloride** | 337.0 | 1.0 | 0.002967359 |
| **i-Inositol** | 180.0 | 2.0 | 0.011111111 |
| **Inorganic Salts** | | | |
| **Calcium Chloride (CaCl2-2H2O)** | 147.0 | 264.0 | 1.7959183 |
| **Magnesium Sulfate (MgSO4-7H2O)** | 246.0 | 200.0 | 0.8130081 |

| | | | |
|---|---|---|---|
| **Potassium Chloride (KCl)** | 75.0 | 400.0 | 5.3333335 |
| **Sodium Bicarbonate (NaHCO3)** | 84.0 | 2200.0 | 26.190475 |
| **Sodium Chloride (NaCl)** | 58.0 | 6800.0 | 117.24138 |
| **Sodium Phosphate monobasic (NaH2PO4-2H2O)** | 156.0 | 158.0 | 1.0128205 |
| **Other Components** | | | |
| **D-Glucose (Dextrose)** | 180.0 | 1000.0 | 5.5555553 |
| **Phenol Red** | 376.4 | 10.0 | 0.026567481 |

URL:http://www.lifetechnologies.com/uk/en/home/technical-resources/media-formulation.197.html Last accessed 18/12/2015.

## A.4 HBSS (Invitrogen 24020-133/500ml)

| Components | Molecular Weight | Concentration (mg/L) | mM |
|---|---|---|---|
| **Inorganic Salts** | | | |
| **Calcium Chloride (CaCl2) (anhyd.)** | 111.0 | 140.0 | 1.2612612 |
| **Magnesium Chloride (MgCl2-6H2O)** | 203.0 | 100.0 | 0.49261084 |
| **Magnesium Sulfate (MgSO4-7H2O)** | 246.0 | 100.0 | 0.40650406 |
| **Potassium Chloride (KCl)** | 75.0 | 400.0 | 5.3333335 |
| **Potassium Phosphate monobasic (KH2PO4)** | 136.0 | 60.0 | 0.44117647 |
| **Sodium Bicarbonate (NaHCO3)** | 84.0 | 350.0 | 4.1666665 |
| **Sodium Chloride (NaCl)** | 58.0 | 8000.0 | 137.93103 |
| **Sodium Phosphate dibasic (Na2HPO4) anhydrous** | 142.0 | 48.0 | 0.33802816 |
| **Other Components** | | | |
| **D-Glucose (Dextrose)** | 180.0 | 1000.0 | 5.5555553 |
| **Phenol Red** | 376.4 | 10.0 | 0.026567481 |

URL:http://www.thermofisher.com/uk/en/home/technical-resources/media-formulation.152.htm Last accessed 18/12/2015.

## A.5 EBSS (Invitrogen 24020/500ml)

| Components | Molecular Weight | Concentration (mg/L) | mM |
|---|---|---|---|
| **Inorganic Salts** | | | |
| **Calcium Chloride (CaCl2) (anhyd.)** | 111.0 | 200.0 | 1.8018018 |
| **Magnesium Sulfate (MgSO4-7H2O)** | 246.0 | 200.0 | 0.8130081 |
| **Potassium Chloride (KCl)** | 75.0 | 400.0 | 5.3333335 |
| **Sodium Bicarbonate (NaHCO3)** | 84.0 | 2200.0 | 26.190475 |
| **Sodium Chloride (NaCl)** | 58.0 | 6800.0 | 117.24138 |
| **Sodium Phosphate monobasic (NaH2PO4-H2O)** | 138.0 | 140.0 | 1.0144928 |
| **Other Components** | | | |
| **D-Glucose (Dextrose)** | 180.0 | 1000.0 | 5.5555553 |
| **Phenol Red** | 398.0 | 10.0 | 0.0251256 |

URL:http://www.thermofisher.com/uk/en/home/technical-resources/media-formulation.305.html Last accessed 18/12/2015.

## A.6 Concentration of amino acids added to EBSS to make L-Methionine depleted MEM.

Source of Amino acids: Sigma kit LAA-21

| Amino acid | Mg/L |
|---|---|
| L-Arginine.HCl | 126 |
| L-Cystine | 24 |
| L-Glutamine | NONE |
| L-Histidine.HCl.H2O | 42 |
| L-Isoleucine | 52 |
| L-Leucine | 52 |
| L-Lysine.HCl | 73 |
| L-Methionine | NONE |

| | |
|---|---|
| L-Phenylalanine | 32 |
| L-Threonine | 48 |
| L-Tryptophan | 10 |
| L-Tyrosine | 36 |
| L-Valine | 46 |

Recipe: From Invitrogen catalogue “REF 21090”
URL:http://www.thermofisher.com/uk/en/home/technical-resources/media-formulation.197.html Last accessed 18/12/2015.

### A.7 MEM Vitamin Solution (100X) (Invitrogen11120-052)

| Components | Molecular Weight | Concentration (mg/L) | mM |
|---|---|---|---|
| **Vitamins** | | | |
| **Choline chloride** | | 100.0 | Infinity |
| **D-Calcium pantothenate** | 477.0 | 100.0 | 0.2096436 |
| **Folic Acid** | 441.0 | 100.0 | 0.22675736 |
| **Nicotinamide** | | 100.0 | Infinity |
| **Pyridoxal hydrochloride** | | 100.0 | Infinity |
| **Riboflavin** | | 10.0 | Infinity |
| **Thiamine hydrochloride** | | 100.0 | Infinity |
| **i-Inositol** | | 200.0 | Infinity |
| **Inorganic Salts** | | | |
| **Sodium Chloride (NaCl)** | | 8500.0 | Infinity |

URL:http://www.thermofisher.com/uk/en/home/technical-resources/media-formulation.163.html Last accessed 18/12/2015.

### A.8 Hepes Buffered Saline (HBS) (1Litre)

| Component | Formula Weight | Weight (g) | Concentration (mM/L) |
|---|---|---|---|
| NaCl | 58.44 | 8.1816 | 140 |
| Hepes Acid | 238.3 | 4.7660 | 20 |
| $MgSO_4.7H_2O$ | 246.5 | 0.6163 | 2.5 |
| KCl | 74.55 | 0.3728 | 5.0 |
| $CaCl_2.2H_2O$ | 147.02 | 0.1470 | 1.0 |
| Phenol Red | ---------- | 0.010g | 10mg/L |

The above components were dissolved in about 750ml of freshly drawn ultra-pure water by stirring to dissolve with a magnetic stirrer bar. The pH was adjusted to 7.4 at room temperature by titrating about 18-20ml of 0.5M NaOH into the solution. The volume made up to 1 L and stored it at +4°C.

### A.9 Ham's F-10 Nutrient Mix, GlutaMAX ™ (Gibco-41550-021)

| Components | Molecular Weight | Concentration (mg/L) | mM |
|---|---|---|---|
| **Amino Acids** | | | |
| Glycine | 75.0 | 7.5 | 0.1 |
| L-Alanine | 89.0 | 9.0 | 0.101123594 |
| L-Alanyl-L-Glutamine | 217.0 | 217.0 | 1.0 |
| L-Arginine hydrochloride | 211.0 | 211.0 | 1.0 |
| L-Asparagine-H2O | 150.0 | 15.0 | 0.1 |
| L-Aspartic acid | 133.0 | 13.0 | 0.09774436 |
| L-Cysteine | 121.0 | 25.0 | 0.20661157 |
| L-Glutamic Acid | 147.0 | 14.7 | 0.1 |
| L-Histidine hydrochloride-H2O | 210.0 | 23.0 | 0.10952381 |
| L-Isoleucine | 131.0 | 2.6 | 0.019847328 |
| L-Leucine | 131.0 | 13.0 | 0.099236645 |
| L-Lysine hydrochloride | 183.0 | 29.0 | 0.15846995 |
| L-Methionine | 149.0 | 4.5 | 0.030201342 |
| L-Phenylalanine | 165.0 | 5.0 | 0.030303031 |
| L-Proline | 115.0 | 11.5 | 0.1 |
| L-Serine | 105.0 | 10.5 | 0.1 |
| L-Threonine | 119.0 | 3.6 | 0.0302521 |
| L-Tryptophan | 204.0 | 0.6 | 0.0029411765 |

| Components | Molecular Weight | Concentration (mg/L) | mM |
|---|---|---|---|
| L-Tyrosine | 181.0 | 1.8 | 0.009944751 |
| L-Valine | 117.0 | 3.5 | 0.02991453 |
| **Vitamins** | | | |
| Biotin | 244.0 | 0.024 | 9.836066E-5 |
| Choline chloride | 140.0 | 0.7 | 0.005 |
| D-Calcium pantothenate | 477.0 | 0.7 | 0.0014675052 |
| Folic Acid | 441.0 | 1.3 | 0.0029478457 |
| Niacinamide | 122.0 | 0.6 | 0.004918033 |
| Pyridoxine hydrochloride | 206.0 | 0.2 | 9.708738E-4 |
| Riboflavin | 376.0 | 0.4 | 0.0010638298 |
| Thiamine hydrochloride | 337.0 | 1.0 | 0.002967359 |
| Vitamin B12 | 1355.0 | 1.4 | 0.0010332103 |
| i-Inositol | 180.0 | 0.5 | 0.0027777778 |
| **Inorganic Salts** | | | |
| Calcium Chloride (CaCl2-2H2O) | 147.0 | 44.0 | 0.2993197 |
| Cupric sulfate (CuSO4-5H2O) | 250.0 | 0.0025 | 1.0E-5 |
| Ferric sulfate (FeSO4-7H2O) | 278.0 | 0.834 | 0.003 |
| Magnesium Sulfate (MgSO4-7H2O) | 246.0 | 153.0 | 0.6219512 |
| Potassium Chloride (KCl) | 75.0 | 285.0 | 3.8 |
| Potassium Phosphate monobasic (KH2PO4) | 136.0 | 83.0 | 0.6102941 |
| Sodium Bicarbonate (NaHCO3) | 84.0 | 1200.0 | 14.285714 |
| Sodium Chloride (NaCl) | 58.0 | 7400.0 | 127.586205 |
| Sodium Phosphate dibasic (Na2HPO4) anhydrous | 142.0 | 154.5 | 1.0880282 |
| Zinc sulfate (ZnSO4-7H2O) | 288.0 | 0.03 | 1.0416666E-4 |
| **Other Components** | | | |
| D-Glucose (Dextrose) | 180.0 | 1100.0 | 6.111111 |
| Hypoxanthine | 136.0 | 4.0 | 0.029411765 |
| Lipoic Acid | 206.0 | 0.2 | 9.708738E-4 |
| Phenol Red | 376.4 | 1.2 | 0.0031880978 |
| Sodium Pyruvate | 110.0 | 110.0 | 1.0 |
| Thymidine | 242.0 | 0.7 | 0.002892562 |

URL:http://www.thermofisher.com/uk/en/home/technical-resources/media-formulation.222.html Last accessed 17/05/17.

## A.10 DMEM Low glucose (Gibco-11885-084)

| Components | Molecular Weight | Concentration (mg/L) | mM |
|---|---|---|---|
| **Amino Acids** | | | |
| Glycine | 75.0 | 30.0 | 0.4 |
| L-Arginine hydrochloride | 211.0 | 84.0 | 0.39810428 |
| L-Cystine 2HCl | 313.0 | 63.0 | 0.20127796 |
| L-Glutamine | 146.0 | 584.0 | 4.0 |
| L-Histidine hydrochloride-H2O | 210.0 | 42.0 | 0.2 |
| L-Isoleucine | 131.0 | 105.0 | 0.8015267 |
| L-Leucine | 131.0 | 105.0 | 0.8015267 |
| L-Lysine hydrochloride | 183.0 | 146.0 | 0.7978142 |
| L-Methionine | 149.0 | 30.0 | 0.20134228 |
| L-Phenylalanine | 165.0 | 66.0 | 0.4 |
| L-Serine | 105.0 | 42.0 | 0.4 |
| L-Threonine | 119.0 | 95.0 | 0.79831934 |
| L-Tryptophan | 204.0 | 16.0 | 0.078431375 |
| L-Tyrosine disodium salt dihydrate | 261.0 | 104.0 | 0.39846742 |
| L-Valine | 117.0 | 94.0 | 0.8034188 |
| **Vitamins** | | | |
| Choline chloride | 140.0 | 4.0 | 0.028571429 |
| D-Calcium pantothenate | 477.0 | 4.0 | 0.008385744 |
| Folic Acid | 441.0 | 4.0 | 0.009070295 |
| Niacinamide | 122.0 | 4.0 | 0.032786883 |
| Pyridoxine hydrochloride | 204.0 | 4.0 | 0.019607844 |
| Riboflavin | 376.0 | 0.4 | 0.0010638298 |
| Thiamine hydrochloride | 337.0 | 4.0 | 0.011869436 |
| i-Inositol | 180.0 | 7.2 | 0.04 |
| **Inorganic Salts** | | | |
| Calcium Chloride (CaCl2) (anhyd.) | 111.0 | 200.0 | 1.8018018 |
| Ferric Nitrate (Fe(NO3)3"9H2O) | 404.0 | 0.1 | 2.4752476E-4 |
| Magnesium Sulfate (MgSO4) (anhyd.) | 120.0 | 97.67 | 0.8139166 |
| Potassium Chloride (KCl) | 75.0 | 400.0 | 5.3333335 |
| Sodium Bicarbonate (NaHCO3) | 84.0 | 3700.0 | 44.04762 |
| Sodium Chloride (NaCl) | 58.0 | 6400.0 | 110.344826 |
| Sodium Phosphate monobasic (NaH2PO4-H2O) | 138.0 | 125.0 | 0.9057971 |
| **Other Components** | | | |

| Components | Molecular Weight | Concentration (mg/L) | mM |
|---|---|---|---|
| D-Glucose (Dextrose) | 180.0 | 1000.0 | 5.5555553 |
| Phenol Red | 376.4 | 15.0 | 0.039851222 |
| Sodium Pyruvate | 110.0 | 110.0 | 1.0 |

URL:http://www.thermofisher.com/uk/en/home/technical-resources/media-formulation.48.html Last accessed 17/05/17.

# Appendix B (Buffers and Reagents)

### B.1 0.5 M Sodium Hydroxide (NaOH)

To prepare 500 ml of 0.5M NaOH, dissolve 10g of pellets (Sigma S-8045 FW: 40.00) in nearly 250 ml of ultra-pure water then bring up the volume to 500 ml by using volumetric flask and store in room temperature.

### B.2 Lowry (Folin) Reagent A (L)

Dissolve the following composition in 500 ml ultra-pure water:

- 20.00 g Sodium Carbonate “Anhydrous” (Sigma S-2127 FW 106.0)
- 4.00 g Sodium hydroxide (Sigma S-8045 FW: 40.00)
- 0.2 g Potassium Sodium (+)-tartrate.4$H_2O$ (BDH AR 10219 FW: 282.22)

Then make up to 1L in a volumetric flask and store in 4°C.

### B.3 Lowry (Folin) Reagent B (L)

Dissolve 5g of Cupric Sulphate (BDH AR 10091 FW: 249.68) in 500 ml ultra-pure water and make up the volume to 1L in a volumetric flask then store 4°C.

### B.4 Lowry (Folin) standards

Make up a stock solution (S) first, weigh out 0.05 g of Bovine Serum Albumin (BSA: Sigma A-7638) and add 20 ml of 0.5M NaOH. Dissolve it with magnetic stirrer then make the standards as follows:

| **Final BSA(µg/ml)** | 0 | 50 | 100 | 150 | 200 | 300 | 400 | 500 |
|---|---|---|---|---|---|---|---|---|
| **Volume of Stock (S) (µl)** | 0 | 50 | 100 | 150 | 200 | 300 | 400 | 500 |
| **Volume of 0.5M NaOH (ml)** | 2.5 | 2.45 | 2.4 | 2.35 | 2.3 | 2.2 | 2.1 | 2.0 |

### B.5 Buffers and Solutions for Tyrosine (PTP) Phosphatases Assay

#### B.5.1 Phosphatase Storage Buffer

25mM Tris.HCl pH 7.5
2mM EDTA
10mM beta-mercaptoethanol (FW = 78.13)

#### B.5.2 Sephadex® G-25 storage buffer

10mM Tris (pH 7.5)
1mM EDTA
0.02% sodium azide

#### B.5.3 Phosphate Standard

50µM Pi Standard (Dilute the 1mM Pi standard provided in the kit 20-fold to give a 50µM Pi Standard, by mixing 10µl of the 1mM standard plus 190ul of Pi-free water from the kit).

## B.6 Western Blot buffers

### B.6.1 Reducing Lysis buffer

| Stock Solutions | For 10ml | Final concentration |
|---|---|---|
| 1M pH 7.4 beta glycerophosphate | 100ul | 10mM |
| 0.5M pH 8 EDTA | 20ul | 1mM |
| 40mM EGTA | 250ul | 1mM |
| 1M pH 7.5 Tris-HCl | 500ul | 50mM |
| 100mM Na Orthovanadate | 100ul | 1mM |
| 1M Benzamidine | 10ul | 1mM |
| 100mM PMSF | 20ul | 0.2mM |
| 5mg/ml Pepstatin A | 10ul | |
| 5mg/ml Leupeptin | 10ul | |
| Beta-Mercaptoethanol | 10ul | 0.1% |
| 10% Triton X-100 | 1ml | 1% |
| 500mM Na Fluoride | 1ml | 50mM |
| Nano-pure water | 6.97ml | |

### B.6.2 Sample Buffer

| Component | Volume (ml) |
|---|---|
| Water | 4.00 |
| 0.5m TRIS HCl pH6.8 | 1.00 |
| Glycerol | 0.80 |
| 10% (w/v) SDS | 1.60 |
| 2-β-mercaptoethanol | 0.40 |
| 0.05% (w/v) bromophenol blue | 0.20 |

### B.6.3 Resolving and Stacking Gel for Western Blot (×1 gel)

| Stock solutions | 12% Resolving gel | 10% Resolving gel | 12% Stacking gel |
|---|---|---|---|
| Water (Nano-pure) | 3.35 ml | 3.1 ml | 3.03 ml |
| Acrylamide[1] (30 w/v) | 4 ml | 2.5 ml | 0.65 ml |
| 1.5M Tris HCl (pH:8.8) | 2.5 ml | 1.875 | --- |
| 0.5M Tris HCl(pH:6.8) | --- | --- | 1.25 ml |
| SDS(10% w/v) | 100 µl | 75 µl | 50 µl |
| APS[2] | 50 µl | 37.5 µl | 25 µl |
| TEMED[3] | 5 µl | 10 µl | 5 µl |

1 Acrylamide: Sigma A3699-100ml
2 APS: Ammonium persulphate.
3 N,N,N',N'- Tetramethylene diamine (Sigma T9281-25ml).

### B.6.4 Western Transfer buffer (1litre)

3.03g Tris-base
14.4g Glycine
200ml Methanol

### B.6.5 SDS-PAGE Running buffer (1litre)

3.03g Tris-base
14.4g glycine
50ml 20% w/v SDS

### B.6.6 Tris-buffered saline 10 X (TBS) (1 litre)

6.055g Trizma Base
8.766g NaCl
Adjust to pH 7.6 with HCl

### B.6.7 TBS-Tween 1 X (1 litre)

100ml 10X TBS
900ml De-ionised $H_2O$
1ml Tween 20

**B.7 Hepes Buffered Saline (2X HBS) (500ml).**

NaCl 8g

$Na_2HPO_4$-$7H_2O$ 0.2g (0.14g if using dihydrate; [phosphate] must be 1.5mM)

HEPES 6.5g

Dissolve above in about 300ml of ultra-pure water, adjust pH to 7.0 using HCl. make up the volume to 500ml and re-pH at the end because it can change filter sterilize using 0.2µm Acrodisc filter. Aliquot and store at -20°C. The solution can be freezed/thawed once for future use.

**B.8 2M $CaCl_2$ (200ml)**

$CaCl_2.6H_2O$ 87.6g, dissolve in 200ml ultra-pure water filter sterile and keep it in 4°C (Do not freeze).

**B.9 Buffers and reagents used for L6 cells Immunohistochemistry**

**B.9.1 Phosphate buffer saline (X1 PBS)**

Dissolve 1 tablet of PBS (Sigma-P4417) in 200ml ultra-pure water.

**B.9.2 Fixation buffer**

2% Paraformaldehyde+ 4% Sucrose in x1 PBS

# Appendix C (SNAT2 constructs sequences)

**C.1. SNAT2-eGFP (F)**

PNACL sequencing result:

NNNNNNNNNNNNNNNNNNNNNNNCTGGTTNAGNGNNNGTCAGATCCGCTAGCGCTACCGGACTCAG
ATCTCGAGATGAAGAAGGCCGAAATGGGACGATTCAGTATTTCCCCGGATGAAGACAGCAGCAGCTA
CAGTTCCAACAGCGACTTCAACTACTCCTACCCCACCAAGCAAGCTGCTCTGAAAAGCCATTATGCA
GATGTAGATCCTGAAAACCAGAACTTTTTACTTGAATCGAATTTGGGGAAGAAGAAGTATGAAACAG
AATTTCATCCAGGTACTACTTCCTTTGGAATGTCAGTATTTAATCTGAGCAATGCGATTGTGGGCAG
TGGAATCCTTGGGCTTTCTTATGCCATGGCTAATACTGGAATTGCTCTTTTTATAATTCTCTTGACA
TTTGTGTCAATATTTTCCCTGTATTCTGTTCATCTCCTTTTGAAGACTGCCAATGAAGGAGGGTCTT
TATTATATGAACAATTGGGATATAAGGCATTTGGATTAGTTGGAAAGCTTGCAGCATCTGGATCAAT
TACAATGCAGAACATTGGAGCTATGTCAAGCTACCTCTTCATAGTGAAATATGAGTTGCCTTTGGTG
ATCCAGGCATTAACGAACATTGAAGATAAAACTGGATTGTGGTATCTGAACGGGAACTATTTGGTTC
TGTTGGTGTCATTGGTGGTCATTCTTCCTTTGTCGCTGTTTAGAAATTTAGGATATTTGGGATATAC
CAGTGGCCTTTCCTTGTTGTGTATGGTGTTCTTTCTGATTGTGGTCATTTGCAAGAAATTTCNNNTT
CCGTGTCCTGTGGAAGCTGCTTTGATAATTAACGAAACAATAAACACCACCTTAACACAGCCAACAG
CTCTTGTACCTGCTTTGTCACATAACGTGACTGAAAATGACTCTTGCAGACCTCACTATTTTATTTT
CAACTCACAGACTGTCTATGCTGTGCCAATTCTGATCTTTTCATTTGTCTGTCATCCTGCTGTTCTT
CCCATCTATGAANAACTGAAANACCGCANCCGTANAANAATGATGAATGNGTCCAANANTTCATTTT
TTGCTANGNTTNNTCANGNNNCNGCTTNCCGCCCTCNTTNGNNNNCNNNANNNTTTACNAANNTNNN
NGTCNNATNGNNNNNNNCTACNNNTNNNNNNNTGGNNACNGNANNNNNNNNTNNNCNNNNNNNNNNN
GNNTNNNNNNNNNNNNNNNNNCNGNNNNNNNNNNNNNNNNTTNNNNNNNNNNNNNNNNNNNNNNN
NNNNNNNNNNGNNNNNNNNNNANNNNNNNNNTNNNNNNNNN

**NCBI BLAST result:**

Range 2: 46729367 to 46729482GenBankGraphics Next Match Previous Match First Match

Alignment statistics for match #2

| Score | Expect | Identities | Gaps | Strand | Frame |
|---|---|---|---|---|---|
| 215 bits (116) | 1e-52() | 116/116(100%) | 0/116(0%) | Plus/Minus | |

Features:
sodium-coupled neutral amino acid transporter 2

```
Query  274       CATCCAGGTACTACTTCCTTTGGAATGTCAGTATTTAATCTGAGCAATGCGATTGTGGGC  333
                  ||||||||||||||||||||||||||||||||||||||||||||||||||||||||||||
Sbjct  46729482  CATCCAGGTACTACTTCCTTTGGAATGTCAGTATTTAATCTGAGCAATGCGATTGTGGGC  46729423

Query  334       AGTGGAATCCTTGGGCTTTCTTATGCCATGGCTAATACTGGAATTGCTCTTTTTAT  389
                  ||||||||||||||||||||||||||||||||||||||||||||||||||||||||
Sbjct  46729422  AGTGGAATCCTTGGGCTTTCTTATGCCATGGCTAATACTGGAATTGCTCTTTTTAT  46729367
```

## C.2. SNAT2-eGFP (R)

PNACL sequencing result:

CNNNNNNNNNNNNNNNNNCNNNNNGCTCNCCNTGGTGGCGACCGGTNNNNNNCGGGCCCGCGGTACC
GTCGACTGCATGAATTCATGGCCACCTCCAGGTGCATTGTGTACCCAATCCAAAACAATCAAGGCCA
TGCTTCCGGTCATCACCAGTACACCACTTAACAGGAAGAACAAAGCCCCAATCTTTTGTACAGATTT
CATAGGTTCTTTCTTCACCAACTTGATATAGAAGGCAGAAGGAAGAATAAAAATCAACATAGAAGCT
GCAGATGCACCAATAAAACCAAAGATATCCCTAATAGTTGGGACAAAGATGACAAGTAAATTGGTAA
ATGCCAAGATAGACACTGTAATGAGACTATGACGCCACCAACTGAAATCTTTTGATGCACACAAAAG
TGAGTTACAGAACTCCGGATTGGGAAAATAACTACTGGTACTGTCAGGGTCACAGCCATTAACACAG
CCAGACGGACAATGAGAAGAAGAATATCAGTTCCCAAGATAGAAGAGTAGGTATGAAGCAATTCTGA
CTCAACATGTTCGTAAAATGTTAGGTATCCAAAGAGGGCGGCAAGCAGATACATGAGAAACATAGCA

AAAAATGAAATCTTGGACACATTCATCATTCTTCTACGGCTGCGGTCTTTCAGTTCTTCATAGATGG
GAAGAACAGCAGGATGACAGACAAATGAAAAGATCAGAATTGGCACAGCATAGACAGTCTGTGAGTT
GAAAATAAAATAGTGAGGTCTGCAAGAGTCATTTTCAGTCACGTTATGTGACAAAGCNNTACAAGAG
CTGTTGGCTGTGTTAAGGTGGTGTTTATTGTTTCGTTAATTATCAAAGCAGCTTCCACAGGACACGG
AACCTGAAATTTCTTGCAAATGACCACAATCAGAAAGAACACCATACACAACNANGAAAGGCNACTG
GNATATCCCAAATATCCTAAATTTCTAAACAGCGACAANGGAAGAATGACNNCCNNTGANNNCNNCA
GAANNAANTAGTTCCCGNTCANANACCACAATCCANTTTNATNNNANNNNNNNAANGNCTNNNCNNN
NNNNNTNNNNTTTNNNTANNANAGNANCTGNNNTANCTNNNNNNCTGCNTNNNNNNNCNNANNCNGC
ANNNTTNNNTANNNANNNNNNNNNNNNNNNNNNNNNNNNNNNAANNNNNCTNNNNNNNNNNNNNNNN
NNNNNNNNNNNNNNNNNNNNNNNNNNNNNNNN

## NCBI BLAST result:

Range 2: 46721345 to 46721491GenBankGraphics Next Match Previous Match First Match

Alignment statistics for match #2

| Score | Expect | Identities | Gaps | Strand | Frame |
|---|---|---|---|---|---|
| 272 bits(147) | 7e-70() | 147/147(100%) | 0/147(0%) | Plus/Plus | |

Features:

sodium-coupled neutral amino acid transporter 2

```
Query 277       ACCAATAAAACCAAAGATATCCCTAATAGTTGGGACAAAGATGACAAGTAAATTGGTAAA 336
                ||||||||||||||||||||||||||||||||||||||||||||||||||||||||||||
Sbjct 4672134   ACCAATAAAACCAAAGATATCCCTAATAGTTGGGACAAAGATGACAAGTAAATTGGTAAA 46721404

Query 337        TGCCAAGATAGACACTGTAATGAGACTATGACGCCACCAACTGAAATCTTTTGATGCACA 396
                 ||||||||||||||||||||||||||||||||||||||||||||||||||||||||||||
Sbjct 46721405   TGCCAAGATAGACACTGTAATGAGACTATGACGCCACCAACTGAAATCTTTTGATGCACA 46721464

Query 397        CAACAAGTGAGTTACAGAACTCCGGAT 423
                 |||||||||||||||||||||||||||
Sbjct 46721465   CAACAAGTGAGTTACAGAACTCCGGAT 46721491
```

## C.3. SNAT2-HisFLAG (F)

PNACL sequencing result:

NNNNNNNNNNNNNNNNNNNNNNNNCGANTGGGACGATTCAGTATTTCCCCGGATGAAGACAGCAGC
AGCTACAGTTCCAACAGCGACTTCAACTACTCCTACCCCACCAAGCAAGCTGCTCTGAAAAGCCATT
ATGCAGATGTAGATCCTGAAAACCAGAACTTTTTACTTGAATCGAATTTGGGGAAGAAGAAGTATGA
AACAGAATTTCATCCAGGTACTACTTCCTTTGGAATGTCAGTATTTAATCTGAGCAATGCGATTGTG
GGCAGTGGAATCCTTGGGCTTTCTTATGCCATGGCTAATACTGGAATTGCTCTTTTTATAATTCTCT
TGACATTTGTGTCAATATTTTCCCTGTATTCTGTTCATCTCCTTTTGAAGACTGCCAATGAAGGAGG
GTCTTTATTATATGAACAATTGGGATATAAGGCATTTGGATTAGTTGGAAAGCTTGCAGCATCTGGA
TCAATTACAATGCAGAACATTGGAGCTATGTCAAGCTACCTCTTCATAGTGAAATATGAGTTGCCTT
TGGTGATCCAGGCATTAACGAACATTGAAGATAAAACTGGATTGTGGTATCTGAACGGGAACTATTT
GGTTCTGTTGGTGTCATTGGTGGTCATTCTTCCTTTGTCGCTGTTTAGAAATTTAGGATATTTGGGA
TATACCAGTGGCCTTTCCTTGTTGTGTATGGTGTTCTTTCTGATTGTGGTCATTTGCAAGAAATTTC
AGGTTCCGTGTCCTGTGGAAGCTGCTTTGATAATTAACGAAACAATAAACACCACCTTAACACAGCC
AACAGCTCTTGTACCTGCTTTGTCACATAACGTGACTGAAAATGACTCTTGCANANCTCACTATTTT
ATTTTCAACTCACAGACTGTCTATGCTGTGCCAATTCTGATCTTTTCATTTGTCTGTCATCCTGCTG
TTCTTCCCATCTATGAANAACTGAAANANCGCAGCCGTANAANAANGATGAATGNGNNCNANATTTC
ATTTTTTGCTATGTTTCTCATGNATCTGCTTGCCNCCNNNNTTGGATACCTANNTTTTNCNANNTGA
GTCNNANNGNTNCNNNNNTACNNNTCNNNNNTTGGNNACTGANNNNNCNTNTNCNCNTNNCGNN

Range 2: 46729367 to 46729482GenBankGraphics Next Match Previous Match First Match

Alignment statistics for match #2

| Score | Expect | Identities | Gaps | Strand | Frame |
|---|---|---|---|---|---|
| 215 bits(116) | 1e-52() | 116/116(100%) | 0/116(0%) | Plus/Minus | |

Features:

sodium-coupled neutral amino acid transporter 2

```
Query  212       CATCCAGGTACTACTTCCTTTGGAATGTCAGTATTTAATCTGAGCAATGCGATTGTGGGC  271
                  ||||||||||||||||||||||||||||||||||||||||||||||||||||||||||||
Sbjct  46729482  CATCCAGGTACTACTTCCTTTGGAATGTCAGTATTTAATCTGAGCAATGCGATTGTGGGC
46729423

Query  272       AGTGGAATCCTTGGGCTTTCTTATGCCATGGCTAATACTGGAATTGCTCTTTTTAT  327
                  |||||||||||||||||||||||||||||||||||||||||||||||||||||
Sbjct  46729422  AGTGGAATCCTTGGGCTTTCTTATGCCATGGCTAATACTGGAATTGCTCTTTTTAT  46729367
```

## C.4. SNAT2-HisFLAG (R)

### PNACL sequencing result

```
NNNNNNNNNNNNNNNNNNNNNNNNNNNNAATAGGGCCCTCTAGATGCATGCTCGATTAGTTTTCGG
AGCCTTTGTCATCGTCATCCTTATAATCTTTGTCATCGTCATCCTTATAGTCTTTGTCATCGTCATC
CTTATAATCGTGATGGTGATGCGCGCCCTGAAAATACAGGTTCTCGAGATGGCCACCTCCAGGTGCA
TTGTGTACCCAATCCAAAACAATCAAGGCCATGCTTCCGGTCATCACCAGTACACCACTTAACAGGA
AGAACAAAGCCCCAATCTTTTGTACAGATTTCATAGGTTCTTTCTTCACCAACTTGATATAGAAGGC
AGAAGGAAGAATAAAAATCAACATAGAAGCTGCAGATGCACCAATAAAACCAAAGATATCCCTAATA
GTTGGGACAAAGATGACAAGTAAATTGGTAAATGCCAAGATAGACACTGTAATGAGACTATGACGCC
ACCAACTGAAATCTTTTGATGCACACAACAAGTGAGTTACAGAACTCCGGATTGGGAAAATAACTAC
TGGTACTGTCAGGGTCACAGCCATTAACACAGCCAGACGGACAATGAGAAGAAGAATATCAGTTCCC
AAGATAGAAGAGTAGGTATGAAGCAATTCTGACTCAACATGTTCGTAAAATGTTAGGTATCCAAAGA
GGGCGGCAAGCAGATACATGAGAAACATAGCAAAAAATGAAATCTTGGACACATTCATCATTCTTCT
ACGGCTGCGGTCTTTCAGTTCTTCATAGATGGGAAGAACAGCAGGATGACAGACAAATGAAAAGATC
AGAATTGGCACAGCATAGACAGTCTGTGAGTTGAAAATAAAATAGTGAGGTCTGCAAGANTCATTTT
CAGTCACGTTATGTGACAAAGCNNNACAAGAGCTGTTGGCTGTGNTAAGNNGGNGTTTATTGTTTCG
TTAATTATCAAAGCAGCTTCCACAGGACACGGANNCTGAAATTTCTTGCAATGACCNCNATCAGAAA
NANNNNCNTACACNANANGNAANNNNNNCNGGNNTATCCNNANNNTNNNNANTTTCTAANCANCGAN
NANGNANNNNACCNCANNACNNNNNNNNNANTNNNNNCNNNNANNNNCNNANCNNTTNNNCNTNNNN
NTCNNNNNCNNNNNNNNNNNNNNNNNNNNNNTNNNNNNNNNNNNNCNNNNNNNNNNNNNNNNGNN
NNNNNNNNNNNANNNNNNNNNNNTNNNNNNNNNNNN
```

### NCBI BLAST result:

Range 1: 46721345 to 46721491GenBankGraphics Next Match Previous Match First Match

Alignment statistics for match #1

| Score | Expect | Identities | Gaps | Strand | Frame |
|---|---|---|---|---|---|
| 272 bits (147) | 7e-70() | 147/147(100%) | 0/147(0%) | Plus/Plus | |

Features:

sodium-coupled neutral amino acid transporter 2

```
Query  375       ACCAATAAAACCAAAGATATCCCTAATAGTTGGGACAAAGATGACAAGTAAATTGGTAAA  434
                 ||||||||||||||||||||||||||||||||||||||||||||||||||||||||||||
Sbjct  46721345  ACCAATAAAACCAAAGATATCCCTAATAGTTGGGACAAAGATGACAAGTAAATTGGTAAA  46721404

Query  435       TGCCAAGATAGACACTGTAATGAGACTATGACGCCACCAACTGAAATCTTTTGATGCACA  494
                 ||||||||||||||||||||||||||||||||||||||||||||||||||||||||||||
Sbjct  46721405  TGCCAAGATAGACACTGTAATGAGACTATGACGCCACCAACTGAAATCTTTTGATGCACA  46721464

Query  495       CAACAAGTGAGTTACAGAACTCCGGAT  521
                 |||||||||||||||||||||||||||
Sbjct  46721465  CAACAAGTGAGTTACAGAACTCCGGAT  46721491
```

## C.5. SNAT2-origional sequence

GTACAAAAAA GCAGGCTCCA CCATGAAGAA GGCCGAAATG GGACGATTCA GTATTTCCCC
GGATGAAGAC AGCAGCAGCT ACAGTTCCAA CAGCGACTTC AACTACTCCT ACCCCACCAA
GCAAGCTGCT CTGAAAAGCC ATTATGCAGA TGTAGATCCT GAAAACCAGA ACTTTTTACT
TGAATCGAAT TTGGGGAAGA AGAAGTATGA AACAGAATTT CATCCAGGTA CTACTTCCTT
TGGAATGTCA GTATTTAATC TGAGCAATGC GATTGTGGGC AGTGGAATCC TTGGGCTTTC
TTATGCCATG GCTAATACTG GAATTGCTCT TTTTATAATT CTCTTGACAT TTGTGTCAAT
ATTTTCCCTG TATTCTGTTC ATCTCCTTTT GAAGACTGCC AATGAAGGAG GGTCTTTATT
ATATGAACAA TTGGGATATA AGGCATTTGG ATTAGTTGGA AAGCTTGCAG CATCTGGATC
AATTACAATG CAGAACATTG GAGCTATGTC AAGCTACCTC TTCATAGTGA AATATGAGTT
GCCTTTGGTG ATCCAGGCAT TAACGAACAT TGAAGATAAA ACTGGATTGT GGTATCTGAA
CGGGAACTAT TTGGTTCTGT TGGTGTCATT GGTGGTCATT CTTCCTTTGT CGCTGTTTAG
AAATTTAGGA TATTTGGGAT ATACCAGTGG CCTTTCCTTG TTGTGTATGG TGTTCTTTCT
GATTGTGGTC ATTTGCAAGA AATTTCAGGT TCCGTGTCCT GTGGAAGCTG CTTTGATAAT
TAACGAAACA ATAAACACCA CCTTAACACA GCCAACAGCT CTTGTACCTG CTTTGTCACA
TAACGTGACT GAAAATGACT CTTGCAGACC TCACTATTTT ATTTTCAACT CACAGACTGT
CTATGCTGTG CCAATTCTGA TCTTTTCATT TGTCTGTCAT CCTGCTGTTC TTCCCATCTA
TGAAGAACTG AAAGACCGCA GCCGTAGAAG AATGATGAAT GTGTCCAAGA TTTCATTTTT
TGCTATGTTT CTCATGTATC TGCTTGCCGC CCTCTTTGGA TACCTAACAT TTTACGAACA
TGTTGAGTCA GAATTGCTTC ATACCTACTC TTCTATCTTG GGAACTGATA TTCTTCTTCT
CATTGTCCGT CTGGCTGTGT TAATGGCTGT GACCCTGACA GTACCAGTAG TTATTTTCCC
AATCCGGAGT TCTGTAACTC ACTTGTTGTG TGCATCAAAA GATTTCAGTT GGTGGCGTCA
TAGTCTCATT ACAGTGTCTA TCTTGGCATT TACCAATTTA CTTGTCATCT TTGTCCCAAC
TATTAGGGAT ATCTTTGGTT TTATTGGTGC ATCTGCAGCT TCTATGTTGA TTTTTATTCT
TCCTTCTGCC TTCTATATCA AGTTGGTGAA GAAAGAACCT ATGAAATCTG TACAAAAGAT
TGGGGCTTTG TTCTTCCTGT TAAGTGGTGT ACTGGTGATG ACCGGAAGCA TGGCCTTGAT
TGTTTTGGAT TGGGTACACA ATGCACCTGG AGGTGGCCAT TAGGACCCAG CTTTCTTGTAC

**C.6. Multiple alignment of SNAT2 DNA sequence (SNAT2-eGFP, SNAT2-origional and SNAT2-HisFLAG)**

```
SNAT2-eGFP          GCCGAAATGGGACGATTCAGTATTTCCCCGGATGAAGACAGCAGCAGCTACAGTTCCAAC
SNT2                GCCGAAATGGGACGATTCAGTATTTCCCCGGATGAAGACAGCAGCAGCTACAGTTCCAAC
SNAT2-HisFLAG       ---CGANTGGGACGATTCAGTATTTCCCCGGATGAAGACAGCAGCAGCTACAGTTCCAAC
                         * **************************************************

SNAT2-eGFP          AGCGACTTCAACTACTCCTACCCCACCAAGCAAGCTGCTCTGAAAAGCCATTATGCAGAT
SNT2                AGCGACTTCAACTACTCCTACCCCACCAAGCAAGCTGCTCTGAAAAGCCATTATGCAGAT
SNAT2-HisFLAG       AGCGACTTCAACTACTCCTACCCCACCAAGCAAGCTGCTCTGAAAAGCCATTATGCAGAT
                    ************************************************************

SNAT2-eGFP          GTAGATCCTGAAAACCAGAACTTTTTACTTGAATCGAATTTGGGGAAGAAGAAGTATGAA
SNT2                GTAGATCCTGAAAACCAGAACTTTTTACTTGAATCGAATTTGGGGAAGAAGAAGTATGAA
SNAT2-HisFLAG       GTAGATCCTGAAAACCAGAACTTTTTACTTGAATCGAATTTGGGGAAGAAGAAGTATGAA
                    ************************************************************

SNAT2-eGFP          ACAGAATTTCATCCAGGTACTACTTCCTTTGGAATGTCAGTATTTAATCTGAGCAATGCG
SNT2                ACAGAATTTCATCCAGGTACTACTTCCTTTGGAATGTCAGTATTTAATCTGAGCAATGCG
SNAT2-HisFLAG       ACAGAATTTCATCCAGGTACTACTTCCTTTGGAATGTCAGTATTTAATCTGAGCAATGCG
                    ************************************************************

SNAT2-eGFP          ATTGTGGGCAGTGGAATCCTTGGGCTTTCTTATGCCATGGCTAATACTGGAATTGCTCTT
SNT2                ATTGTGGGCAGTGGAATCCTTGGGCTTTCTTATGCCATGGCTAATACTGGAATTGCTCTT
SNAT2-HisFLAG       ATTGTGGGCAGTGGAATCCTTGGGCTTTCTTATGCCATGGCTAATACTGGAATTGCTCTT
                    ************************************************************

SNAT2-eGFP          TTTATAATTCTCTTGACATTTGTGTCAATATTTTCCCTGTATTCTGTTCATCTCCTTTTG
SNT2                TTTATAATTCTCTTGACATTTGTGTCAATATTTTCCCTGTATTCTGTTCATCTCCTTTTG
SNAT2-HisFLAG       TTTATAATTCTCTTGACATTTGTGTCAATATTTTCCCTGTATTCTGTTCATCTCCTTTTG
                    ************************************************************

SNAT2-eGFP          AAGACTGCCAATGAAGGAGGGTCTTTATTATATGAACAATTGGGATATAAGGCATTTGGA
SNT2                AAGACTGCCAATGAAGGAGGGTCTTTATTATATGAACAATTGGGATATAAGGCATTTGGA
SNAT2-HisFLAG       AAGACTGCCAATGAAGGAGGGTCTTTATTATATGAACAATTGGGATATAAGGCATTTGGA
                    ************************************************************

SNAT2-eGFP          TTAGTTGGAAAGCTTGCAGCATCTGGATCAATTACAATGCAGAACATTGGAGCTATGTCA
SNT2                TTAGTTGGAAAGCTTGCAGCATCTGGATCAATTACAATGCAGAACATTGGAGCTATGTCA
SNAT2-HisFLAG       TTAGTTGGAAAGCTTGCAGCATCTGGATCAATTACAATGCAGAACATTGGAGCTATGTCA
                    ************************************************************

SNAT2-eGFP          AGCTACCTCTTCATAGTGAAATATGAGTTGCCTTTGGTGATCCAGGCATTAACGAACATT
SNT2                AGCTACCTCTTCATAGTGAAATATGAGTTGCCTTTGGTGATCCAGGCATTAACGAACATT
SNAT2-HisFLAG       AGCTACCTCTTCATAGTGAAATATGAGTTGCCTTTGGTGATCCAGGCATTAACGAACATT
                    ************************************************************

SNAT2-eGFP          GAAGATAAAACTGGATTGTGGTATCTGAACGGGAACTATTTGGTTCTGTTGGTGTCATTG
SNT2                GAAGATAAAACTGGATTGTGGTATCTGAACGGGAACTATTTGGTTCTGTTGGTGTCATTG
SNAT2-HisFLAG       GAAGATAAAACTGGATTGTGGTATCTGAACGGGAACTATTTGGTTCTGTTGGTGTCATTG
                    ************************************************************

SNAT2-eGFP          GTGGTCATTCTTCCTTTGTCGCTGTTTAGAAATTTAGGATATTTGGGATATACCAGTGGC
SNT2                GTGGTCATTCTTCCTTTGTCGCTGTTTAGAAATTTAGGATATTTGGGATATACCAGTGGC
SNAT2-HisFLAG       GTGGTCATTCTTCCTTTGTCGCTGTTTAGAAATTTAGGATATTTGGGATATACCAGTGGC
                    ************************************************************

SNAT2-eGFP          CTTTCCTTGTTGTGTATGGTGTTCTTTCTGATTGTGGTCATTTGCAAGAAATTTCNNNTT
SNT2                CTTTCCTTGTTGTGTATGGTGTTCTTTCTGATTGTGGTCATTTGCAAGAAATTTCAGGTT
SNAT2-HisFLAG       CTTTCCTTGTTGTGTATGGTGTTCTTTCTGATTGTGGTCATTTGCAAGAAATTTCAGGTT
                    ********************************************************   **
```

URL:[http://www.ebi.ac.uk/Tools/services/web/toolresult.ebi?jobId=clustalo-I20170704-134854-0527-56992315-oy](http://www.ebi.ac.uk/Tools/services/web/toolresult.ebi?jobId=clustalo-I20170704-134854-0527-56992315-oy)

## Appendix D a full list of proteins detected in B1 band (Figure 4.12 )

| | | |
|---|---|---|
| **Protein hits:** | P35579 | Myosin-9 OS=Homo sapiens GN=MYH9 PE=1 SV=4 |
| | P09874 | Poly [ADP-ribose] polymerase 1 OS=Homo sapiens GN=PARP1 PE=1 SV=4 |
| | P04264 | Keratin, type II cytoskeletal 1 OS=Homo sapiens GN=KRT1 PE=1 SV=6 |
| | Q9Y5B9 | FACT complex subunit SPT16 OS=Homo sapiens GN=SUPT16H PE=1 SV=1 |
| | P35908 | Keratin, type II cytoskeletal 2 epidermal OS=Homo sapiens GN=KRT2 PE=1 SV=2 |
| | P13645 | Keratin, type I cytoskeletal 10 OS=Homo sapiens GN=KRT10 PE=1 SV=6 |
| | P35527 | Keratin, type I cytoskeletal 9 OS=Homo sapiens GN=KRT9 PE=1 SV=3 |
| | Q08211 | ATP-dependent RNA helicase A OS=Homo sapiens GN=DHX9 PE=1 SV=4 |
| | P35580 | Myosin-10 OS=Homo sapiens GN=MYH10 PE=1 SV=3 |
| | P48668 | Keratin, type II cytoskeletal 6C OS=Homo sapiens GN=KRT6C PE=1 SV=3 |
| | P02538 | Keratin, type II cytoskeletal 6A OS=Homo sapiens GN=KRT6A PE=1 SV=3 |
| | P04259 | Keratin, type II cytoskeletal 6B OS=Homo sapiens GN=KRT6B PE=1 SV=5 |
| | Q00839 | Heterogeneous nuclear ribonucleoprotein U OS=Homo sapiens GN=HNRNPU PE=1 SV=6 |
| | O60264 | SWI/SNF-related matrix-associated actin-dependent regulator of chromatin subfamily A member 5 OS=Homo sapiens GN=SMARCA5 PE=1 SV=1 |
| | Q08945 | FACT complex subunit SSRP1 OS=Homo sapiens GN=SSRP1 PE=1 SV=1 |
| | P23246 | Splicing factor, proline- and glutamine-rich OS=Homo sapiens GN=SFPQ PE=1 SV=2 |
| | P13647 | Keratin, type II cytoskeletal 5 OS=Homo sapiens GN=KRT5 PE=1 SV=3 |
| | P08779 | Keratin, type I cytoskeletal 16 OS=Homo sapiens GN=KRT16 PE=1 SV=4 |
| | P02533 | Keratin, type I cytoskeletal 14 OS=Homo sapiens GN=KRT14 PE=1 SV=4 |
| | B7ZLQ5 | Probable global transcription activator SNF2L1 OS=Homo sapiens GN=SMARCA1 PE=1 SV=1 |
| | P12035 | Keratin, type II cytoskeletal 3 OS=Homo sapiens GN=KRT3 PE=1 SV=3 |
| | O95239 | Chromosome-associated kinesin KIF4A OS=Homo sapiens GN=KIF4A PE=1 SV=3 |
| | A0A0R4J2E8 | Matrin-3 OS=Homo sapiens GN=MATR3 PE=1 SV=1 |
| | Q01546 | Keratin, type II cytoskeletal 2 oral OS=Homo sapiens GN=KRT76 PE=1 SV=2 |
| | Q14008 | Cytoskeleton-associated protein 5 OS=Homo sapiens GN=CKAP5 PE=1 SV=3 |
| | P05787 | Keratin, type II cytoskeletal 8 OS=Homo sapiens GN=KRT8 PE=1 SV=7 |
| | J3QS39 | Polyubiquitin-B (Fragment) OS=Homo sapiens GN=UBB PE=1 SV=1 |

| | |
|---|---|
| P11388 | DNA topoisomerase 2-alpha OS=Homo sapiens GN=TOP2A PE=1 SV=3 |
| O43707 | Alpha-actinin-4 OS=Homo sapiens GN=ACTN4 PE=1 SV=2 |
| P07900 | Heat shock protein HSP 90-alpha OS=Homo sapiens GN=HSP90AA1 PE=1 SV=5 |
| Q12906 | Interleukin enhancer-binding factor 3 OS=Homo sapiens GN=ILF3 PE=1 SV=3 |
| P35749 | Myosin-11 OS=Homo sapiens GN=MYH11 PE=1 SV=3 |
| P13639 | Elongation factor 2 OS=Homo sapiens GN=EEF2 PE=1 SV=4 |
| P08238 | Heat shock protein HSP 90-beta OS=Homo sapiens GN=HSP90AB1 PE=1 SV=4 |
| P19012 | Keratin, type I cytoskeletal 15 OS=Homo sapiens GN=KRT15 PE=1 SV=3 |
| K7ERE3 | Keratin, type I cytoskeletal 13 OS=Homo sapiens GN=KRT13 PE=1 SV=1 |
| P43246 | DNA mismatch repair protein Msh2 OS=Homo sapiens GN=MSH2 PE=1 SV=1 |
| Q5XKE5 | Keratin, type II cytoskeletal 79 OS=Homo sapiens GN=KRT79 PE=1 SV=2 |
| Q13111 | Chromatin assembly factor 1 subunit A OS=Homo sapiens GN=CHAF1A PE=1 SV=2 |
| P08729 | Keratin, type II cytoskeletal 7 OS=Homo sapiens GN=KRT7 PE=1 SV=5 |
| P19013 | Keratin, type II cytoskeletal 4 OS=Homo sapiens GN=KRT4 PE=1 SV=4 |
| G8JLG1 | Structural maintenance of chromosomes protein OS=Homo sapiens GN=SMC1A PE=1 SV=2 |
| P14625 | Endoplasmin OS=Homo sapiens GN=HSP90B1 PE=1 SV=1 |
| Q7Z406 | Myosin-14 OS=Homo sapiens GN=MYH14 PE=1 SV=2 |
| A0A087WTW0 | E3 ubiquitin-protein ligase UHRF1 OS=Homo sapiens GN=UHRF1 PE=1 SV=1 |
| P22629 | Streptavidin OS=Streptomyces avidinii PE=1 SV=1 |
| P19338 | Nucleolin OS=Homo sapiens GN=NCL PE=1 SV=3 |
| Q96QD8 | Sodium-coupled neutral amino acid transporter 2 OS=Homo sapiens GN=SLC38A2 PE=1 SV=2 |
| A0A087WVQ6 | Clathrin heavy chain OS=Homo sapiens GN=CLTC PE=1 SV=1 |
| Q04695 | Keratin, type I cytoskeletal 17 OS=Homo sapiens GN=KRT17 PE=1 SV=2 |
| A0A0C4DGB6 | Serum albumin OS=Homo sapiens GN=ALB PE=1 SV=1 |
| Q15424 | Scaffold attachment factor B1 OS=Homo sapiens GN=SAFB PE=1 SV=4 |
| P14136 | Glial fibrillary acidic protein OS=Homo sapiens GN=GFAP PE=1 SV=1 |
| Q9UQE7 | Structural maintenance of chromosomes protein 3 OS=Homo sapiens GN=SMC3 PE=1 SV=2 |
| Q14151 | Scaffold attachment factor B2 OS=Homo sapiens GN=SAFB2 PE=1 SV=1 |
| O75643 | U5 small nuclear ribonucleoprotein 200 kDa helicase OS=Homo sapiens GN=SNRNP200 PE=1 SV=2 |
| I3VM54 | Lysine-specific demethylase 2A OS=Homo sapiens GN=KDM2A PE=1 SV=1 |
| P11387 | DNA topoisomerase 1 OS=Homo sapiens GN=TOP1 PE=1 SV=2 |
| Q15393 | Splicing factor 3B subunit 3 OS=Homo sapiens GN=SF3B3 PE=1 SV=4 |
| P22314 | Ubiquitin-like modifier-activating enzyme 1 OS=Homo sapiens GN=UBA1 PE=1 SV=3 |
| P05023 | Sodium/potassium-transporting ATPase subunit alpha-1 OS=Homo sapiens GN=ATP1A1 PE=1 SV=1 |

P49916 DNA ligase 3 OS=Homo sapiens GN=LIG3 PE=1 SV=2
Q14444 Caprin-1 OS=Homo sapiens GN=CAPRIN1 PE=1 SV=2
O43143 Pre-mRNA-splicing factor ATP-dependent RNA helicase DHX15 OS=Homo sapiens GN=DHX15 PE=1 SV=2
A0A087WZZ5 Splicing factor 3B subunit 2 OS=Homo sapiens GN=SF3B2 PE=1 SV=1
Q9Y2W1 Thyroid hormone receptor-associated protein 3 OS=Homo sapiens GN=THRAP3 PE=1 SV=2
P13010 X-ray repair cross-complementing protein 5 OS=Homo sapiens GN=XRCC5 PE=1 SV=3
Q9NR30 Nucleolar RNA helicase 2 OS=Homo sapiens GN=DDX21 PE=1 SV=5
Q16531 DNA damage-binding protein 1 OS=Homo sapiens GN=DDB1 PE=1 SV=1
Q14697 Neutral alpha-glucosidase AB OS=Homo sapiens GN=GANAB PE=1 SV=3
P46100 Transcriptional regulator ATRX OS=Homo sapiens GN=ATRX PE=1 SV=5
P53621 Coatomer subunit alpha OS=Homo sapiens GN=COPA PE=1 SV=2
P20585 DNA mismatch repair protein Msh3 OS=Homo sapiens GN=MSH3 PE=1 SV=4
Q1KMD3 Heterogeneous nuclear ribonucleoprotein U-like protein 2 OS=Homo sapiens GN=HNRNPUL2 PE=1 SV=1
A0A087X2G1 ATP-dependent RNA helicase DDX1 OS=Homo sapiens GN=DDX1 PE=1 SV=1
P27824 Calnexin OS=Homo sapiens GN=CANX PE=1 SV=2
Q7Z794 Keratin, type II cytoskeletal 1b OS=Homo sapiens GN=KRT77 PE=2 SV=3
Q86Y46 Keratin, type II cytoskeletal 73 OS=Homo sapiens GN=KRT73 PE=1 SV=1
P55072 Transitional endoplasmic reticulum ATPase OS=Homo sapiens GN=VCP PE=1 SV=4
Q7KZF4 Staphylococcal nuclease domain-containing protein 1 OS=Homo sapiens GN=SND1 PE=1 SV=1
Q14152 Eukaryotic translation initiation factor 3 subunit A OS=Homo sapiens GN=EIF3A PE=1 SV=1
P26358 DNA (cytosine-5)-methyltransferase 1 OS=Homo sapiens GN=DNMT1 PE=1 SV=2
A0A0C4DG88 POU domain protein (Fragment) OS=Homo sapiens GN=POU2F1 PE=1 SV=1
Q92878 DNA repair protein RAD50 OS=Homo sapiens GN=RAD50 PE=1 SV=1
Q14974 Importin subunit beta-1 OS=Homo sapiens GN=KPNB1 PE=1 SV=2
A0A087WWJ1 DNA mismatch repair protein Msh6 OS=Homo sapiens GN=MSH6 PE=1 SV=1
A0A0A0MT49 Transcription activator BRG1 OS=Homo sapiens GN=SMARCA4 PE=1 SV=1
Q02880 DNA topoisomerase 2-beta OS=Homo sapiens GN=TOP2B PE=1 SV=3
A0A024RCR6 HLA-B associated transcript 3, isoform CRA_a OS=Homo sapiens GN=BAT3 PE=1 SV=1
A0A075B6Z2 Protein TRAJ56 (Fragment) OS=Homo sapiens GN=TRAJ56 PE=4 SV=1
F5H2F4 C-1-tetrahydrofolate synthase, cytoplasmic OS=Homo sapiens GN=MTHFD1 PE=1 SV=1
Q15029 116 kDa U5 small nuclear ribonucleoprotein component OS=Homo sapiens GN=EFTUD2 PE=1 SV=1
P81605 Dermcidin OS=Homo sapiens GN=DCD PE=1 SV=2

| | |
|---|---|
| S4R3H4 | Apoptotic chromatin condensation inducer in the nucleus OS=Homo sapiens GN=ACIN1 PE=1 SV=1 |
| Q13263 | Transcription intermediary factor 1-beta OS=Homo sapiens GN=TRIM28 PE=1 SV=5 |
| B5ME19 | Eukaryotic translation initiation factor 3 subunit C-like protein OS=Homo sapiens GN=EIF3CL PE=3 SV=1 |
| E9PLK3 | Puromycin-sensitive aminopeptidase OS=Homo sapiens GN=NPEPPS PE=1 SV=1 |
| E9PK91 | Bcl-2-associated transcription factor 1 OS=Homo sapiens GN=BCLAF1 PE=1 SV=1 |
| Q9UHB6 | LIM domain and actin-binding protein 1 OS=Homo sapiens GN=LIMA1 PE=1 SV=1 |
| O75533 | Splicing factor 3B subunit 1 OS=Homo sapiens GN=SF3B1 PE=1 SV=3 |
| F8VXC8 | SWI/SNF complex subunit SMARCC2 OS=Homo sapiens GN=SMARCC2 PE=1 SV=1 |
| Q9NSB2 | Keratin, type II cuticular Hb4 OS=Homo sapiens GN=KRT84 PE=2 SV=2 |
| A0A0U1RRH6 | PHD finger protein 14 OS=Homo sapiens GN=PHF14 PE=1 SV=1 |
| C9JZG1 | Eukaryotic translation initiation factor 3 subunit B (Fragment) OS=Homo sapiens GN=EIF3B PE=1 SV=1 |
| K7EJ74 | 116 kDa U5 small nuclear ribonucleoprotein component (Fragment) OS=Homo sapiens GN=EFTUD2 PE=1 SV=1 |
| H3BMZ1 | Very-long-chain (3R)-3-hydroxyacyl-CoA dehydratase 3 (Fragment) OS=Homo sapiens GN=HACD3 PE=1 SV=1 |
| U3KQ96 | POU domain, class 2, transcription factor 2 (Fragment) OS=Homo sapiens GN=POU2F2 PE=1 SV=1 |
| A0A096LNL9 | Transcriptional regulator ATRX (Fragment) OS=Homo sapiens GN=ATRX PE=1 SV=1 |
| P35609 | Alpha-actinin-2 OS=Homo sapiens GN=ACTN2 PE=1 SV=1 |
| Q14CN4 | Keratin, type II cytoskeletal 72 OS=Homo sapiens GN=KRT72 PE=1 SV=2 |
| Q15323 | Keratin, type I cuticular Ha1 OS=Homo sapiens GN=KRT31 PE=1 SV=3 |
| F8VZY9 | Keratin, type I cytoskeletal 18 OS=Homo sapiens GN=KRT18 PE=1 SV=1 |
| Q12931 | Heat shock protein 75 kDa, mitochondrial OS=Homo sapiens GN=TRAP1 PE=1 SV=3 |
| E9PDF6 | Unconventional myosin-Ib OS=Homo sapiens GN=MYO1B PE=1 SV=1 |
| Q99459 | Cell division cycle 5-like protein OS=Homo sapiens GN=CDC5L PE=1 SV=2 |
| Q86YZ3 | Hornerin OS=Homo sapiens GN=HRNR PE=1 SV=2 |
| A5A3E0 | POTE ankyrin domain family member F OS=Homo sapiens GN=POTEF PE=1 SV=2 |
| H3BSK9 | Ataxin-2-like protein (Fragment) OS=Homo sapiens GN=ATXN2L PE=1 SV=1 |
| Q9H307 | Pinin OS=Homo sapiens GN=PNN PE=1 SV=4 |
| A0A087X0K9 | Tight junction protein ZO-1 OS=Homo sapiens GN=TJP1 PE=1 SV=1 |
| B1AHB1 | DNA helicase OS=Homo sapiens GN=MCM5 PE=1 SV=1 |
| Q9H0D6 | 5'-3' exoribonuclease 2 OS=Homo sapiens GN=XRN2 PE=1 SV=1 |
| A0A075B729 | Ribosome biogenesis protein BOP1 (Fragment) OS=Homo sapiens GN=BOP1 PE=1 SV=1 |
| A0A087WTA8 | Collagen alpha-2(I) chain OS=Homo sapiens GN=COL1A2 PE=1 SV=1 |
| P55060 | Exportin-2 OS=Homo sapiens GN=CSE1L PE=1 SV=3 |
| P18206 | Vinculin OS=Homo sapiens GN=VCL PE=1 SV=4 |

A0A0A0MRA5 Heterogeneous nuclear ribonucleoprotein U-like protein 1 OS=Homo sapiens GN=HNRNPUL1 PE=1 SV=1
P05109 Protein S100-A8 OS=Homo sapiens GN=S100A8 PE=1 SV=1
D6RIA2 Matrin-3 (Fragment) OS=Homo sapiens GN=MATR3 PE=1 SV=1
Q13200 26S proteasome non-ATPase regulatory subunit 2 OS=Homo sapiens GN=PSMD2 PE=1 SV=3
Q58FG1 Putative heat shock protein HSP 90-alpha A4 OS=Homo sapiens GN=HSP90AA4P PE=5 SV=1
B4DEB1 Histone H3 OS=Homo sapiens GN=H3F3A PE=1 SV=1
O14776 Transcription elongation regulator 1 OS=Homo sapiens GN=TCERG1 PE=1 SV=2
Q9NQH7 Probable Xaa-Pro aminopeptidase 3 OS=Homo sapiens GN=XPNPEP3 PE=1 SV=1
Q5QJE6 Deoxynucleotidyltransferase terminal-interacting protein 2 OS=Homo sapiens GN=DNTTIP2 PE=1 SV=2
Q96SI9 Spermatid perinuclear RNA-binding protein OS=Homo sapiens GN=STRBP PE=1 SV=1
P55265 Double-stranded RNA-specific adenosine deaminase OS=Homo sapiens GN=ADAR PE=1 SV=4
A0A0C4DG79 Constitutive coactivator of PPAR-gamma-like protein 1 (Fragment) OS=Homo sapiens GN=FAM120A PE=1 SV=1
A0A0U1RQZ9 Probable global transcription activator SNF2L2 OS=Homo sapiens GN=SMARCA2 PE=1 SV=1
Q14980 Nuclear mitotic apparatus protein 1 OS=Homo sapiens GN=NUMA1 PE=1 SV=2
Q9H2P0 Activity-dependent neuroprotector homeobox protein OS=Homo sapiens GN=ADNP PE=1 SV=1
P02452 Collagen alpha-1(I) chain OS=Homo sapiens GN=COL1A1 PE=1 SV=5
A0A0A0MSX9 Isoleucine--tRNA ligase, cytoplasmic OS=Homo sapiens GN=IARS PE=1 SV=1
P12036 Neurofilament heavy polypeptide OS=Homo sapiens GN=NEFH PE=1 SV=4
P16403 Histone H1.2 OS=Homo sapiens GN=HIST1H1C PE=1 SV=2
P16402 Histone H1.3 OS=Homo sapiens GN=HIST1H1D PE=1 SV=2
Q9NZB2 Constitutive coactivator of PPAR-gamma-like protein 1 OS=Homo sapiens GN=FAM120A PE=1 SV=2
Q15059 Bromodomain-containing protein 3 OS=Homo sapiens GN=BRD3 PE=1 SV=1
O60885 Bromodomain-containing protein 4 OS=Homo sapiens GN=BRD4 PE=1 SV=2
I3L0J9 Pre-mRNA-processing-splicing factor 8 (Fragment) OS=Homo sapiens GN=PRPF8 PE=1 SV=8
H0YGW7 ATP-binding cassette sub-family F member 1 (Fragment) OS=Homo sapiens GN=ABCF1 PE=1 SV=1
Q96JG8 Melanoma-associated antigen D4 OS=Homo sapiens GN=MAGED4 PE=1 SV=3
B9ZVT1 RNA-binding protein 12B OS=Homo sapiens GN=RBM12B PE=1 SV=2
C9JY79 Non-erythrocytic beta-spectrin 4 OS=Homo sapiens GN=SPTBN4 PE=1 SV=2
P15924 Desmoplakin OS=Homo sapiens GN=DSP PE=1 SV=3
Q96T23 Remodeling and spacing factor 1 OS=Homo sapiens GN=RSF1 PE=1 SV=2
A0A0A0MRM8 Unconventional myosin-VI OS=Homo sapiens GN=MYO6 PE=1 SV=1
Q96L93 Kinesin-like protein KIF16B OS=Homo sapiens GN=KIF16B PE=1 SV=2

| | |
|---|---|
| A0A087X011 | Kinesin-like protein OS=Homo sapiens GN=KIF3A PE=1 SV=1 |
| A0A087WV73 | Probable 28S rRNA (cytosine(4447)-C(5))-methyltransferase OS=Homo sapiens GN=NOP2 PE=1 SV=1 |
| O75691 | Small subunit processome component 20 homolog OS=Homo sapiens GN=UTP20 PE=1 SV=3 |
| O95294 | RasGAP-activating-like protein 1 OS=Homo sapiens GN=RASAL1 PE=1 SV=3 |
| Q8N3U4 | Cohesin subunit SA-2 OS=Homo sapiens GN=STAG2 PE=1 SV=3 |
| Q8WVM7 | Cohesin subunit SA-1 OS=Homo sapiens GN=STAG1 PE=1 SV=3 |
| Q18PE1 | Protein Dok-7 OS=Homo sapiens GN=DOK7 PE=1 SV=1 |
| Q9BTV7 | CDK5 and ABL1 enzyme substrate 2 OS=Homo sapiens GN=CABLES2 PE=1 SV=3 |
| A0A0A0MSA0 | Laminin subunit alpha-3 OS=Homo sapiens GN=LAMA3 PE=1 SV=1 |
| H0YJ79 | Echinoderm microtubule-associated protein-like 5 (Fragment) OS=Homo sapiens GN=EML5 PE=4 SV=1 |
| A0A087WTS8 | Heat shock 70 kDa protein 4 OS=Homo sapiens GN=HSPA4 PE=1 SV=1 |
| Q12788 | Transducin beta-like protein 3 OS=Homo sapiens GN=TBL3 PE=1 SV=2 |
| Q8NB90 | Spermatogenesis-associated protein 5 OS=Homo sapiens GN=SPATA5 PE=1 SV=3 |
| I1E4Y6 | PERQ amino acid-rich with GYF domain-containing protein 2 OS=Homo sapiens GN=GIGYF2 PE=1 SV=1 |
| H7C5W9 | Sarcoplasmic/endoplasmic reticulum calcium ATPase 2 (Fragment) OS=Homo sapiens GN=ATP2A2 PE=1 SV=1 |
| Q9HAU5 | Regulator of nonsense transcripts 2 OS=Homo sapiens GN=UPF2 PE=1 SV=1 |
| Q5T085 | Alpha-amylase 1 (Fragment) OS=Homo sapiens GN=AMY1B PE=1 SV=1 |
| B1AN99 | Trypsin-3 (Fragment) OS=Homo sapiens GN=PRSS3 PE=1 SV=7 |
| O60882 | Matrix metalloproteinase-20 OS=Homo sapiens GN=MMP20 PE=1 SV=3 |
| A0A0G2JIW1 | Heat shock 70 kDa protein 1B OS=Homo sapiens GN=HSPA1B PE=1 SV=1 |
| P42704 | Leucine-rich PPR motif-containing protein, mitochondrial OS=Homo sapiens GN=LRPPRC PE=1 SV=3 |
| A0A087WXG2 | Uncharacterized aarF domain-containing protein kinase 2 OS=Homo sapiens GN=ADCK2 PE=1 SV=1 |
| O95263 | High affinity cAMP-specific and IBMX-insensitive 3',5'-cyclic phosphodiesterase 8B OS=Homo sapiens GN=PDE8B PE=1 SV=2 |
| I3L104 | Unconventional prefoldin RPB5 interactor 1 (Fragment) OS=Homo sapiens GN=URI1 PE=1 SV=1 |
| A0A087WW66 | 26S proteasome non-ATPase regulatory subunit 1 OS=Homo sapiens GN=PSMD1 PE=1 SV=1 |
| A0A0A0MSJ0 | ATP-dependent RNA helicase DDX42 OS=Homo sapiens GN=DDX42 PE=1 SV=1 |
| Q5VYL4 | Abnormal spindle-like microcephaly-associated protein OS=Homo sapiens GN=ASPM PE=1 SV=1 |
| H0Y3P2 | Eukaryotic translation initiation factor 4 gamma 2 OS=Homo sapiens GN=EIF4G2 PE=1 SV=1 |
| Q8NFC6 | Biorientation of chromosomes in cell division protein 1-like 1 OS=Homo sapiens GN=BOD1L1 PE=1 SV=2 |
| Q8TDI0 | Chromodomain-helicase-DNA-binding protein 5 OS=Homo sapiens GN=CHD5 PE=1 SV=1 |

| | |
|---|---|
| Q12873 | Chromodomain-helicase-DNA-binding protein 3 OS=Homo sapiens GN=CHD3 PE=1 SV=3 |
| A0A0C4DGG9 | Chromodomain-helicase-DNA-binding protein 4 OS=Homo sapiens GN=CHD4 PE=1 SV=1 |
| H0YA27 | Cyclin-I (Fragment) OS=Homo sapiens GN=CCNI PE=1 SV=1 |
| P49756 | RNA-binding protein 25 OS=Homo sapiens GN=RBM25 PE=1 SV=3 |
| Q86UP2 | Kinectin OS=Homo sapiens GN=KTN1 PE=1 SV=1 |
| O60216 | Double-strand-break repair protein rad21 homolog OS=Homo sapiens GN=RAD21 PE=1 SV=2 |
| Q15459 | Splicing factor 3A subunit 1 OS=Homo sapiens GN=SF3A1 PE=1 SV=1 |
| A0A087WY55 | Chromosome 6 open reading frame 55, isoform CRA_b OS=Homo sapiens GN=VTA1 PE=1 SV=1 |
| Q4G0J3 | La-related protein 7 OS=Homo sapiens GN=LARP7 PE=1 SV=1 |
| P78386 | Keratin, type II cuticular Hb5 OS=Homo sapiens GN=KRT85 PE=1 SV=1 |
| Q8N1N4 | Keratin, type II cytoskeletal 78 OS=Homo sapiens GN=KRT78 PE=2 SV=2 |
| A8MVM7 | Putative uncharacterized protein ENSP00000382790 OS=Homo sapiens PE=5 SV=3 |
| Q86VN1 | Vacuolar protein-sorting-associated protein 36 OS=Homo sapiens GN=VPS36 PE=1 SV=1 |
| Q5QP74 | |
| A0A0C4DGH5 | Cullin-associated NEDD8-dissociated protein 1 (Fragment) OS=Homo sapiens GN=CAND1 PE=1 SV=1 |
| H0Y8D9 | U2 snRNP-associated SURP motif-containing protein (Fragment) OS=Homo sapiens GN=U2SURP PE=1 SV=1 |
| E7ET15 | U2 snRNP-associated SURP motif-containing protein OS=Homo sapiens GN=U2SURP PE=1 SV=1 |
| O15226 | NF-kappa-B-repressing factor OS=Homo sapiens GN=NKRF PE=1 SV=2 |
| Q14D04 | Ventricular zone-expressed PH domain-containing protein homolog 1 OS=Homo sapiens GN=VEPH1 PE=2 SV=1 |
| Q6PKX4 | Docking protein 6 OS=Homo sapiens GN=DOK6 PE=1 SV=1 |
| E7ERT8 | Homeobox protein Hox-A1 OS=Homo sapiens GN=HOXA1 PE=4 SV=1 |
| K7ES05 | KN motif and ankyrin repeat domain-containing protein 2 (Fragment) OS=Homo sapiens GN=KANK2 PE=1 SV=7 |

# References


Aas, V., Bakke, S., Feng, Y., Kase, E., Jensen, J., Bajpeyi, S., Thoresen, G. & Rustan, A. 2013, "Are cultured human myotubes far from home?", *Cell and Tissue Research,* vol. 354, no. 3, pp. 671-682.

Almon, R.R., Dubois, D.C., Jin, J.Y. & Jusko, W.J. 2005, "Temporal profiling of the transcriptional basis for the development of corticosteroid-induced insulin resistance in rat muscle", *The Journal of endocrinology,* vol. 184, no. 1, pp. 219-232.

Argiles, J.M., Lopez-Soriano, F.J. & Busquets, S. 2009, "Therapeutic potential of interleukin-15: a myokine involved in muscle wasting and adiposity", *Drug discovery today,* vol. 14, no. 3-4, pp. 208-213.

Baird, F.E., Kevin J. Bett, Catherine MacLean, Andrew R. Tee, Harinder S. Hundal & Peter M. Taylor 2009, "Tertiary active transport of amino acids reconstituted by coexpression of System A and L transporters in Xenopus oocytes", *American Journal of Physiology - Endocrinology And Metabolism,* vol. 297, no. 3, pp. 822-829.

Baird, F.E., Pinilla-Tenas, J.J., Ogilvie, W.L., Ganapathy, V., Hundal, H.S. & Taylor, P.M. 2006, "Evidence for allosteric regulation of pH-sensitive System A (SNAT2) and System N (SNAT5) amino acid transporter activity involving a conserved histidine residue", *The Biochemical journal,* vol. 397, no. 2, pp. 369-375.

Bell, S. & Terentjev, E.M. 2017, "Focal Adhesion Kinase: The Reversible Molecular Mechanosensor", *Biophysical Journal,* vol. 112, no. 11, pp. 2439.

Beltran, V.D. 2017, *System L amino acid transporters & their relation to cellular energy status & glucose*, Leicester.

Bergstrom, J., Alvestrand, A. & Furst, P. 1990, "Plasma and muscle free amino acids in maintenance hemodialysis patients without protein malnutrition", *Kidney international,* vol. 38, no. 1, pp. 108-114.

Breen, L. & Phillips, S.M. 2011, "Skeletal muscle protein metabolism in the elderly: Interventions to counteract the 'anabolic resistance' of ageing", Nutrition & metabolism, vol. 8, no. 1, pp. 68.

Burd, N.A., Gorissen, S.H. & van Loon, L J C 2013, "Anabolic resistance of muscle protein synthesis with aging", Exercise and Sport Sciences Reviews, vol. 41, no. 3, pp. 169-173.

Bevington, A., Brown, J., Butler, H., Govindji, S., M-Khalid, K., Sheridan, K. & Walls, J. 2002, "Impaired system A amino acid transport mimics the catabolic effects of acid in L6 cells", *European journal of clinical investigation,* vol. 32, no. 8, pp. 590-602.

Bevington, A., Brown, J., Pratt, A., Messer, J. & Walls, J. 1998, "Impaired glycolysis and protein catabolism induced by acid in L6 rat muscle cells", *European journal of clinical investigation,* vol. 28, no. 11, pp. 908-917.

Bevington, A., Brown, J. & Walls, J. 2001, "Leucine suppresses acid- induced protein wasting in L6 rat muscle cells", *European Journal of Clinical Investigation,* vol. 31, no. 6, pp. 497-503.

Bobrow, C.S. & Soothill, P.W. 1999, "Causes and consequences of fetal acidosis", *Archives of disease in childhood. Fetal and neonatal edition,* vol. 80, no. 3, pp. F249.

Brandt, C. & Pedersen, B.K. 2010, "The Role of Exercise-Induced Myokines in Muscle Homeostasis and the Defense against Chronic Diseases", *Journal of Biomedicine and Biotechnology,* vol. 2010, pp. 1-6.

Bröer, S. 2014, "The SLC38 family of sodium–amino acid co-transporters", *Pflügers Archiv - European Journal of Physiology,* vol. 466, no. 1, pp. 155-172.

Brooks, S.V. 2003, "Current topics for teaching skeletal muscle physiology", *Advances in Physiology Education,* vol. 27, no. 4, pp. 171-182.

Buehlmeier, J., Remer, T., Frings-Meuthen, P., Maser-Gluth, C. & Heer, M. 2016, "Glucocorticoid activity and metabolism with NaCl-induced low-grade metabolic acidosis and oral alkalization: results of two randomized controlled trials", *Endocrine,* vol. 52, no. 1, pp. 139-147.

Carrero, J.J., Johansen, K.L., Lindholm, B., Stenvinkel, P., Cuppari, L. & Avesani, C.M. 2016, "Screening for muscle wasting and dysfunction in patients with chronic kidney disease", *Kidney international,* vol. 90, no. 1, pp. 53-66.

Castillero, E., Alamdari, N., Lecker, S.H. & Hasselgren, P. 2013, "Suppression of atrogin-1 and MuRF1 prevents dexamethasone-induced atrophy of cultured myotubes", *Metabolism,* vol. 62, no. 10, pp. 1495-1502.

Cerioni, L., Palomba, L. & Cantoni, O. 2003, "The Raf/MEK inhibitor PD98059 enhances ERK1/2 phosphorylation mediated by peroxynitrite via enforced mitochondrial formation of reactive oxygen species", *FEBS Letters,* vol. 547, no. 1, pp. 92-96.

Chaudhry, F.A., Schmitz, D., Reimer, R.J., Larsson, P., Gray, A.T., Nicoll, R., Kavanaugh, M. & Edwards, R.H. 2002, "Glutamine uptake by neurons: interaction of protons with system a transporters", *The Journal of neuroscience : the official journal of the Society for Neuroscience,* vol. 22, no. 1, pp. 62.

Chalil, S., Pierre, N., Bakker, A.D., Manders, R.J., Pletsers, A., Francaux, M., Klein-Nulend, J., Jaspers, R.T. & Deldique, L. 2015, "Aging related ER stress is not responsible for anabolic resistance in mouse skeletal muscle", *Biochemical and Biophysical Research Communications,* vol. 468, no. 4, pp. 702-707.Chen, W. & Abramowitz, M.K. 2014, "Metabolic acidosis and the progression of chronic kidney disease", *BMC Nephrology,* vol. 15, no. 1, pp. 55.

Cheung, W.W., Paik, K.H. & Mak, R.H. 2010, "Inflammation and cachexia in chronic kidney disease", *Pediatric nephrology (Berlin, Germany),* vol. 25, no. 4, pp. 711-724.

Clapp, E.L. 2010, *The Effect of Therapeutic Exercise and Metabolic Acidosis on Skeletal Muscle Metabolism in Chronic Kidney Disease,* © Emma Louise Clapp.

Clapp, E.L. & Bevington, A. 2011, "Exercise-induced Biochemical Modifications in Muscle in Chronic Kidney Disease: Occult Acidosis as a Potential Factor Limiting the Anabolic Effect of Exercise", *Journal of Renal Nutrition,* vol. 21, no. 1, pp. 57-60.

Conigrave, A.D. & Hampson, D.R. 2010, "Broad-spectrum amino acid-sensing class C G-protein coupled receptors: Molecular mechanisms, physiological significance and options for drug development", *Pharmacology & therapeutics,* vol. 127, no. 3, pp. 252-260.

Costill, D.L., J. Daniels, W. Evans, W. Fink, G. Krahenbuhl & B. Saltin 1976, "Skeletal muscle enzymes and fiber composition in male and female track athletes", *Journal of Applied Physiology,* vol. 40, no. 2, pp. 149-154.

Costill, D., Fink, W., Flynn, M. & Kirwan, J. 1987, "Muscle Fiber Composition and Enzyme Activities in Elite Female Distance Runners", *Int J Sports Med,* vol. 8, no. S 2, pp. S106.

Damm, T.B. & Egli, M. 2014, "Calcium's Role in Mechanotransduction during Muscle Development", *Cellular Physiology and Biochemistry,* vol. 33, no. 2, pp. 249-272.

Dickinson, J. & Rasmussen, B. 2013, "Amino acid transporters in the regulation of human skeletal muscle protein metabolism", *Current Opinion in Clinical Nutrition and Metabolic Care,* vol. 16, no. 6, pp. 638-644.

Dong, L., Li, Z., Leffler, N.R., Asch, A.S., Chi, J. & Yang, L.V. 2013, "Acidosis activation of the proton-sensing GPR4 receptor stimulates vascular endothelial cell inflammatory responses revealed by transcriptome analysis", *PloS one,* vol. 8, no. 4, pp. e61991.

Drummond, M.J., Fry, C.S., Glynn, E.L., Dreyer, H.C., Dhanani, S., Timmerman, K.L., Volpi, E. & Rasmussen, B.B. 2009, "Rapamycin administration in humans blocks the contraction-induced increase in skeletal muscle protein synthesis", *The Journal of Physiology,* vol. 587, no. 7, pp. 1535-1546.

Elsner, P., Quistorff, B., Hermann, T.S., Dich, J. & Grunnet, N. 1998, "Regulation of glycogen accumulation in L6 myotubes cultured under optimized differentiation conditions", *The American Journal of Physiology,* vol. 275, no. 6 Pt 1, pp. 925.

Emeis, M., Josef Sonntag, Carsten Willam, Evelyn Strauss, Matthias M. Walka & Michael Obladen 1998, "Acidosis activates complement system in vitro", *Mediators of Inflammation,* vol. 7, no. 6, pp. 417-420.

Eunjung, K. 2009, "Mechanisms of amino acid sensing in mTOR signaling pathway", *Nutrition Research and Practice,* vol. 3, no. 1, pp. 64-71.

Evans, K., Nasim, Z., Brown, J., Butler, H., Kauser, S., Varoqui, H., Erickson, J.D., Herbert, T.P. & Bevington, A. 2007, "Acidosis-sensing glutamine pump SNAT2 determines amino acid levels and mammalian target of rapamycin signalling to protein synthesis in L6 muscle cells", *Journal of the American Society of Nephrology : JASN,* vol. 18, no. 5, pp. 1426-1436.

Evans, K., Nasim, Z., Brown, J., Clapp, E., Amin, A., Yang, B., Herbert, T.P. & Bevington, A. 2008, "Inhibition of SNAT2 by metabolic acidosis enhances proteolysis in skeletal muscle", *Journal of the American Society of Nephrology : JASN,* vol. 19, no. 11, pp. 2119-2129.

Evans, K.F. 2009, *The effects of acidosis, glutamine starvation and inhibition of the pH sensitive SNAT 2 amino acid transporter on protein metabolism in L6 muscle cells*, University of Leicester.

Foley, R., Parfrey, P. & Sarnak, M. 1998, "Clinical epidemiology of cardiovascular disease in chronic renal disease", *American Journal of Kidney Diseases,* vol. 32, no. 5, pp. S119.

Frontera, W.R. & Ochala, J. 2015, "Skeletal muscle: a brief review of structure and function", *Calcified tissue international,* vol. 96, no. 3, pp. 183-195.

Gaccioli, F., Huang, C.C., Wang, C., Bevilacqua, E., Franchi-Gazzola, R., Gazzola, G.C., Bussolati, O., Snider, M.D. & Hatzoglou, M. 2006, "Amino acid starvation induces the SNAT2 neutral amino acid transporter by a mechanism that involves eukaryotic initiation factor 2alpha phosphorylation and cap-independent translation", *The Journal of biological chemistry,* vol. 281, no. 26, pp. 17929-17940.

Galpin, A.J., Fry, A.C., Chiu, L.Z.F., Thomason, D.B. & Schilling, B.K. 2012, "High-power resistance exercise induces MAPK phosphorylation in weightlifting trained men", *Applied physiology, nutrition, and metabolism = Physiologie appliquée, nutrition et métabolisme,* vol. 37, no. 1, pp. 80.

Garibotto, G., Sofia, A., Saffioti, S., Bonanni, A., Mannucci, I. & Verzola, D. 2010, "Amino acid and protein metabolism in the human kidney and in patients with chronic kidney disease", *Clinical Nutrition,* vol. 29, no. 4, pp. 424 433.

Goberdhan, D.I., Wilson, C. & Harris, A. 2016, "Amino Acid Sensing by mTORC1: Intracellular Transporters Mark the Spot", *Cell Metabolism,* vol. 23, no. 4, pp. 580-589.

Golberg, N., Druzhevskaya, A., Rogozkin, V. & Ahmetov, I. 2014, "Role of mTOR in the regulation of skeletal muscle metabolism", *Human Physiology,* vol. 40, no. 5, pp. 580-588.

Gong, B., Radulovic, M., Figueiredo-Pereira, M.E. & Cardozo, C. 2016a, "The Ubiquitin-Proteasome System: Potential Therapeutic Targets for Alzheimer's Disease and Spinal Cord Injury", *Frontiers in molecular neuroscience,* vol. 9, pp. 4.

Gong, H., Liu, L., Ni, C., Zhang, Y., Su, W., Lian, Y., Peng, W., Zhang, J. & Jiang, C. 2016b, "Dexamethasone rapidly inhibits glucose uptake via non-genomic mechanisms in contracting myotubes", *Archives of biochemistry and biophysics,* vol. 603, pp. 102-109.

Goodman, C.A., Miu, M.H., Frey, J.W., Mabrey, D.M., Lincoln, H.C., Ge, Y., Chen, J. & Hornberger, T.A. 2010, "A phosphatidylinositol 3-kinase/protein kinase B-independent activation of mammalian target of rapamycin signaling is sufficient to induce skeletal muscle hypertrophy", *Molecular biology of the cell,* vol. 21, no. 18, pp. 3258-3268.

Greig, C.A. & Jones, D.A. 2010, "Muscle physiology", *Surgery (Oxford),* vol. 28, no. 2, pp. 55-59.

Grice & Nathan, J.A. 2016, *Reports from University of Cambridge Highlight Recent Findings in Ubiquitins (The recognition of ubiquitinated proteins by the proteasome)*, NewsRX LLC.

Guo, X., Greene, K., Akanda, N., Smith, A.S.T., Stancescu, M., Lambert, S., Vandenburgh, H. & Hickman, J.J. 2014, "In vitro differentiation of functional human skeletal myotubes in a defined system", *Biomater. Sci,* vol. 2, no. 1, pp. 131-138.

Gupta, A. & Gupta, Y. 2013, "Glucocorticoid-induced myopathy: Pathophysiology, diagnosis, and treatment", *Indian journal of endocrinology and metabolism,* vol. 17, no. 5, pp. 913-916.

Hägglund, M.G.A., Hellsten, S.V., Bagchi, S., Philippot, G., Löfqvist, E., Nilsson, V.C.O., Almkvist, I., Karlsson, E., Sreedharan, S., Tafreshiha, A. & Fredriksson, R. 2015, "Transport of L-glutamine, L-alanine, L-arginine and L-histidine by the neuron-specific Slc38a8 (SNAT8) in CNS", *Journal of molecular biology,* vol. 427, no. 6 Pt B, pp. 1495-1512.

Hall, D.T., Ma, J.F., Marco, S.D. & Gallouzi, I.E. 2011a, "Inducible nitric oxide synthase (iNOS) in muscle wasting syndrome, sarcopenia, and cachexia", *Aging,* vol. 3, no. 8, pp. 702-715.

Hall, M.N., Corbett, A.H. & Pavlath, G.K. 2011b, "Regulation of Nucleocytoplasmic Transport in Skeletal Muscle", *Current Topics in Developmental Biology,* vol. 96, pp. 273-302.

Hatanaka, T., Yasue Hatanaka & Mitsutoshi Setou 2006, "Regulation of Amino Acid Transporter ATA2 by Ubiquitin Ligase Nedd4-2", *Journal of Biological Chemistry,* vol. 281, no. 47, pp. 35922-35930.

Hediger, Clémençon, B., Burrier, R.E. & Bruford, E.A. 2013, *The ABCs of membrane transporters in health and disease (SLC series): Introduction*.

Heitzer, M., Wolf, I., Sanchez, E., Witchel, S. & DeFranco, D. 2007, "Glucocorticoid receptor physiology", *Reviews in Endocrine and Metabolic Disorders,* vol. 8, no. 4, pp. 321-330.

Hellsten, S.V., Hägglund, M.G., Eriksson, M.M. & Fredriksson, R. 2017, "The neuronal and astrocytic protein SLC38A10 transports glutamine, glutamate, and aspartate, suggesting a role in neurotransmission", *FEBS Open Bio,* vol. 7, no. 6, pp. 730-746.

Hornberger, T.A., W. K. Chu, Y. W. Mak, J. W. Hsiung, S. A. Huang & S. Chien 2006, "The Role of Phospholipase D and Phosphatidic Acid in the Mechanical Activation of MTOR Signaling in Skeletal Muscle", *Proceedings of the National Academy of Sciences of the United States of America,* vol. 103, no. 12, pp. 4741-4746.

Hornberger, T.A., Stuppard, R., Conley, K.E., Fedele, M.J., Fiorotto, M.L., Chin, E.R. & Esser, K.A. 2004, "Mechanical stimuli regulate rapamycin-sensitive signalling by a phosphoinositide 3-kinase-, protein kinase B- and growth factor-independent mechanism", *The Biochemical journal,* vol. 380, no. Pt 3, pp. 795-804.

Hu, Z., Wang, H., Lee, I.H., Du, J. & Mitch, W.E. 2009, "Endogenous glucocorticoids and impaired insulin signalling are both required to stimulate muscle wasting under pathophysiological conditions in mice", The Journal of clinical investigation, vol. 119, no. 10, pp. 3059-3069.

Hundal, H.S. & Taylor, P.M. 2009, "Amino acid transceptors: gate keepers of nutrient exchange and regulators of nutrient signaling", *American Journal of Physiology - Endocrinology And Metabolism,* vol. 296, no. 4, pp. 603-613.

Hyde, R., Christie, G.R., Litherland, G.J., Hajduch, E., Taylor, P.M. & Hundal, H.S. 2001, "Subcellular localization and adaptive up-regulation of the System A (SAT2) amino acid transporter in skeletal-muscle cells and adipocytes", *The Biochemical journal,* vol. 355, no. Pt 3, pp. 563-568.

Hyde, R., Cwiklinski, E.L., MacAulay, K., Taylor, P.M. & Hundal, H.S. 2007, "Distinct sensor pathways in the hierarchical control of SNAT2, a putative amino acid transceptor, by amino acid availability", *The Journal of biological chemistry,* vol. 282, no. 27, pp. 19788-19798.

Hyde, R., Karine Peyrollier & Harinder S. Hundal 2002, "Insulin Promotes the Cell Surface Recruitment of the SAT2/ATA2 System A Amino Acid Transporter from an Endosomal Compartment in Skeletal Muscle Cells", *Journal of Biological Chemistry,* vol. 277, no. 16, pp. 13628-13634.

Hyde, R., Taylor, P.M. & Hundal, H.S. 2003, "Amino acid transporters: roles in amino acid sensing and signalling in animal cells", *The Biochemical journal,* vol. 373, no. Pt 1, pp. 1-18.

Janssen, I., Heymsfield, S.B. & Ross, R. 2002, "Low Relative Skeletal Muscle Mass (Sarcopenia) in Older Persons Is Associated with Functional Impairment and Physical Disability", *Journal of the American Geriatrics Society,* vol. 50, no. 5, pp. 889-896.

Janssen, I., Heymsfield, S.B., Wang, Z. & Ross, R. 2000, "Skeletal muscle mass and distribution in 468 men and women aged 18-88 yr", *Journal of Applied Physiology,* vol. 89, no. 1, pp. 81.

Johansen, K.L. & Lee, C. 2015, "Body composition in chronic kidney disease", *Current opinion in nephrology and hypertension,* vol. 24, no. 3, pp. 268.

Johnson, M.A., Polgar, J., Weightman, D. & Appleton, D. 1973, "Data on the distribution of fibre types in thirty-six human muscles", *Journal of the Neurological Sciences,* vol. 18, no. 1, pp. 111-129.

Jung, J., Genau, H.M. & Behrends, C. 2015, "Amino Acid-Dependent mTORC1 Regulation by the Lysosomal Membrane Protein SLC38A9", *Molecular and cellular biology,* vol. 35, no. 14, pp. 2479-2494.

Jung, U.J. & Choi, M. 2014, "Obesity and its metabolic complications: the role of adipokines and the relationship between obesity, inflammation, insulin resistance, dyslipidemia and nonalcoholic fatty liver disease", *International journal of molecular sciences,* vol. 15, no. 4, pp. 6184-6223.

Kalantar-Zadeh, K., Mehrotra, R., Fouque, D. & Kopple, J.D. 2004, "Metabolic Acidosis and Malnutrition-Inflammation Complex Syndrome in Chronic Renal Failure", *Seminars in Dialysis,* vol. 17, no. 6, pp. 455-465.

Kashiwagi, H., Yamazaki, K., Takekuma, Y., Ganapathy, V. & Sugawara, M. 2009, "Regulatory mechanisms of SNAT2, an amino acid transporter, in L6 rat skeletal muscle cells by insulin, osmotic shock and amino acid deprivation", *Amino Acids,* vol. 36, no. 2, pp. 219-230.

Kenawy, H.I., Boral, I. & Bevington, A. 2015, "Complement-Coagulation Cross-Talk: A Potential Mediator of the Physiological Activation of Complement by Low pH", *Frontiers in immunology,* vol. 6, pp. 215.

Kilberg, M.S., Shan, J. & Su, N. 2009, "ATF4-dependent transcription mediates signaling of amino acid limitation", *Trends in Endocrinology & Metabolism,* vol. 20, no. 9, pp. 436-443.

Kim, D.K., Kim, I.J., Hwang, S., Kook, J.H., Lee, M., Shin, B.A., Bae, C.S., Yoon, J.H., Ahn, S.G., Kim, S.A., Kanai, Y., Endou, H. & Kim, J. 2004, "System l-amino acid transporters are differently expressed in rat astrocyte and C6 glioma cells", *Neuroscience research,* vol. 50, no. 4, pp. 437-446.

Klein, G.L. 2015, "The effect of glucocorticoids on bone and muscle", *Osteoporosis and sarcopenia,* vol. 1, no. 1, pp. 39-45.

Kobilka, B.K. 2007, "G protein coupled receptor structure and activation", *Biochimica et biophysica acta,* vol. 1768, no. 4, pp. 794.

Kotler, D.P. 2000, "Cachexia", *Annals of Internal Medicine,* vol. 133, no. 8, pp. 622-634.

Kraut, J.A. & Kurtz, I. 2005, "Metabolic Acidosis of CKD: Diagnosis, Clinical Characteristics, and Treatment", *American Journal of Kidney Diseases,* vol. 45, no. 6, pp. 978 993.

Kraut, J.A. & Madias, N.E. 2016, "Metabolic Acidosis of CKD: An Update", *American journal of kidney diseases : the official journal of the National Kidney Foundation,* vol. 67, no. 2, pp. 307-317.

Lacraz, G., Volatiana Rakotoarivelo, Sebastien M Labbé, Mathieu Vernier, Christophe Noll, Marian Mayhue, Jana Stankova, Adel Schwertani, Guillaume Grenier, André Carpentier, Denis Richard, Gerardo Ferbeyre, Julie Fradette, Marek Rola-Pleszczynski, Alfredo Menendez, Marie-France Langlois & Subburaj Ilangumaran 2016, "Deficiency of Interleukin-15 Confers Resistance to Obesity by Diminishing Inflammation and Enhancing the Thermogenic Function of Adipose Tissues", *PLoS One,* vol. 11, no. 9, pp. e0162995.

Lardner, A. 2001, "The effects of extracellular pH on immune function", *Journal of leukocyte biology,* vol. 69, no. 4, pp. 522-530.

Lfberg, E., Gutierrez, A., Wernerman, J., Anderstam, B., Mitch, W.E., Price, S.R., Bergstrm, J. & Alvestrand, A. 2002, "Effects of high doses of glucocorticoids on free amino acids, ribosomes and protein turnover in human muscle", *European journal of clinical investigation,* vol. 32, no. 5, pp. 345-353.

Limon, J.J. & Fruman, D.A. 2012, "Akt and mTOR in B Cell Activation and Differentiation", *Frontiers in immunology,* vol. 3, pp. 228.

Lin, Y., Boone, M., Meuris, L., Lemmens, I., Van Roy, N., Soete, A., Reumers, J., Moisse, M., Plaisance, S., Drmanac, R., Chen, J., Speleman, F., Lambrechts, D., Van de Peer, Y., Tavernier, J. & Callewaert, N. 2014, "Genome dynamics of the human embryonic kidney 293 lineage in response to cell biology manipulations", *Nature communications,* vol. 5, no. 1, pp. 4767.

Liu, J., Peng, Y., Wang, X., Fan, Y., Qin, C., Shi, L., Tang, Y., Cao, K., Li, H., Long, J. & Liu, J. 2016, "Mitochondrial Dysfunction Launches Dexamethasone-

Induced Skeletal Muscle Atrophy via AMPK/FOXO3 Signaling", *Molecular pharmaceutics,* vol. 13, no. 1, pp. 73.

López-Fontanals, M., Rodríguez-Mulero, S., Casado, F.J., Dérijard, B. & Pastor-Anglada, M. 2003, "The osmoregulatory and the amino acid-regulated responses of system A are mediated by different signal transduction pathways", *The Journal of general physiology,* vol. 122, no. 1, pp. 5-16.

Lowry, O.H., Rosebrough, N.J., Farr, A.L. & Randall, R.J. 1951, "Protein measurement with the Folin phenol reagent", *The Journal of biological chemistry,* vol. 193, no. 1, pp. 265-275.

Luo, J., Liang, A., Liang, M., Xia, R., Rizvi, Y., Wang, Y. & Cheng, J. 2016, "Serum Glucocorticoid-Regulated Kinase 1 Blocks CKD-Induced Muscle Wasting Via Inactivation of FoxO3a and Smad2/3", *Journal of the American Society of Nephrology : JASN,* vol. 27, no. 9, pp. 2797.

Lützner, N., Kalbacher, H., Krones-Herzig, A. & Rösl, F. 2012, "FOXO3 is a glucocorticoid receptor target and regulates LKB1 and its own expression based on cellular AMP levels via a positive autoregulatory loop", *PloS one,* vol. 7, no. 7, pp. e42166.

Mackenzie, B. & Erickson, J. 2004, "Sodium-coupled neutral amino acid (System N/A) transporters of the SLC38 gene family", *Pflügers Archiv - European Journal of Physiology,* vol. 447, no. 5, pp. 784-795.

Malavaki, C., Sakkas, G., Mitrou, G., Kalyva, A., Stefanidis, I., Myburgh, K. & Karatzaferi, C. 2015, "Skeletal muscle atrophy: disease-induced mechanisms may mask disuse atrophy", *Journal of Muscle Research and Cell Motility,* vol. 36, no. 6, pp. 405-421.

Maurer, M., Riesen, W., Muser, J., Hulter, H.N. & Krapf, R. 2003, "Neutralization of Western diet inhibits bone resorption independently of K intake and reduces cortisol secretion in humans", *American journal of physiology.Renal physiology,* vol. 284, no. 1, pp. 32.

May, R.C., Kelly, R.A. & Mitch, W.E. 1986, "Metabolic acidosis stimulates protein degradation in rat muscle by a glucocorticoid-dependent mechanism", *The Journal of clinical investigation,* vol. 77, no. 2, pp. 614-621.

Mayer, C. & Grummt, I. 2006, "Ribosome biogenesis and cell growth: mTOR coordinates transcription by all three classes of nuclear RNA polymerases", *Oncogene,* vol. 25, no. 48, pp. 6384-6391.

McCarthy, J. & Esser, K. 2010, "Anabolic and catabolic pathways regulating skeletal muscle mass", *Current Opinion in Clinical Nutrition and Metabolic Care,* vol. 13, no. 3, pp. 230-235.

McCubrey, Steelman, L.S., Chappell, W.H., Abrams, S.L., Wong, E.W.T., Chang, F., Lehmann, B., Terrian, D.M., Milella, M., Tafuri, A., Stivala, F., Libra, M.,

Basecke, J., Evangelisti, C., Martelli, A.M. & Franklin, R.A. 2007, *Roles of the Raf/MEK/ERK pathway in cell growth, malignant transformation and drug resistance*.

McGivan, J.D. & Pastor-Anglada, M. 1994, "Regulatory and molecular aspects of mammalian amino acid transport", *The Biochemical journal,* vol. 299 ( Pt 2), no. Pt 2, pp. 321-334.

McLeod, M., Breen, L., Hamilton, D.L. & Philp, A. 2016, "Live strong and prosper: the importance of skeletal muscle strength for healthy ageing", *Biogerontology,* vol. 17, no. 3, pp. 497-510.

Menconi, M., Gonnella, P., Petkova, V., Lecker, S. & Hasselgren, P. 2008, "Dexamethasone and corticosterone induce similar, but not identical, muscle wasting responses in cultured L6 and C2C12 myotubes", *Journal of cellular biochemistry,* vol. 105, no. 2, pp. 353-364.

Menon, M.C. & He, J.C. 2016, "Glucocorticoid-Regulated Kinase: Linking Azotemia and Muscle Wasting in CKD", *Journal of the American Society of Nephrology : JASN,* vol. 27, no. 9, pp. 2545.

Methenitis, S., Spengos, K., Zaras, N., Stasinaki, A., Papadimas, G., Karampatsos, G., Arnaoutis, G. & terzis, G. 2017, "Fiber Type Composition And Rate Of Force Development In Endurance And Resistance Trained Individuals", *Journal of Strength and Conditioning Research,* .

Mihaylova, M.M. & Shaw, R.J. 2011, "The AMPK signalling pathway coordinates cell growth, autophagy and metabolism", *Nature cell biology,* vol. 13, no. 9, pp. 1016.

Milkereit, R., Avinash Persaud, Liviu Vanoaica, Adriano Guetg, Francois Verrey & Daniela Rotin 2015, "LAPTM4b recruits the LAT1-4F2hc Leu transporter to lysosomes and promotes mTORC1 activation", *Nature Communications,* vol. 6, pp. 7250.

Moore, D.R., Atherton, P.J., Rennie, M.J., Tarnopolsky, M.A. & Phillips, S.M. 2011, "Resistance exercise enhances mTOR and MAPK signalling in human muscle over that seen at rest after bolus protein ingestion", *Acta Physiologica,* vol. 201, no. 3, pp. 365-372.

Morley, J.E., Thomas, D.R. & Wilson, M.M. 2006, "Cachexia: pathophysiology and clinical relevance", *The American Journal of Clinical Nutrition,* vol. 83, no. 4, pp. 735-743.

Müller, T., Perez-Tilve, D., Tong, J., Pfluger, P. & Tschöp, M. 2010, "Ghrelin and its potential in the treatment of eating/wasting disorders and cachexia", *Journal of Cachexia, Sarcopenia and Muscle,* vol. 1, no. 2, pp. 159-167.

Nader, G.A., Thomas J. McLoughlin & Karyn A. Esser 2005, "mTOR function in skeletal muscle hypertrophy: increased ribosomal RNA via cell cycle regulators", *American Journal of Physiology - Cell Physiology,* vol. 289, no. 6, pp. 1457-1465.

Náray-Fejes-Tóth, A., Fejes-Tóth, G., Volk, K.A. & Stokes, J.B. 2000, "SGK is a primary glucocorticoid-induced gene in the human", *Journal of Steroid Biochemistry and Molecular Biology,* vol. 75, no. 1, pp. 51-56.

Nardi, F., Hoffmann, T.M., Stretton, C., Cwiklinski, E., Taylor, P.M. & Hundal, H.S. 2015, "Proteasomal modulation of cellular SNAT2 (SLC38A2) abundance and function by unsaturated fatty acid availability", *Journal of Biological Chemistry,* vol. 290, no. 13, pp. 8173-8184.

Nascimento, M.M., Pecoits-Filho, R., Lindholm, B., Riella, M.C. & Stenvinkel, P. 2002, "Inflammation, Malnutrition and Atherosclerosis in End-Stage Renal Disease: A Global Perspective", *Blood Purification,* vol. 20, no. 5, pp. 454-458.

Newton, R., Cambridge, L., Hart, L.A., Stevens, D.A., Lindsay, M.A. & Barnes, P.J. 2000, "The MAP kinase inhibitors, PD098059, UO126 and SB203580, inhibit IL-1β-dependent PGE2 release via mechanistically distinct processes", *British journal of pharmacology,* vol. 130, no. 6, pp. 1353-1361.

Nielsen, S. & Pedersen, B.K. 2008, "Skeletal muscle as an immunogenic organ", *Current opinion in pharmacology,* vol. 8, no. 3, pp. 346-351.

Nissen-Meyer, L.S.H. & Chaudhry, F.A. 2013, "Protein Kinase C Phosphorylates the System N Glutamine Transporter SN1 (Slc38a3) and Regulates Its Membrane Trafficking and Degradation", *Frontiers in endocrinology,* vol. 4, pp. 138.

Oakley, R.H. & Cidlowski, J.A. 2013, "The biology of the glucocorticoid receptor: new signaling mechanisms in health and disease", *The Journal of allergy and clinical immunology,* vol. 132, no. 5, pp. 1033.

Okajima, F. 2013, "Regulation of inflammation by extracellular acidification and proton-sensing GPCRs", *Cellular signalling,* vol. 25, no. 11, pp. 2263-2271.

Palacn, M., Estvez, R., Bertran, J. & Zorzano, A. 1998, "Molecular biology of mammalian plasma membrane amino acid transporters", *Physiological Reviews,* vol. 78, no. 4, pp. 969-1054.

Palii, S.S., Hong Chen & Michael S. Kilberg 2004, "Transcriptional Control of the Human Sodium-coupled Neutral Amino Acid Transporter System A Gene by Amino Acid Availability Is Mediated by an Intronic Element", *Journal of Biological Chemistry,* vol. 279, no. 5, pp. 3463-3471.

Pallafacchina, G., Blaauw, B. & Schiaffino, S. 2013, "Role of satellite cells in muscle growth and maintenance of muscle mass", *Nutrition, Metabolism and Cardiovascular Diseases,* vol. 23 Suppl 1, pp. S18.

Palmisano, M.G., Bremner, S.N., Hornberger, T.A., Meyer, G.A., Domenighetti, A.A., Shah, S.B., Kiss, B., Kellermayer, M., Ryan, A.F. & Lieber, R.L. 2015, "Skeletal muscle intermediate filaments form a stress-transmitting and stress-signaling network", *Journal of cell science,* vol. 128, no. 2, pp. 219-224.

Pasiakos, S.M. 2012, "Exercise and amino acid anabolic cell signaling and the regulation of skeletal muscle mass", *Nutrients,* vol. 4, no. 7, pp. 740-758.

Pecoits-Filho, R., Lindholm, B. & Stenvinkel, P. 2002, "The malnutrition, inflammation, and atherosclerosis (MIA) syndrome -- the heart of the matter", *Nephrology, dialysis, transplantation : official publication of the European Dialysis and Transplant Association - European Renal Association,* vol. 17 Suppl 11, pp. 28-31.

Petersen, A.M. & Pedersen, B.K. 2005, "The anti-inflammatory effect of exercise", *Journal of applied physiology (Bethesda, Md.: 1985),* vol. 98, no. 4, pp. 1154-1162.

Pfaffl, M.W. 2001, "A new mathematical model for relative quantification in real-time RT-PCR", *Nucleic acids research,* vol. 29, no. 9, pp. 45.

Philp, A., Joaquin Perez-Schindler, Charlotte Green, D. Lee Hamilton & Keith Baar 2010, "Pyruvate suppresses PGC1α expression and substrate utilization despite increased respiratory chain content in C2C12 myotubes", *American Journal of Physiology - Cell Physiology,* vol. 299, no. 2, pp. 240-250.

Philp, A., Micah Y. Belew, Ashleigh Evans, Don Pham, Itwinder Sivia, Ai Chen, Simon Schenk & Keith Baar 2011, "The PGC-1α-related coactivator promotes mitochondrial and myogenic adaptations in C2C12 myotubes", *American Journal of Physiology - Regulatory, Integrative and Comparative Physiology,* vol. 301, no. 4, pp. 864-872.

Philp, A., Schenk, S., Perez-Schindler, J., Hamilton, D. ., Breen, L., Laverone, E., Jeromson, S., Phillips, S.M. & Baar, K. 2015, "Rapamycin does not prevent increases in myofibrillar or mitochondrial protein synthesis following endurance exercise", *The Journal of Physiology,* vol. 593, no. 18, pp. 4275-4284.

Pickering, W., Cheng, M.K., Brown, J., Butler, H., Walls, J. & Bevington, A. 2003, "Stimulation of protein degradation by low pH in L6G8C5 skeletal muscle cells is independent of apoptosis but dependent on differentiation state", *Nephrology, dialysis, transplantation: official publication of the European Dialysis and Transplant Association - European Renal Association,* vol. 18, no. 8, pp. 1466-1474.

Pinilla, J., Aledo, J.C., Cwiklinski, E., Hyde, R., Taylor, P.M. & Hundal, H.S. 2011, "SNAT2 transceptor signalling via mTOR: a role in cell growth and proliferation?", Frontiers in bioscience (Elite edition), vol. 3, no. 4, pp. 1289-1299.

Pistilli, E.E. & Quinn, L.S. 2013, "From anabolic to oxidative: reconsidering the roles of IL-15 and IL-15Rα in skeletal muscle", *Exercise and sport sciences reviews,* vol. 41, no. 2, pp. 100-106.

Prasad, S. & Aggarwal, B.B. 2014, "Chronic diseases caused by chronic inflammation require chronic treatment: anti-inflammatory role of dietary spices", *Journal of Clinical & Cellular Immunology,* vol. 2014.

Putney, L.K., Brandt, J.D. & O'Donnell, M.E. 1997, "Effects of dexamethasone on sodium-potassium-chloride cotransport in trabecular meshwork cells", *Investigative Ophthalmology & Visual Science,* vol. 38, no. 6, pp. 1229.

Quinn, L.S., Anderson, B.G., Drivdahl, R.H., Alvarez, B. & Argilés, J.M. 2002, "Overexpression of Interleukin-15 Induces Skeletal Muscle Hypertrophy in Vitro: Implications for Treatment of Muscle Wasting Disorders", *Experimental Cell Research,* vol. 280, no. 1, pp. 55-63.

Ramamoorthy, S., Devadoss J. Samuvel, Eric R. Buck, Gary Rudnick & Lankupalle D. Jayanthi 2007, "Phosphorylation of Threonine Residue 276 Is Required for Acute Regulation of Serotonin Transporter by Cyclic GMP", *Journal of Biological Chemistry,* vol. 282, no. 16, pp. 11639-11647.

Raschke, S. & Eckel, J. 2013, "Adipo-myokines: two sides of the same coin--mediators of inflammation and mediators of exercise", *Mediators of inflammation,* vol. 2013, pp. 320724.

Rebsamen, M., Lorena Pochini, Taras Stasyk, Mariana E G de Araújo, Michele Galluccio, Richard K Kandasamy, Berend Snijder, Astrid Fauster, Elena L Rudashevskaya, Manuela Bruckner, Stefania Scorzoni, Przemyslaw A Filipek, Kilian V M Huber, Johannes W Bigenzahn, Leonhard X Heinz, Claudine Kraft, Keiryn L Bennett, Cesare Indiveri, Lukas A Huber & Giulio Superti-Furga 2015, "SLC38A9 is a component of the lysosomal amino acid sensing machinery that controls mTORC1", *Nature,* vol. 519, no. 7544, pp. 477-481.

Relaix, F. & Zammit, P.S. 2012, "Satellite cells are essential for skeletal muscle regeneration: the cell on the edge returns centre stage", *Development (Cambridge, England),* vol. 139, no. 16, pp. 2845-2856.

Rom, O. & Reznick, A.Z. 2016, "The role of E3 ubiquitin-ligases MuRF-1 and MAFbx in loss of skeletal muscle mass", *Free radical biology & medicine,* vol. 98, pp. 218-230.

Romanick, M., Thompson, L.V. & Brown-Borg, H.M. 2013, "Murine models of atrophy, cachexia, and sarcopenia in skeletal muscle", *Biochimica et Biophysica Acta (BBA) - Molecular Basis of Disease,* vol. 1832, no. 9, pp. 1410-1420.

Rosa, D.A., Tatjana Coric, Natasa Todorovic, Deren Shao, Tong Wang & Cecilia M Canessa 2003, "Distribution and regulation of expression of serum- and glucocorticoid-induced kinase-1 in the rat kidney", *The Journal of Physiology,* vol. 551, no. 2, pp. 455-466.

Rosario, F.J., Dimasuay, K.G., Kanai, Y., Powell, T.L. & Jansson, T. 2016, "Regulation of amino acid transporter trafficking by mTORC1 in primary human trophoblast cells is mediated by the ubiquitin ligase Nedd4-2", *Clinical science (London, England : 1979),* vol. 130, no. 7, pp. 499.

Rosman, P.M., Farag, A., Peckham, R., Benn, R., Tito, J., Bacci, V. & Wallace, E.Z. 1982, "Pituitary-adrenocortical function in chronic renal failure: blunted suppression and early escape of plasma cortisol levels after intravenous dexamethasone", *The Journal of clinical endocrinology and metabolism,* vol. 54, no. 3, pp. 528-533.

Ross, A. & Leveritt, M. 2001, "Long-term metabolic and skeletal muscle adaptations to short-sprint training", *Sports Medicine,* vol. 31, no. 15, pp. 1063-1082.

Roux, p.p. & Blenis, J. 2004, "ERK and p38 MAPK-Activated Protein Kinases: a Family of Protein Kinases with Diverse Biological Functions", *Microbiology and Molecular Biology Reviews,* vol. 68, no. 2, pp. 320-344.

Sakuma, K. & Yamaguchi, A. 2012, "Sarcopenia and Age-Related Endocrine Function", *International Journal of Endocrinology,* vol. 2012, pp. 1-10.

Schakman, O., Kalista, S., Barbe, C., Loumaye, A. & Thissen, J.P. 2013, "Glucocorticoid-induced skeletal muscle atrophy", *The international journal of biochemistry & cell biology,* vol. 45, no. 10, pp. 2163-2172.

Serhan, C.N., Ward, P.A. & Gilroy, D.W. 2010, *Fundamentals of inflammation,* 1st edition edn, Cambridge University Press.

Shaw, K.A., Srikanth, V.K., Fryer, J.L., Blizzard, L., Dwyer, T. & Venn, A.J. 2007, "Dual energy X-ray absorptiometry body composition and aging in a population-based older cohort", *International Journal of Obesity,* vol. 31, no. 2, pp. 279-284.

Sheridan, D.L., Kong, Y., Parker, S.A., Dalby, K.N. & Turk, B.E. 2008, "Substrate Discrimination among Mitogen-activated Protein Kinases through Distinct Docking Sequence Motifs", *Journal of Biological Chemistry,* vol. 283, no. 28, pp. 19511-19520.

Shigemitsu, K., Tsujishita, Y., Miyake, H., Hidayat, S., Tanaka, N., Hara, K. & Yonezawa, K. 1999, "Structural requirement of leucine for activation of p70 S6 kinase", *FEBS letters,* vol. 447, no. 2–3, pp. 303-306.

Simms, N., (2013) MSc thesis, University of Leicester.

Simoneau, J.A. & Bouchard, C. 1995, "Genetic determinism of fiber type proportion in human skeletal muscle.", *The FASEB Journal,* vol. 9, no. 11, pp. 1091-1095.

Sonntag, J., Emeis, M., Strauss, E. & Obladen, M. 1998, "In vitro activation of complement and contact system by lactic acidosis", *Mediators of inflammation,* vol. 7, no. 1, pp. 49-51.

Spangenburg, E.E., Derek Le Roith, Chris W. Ward & Sue C. Bodine 2008, "A functional insulin-like growth factor receptor is not necessary for load-induced skeletal muscle hypertrophy", *The Journal of Physiology,* vol. 586, no. 1, pp. 283-291.

Stolarczyk, E.I., Cassandra J. Reiling & Christian M. Paumi 2011, "Regulation of ABC Transporter Function Via Phosphorylation by Protein Kinases", *Current Pharmaceutical Biotechnology,* vol. 12, no. 4, pp. 621-635.

Stubbs, A.K., Wheelhouse, N.M., Lomax, M.A. & Hazlerigg, D.G. 2002, "Nutrient-hormone interaction in the ovine liver: methionine supply selectively modulates growth hormone-induced IGF-I gene expression", *Journal of Endocrinology,* vol. 174, no. 2, pp. 335-341.

Tan, N. & Lansman, J.B. 2014, "Utrophin regulates modal gating of mechanosensitive ion channels in dystrophic skeletal muscle", *The Journal of Physiology,* vol. 592, no. 15, pp. 3303-3323.

Taylor, P.M. 2014, "Role of amino acid transporters in amino acid sensing1234", *The American Journal of Clinical Nutrition,* vol. 99, no. 1, pp. 230S.

Tesseraud, S., Bigot, K. & Taouis, M. 2003, "Amino acid availability regulates S6K1 and protein synthesis in avian insulin-insensitive QM7 myoblasts", *FEBS letters,* vol. 540, no. 1–3, pp. 176-180.

Thomas, P. & Smart, T.G. 2005, "HEK293 cell line: A vehicle for the expression of recombinant proteins", *Journal of pharmacological and toxicological methods,* vol. 51, no. 3, pp. 187-200.

Thomas, S. & Mitch, W. 2013, "Mechanisms stimulating muscle wasting in chronic kidney disease: the roles of the ubiquitin-proteasome system and myostatin", *Clinical and Experimental Nephrology,* vol. 17, no. 2, pp. 174-182.

Thoroed, S.M., Bryan-Sisneros, A. & Doroshenko, P. 1999, "Protein phosphotyrosine phosphatase inhibitors suppress regulatory volume decrease and the volume-sensitive Cl- conductance in mouse fibroblasts", *Pflugers Archiv : European journal of physiology,* vol. 438, no. 2, pp. 133-140.

Vanek, M., Hofstetter, H., Wolf, R.M., Gasser, J.A., Junker, U., Guerini, D., Ludwig, M., Seuwen, K. & Jones, C.E. 2003, "Proton-sensing G-protein-coupled receptors", *Nature,* vol. 425, no. 6953, pp. 93-98.

Verdijk, L., Snijders, T., Drost, M., Delhaas, T., Kadi, F. & van Loon, L. 2014, "Satellite cells in human skeletal muscle; from birth to old age", *AGE,* vol. 36, no. 2, pp. 545-557.

Verdon, Q., Boonen, M., Ribes, C., Jadot, M., Gasnier, B. & Sagn, C. 2017, "SNAT7 is the primary lysosomal glutamine exporter required for extracellular protein-dependent growth of cancer cells", *Proceedings of the National Academy of Sciences,* vol. 114, no. 18, pp. E3611.

Viana, J.L., Kosmadakis, G.C., Watson, E.L., Bevington, A., Feehally, J., Bishop, N.C. & Smith, A.C. 2014, "Evidence for anti-inflammatory effects of exercise in CKD", *Journal of the American Society of Nephrology : JASN,* vol. 25, no. 9, pp. 2121-2130.

von Haehling, S. & Anker, S. 2014, "Prevalence, incidence and clinical impact of cachexia: facts and numbers—update 2014", *Journal of Cachexia, Sarcopenia and Muscle,* vol. 5, no. 4, pp. 261-263.

von Haehling, S. & Anker, S. 2010, "Cachexia as a major underestimated and unmet medical need: facts and numbers", *Journal of Cachexia, Sarcopenia and Muscle,* vol. 1, no. 1, pp. 1-5.

Wang, S., Tsun, Z., Wolfson, R., Shen, K., Wyant, G.A., Plovanich, M.E., Yuan, E.D., Jones, T.D., Chantranupong, L. & Comb, W. 2015, "The amino acid transporter SLC38A9 is a key component of a lysosomal membrane complex that signals arginine sufficiency to mTORC1", *Science (New York, NY),* vol. 347, no. 6218, pp. 188.

Wang, X.H. & Mitch, W.E. 2013, "Muscle wasting from kidney failure-a model for catabolic conditions", *The international journal of biochemistry & cell biology,* vol. 45, no. 10, pp. 2230-2238.

Wang, X.H., Hu, Z., Klein, J.D., Zhang, L., Fang, F. & Mitch, W.E. 2011, "Decreased miR-29 suppresses myogenesis in CKD", *Journal of the American Society of Nephrology : JASN,* vol. 22, no. 11, pp. 2068-2076.

Wang, X. & Proud, C.G. 2006, "The mTOR Pathway in the Control of Protein Synthesis", *Physiology,* vol. 21, no. 5, pp. 362-369.

Watson, E.L., Kosmadakis, G.C., Smith, A.C., Viana, J.L., Brown, J.R., Molyneux, K., Pawluczyk, I.Z., Mulheran, M., Bishop, N.C., Shirreffs, S., Maughan, R.J., Owen, P.J., John, S.G., McIntyre, C.W., Feehally, J. & Bevington, A. 2013, "Combined walking exercise and alkali therapy in patients with CKD4-5 regulates intramuscular free amino acid pools and ubiquitin E3 ligase expression", *European journal of applied physiology,* vol. 113, no. 8, pp. 2111-2124.

Watson, K. & Baar, K. 2014, "mTOR and the health benefits of exercise", *Seminars in cell & developmental biology,* vol. 36, pp. 130-139.

Wells, J. & Fewtrell, M.S. 2006, "Measuring body composition", *Archives of Disease in Childhood,* vol. 91, no. 7, pp. 612-617.

Wendowski, O., Redshaw, Z. & Mutungi, G. 2017, "Dihydrotestosterone treatment rescues the decline in protein synthesis as a result of sarcopenia in

isolated mouse skeletal muscle fibres", *Journal of Cachexia, Sarcopenia and Muscle,* vol. 8, no. 1, pp. 48-56.

Wolfe, R.R. 2006, "The underappreciated role of muscle in health and disease", *The American journal of clinical nutrition,* vol. 84, no. 3, pp. 475.

Wong, Port, F.K., Hulbert-Shearon, T.E., Carroll, C.E., Wolfe, R.A., Agodoa, L.Y.C. & Daugirdas, J.T. 1999, *Survival advantage in Asian American end-stage renal disease patients11See Editorial by Breyer-Lewis, p. 2528.*

Yablonka-Reuveni, Z. 2011, "The Skeletal Muscle Satellite Cell:Still Young and Fascinating at 50", *Journal of Histochemistry & Cytochemistry,* vol. 59, no. 12, pp. 1041-1059.

Yaffe, D. 1968, "Retention of differentiation potentialities during prolonged cultivation of myogenic cells", *Proceedings of the National Academy of Sciences of the United States of America,* vol. 61, no. 2, pp. 477-483.

Yang, L., Sanderlin, E., Justus, C. & Krewson, E. 2015, "Emerging roles for the pH-sensing G protein-coupled receptors in response to acidotic stress", *Cell Health and Cytoskeleton,* vol. 2015, pp. 99-109.

Yao, D., Mackenzie, B., Ming, H., Varoqui, H., Zhu, H., Hediger, M.A. & Erickson, J.D. 2000, "A novel system A isoform mediating Na+/neutral amino acid cotransport", *The Journal of biological chemistry,* vol. 275, no. 30, pp. 22790-22797.

Yeun, J.Y., Levine, R.A., Mantadilok, V. & Kaysen, G.A. 2000, "C-reactive protein predicts all-cause and cardiovascular mortality in hemodialysis patients", *American Journal of Kidney Diseases,* vol. 35, no. 3, pp. 469-476.

Yoon, M., Son, K., Arauz, E., Han, J.M., Kim, S. & Chen, J. 2016, "Leucyl-tRNA Synthetase Activates Vps34 in Amino Acid-Sensing mTORC1 Signaling", *Cell reports,* vol. 16, no. 6, pp. 1510-1517.

Yoshida, T. & Delafontaine, P. 2015, "Mechanisms of Cachexia in Chronic Disease States", *The American Journal of the Medical Sciences,* vol. 350, no. 4, pp. 250-256.

You, J., Anderson, G.B., Dooley, M.S. & Hornberger, T.A. 2015, "The role of mTOR signaling in the regulation of protein synthesis and muscle mass during immobilization in mice", *Disease models & mechanisms,* vol. 8, no. 9, pp. 1059-1069.

Yuan, S.Y., Jue Liu, Jun Zhou, Wei Lu, Hai-Yun Zhou, Li-Hong Long, Zhuang-Li Hu, Lan Ni, Yi Wang, Jian-Guo Chen & Fang Wang 2016, "AMPK Mediates Glucocorticoids Stress-Induced Downregulation of the Glucocorticoid Receptor in Cultured Rat Prefrontal Cortical Astrocytes", *PLoS One,* vol. 11, no. 8, pp. e0159513.

Zhang, L., Du, J., Hu, Z., Han, G., Delafontaine, P., Garcia, G. & Mitch, W.E. 2009a, "IL-6 and serum amyloid A synergy mediates angiotensin II-induced muscle wasting", *Journal of the American Society of Nephrology : JASN,* vol. 20, no. 3, pp. 604-612.

Zhang, Z., Thomas Albers, Heather L. Fiumera, Armanda Gameiro & Christof Grewer 2009b, "A Conserved Na+ Binding Site of the Sodium-coupled Neutral Amino Acid Transporter 2 (SNAT2)", *Journal of Biological Chemistry,* vol. 284, no. 37, pp. 25314-25323.

Zhang, Z., Gameiro, A. & Grewer, C. 2008, "Highly Conserved Asparagine 82 Controls the Interaction of Na+ with the Sodium-coupled Neutral Amino Acid Transporter SNAT2", *Journal of Biological Chemistry,* vol. 283, no. 18, pp. 12284-12292.

Zheng, B., Ohkawa, S., Li, H., Roberts-Wilson, T.K. & Price, S.R. 2010, "FOXO3a mediates signaling crosstalk that coordinates ubiquitin and atrogin-1/MAFbx expression during glucocorticoid-induced skeletal muscle atrophy", *FASEB journal : official publication of the Federation of American Societies for Experimental Biology,* vol. 24, no. 8, pp. 2660-2669.

Zheng, L., Zhang, W., Zhou, Y., Li, F., Wei, H. & Peng, J. 2016, "Recent Advances in Understanding Amino Acid Sensing Mechanisms that Regulate mTORC1", *International Journal of Molecular Sciences,* vol. 17, no. 10, pp. 1636.

http://lifecenter.sgst.cn/SysPTM/search.do?pager_totalCount=29&searchOrder.sitesAA=&search.proteinNames=&search.histon=&searchOrder.species=&search.species=&search.site=&searchOrder.geneName=desc&search.idsOrAccessionsFileName=&search.idsOrAccessions=Q96QD8&search.ptmSourceType=&search.cellLine=&searchOrder.pip=&searchOrder.ptmType=&searchOrder.proteinId=&search.sequenceFileName=&search.tissue=&search.pmid=&search.ptmType=&search.sequence=&search.ptmSubType=&search.proteinNamesFileName=&pager_currentPage=1&pager_pageSize=20&pager_offset=0.